Visual and vestibular integration for gaze stabilization in the mouse model

Louise Schenberg

Sorbonne Université

Ecole doctorale ED3C

Integrative Neuroscience and Cognition Center – Spatial Orientation Team

Visual and vestibular integration for gaze stabilization in the mouse model

Intégration visuo-vestibulaire dans la stabilisation du regard chez le modèle murin

Par Louise Schenberg

Thèse de doctorat de Neuroscience

Dirigée par Mathieu Beraneck

Présentée et soutenue publiquement le 16 décembre 2022

Devant un jury composé de :

Pr. Dr. Hans STRAKA	Rapporteur
Dr. Brahim TIGHILET	Rapporteur
Dr. Volker BORMUTH	Examinateur
Dr. Fekrije SELIMI	Présidente du Jury
Dr. Alexandra SEVERAC-CAUQUIL	Examinatrice
Dr. Mathieu BERANECK	Directeur de thèse

“This is how you do it: you sit down at the keyboard and you put one word after another until its done. It's that easy, and that hard.”

— Neil Gaiman
(1960-)

“You will ride life straight to perfect laughter. It's the only good fight there is.”

— Charles Bukowski
(1920-1994)

Acknowledgement

Before everything, I would like to gratefully thank all thesis committee members who have accepted to read and evaluate my work: Pr.Dr. Hans Straka and Dr. Brahim Tighilet as reviewers and Dr. Fekrije Selimi, Dr. Alexandra Severac-Cauquil and Dr. Volker Bormuth as examiners.

Je voudrais adresser un immense merci à Mathieu pour ces quatre dernières années et des poussières. Je voudrais te remercier du fond du coeur pour ta patience à toute épreuve, ton soutien continu et tout ce que tu m'as appris. Merci également pour ces nombreuses conversations autour de la machine à café, toujours agrémentées d'une nouvelle expression quasi-inconnue, et d'accepter (ou pas) les couleurs que j'utilise pour les graphiques. Pleins d'éléments qui m'ont aidé de faire de cette thèse une expérience incroyable aussi bien humainement que scientifiquement. Merci aussi pour ta confiance et les opportunités que tu continues de m'offrir.

Et également merci, à toi et à Desdemona d'avoir réuni une superbe équipe. Avant de faire une thèse, on ne se rend pas compte que l'environnement de travail, l'équipe dans laquelle on évolue, joue pour beaucoup. Et l'équipe Orientation Spatiale a été un soutien incroyable tout au long de ces dernières années.

Un grand merci à Michele pour tous tes conseils scientifiques mais pas que, et pour toute l'aide et la rigueur que tu m'as apporté sur tous les projets de ma thèse. Merci aussi pour toutes ces discussions cinéphiles, j'ai quelques films à rattraper mais promis mes critiques resteront sobres. Je te remercie également de m'avoir offert l'opportunité de réaliser des vols paraboliques ! Merci à Desdemona pour tes conseils toujours disponibles et bienveillants. Merci François pour tes conseils et ces instants de consternations partagés qui m'ont toujours fait bien rire. Merci David pour ton humour et tes discussions sur tout et rien. To the last (but not the least) of the PhD students, Marin and Dongkyun, thank you for always being up for team meetings on the 7th, and I hope we did not spoil the PhD experience with our most recent bouts of complaining. Good luck for you all.

Je voudrais également remercier l'ensemble du labo INCC, pour leur accueil et particulièrement Pascale, Patrick, Carole et Francesca pour leur aide continuelle, leur gentillesse et leur humour.

I would also like to thank Jordi Llorens and Aida Palou for their incredible contribution to our IDPN project. Sorry for making you, Aida, come to Paris to get the samples but I'm really happy with what we have achieved in the end and I hope for the best for the rest of your PhD.

A Louis, mon double maléfique (je me permets de rétablir la vérité sur ce point-là). Je voudrais te remercier pour ton amitié, ces moments partagés (ainsi que beaucoup de choses comme par exemple un mois d'anniversaire, un signe astrologique et des blagues douteuses), ou encore ces soirées marathons entrechoquées par des coups de coudes compulsifs pour se maintenir éveillés (avec beaucoup d'échec il faut se l'avouer). Merci aussi pour ton soutien du début à la fin !

I would also like to properly thank Filipa. You were one of the first people I've met in this amazing team and I've been pretty lucky to do so. You've taught me a lot, but you've made me laugh a lot more. Thank you for your never-ending positive attitude about everything, it was such a blessing to work with you. I really hope we'll get the lab lab one day!

I could not do the list of people to thank without including Flavia who managed admirably the tough job of transferring from electrophysiological recordings saviour to nerve saving friend. You've always made the lab livelier (maybe because you can actually keep a plant alive?) and I miss how we could just both curse in sync. I hope you and Louis have a great time in Chicago, and I can't wait to come to see you both!

En ces jours de fin de thèse où l'on se traine, à la limite de la joie et de la haine, je voudrais remercier Jules et Corentin. Ce petit triangle de fou-rires nerveux, de questionnement incessant sur les méandres administratifs de la soutenance de thèse, et de théories sur la réelle identité de Sauron était un véritable baume au cœur.

Petite pensée aussi pour ces anciens du labo Jothini, Martina, Merouann et Susie, avec qui j'ai toujours partagé d'excellent moments qui m'ont apporté soutien et rires.

Je voudrais remercier également ma famille pour leurs encouragements et leur soutien inébranlable, notamment ma mère et à mon père à qui je dois beaucoup. De mes plus jeunes rêves de devenir archéologue en passant par chercheuse en math sans oublier bien sûr chanteuse (rêve oublié suite à un constat certain d'une absence totale de talent pour lequel je vous remercie moins), vous m'avez toujours épaulé et porté vers l'avant. Que ce soit en s'intéressant à ce que je faisais dans ce monde étrange du laboratoire, ou en me demandant mes codes netflix, vous avez toujours été là veiller à ce que tout se passe bien. Merci à mes frères, Grégoire et Tristan, qui m'ont montré à de très nombreuses reprises qu'ils étaient toujours là quand j'en avais besoin. A Eve (et Hypnos) également et spécialement parce que c'est elle qui a eu la lourde peine de devoir me supporter pendant la période d'écriture, pénible autant pour moi que pour elle, et qui pourtant a trouvé la force de faire seule les courses le dimanche pour me laisser travailler plus longtemps.

Un dernier merci à mes amis de longue date Elsa, Tim, Fantine, Marguerite, Bénédicte et Camille qui m'ont vu évoluée pendant ces longues années, entre l'assurance des premières au stress des dernières. Merci de votre soutien, de ces soirées durant lesquelles je pouvais décompresser.

Table of contents

「 · CHAPITRE 1 · 」

═ INTRODUCTION ═

OVERVIEW

Let's take an almost banal example: we are walking in a crowded street in Paris, not yet deep into winter. Two things are clear: 1) we are walking, i.e. our body is actively moving 2) the world around us is also moving. However, both of these things are happening at the same time. We must therefore be able to distinguish between movements that originate from us (i.e. walking), and external movements (i.e. what we observe around us). These two sources of information are transmitted by distinct, but related systems; the vestibular and postural systems allow us to be aware of our movement in space, while the visual system provides us with information about external movements.
However, when we move, the world also 'moves', resulting in a visual blur. Indeed, images are perceived by the retina and sent to the brain, but movement can disrupt this impression of a clear image. We must therefore find a way to obtain a clear image when we move our head or when the environment around us is moving.

To do this, precise and rapid reflexes integrate visual, vestibular and postural information in order to stabilize the gaze. They compensate for the movement of the head or the environment with counteracting movements of the eyes using inputs from different organs such as the eye (visual), inner ear (vestibular) and the proprioceptors (postural). There are several oculomotor reflexes, called as such because they act *in fine* on the muscles that allow the eyes to move. However, during the work of this thesis, I am mainly interested in two of them, whose inputs are either vestibular or visual. The first is the vestibulo-ocular reflex (VOR) which induces a compensatory movement of the eye in response to a movement of the head in a given direction. The second reflex is called optokinetic reflex (OKR) and responds to a moving environment by performing a movement of the eye in the same direction.

Although animal model species differ in anatomical aspects (the location of the eyes on the head, or visual acuity) or physiological properties, these two reflexes are present in a similar way in vertebrates. Thus, in tadpoles, monkeys or mice, gaze

stabilization reflexes serve the same purpose, and can be used as sensorimotor models to understand visual and vestibular integration.

This multisensory integration is the focus of the work of my thesis. The use of these reflexes as physiological reporters of good integration relies partly on the multiple advantages they possess. Indeed, activating one of these reflexes by vestibular or visual stimulations is easy and quantifiable. Thus, it is possible to modify the intensity of these stimulations by controlling different parameters such as amplitude, and frequency or to carry out constantly changing (e.g. sinusoidal) or constant speed (continuous rotation). This set of possible stimulations makes it possible to test the efficiency of reflexes under different conditions and to observe whether one reflex is physiologically preferable to another for one specific condition. It is also possible to reproduce optimal conditions of gaze control, with combined visual and vestibular inputs resulting in optimal compensatory eye movements or, on the contrary, causing visual and vestibular conflict in order to modulate either system and drive them toward adaptation. Similarly, reflex responses, i.e. compensatory eye movements, have been easily quantifiable for several years. Several techniques exist but video-oculography, used in all studies of this thesis, is notably practical because it is precise and non-invasive. Thus, it is possible to modify the visual and vestibular inputs necessary for the generation of these two reflexes and to quantify the modulations created in the reflex, by measuring the oculomotor responses.

The work presented in this thesis deals with the adaptation and integration of visual and vestibular inputs with two main articles centered on the plasticity of VOR and OKR following perturbation, either in the form of a visual mismatch or pharmacological-induced bilateral vestibular lesion. In order to properly review the context behind the studies presented further, in this introduction, I will first address the anatomical and physiological description of the sensory organs from which the visual and vestibular information originates as well as the oculomotor system, which will generate compensatory eye movements in response to stimuli. In the second part, I will describe the characteristics and physiological properties of the vestibular-related reflexes to finish with a third and final section on the adaptation and plasticity of the OKR and VOR.

SENSORY PATHWAY

I· ANATOMY AND PHYSIOLOGY OF THE VESTIBULAR SYSTEM

The vestibular system consists of different anatomical structures: the peripheral vestibular system, composed of the vestibular organs located in the inner ear and the vestibular nerve, and the central vestibular system, composed of nuclei of neurons. The peripheral system will detect and encode the 3D head movement and orientation relative to gravity and will, through the VIIIth vestibular-auditory nerve, send this information to the central vestibular nuclei to be further processed and integrated. This chapter will attend to give an overview of the peripheral and central vestibular systems.

i· PERIPHERAL SYSTEM

The peripheral system of the vestibular apparatus consists of 5 small pairs of structures found in both inner ears: 2 otolithic organs and 3 semi-circular canals on each side of the brain. The inner ear is composed of a bony labyrinth and a membranous labyrinth, bilaterally located in the temporal bone. The bony labyrinth contains and protects the membranous labyrinth, formed by the semi-circular canals, the otolithic organs (saccule and utricule), and the cochlea **(Figure 1).** The cochlea contains the Organ of Corti, the receptor of sounds and hearing, and will not be addressed further as it is not part of the vestibular apparatus. The bony labyrinth is filled with a fluid, separating it from the membranous labyrinth, the perilymph (similar in composition to the cerebrospinal fluid, with a high level of chloride and sodium that is continuous and drained by the perilymphatic duct into the subarachnoid space (Khan and Chang, 2013). The fluid inside the membranous labyrinth is called endolymph, composed of a high level of potassium and low sodium, and is produced by the capillaries in the wall of the cochlear duct.

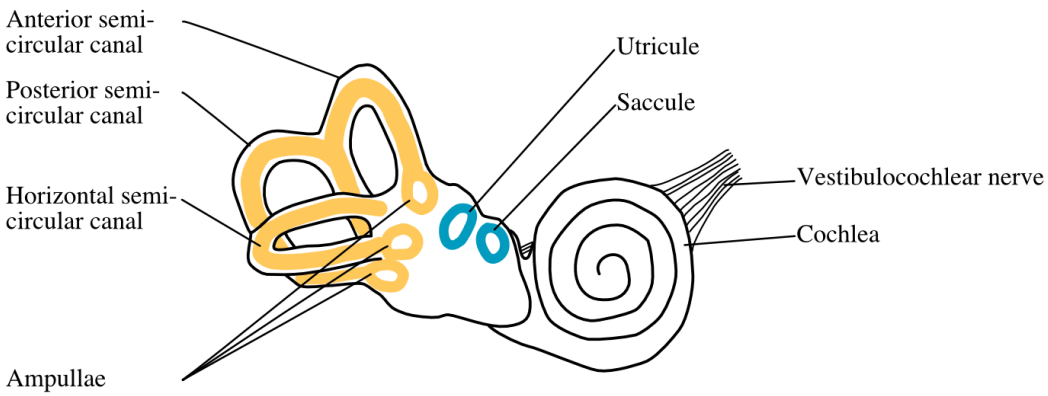

Figure 1: Inner ear. The inner ears are located bilaterally, on each side of the brain and are each composed of three semi-circular canals (in yellow), and two otolithic organs, the saccule and utricule (in blue). The vestibular and cochlear information are transmitted to the brain through the vestibulocochlear nerve. (From L. Schenberg)

Otoliths organs

The utricule and saccule contained in the vestibule encode the orientation of the head in space relative to gravity, they are activated by linear acceleration and tilt of the head (Angelaki, 2004). Inside the sensory neuroepithelium, called the macula, is a gelatinous membrane containing small calcium carbonate particles, stone-like, that are called otoliths or otoconia. When the head is tilted, or when there is a linear acceleration, a tension created between the gelatinous membrane and the macula will bend the cilia of hair cells. The utricule and saccule code for different planes to optimize head motion detection, as the utricule encodes horizontal motions while the saccule codes motion in the vertical plane. Single hair cells, in both organs, have different orientations compared to the neighbouring hair cells and are organized through the striola. The striola is a curvilinear line towards which the stereocilia in the utricule are oriented and away from the stereocilia inside the saccule (Desai et al., 2005b). This line separates the organ into two zones: striolar and extrastriolar **(Figure 2).** A motion will trigger the activation of a bundle of hair cells whose orientation can encode the

movement and inhibition of the other bundles not affected by the movement orientation.

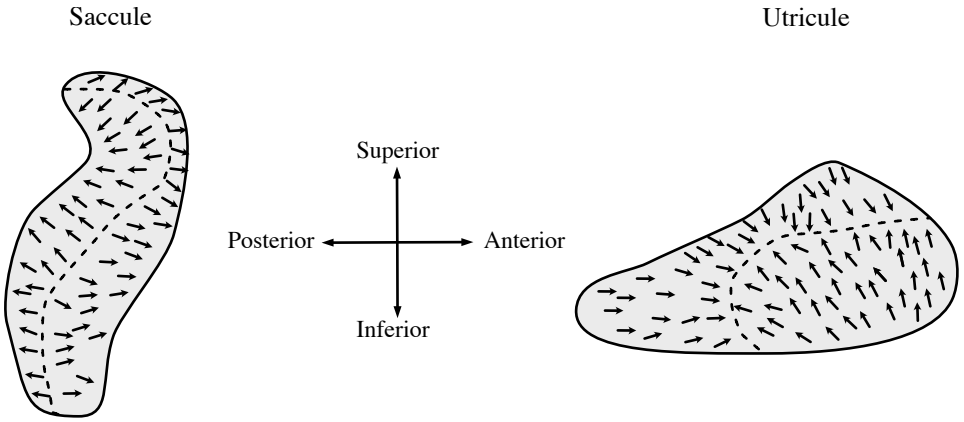

Figure 2: Otolithic hair cell orientation in the saccule (left) and the utricule (right). The dotted line represents the striola, separating the organ into the central and peripheral parts (i.e extrastriolar). (Adapted from Simon et al., 2021).

Semi-circular canals

The semi-circular canals code angular acceleration or rotation of the head (Goldberg and Fernandez, 1975). They are oriented perpendicularly from one to the other and canals are sensitive to a specific plane, so this distribution with three semi-circular canals, one horizontal and two verticals (anterior and posterior) allows a 3D representation of the head rotational motion **(Figure 3)**. The ampulla at the end of each canal contains the sensor epithelium called the crista ampullaris, which can be divided into a central and peripheral part. The hair cells that composed the epithelium are positioned inside a gelatinous substance called the cupula that caps the epithelium (Khan & Chang, 2013). While the crista ampullaris are similar to the macula, it does not contain otoliths. When there is a rotational motion, the endolymph will move and displace the cupula causing the hair cells to bend in the other direction of the movement, leading to an activation of the afferent fibres. If the motion is constant, after

the bend of the hair cells, the cupula falls back to its initial position. This leads to a deceleration as the displacement of the cupula is now in the same direction as the movement (Khan & Chang, 2013).

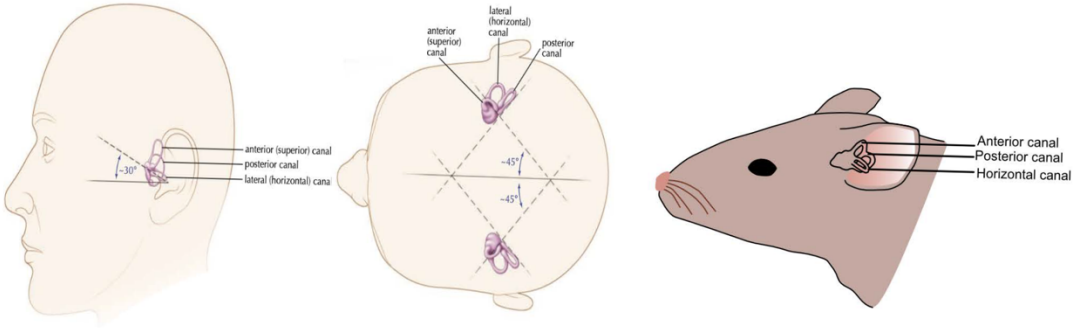

Figure 3: Spatial orientation of the three semi-circular canals in humans (From Parnes et al., 2003) and in mice (adapted from Groves and Fekete, 2012). The semi-circular canals are able to encode movements in distinct and specific orientations.

Hair cells

The sensory epithelium in the vestibular system contains hair cells (HC), sensory mechanoreceptors formed like a rod. In each mouse labyrinth, around 10 000 hair cells are equally divided between the semi-circular canals and the otolithic organs (Desai et al., 2005a). Every hair cell bundle on its apical end is composed of a single kinocilium and dozens of specialized microvilli called stereocilia organised in a row-like manner from the tallest next to the kinocilium to the shortest (Eatock, 2000). Adjacent stereocilia are connected through tip links binding the tip of the shorter one to the body of the adjoined taller stereocilia. Head motions induce a tilt of the stereocilia toward the kinocilium, resulting in a shift in the tip links that triggers open the K+ channels. The increase of K+ concentration inside the hair cells depolarizes it, leading to an influx of calcium and the release of neurotransmitters into the synapse of vestibular afferent nerve fibres. On the other hand, when the stereocilia separate from the kinocilium, the

tension in the tip links decreases, leading to a closure of the K+ channels thus leading to a decrease in activation of the vestibular fibres (Lim et al., 2011). On their basal end, hair cells have a synaptic pole from which their information will be transmitted to a vestibular afferent (reviewed in Rabbitt, 2019), and can be modulated through efferent fibres see **Figure 4**.

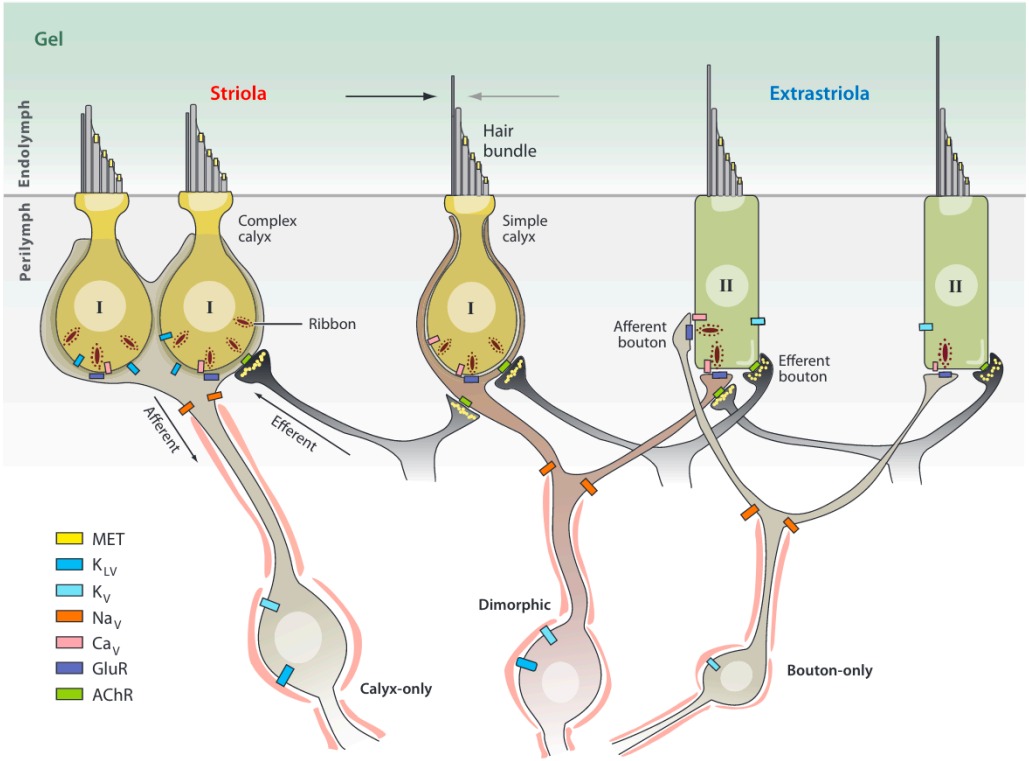

Figure 4: Hair cells type I and type II and their respective afferent fibres. Type I HC are found mainly in the central zones of the vestibular organs, and type II HC in the peripheral zones. Hair cells are innervated by three different kinds of primary afferents that contact either the calyx-shaped terminals of type I HC (calyx-only), bouton terminals of type II HC (bouton-only) or both calyx and bouton terminals (dimorphic)(From Eatock and Songer, 2011).

Hair cells have been classified into two types, I and II, that are segregated by their distribution, shape and innervation properties. Type I HC are mostly located in the central zones of the macula and cristae while type II HC are found at the periphery of the macula and cristae, but also in the auditory system (Fernandez et al 1988). Type I HC have a rounder base, flask-shaped, and their end terminal is completely enveloped

by the calyx end of their single afferent fibre while type II have a bouton synaptic linked to several afferent nerve fibres (Eactock and Singer, 2011). A vestibular afferent will contact the synaptic end of the hair cells (**Figure 4**, see the following section "Vestibular afferents") and its signal will be transmitted to the central vestibular nuclei or to the vestibular-related cerebellum. Recent studies have confirmed that type I HC have faster transmission than type II with higher variability of resting discharge (Contini et al., 2022) and that these non-quantal release dynamics would have a role in type I high-frequency sensitivity (Spaiardi et al., 2022). These results are in line with the theory that type I appeared in evolution after type II as their fast dynamics would be necessary for the high-velocity stimulation of land life (Eatock, 2018).

Modulation of Hair cells by the Vestibular Efferent System

Vestibular periphery inputs can be modulated by efferent fibres (**Figure 5**) that originate, in the mammalian vestibular efferent system, from the e-group (or efferent vestibular nucleus) in the central vestibular nuclei and that connect with type I HC through their calyx-shaped junction with their afferent or directly for type II HC (Goldberg, 2000; Raghu et al., 2019). One of the hypotheses about the vestibular efferent systems' roles is as a way to discriminate between active and passive motions, supported by several studies on fish or Xenopus. During locomotion, the efferent system would act to decrease vestibular sensitivity in the peripheral vestibular organs (Chagnaud et al., 2015). However, in monkeys, the peripheral vestibular inputs do not seem to be modulated during active locomotion (Mackrous et al., 2022). The vestibular efferent system could have a different role in mammals than it has in other species where it down-modulates vestibular inputs during active motions, and as of yet the role in mammals has remained undescribed. Nonetheless, in mice, the vestibular efferent has been shown to play a role in the VOR compensation after a unilateral vestibular lesion (Hübner et al., 2017) and to preferentially modulate the discharge firing rate of irregular afferents (Raghu et al, 2019).

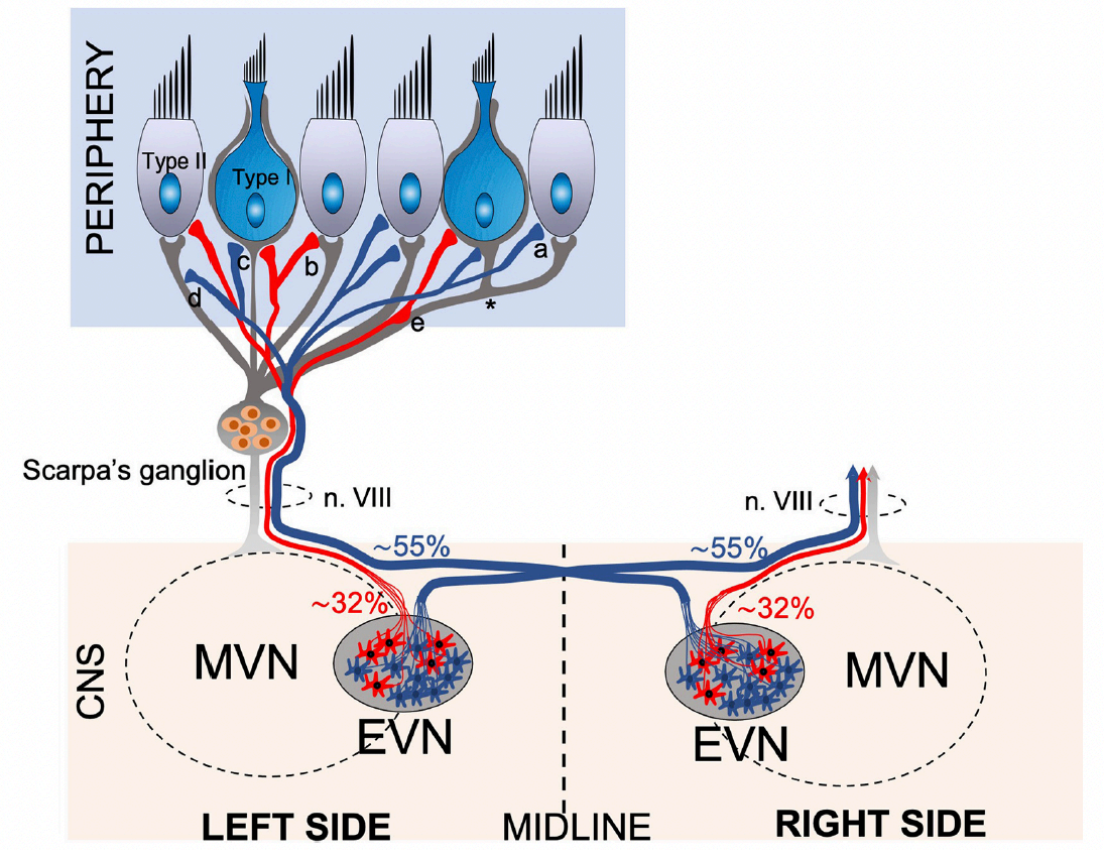

Figure 5: Anatomical projections of the Efferent Vestibular Systems. The efferent fibers (blue and red) cell bodies are located in the EVN in the brainstem and project through the VIIIth nerve to modulate directly Type II hair cells (a), indirectly type I by their calyx terminals (c) or the afferent fibres (b, d, e). In the mice, around 55% of EVN neurons target the contralateral vestibular peripheral system, and 32% the ipsilateral one (Lorincz et al., 2022).

Vestibular afferents

Vestibular afferents, as stated above, connect with the hair cells and transmit their information to the vestibular nuclei in the brainstem. Goldberg and colleagues have shown that all vestibular afferents have a comparable mean discharge rate (100 spikes/s in monkeys, 40 to 50 spikes/s in mice (Lasker et al., 2008)) but with different discharge regularity (the timing between their spikes) and proposed to discriminate two groups: regular and irregular fibres, see **Figure 6** (Goldberg, 2000).

This classification between two primary types of afferents also correlates with their distribution and diameter. Hence, the vestibular afferents' physiology varies with the zone they originate from: peripheral zones of the cristae and the extrastriolar zones of the macula information are preferentially innervated by the regular afferents, while the central and striolar zone are preferentially innervated by irregular afferents (Baird et al., 1988). The number of afferents is therefore linked to the size of the zone, and as such, there are more regular firing afferents than irregular ones. Their distribution would imply that the central fibres, or irregular afferents, receive information from the type I HC ("calyx only") whereas the type II HC would be connected with regular afferents ("bouton only"). However, some afferents also receive inputs from both types of HC and are called ("dimorphic") and those afferents are situated in both the central and peripheric zone (Eatock and Songer, 2011). The size of the regular and irregular fibres differs as well: irregular afferents tend to be larger than their regular counterparts (Goldberg et al, 2000).

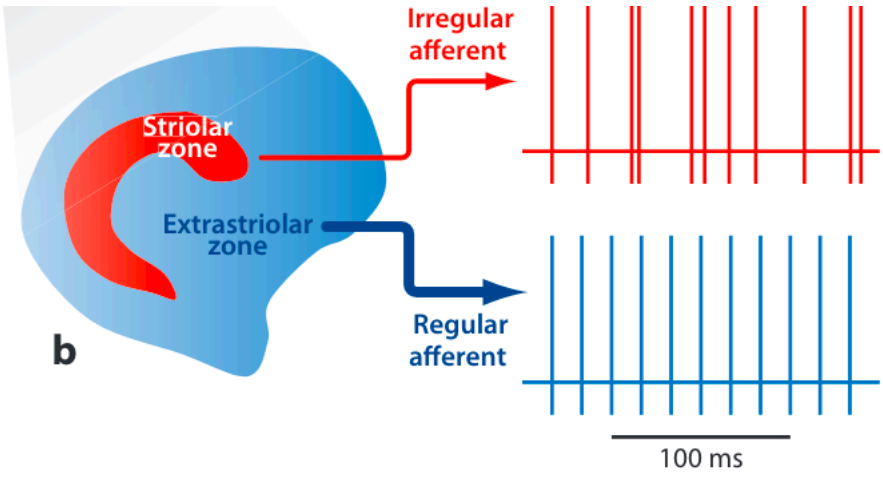

Figure 6: Example of the dynamic of irregular (red) and regular (blue) afferents originating respectively from the striolar and extrastriolar parts of the utricule (From Eatock & Songer, 2011).

The segregation of vestibular afferent fibres into functional subgroups represents the functional need to encode an ensemble of movement (passive, active) of different velocities to cover the natural range of head movements; afferents with varying properties are therefore considered to allow for the precise and accurate encoding of

different parameters of head movements. Both afferents firing discharges have been described in monkey studies and for frequencies obtained in a laboratory set-up, and as such under-sampled, to respond linearly to increasing vestibular stimulation. However, regular and irregular afferents have different sensitivities to selective frequency ranges (see **Table 1**).

Regular afferents can encode, through their firing rates, detailed timing of the stimulation that will be integrated into their target neurons (Jamali et al., 2016). The regular afferents encode generally more signals about head motion than the irregular afferents, as they respond to a wider range of motions, and possess a better detection threshold. They also exhibit a tonic response pattern. On the other hand, the irregular afferents encode high-frequency head movements with a higher gain with a greater phase lead and a phasic-tonic discharge dynamic (reviewed in Cullen, 2019). Contrary to the regular afferents, they can discriminate between diverse stimulations through patterns of precise spike timing (Jamali et al., 2016).

	Irregular afferent	Regular afferent
Traditional type of hair cell	Type I HC	Type II HC
Shapes of their afferent terminals	Calyx	Bouton
Properties of afferent	-High variability of discharge -Greater sensitivity -Phase lead	-Low variability of discharge -Lower detection threshold
Dynamics of afferents	Phasic-tonic	Tonic
Type of vestibular information	Vestibular stimuli of higher frequencies	-More information than irregular afferent -Detailed timing motions

Table 1: Properties of the two distinct afferents making up the two-channel pathways coding vestibular information from the peripheral system to the central nuclei.

In a nutshell, vestibular information is first encoded by two distinct types of hair cells in the five vestibular organs and transmitted to the central pathway through also distinct primary afferents. Those afferents code different ranges of motions and frequencies into two parallel channels that are still apparent in the central vestibular coding (Beraneck and Straka, 2011).

ii· CENTRAL NUCLEI

The vestibular inputs from the peripheral apparatus reach the central vestibular system through the vestibular ganglion and vestibular cochlear nerve. Through these structures, which will be first described, the peripheral information will be used to code different pathways through distinct populations of neurons.

The vestibular ganglion also called Scarpa's ganglion is located in the lateral portion of the auditory meatus. It receives inputs from afferent fibres of the sensory epithelium and is separated into two divisions, superior and inferior, that are connected by the isthmus (Sato et al., 1992). The superior part of the ganglion receives inputs from the utricule, anterior and horizontal canals and the inferior part receives information from the saccule and posterior canal (Hain and Helminski, 2007). The axons of both divisions of the ganglion merge to form the vestibular nerve, which combines with the cochlear nerve to form the vestibulocochlear nerve, the VIIIth cranial nerve. It will then separate after entering the brainstem at the pontomedullary junction. The majority of the fibres go to the ipsilateral vestibular nuclei or join the flocullo-nodular lobe or adjacent vermian cortex of the cerebellum (Highstein and Holstein, 2006).

Anatomy of the central vestibular pathway

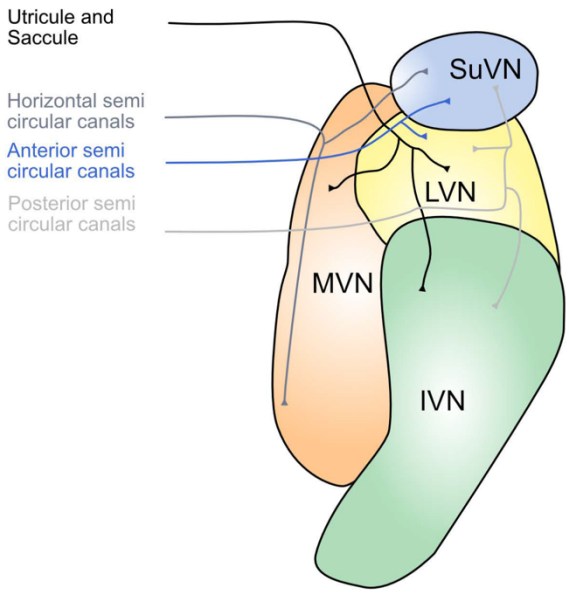

Figure 7: Central vestibular nuclei with and the projections from the peripheral vestibular organs. (MVN: medial vestibular nucleus; LVN: lateral vestibular nucleus; IVN: inferior vestibular nucleus; SuVN: superior vestibular nucleus) (Adapted from Wijesinghe et al., 2015)

The vestibular nuclei are formed by a complex of four nuclei located in the dorsal part of the brainstem, under the 4th ventricle. Similar to Scarpa's ganglion, the division is primarily anatomical but also represents to a certain extent a functional partition, see **Figure 7** (Highstein & Holstein, 2006).

- The medial vestibular nucleus, historically called Schwalbe is topographically divided. It receives inputs from the horizontal semi-circular canals and the flocculus lobe in its magnocellular area. It also receives information in its caudal part from the otoliths. It is the nucleus involved in the horizontal vestibulo-ocular reflex, as axonal fibres climb from the medial vestibular nucleus to the motor nuclei of the extraocular muscles involved in the horizontal eye movements. It is also involved in the vestibular spinal reflex.

- The superior vestibular nucleus (also called Bechterew) receives inputs from three semi-circular canals and as such is also involved in the vertical response of the VOR.

- The lateral vestibular nucleus, or Deiter, receives information from the macula and the crista ampullaris from the posterior and anterior canals) and also from the cerebellum. It is also involved in the vestibular spinal reflex.

- The last vestibular nucleus, the inferior or descending, receives inputs from the utricule, saccule and posterior semi-circular canal. It projects to the other three nuclei and the cerebellum and is also involved in the vestibular spinal reflex.

Small groups of cells, whose roles are mostly still unknown, complete the vestibular nucleus complex, such as the y-group that in its ventral division receives direct saccule inputs (Gacek, 1969) and that projects to the oculomotor nuclei through its dorsal part (Highstein & Holstein 2006). Another small group of neurons is the e-group which contains the cell bodies of the efferent fibres that contact and modulate the hair cells and their afferents.

The bilateral vestibular nuclei are connected through the vestibular commissural pathway to regulate the firing rate of each vestibular nuclei to create a discharge balance between them. This pathway is mainly inhibitory through GABA and glycinergic projections (Barmack, 2003; Malinvaud et al., 2010).

Dynamics of central vestibular nuclei neurons

The vestibular afferents convey information from specific hair cells to the central vestibular nuclei where information will be shared to ensure a multisensory integration of the signals. To do so, several afferents of different vestibular endorgans converge on one vestibular neuron. For example, in monkeys, rotation (canal-related) and translation (otolithic-related) movements modulate is encoded in 50% of the central vestibular neurons (Dickman and Angelaki, 2002). In frogs as well, there is a spatial convergence of primary afferents from different organs with almost 50% of the second-order vestibular neurons receiving otolithic and canalar inputs (Straka et al., 2002). Movements on different planes are also closely integrated as signals coming from at least two semi-circular canals converge on a single central neuron (Carriot et al., 2015).

Vestibular information is interpreted in the central vestibular nuclei through two parallel channels to represent self-motion by encoding different ranges of motion, similar to the pathways found in the primary afferents. This separation is common for most vertebrates, however, neuron properties such as resting discharge and dynamics differ between species. Thus, the designation of central neurons is mostly conventional. Vestibular information in the vestibular neurons is encoded for low frequencies with a phasic dynamic and high frequencies with a tonic dynamic (Beraneck and Straka, 2011). *In vitro* recordings of medial vestibular neurons have revealed that neurons can be parted by their intrinsic membrane properties in 2 main neuronal subtypes: tonic and phasic neurons that in the frog act respectively as low pass and bandpass filters (Straka et al., 2005; Beraneck and Straka, 2011). This separation according to the frequency-selective firing pattern and membrane properties is similarly found in rodents, in the form of type A and B neurons. Type A neuron has a single and large after hyperpolarization while type B is described with a small and biphasic after hyperpolarization, as represented in **Figure 8** (Beraneck and Idoux, 2012). Their neurotransmitter content is partially shared as both types are GABAergic neurons, only fractionally for type B (Eugène et al., 2011). In the mice specifically, as in the frog, both

types are not distributed equally in the medial vestibular nuclei: 75 to 80% of the neurons are type B, and 20-25% are type A (Dutia and Johnston, 1998; Straka et al., 2002).

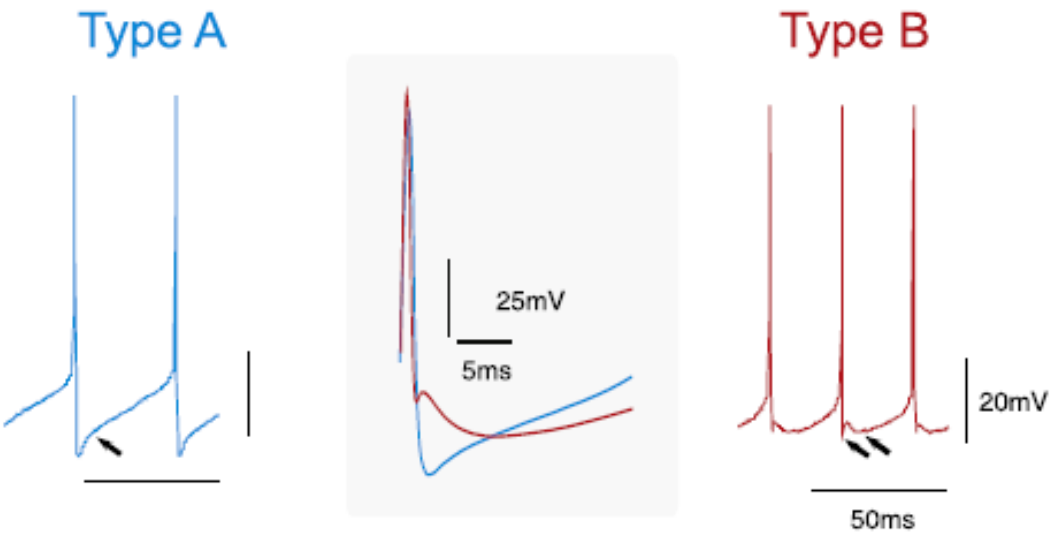

Figure 8: Action potentials of Medial Vestibular Nucleus neurons of type A (blue trace), and type B (red trace). Type A demonstrates a monophasic AHP (single arrow & framed box) and type B a biphasic with an early fast component (double arrow & gray box) and a late slower component (gray box & double red arrow). (From Beraneck and Lambert, 2020, modified from Beraneck et al., 2004).

Diverse populations of neurons in the central vestibular nuclei

Vestibular information coming from the otoliths and the semi-circular canals is not the only one being integrated into the vestibular nuclei. Inputs coming from other areas of the brainstem or cerebellum (flocculus "See "Optokinetic Pathway" chapter) converge in the vestibular nuclei. And in return, vestibular neurons project to different cortical and sub-cortical areas with different sensitivities and coding. Several *in vivo* studies on head-fixed animals (monkeys and mice) have highlighted the diverse neuronal population in the vestibular nuclei, noticeably neurons sensitive to head motion and eye position such as position-vestibular-pause (PVP) neurons, vestibular-only (VO) neurons and eye-head (EH or FTN) neurons (Beraneck and Cullen, 2007, **Figure 9**). PVP neurons are stimulated by modified eye position and vestibular stimulation and their firing discharge pause during saccades. As such, PVP neurons are

the cells that innervate the extra-ocular muscles (EOMs) and are involved in the vestibulo-ocular reflex and the optokinetic. In the case of active gaze direction, the VOR is canceled through modulation of the PVP neurons by the Floccular-target neurons (FTN) (Cullen and Roy, 2004). Those neurons are also involved in the adaptation of the VOR (see "Adaptation of Gaze stabilization"). Vestibular-only (VO) neurons do not encode eye movement or position but passive head motion (Cullen, 2012). Their signal is integrated into other vestibular functions such as posture with the vestibulo-spinal reflex (Gdowski and McCrea, 1999) and self-motion perception notably through the thalamus (Wijesinghe et al, 2015). In mice, 2/3 of the neurons in the vestibular nuclei correspond to VO neurons (Beraneck and Cullen, 2007).

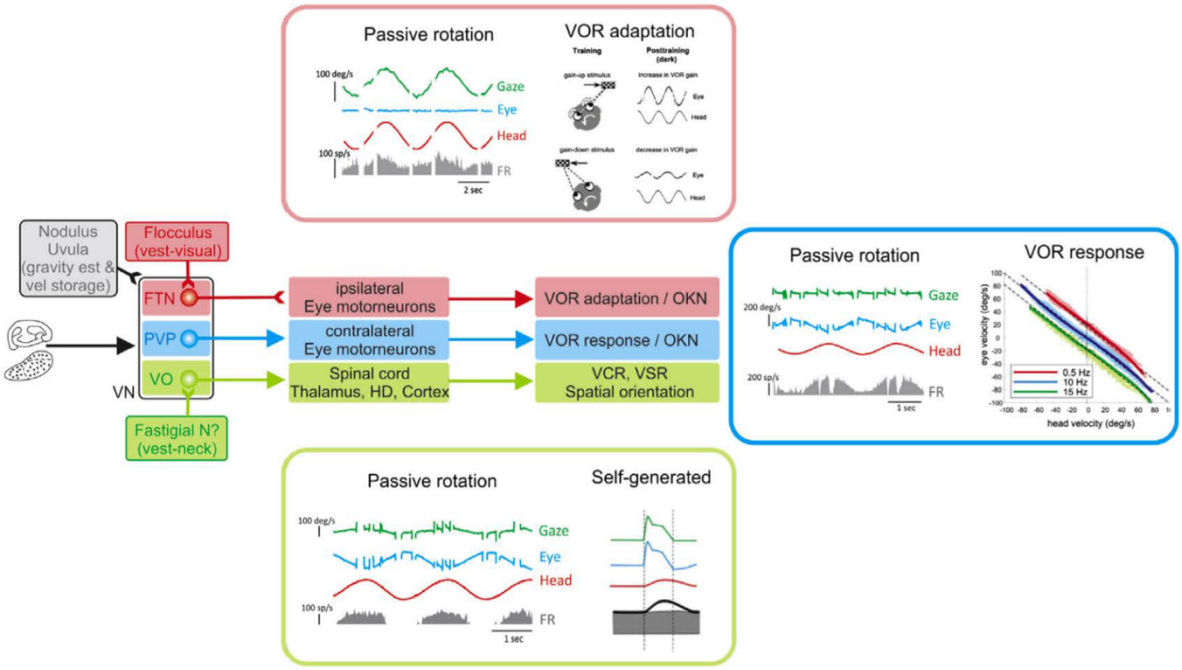

Figure 9: Distinct populations of vestibular neurons and their task-specific pathway. The otolithic and canalar inputs are integrated into the coding of the central neurons that can be divided into three groups of cells. Floccular target neurons (FTN, in red) are part of the VOR cancellation and adaptation pathway and encode both head and eye velocity. Position-vestibular-pause neurons (PVP, in blue) are involved in the VOR pathway and can code head and eye velocity as well. Vestibular-only (VO, in green) neurons are essential for the vestibulo-spinal reflex and higher cortical or sub-cortical function. They code head velocity and can differentiate between passive and active rotation.

(VOR: vestibulo-ocular reflex; HD: head direction, OKN: optokinetic response, VCR: vestibulo-colic reflex, VSR: vestibulo spinal reflex)(From Sadeghi and Beraneck, 2020).

Higher vestibular functions

Vestibular inputs project into several cortical and subcortical areas which are integrative and multisensory (see **Figure 10**). Beyond the gaze stabilization function of the vestibular information (addressed in the chapter "Physiology of the VOR"), a composite signal made of vestibular and other sensory and non-sensory signals is used for posture and orientation as well as computed into higher cortical structures.

Posture stability is maintained due to the vestibulo-spinal reflex that inputs vestibular signals with the "anti-gravity" group of muscles (green box, **Figure 9)**. Those muscles are the neck, trunk and extremities extensor. The vestibular inputs are either directly (lateral and medial vestibulo-spinal tracts) or indirectly (reticulo-spinal tract), through the respective vestibular nuclei, used to stabilize the body. The lateral and medial vestibulo-spinal tracts act on the cervical muscles to stabilize the head, and the reticulo-spinal tract acts on the limb extensor muscles for the posture (Manzoni, 2009).

Visual and auditory signals are processed in specialized cortical areas but this is not the case for vestibular inputs. Instead, vestibular information is relayed to multiple cortical areas by the thalamus (Lopez and Blanke, 2011). The thalamus is a multisensory integrator structure that receives diverse sensory information coming from other brain regions and senses. As reviewed in Wijesinghe et al, 2015, vestibular inputs are conveyed to several subnuclei of the thalamus, the principal ones being the ventro-basal, ventra-lateral, intralaminar nuclei and the geniculate bodies. In the thalamus, vestibular inputs are also integrated into the orientation pathway by the head direction (HD) circuit in the antero-dorsal thalamic nuclei (ADN). HD cells are able to encode a head's preferred direction on a yaw plane to better orientate the animal in its environment (Taube, 2007). Though HD cells are recorded in other cortical and sub-cortical regions, vestibular inputs are necessary for HD cells' stability (Stackman et al., 2002). The vestibular

information is translated into a multisensory signal in the ADN with landmark encoding coming through the retrosplenial cortex and is further used down in the navigation circuit (Yoder and Taube, 2014).

The extent of the reach of vestibular inputs in multisensory integration was further proven by the brain-wide imagery approach in rodents to correlate the activation of the vestibular system to other pathways. Aside from the vestibulo-oculomotor reflex (see "Physiology of the Gaze Stabilization) and vestibulo-cerebellar pathways (that play a role in the adaptation of VOR, see red box Figure 9), vestibular inputs are integrated with auditory and motion cues to improve self-motion (Rancz et al., 2015). Vestibular information is also used in cognition, through several pathways involving either the thalamus or the hippocampal formation or both of these structures, see **Figure 10** (Leong et al., 2019). Moreover, the vestibular contribution in some cognition pathways might depend on the species as the vestibulo-cortical network in primates and humans is quite dense and robust, although it differs between species (Raiser et al., 2020).

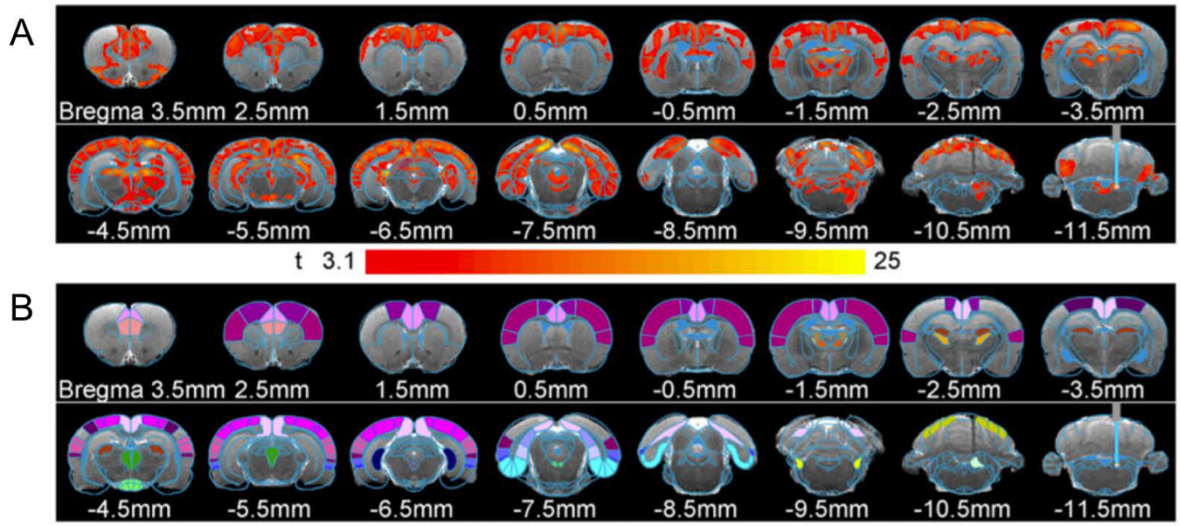

Figure 10: Vestibular-related areas A) Average BOLD (blood-oxygen level dependent) activation maps during optogenetic stimulation of the MVN in the mice (seen in -11.5mm). The regions appearing in red are activated after the stimulation and the coordinates refer to the position from the bregma on the antero-dorsal plane. B) Paxinos atlas with the regions of interest activated after the stimulation: cortical (purple), thalamus (orange/brown), midbrain (green) and the hippocampal formation (blue). (From Leong et al, 2019)

To conclude, the vestibular nuclei receive diverse information originating from the vestibular endorgans to encode motion in multiple planes but also in response to different ranges of stimulation, in two-channel pathways. This separation is found similarly in most vertebrates even though species differences must be taken into account. Vestibular information is already integrated with non-vestibular input in the vestibular nuclei and is integrated further in cortical and sub-cortical areas. The pathway comprising the medial vestibular nucleus and the specific neuronal population of the PVP (or eye-sensitive neurons in rodents) is particularly at the forefront of this thesis work as it is heavily involved in the gaze stabilizing reflexes.

II· ANATOMY AND PHYSIOLOGY OF THE OPTOKINETIC SYSTEM

The optokinetic reflex is the compensatory eye movement of the eye in response to a moving visual field. If the field is moving in one direction, the eye will execute a slow movement in the same direction to compensate for the motion and fast movements to recenter the eye. The combination of the slow and fast phases is called optokinetic nystagmus (OKN) (Büttner and Büttner-Ennever, 2006). To have a mechanical response of the eye, achieved by the extraocular muscles surrounding the globe, the movement of the visual field has to be perceived by the retina. The visual signal is then transferred to a central pathway through retinofugal projections to oculomotor structures (Summers and Feller, 2022). After an overview of the anatomical pathway of the optokinetic reflex, the characteristics of this reflex will be addressed.

Direction-selective ganglion cells of the retina

Velocity is visually perceived by a specific type of retinal ganglion cells found directly in the retina for lateral-eyed animals (Barlow et al., 1964). Such cells, representing around 35% of the ganglion cells in mice are described as direction-selective (direction-selective ganglion cells, DSGC) and can be divided into several

subtypes depending on their receptive field properties. (Bos et al., 2016). Through all DSGC emit strong spiking discharge when the visual stimulus is moving toward a preferred direction and a null response when moving in the opposite direction, ON DSGC respond preferably for low-velocity movements in the anterior, inferior and superior vestibular planes (Oyster and Barlow, 1967). In mice, the preference of the ON DSGC for low velocities (3°/s) is due in part to a high-velocity selective inhibition (Dhande et al., 2013; Summers and Feller, 2022). ON DSGC project to the Accessory Optic System (AOS) and mediates the optokinetic compensatory eye movements by encoding slow motions (Simpson, 1984).

Optokinetic reflex pathway

The axons of the retinal ganglion cells form the optic nerve that is partially decussated once it reaches the optic chiasma and then projects to different visual-related areas, like the lateral geniculate nucleus. The ON DSGC drive the OKR by sending their axons to the contralateral AOS and they innervate several other nuclei: the nucleus of the optic tract (NOT) but also the dorsal, lateral et medial terminal nuclei (DTN, LTN, MTN), see **Figure 9** (Oyster et al., 1972). Because of the ON-DSGC properties to encode direction in several planes, the nucleus targeted by those neurons receives a direction-selective signal: NOT and DTN perceive information about the temporo-nasal direction while the LTN and MTN receive signals about the vertical plane motions (Simpson, 1984).

From the AOS, visual inputs will be forwarded through the inferior olive. NOT and DTN project to the ipsilateral Dorsal cap of Kooy, one subnucleus of the inferior olive that modulates optokinetic information and that projects in turn to the contralateral flocculus and nodulus (Sugihara, 2004). The DC is subdivided into three nuclei that encode different planes of stimulation, similar to the three semi-circular canals that can code 3D directions. (Simpson, 1984).

Inputs from the DNT and NOT can also reach the ipsilateral nucleus prepositus hypoglossi (NPH) that can project directly to the extra-oculomotor nuclei and specifically to the motoneurons of the lateral and medial rectus (Graf et al., 2002). The NPH is a central part of the pathway whose aim is to stabilize the gaze in the horizontal plane as a neural integrator of vestibular and visual signals (Mehlman et al., 2021). Indeed, its inactivation in monkeys leads to the inability to maintain gaze stabilization (Arnold et al., 1999).

Inferior olive inputs are conveyed to the flocculi, a subsection of the cerebellum, and the vestibular nuclei to finally activate the extraocular muscles that will be contracted or inhibited to allow eye movements (Kodama and du Lac, 2016).

For example, let's take a horizontal visual movement toward the right that will stimulate the right eye with an NT direction and the left eye with a TN direction (see **Figure 11**). The left retina and its DSGC will be recruited and the right hemisphere DNT and NOT will be activated. Their signal will be conveyed to several structures including the nucleus reticularis tegmenti pontis (NRTP), Inferior Olive and the flocculus that will project to the medial vestibular nucleus. The right eye stimulation will lead to an activation of the NPH through the NOT and DTN (Yokota et al., 1992). The NPH and MVN are able to induce compensatory eye movements by activating the right lateral rectus and inhibiting the left one (Kodama and du Lac, 2016).

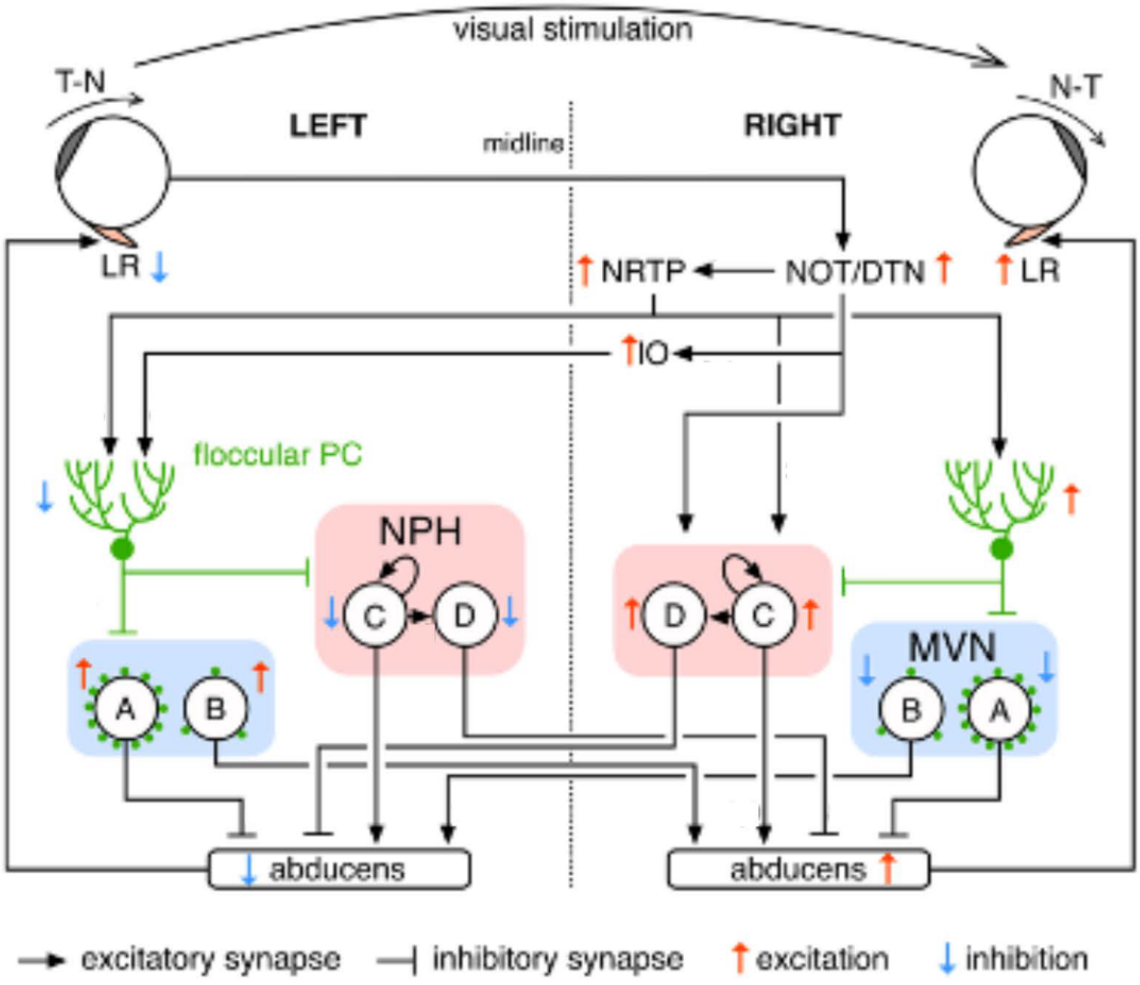

Figure 11: OKR pathway from a visual stimulation effect on the retina to the response of the lateral rectus muscle. The visual inputs are transmitted to the oculomotor nucleus either through the NOT/DTN and NPH, or through the IO, the cerebellum and the medial vestibular nucleus. However, the MVN is reciprocally connected to the NPH. (T-N: temporo-nasal; N-T: naso-temporal; NOT/DTN: nucleus of the optic tract/dorsal terminal nuclei; NRTP: nucleus reticularis tegmenti pontis; IO: inferior olive; NPH: nucleus prepositus hypoglossi; MVN: medial vestibular nucleus; PC: Purkinje cell; LR: lateral recti). (From Kodama & du Lac, 2016).

Optokinetic reflex's characteristics

The OKR responses to slow motions of the visual field can be described as asymmetric. Temporo-nasal (T-N) motion elicits a higher OKR response than the other directions, especially naso-temporal (N-T) (Büttner & Büttner-Ennever, 2006), leading to an asymmetry of the optokinetic response during monocular stimulation. This T-N higher response, and not the other directions, is reliant on the flocculus (Kodama & du Lac, 2016). This asymmetry of response is mainly found in non-foveate, lateral-eyed animals and it might be involved in the suppression of the optokinetic reflex when the animal is moving forward, as a forward movement will elicit a naso-temporal retinal flow (Fritsches and Marshall, 2002).

The compensatory slow phase of the OKR response can be divided into two components: 1) the direct component or ocular-following response occurring immediately after the visual stimulation that is linked to eye pursuit and includes a fast increase of the eye velocity (Inoue et al., 1998) 2) the indirect component of the response, that is demonstrated by the optokinetic after-nystagmus (OKAN) and linked to the eye velocity storage (see "Velocity Storage" in Physiology of Gaze Stabilization) (Büttner & Büttner-Ennever, 2006). Non-foveate animals cannot perform smooth pursuit eye movements and so their OKR consist only of the indirect components. In the mouse noticeably, the OKAN induced by turning off the lights was weakly observed (van Alphen et al., 2001). The mice might depend only on the indirect pathway involving a leaky velocity storage, but their OKR acts, if not in gain, similarly to in humans (Kodama & Du Lac, 2016).

The ON DSGC preference for slow velocities complements the vestibular endorgans' own preference for high-velocity stimulation driven by the proprieties of the semi-circular canals (Angelaki and Cullen, 2008). However, it has been proven that OKR gain can adapt to higher frequencies and velocities (Nagao, 1983) with a higher gain. The OKR-related cerebellum is required for any OKR adaptation and as such, any adaptation toward high frequencies must take place in the flocculus (Kodama and du Lac, 2016).

The OKR performance obtained at velocities above the tuning point of the ON-DSGC might also be the result of another subtype of ganglion cells, the ON-OFF direction-selective cells that code for a larger range of velocities (Weng et al., 2005). While most of the ON-OFF cells project to non-optokinetic related structures such as the lateral geniculate nucleus, some also project to the DTN (Dhande et al, 2013).

III· OCULOMOTOR PATHWAY

The end goal of the oculomotor reflexes is to stabilize the image on the retina, with eye movements in response to vestibular and visual stimulation (Cullen and Roy, 2004; Hoy et al., 2016a). While the compensatory reflexes are quite preserved in evolution, especially in mammals, there are significant differences in the position and visual acuity of the ocular structures. While humans and non-human primates have a front-eyed vision, animals like mice have laterally placed eyes. This placement relative to the skull allows for a greater visual angle but the eye convergence space is limited (40°, Hoy et al., 2016). Binocular vision is still of great importance as the mice hunt by keeping prey in their binocular vision areas with head movements (Michaiel et al., 2020; Johnson et al., 2021). Another difference between species is the presence or absence of a small region in the retina that allows the finest resolution of objects, the fovea, that is present in humans and primates (Walls, 1942). However, the mice are non-foveate animals and as such do not make movements to center a target on the fovea.

i· TYPES OF EYE MOVEMENTS

Several movements of the eyes have been described, as described in **Figure 12** (Büttner & Büttner-Ennever, 2006). While they differ in their mechanisms, the plurality of eye movements aims to improve our orientation relative to surrounding objects or individuals in the environment.

- *Smooth eye pursuit movements* (SPEMs) are voluntary movements used to track a moving target. As the gaze needs to focus on a target, SPEMs require a fovea and as such, mice being non-foveate animals are not able to perform SPEMs (Stahl, 2004).

- *Saccades* correspond to quick movements that will move the eye to a new position. They can be both voluntary or a physiological part of the oculomotor reflexes to recenter the eye.

- *Convergence* concerns mostly frontal-eyed animals; allows different depths of the visual field to be perceived by deconjugated eye movements.

- *Gaze holding* depends on a neural integrator to stabilize the eye position between two consecutive movements, and its failure leads to nystagmus.

- *Compensatory eye movements*, the centre of the works of this thesis, compensates for either head movements (vestibulo-related reflexes) or a moving visual field (optokinetic reflex). They consist of a slow phase of compensation and a quick phase to recenter the eye in the orbit.

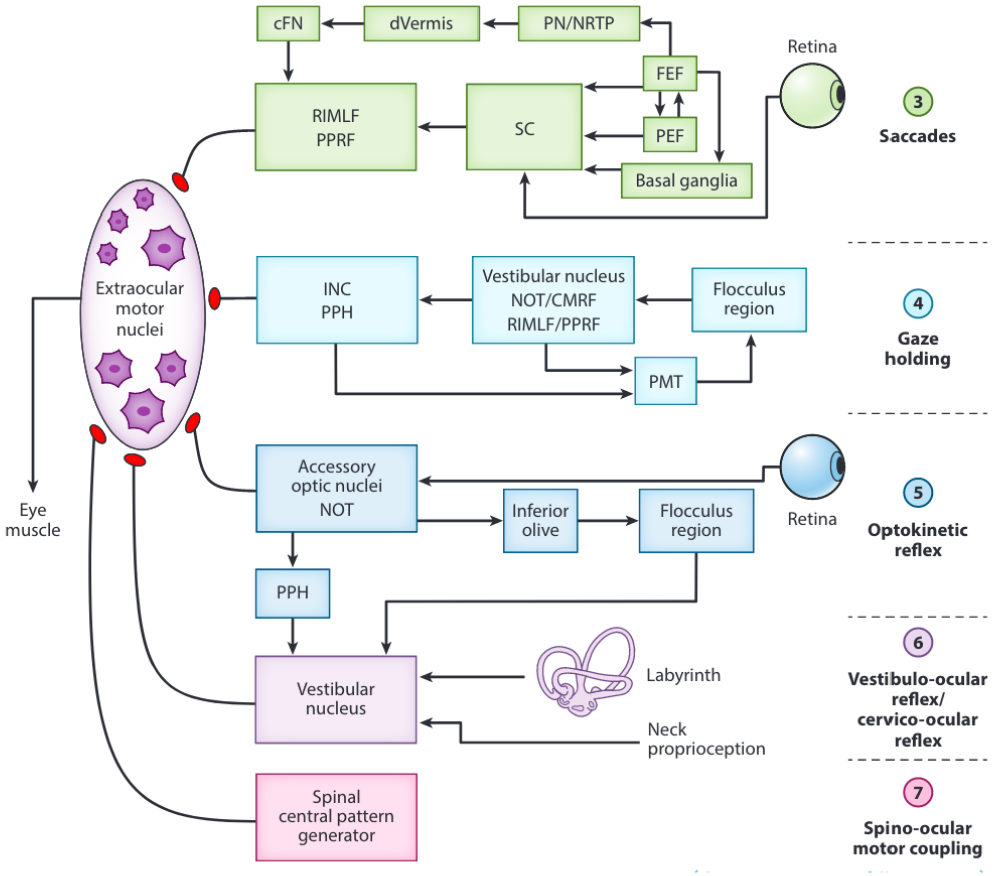

Figure 12: Type of eye movements possible in the mice: saccades, gaze holding, and gaze stabilizing reflexes (Optokinetic reflex, vestibulo-ocular reflex/cervico-ocular reflex and spino-ocular motor coupling). Their pathways converge on the extraocular motor nuclei to induce eye movement. (FEF: frontal eye field; PEF: parietal eye field; PN: pontine nucleus; NRTP: nucleus reticularis tegmenti ponti; cFN: caudal fastigial nucleus; SC: superior colliculus; RIMLF: rostral interstitial nucleus of the medial longitudinal fascicle; PPRF: paramedian pontine reticular formation; PMT: paramedian tract neuron; INC: intersticial nucleus of Cajal; PPH: nucleus prepositus hypoglossi). (Modified from Horn and Straka, 2021).

ii· EXTRA OCULAR MUSCLES (EOMs)

The different types of eye movements are controlled through the different neural pathways, but they converge on motoneurons that will activate the extra-ocular muscles (EOMs).

There are 6 extra-ocular muscles responsible for voluntary and involuntary eye movements in mammals and are highly conserved through evolution and present in a lot of species. They are able to produce the different classes of eye movements explained in the previous chapter (smooth eye pursuit, saccades, convergence, compensatory eye movement and gaze holding) (Spencer and Porter, 2006). In mammals, the seven extra-ocular muscles are quite constant in their location and innervation pattern, but there is some difference between lateral-eyed and front-eyed animals. As the principal model of this thesis are mice, the EOMs description will be centered on the mice.

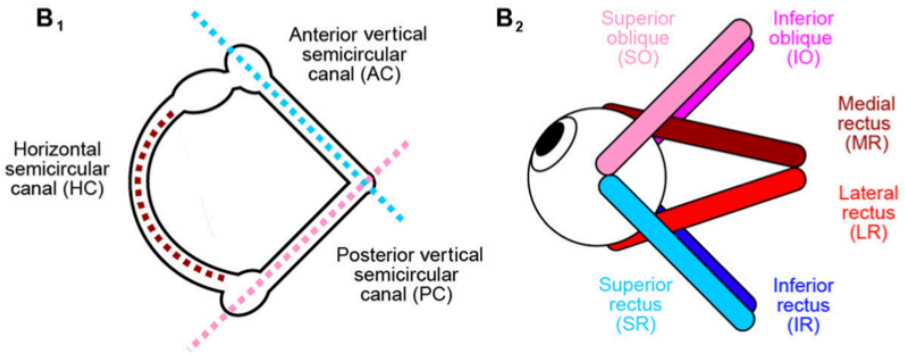

Figure 13: Extra-ocular muscles. A) planar organization of the semi-circular canals, orientated perpendicularly to each other B) Planar organization of the EOMs. Their respective orientations allow for a large range of movements in several planes, limited only by the tendons.(From Branoner et al., 2016).

The EOMS are innerved by motoneurons that originate from 3 different nuclei: oculomotor (3^{rd} nerve), trochlear (4^{th} nerve) and abducens (6^{th} nerve) (Büttner and Büttner-Ennever, 2006) all located in the brainstem.

Motoneurons innervating the EOMs can also be divided into two groups by the pattern of innervation of individual muscle fibres. Singly innervated muscle fibres (SIFs) consist of a fibre with a single neuromuscular junction situated at the centre of the muscle fibre. Multiply innervated muscle fibres (MIFs) are fibres that receive several neuromuscular junctions along the length of the muscle fibres and are smaller (Bohlen et al., 2019). Both groups have different characteristics as SIFs are fatigueable with an "all or none" activation while MIFs act with slow and gradual contractions, and thus are not as fatigueable (Spencer & Porter, 2006). MIFs represent in the rat 20% of the motoneurons (Eberhorn et al., 2006) and are specific of slow eye movements (Hernández et al., 2019).

The 6 EOMs can be divided into 4 recti muscles (lateral and medial forming the horizontal recti, and the superior and inferior forming the vertical recti) and 2 oblique muscles (see **Figure 13**). There are also two other muscles that control the eyelid.

- *Horizontal recti muscles:* the medial rectus muscle is located medially of the globe and the lateral rectus laterally. Both originate from the tendinous ring at the apex of the orbit and dura around the optic nerve. The medial rectus works antagonistically with the lateral rectus, as the adductor (medial) and abductor (lateral) control eye movements. As they are responsible for horizontal movements, the medial and lateral recti are involved in the horizontal response of the VOR (further described in the chapter "Physiology of gaze stabilization"). Movements are limited by the tendons of the muscles attached to the bones lining the orbit. The medial rectus is mainly innervated by the ipsilateral oculomotor nucleus while the lateral rectus is innervated by the ipsilateral abducens nucleus (Bohlen et al., 2019).

- *Vertical recti muscles:* The superior and inferior recti muscles originate, similarly to the horizontal recti, from the tendinous ring and are located respectively in the antero-superior and antero-inferior parts of the globe. The superior rectus muscle is innervated by the contralateral oculomotor nucleus (Bohlen et al., 2019). The ipsilateral oculomotor nucleus is responsible for innervating the inferior rectus muscle. Both muscles function to allow vertical eye movements, as they elevate and lower the eye.

Their close location to each other could be the reason for deconjugated vertical eye movements when the head of the mice is tilted to one side, one of the eyes going down and the other up (Bohlen et al., 2019).

- *Oblique muscles:* The two oblique muscles differ in their origin: the superior oblique muscle arises from the tendinous ring while the inferior oblique muscle stems from the medial wall of the orbit. They are inserted on the globe respectively at the superior and lateral (medially to the LR) part of the globe and are quite prominent in the mice (Bohlen et al., 2019). Their insertion allows them torsional movements; thus, maintaining the gaze stable while the animal is pacing in its environment. The superior oblique is innervated by the contralateral trochlear nucleus and the inferior oblique by the ipsilateral oculomotor nucleus.

The levator palpebrae superioris (LPS) is a mammal-specific EOMs that is inserted in the eyelid's nasal region, which permits the elevation. The LPS is innervated by the contralateral oculomotor nucleus. In some species like cats, rabbits or mice, another muscle controls the eyelid, the retractor bulbi (Bohlen et al., 2019).

To sum up, vestibular inputs originating from the vestibular endorgans and visual information from the DSGC cells on the retina are used in the gaze stabilization reflex pathways to induce compensatory eye movements in order to preserve a stable image on the retina. Both pathways have a specific encoding to maintain a proper compensatory movement for an extended range of motion possible. However, for gaze stabilization to be optimal both inputs need to be integrated and this question will be addressed in further chapters.

PHYSIOLOGY OF GAZE STABILIZATION

To maintain a functional visual acuity, the motion of the head or of the visual surrounding has to be compensated with eye movements. This compensation is made possible by the several reflexes acting synergistically to stabilize the gaze. Those reflexes integrate diverse information, from vestibular to visual and proprioceptive (Angelaki and Cullen, 2008). The physiology of the vestibulo-ocular reflex will be addressed in the first section, followed by an overview of the otolithic-dependent reflexes. The capacity of the system to handle visual-induced error signals would be discussed in the section about velocity storage.

I· ONTOLOGY OF THE VESTIBULO-OCULAR REFLEXES

Of the different reflexes working to facilitate an accurate visual perception, the vestibulo ocular reflexes (VOR) is a major player in gaze stabilization, its primary input being the vestibular information involved in both active and passive motions. VOR and OKR are two highly conserved reflexes among the vertebrate species (Straka and Dieringer, 2004). Vestibular endorgans (semi-circular canals and otoliths) and central structures during developmental stages are similar in several species such as zebrafish, Xenopus and mice (Mackowetzky et al., 2021). In rodents, both the peripheral (vestibular organs and afferents) and the central vestibular system are formed during gestation. The acquisition of a functional VOR and OKR is due to the maturation of the system through several mechanisms that begin i*n utero* and last for the first month of life (see **Figure 14**, Beraneck et al, 2014). This maturation is associated with new electrophysiological proprieties of central vestibular neurons and indeed low VOR gain in juvenile mice is correlated with the incomplete maturation of the membrane properties of the vestibular neurons (Eugène et al., 2007). Type A and type B neurons are predominantly described as mature between P15 to P30 (review in Straka et al., 2005; Beraneck et al., 2014) coinciding with the maturation and functionality of the gaze stabilizing reflexes.

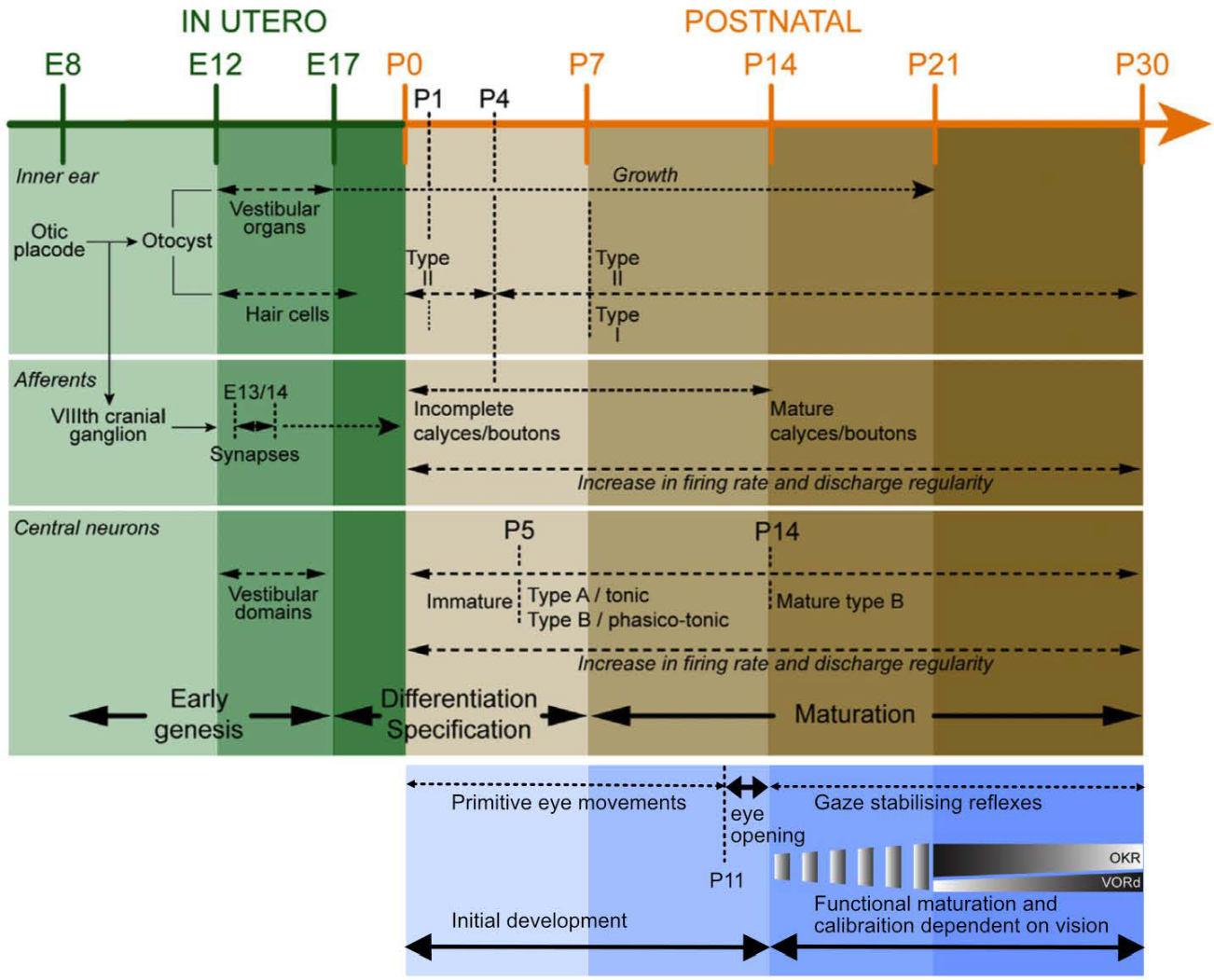

Figure 14: Formation (green) and maturation of the vestibular system (brown) and gaze stabilization reflexes (blue). The timeline presented here corresponds to days *in utero* and after birth (at Po). Early genesis mechanisms occur during gestation that lasts for mice around 20 days. The maturation of the vestibular system takes place during the first month (Modified from Beraneck et al., 2014).

The initial maturation of the gaze-stabilizing reflexes does not depend on visual inputs as mice open their eyes during their second week of life. The vestibular system appears to already be functional very early but it maturates further with the growth of the mice into their adult size (Beraneck et al., 2004). Since vision is instrumental in

properly calibrating gaze stabilizing reflexes, this event is accompanied by the final maturation of VOR and OKR, respectively. Hence, the opening of the eyes induces a quick maturation of the VOR as its gain is already quite high even at a juvenile age and reaches adult gain at P30 (Faulstich et al, 2004). OKR gain is, on the contrary, higher at an early age. However, this superior performance allows for an optimal response of the VOR in the light as the vestibular system is still immature at a juvenile age (Faulstich et al, 2004).

II· VESTIBULO OCULAR REFLEXES

As previously stated, the VOR maintains a stable image on the retina when the head is moving. The eyes will then compensate for the movement by turning in the opposite direction: if the head turns to the right, the VOR will induce an eye movement to the left. There are two components of this compensatory eye movement called vestibular nystagmus. For small and slow movements, the oculomotor system will be able to produce a compensatory movement called the slow phase. However, in the case of large amplitude motion, the eye will reach its physical limitation of movements; a quick phase will then recenter the eye to continue its compensatory movement. The VOR uses both canalar and otolithic inputs to respond to respectively angular and translational movements to compensate for head movements. The angular vestibulo ocular senses angular accelerations through the semi-circular canals and will be first addressed. The otolith-related reflexes will be then developed, as well as other vestibular-related reflexes.

i· ANGULAR VESTIBULO OCULAR REFLEX

First described by Lorente de No in 1933, the aVOR is one of the fastest reflexes, around 5 to 7ms in primates (Huterer and Cullen, 2002), produced by a short and direct pathway called the three neurons-arc. The first-order neurons are the afferent fibres that

connect the hair cells in the vestibular organs to the vestibular complex nuclei. The second-order neurons (premotor) are the vestibular nuclei neurons, finally, the ocular-motor neurons will send the motor command of the EOMs to induce the compensatory eye movement of the VOR.

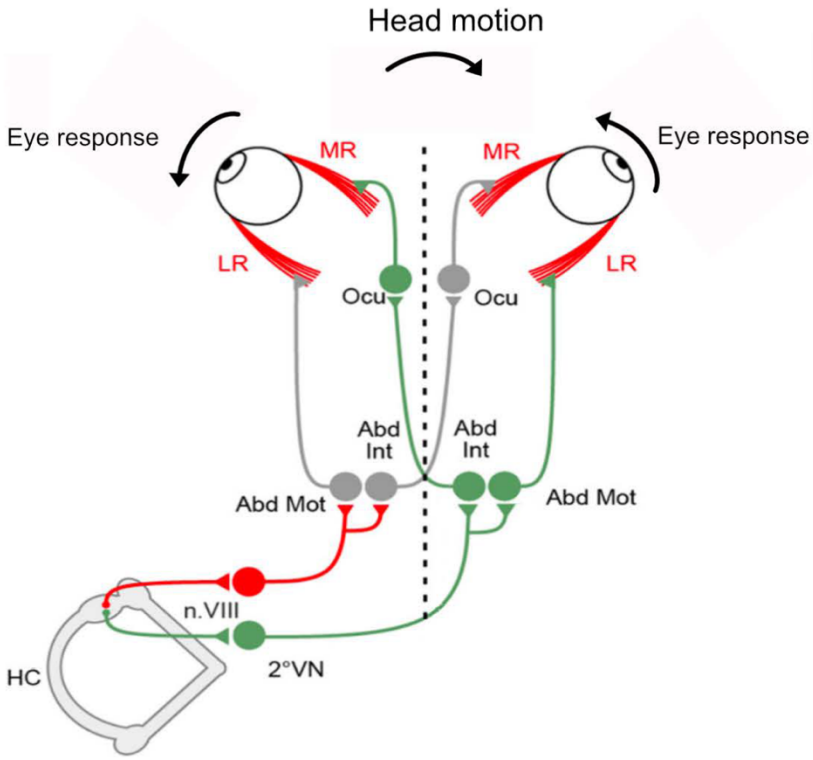

Figure 15: Horizontal angular vestibulo-ocular reflex pathway and the tree neurons arc pathway of the VOR. 1st order neuron: primary afferent connecting the HC to the vestibular nuclei; 2nd order neuron: vestibular nuclei; 3rd order neuron: ocular motor neuron originating for the hVOR from the abducens nucleus. (MR: medial recti, LR: lateral recti; Ocu: oculomotor nucleus; Abd Int: internuclear neurons; Abd Mot: abducens motoneurons; 2° VN: second-order vestibular neurons; HC: horizontal semi-circular canals, From Branoner et al., 2016).

We can, for example, consider a head motion in the horizontal plane in the right direction that will in finite leads to a horizontal eye compensatory movement in the left direction, as represented in **Figure 15**.

- The right horizontal semi-circular canal is then stimulated, which will lead to an increase in its afferents' firing rate (first order).

- That modulation will be translated from the VIIIth nerve into excitatory projections of the ipsilateral (right) vestibular nuclei neurons (2^{nd} order) to the contralateral (left) abducens nucleus (left).

- Through the excitatory drive of the motor abducens neurons, the lateral rectus will be contracted, while the internuclear neurons (in the medial longitudinal fasciculus) will convey excitatory signals to the right medial rectus by crossing the midline. The activation of the right medial rectus can also be induced by ipsilateral projections from the ascending tract of Dieters. This pull and push action of both muscles (contralateral LR and ipsilateral MR) will lead to a compensatory left eye movement.

- At the same time, the antagonist horizontal eye muscles (ipsilateral LR and contralateral MR) will be inhibited in order to suppress any eye movement toward the right. This inhibition is the result of the semi-circular canal hair cells' orientation: as they bend opposite to the movement they will be inhibited and their resting discharge decreased.

ii· CERVICO-OCULAR REFLEX (COR)

The Cervico-ocular reflex supplements the VOR, MOR and OKR to stabilize the visual acuity in response to perturbations induced by head motions during active head-on-body rotations (Cullen & Roy, 2004). The COR will be activated by neck spindle afferents stimulations (Manzoni, 2009) during active movements. Several studies have

shown that the COR is inconsequential in several species such as the monkey as the vestibular nuclei neurons are not modulated by dynamic or static neck stimulations (Cullen and Roy, 2004). The COR is controlled by the same neurons that mediate the VOR, and so might be modulated as well by the flocculus (Gdowski et al., 2001). Coincidentally, bilateral vestibular dysfunction leads to an increase in the activity of the COR that substitutes the sensory loss to improve gaze stabilization (Sadeghi et al., 2012).

iii· OTOLITHIC OCULAR REFLEXES

There are several types of otolithic-related reflexes and different responses to otolithic stimulations. Translations movements will generate the compensatory reflex tVOR (translational vestibulo-ocular reflex) sensed by the otolithic sensory epithelium, the maculae (Angelaki, 2004). As the tVOR is only well developed in foveal animals (such as humans or non-human primates), it will not be further addressed in this thesis.

Ocular Counter Roll (OCR)l responses

When the head is tilted or pitched, the eye will be orientated to a compensatory position to maintain a stable visual acuity, through movements that tend to keep the eye in the azimuth plane. Additionally, a dynamic tilt will induce an activation of otolithic and semi-circular canals, static tilt is associated with the stimulation of only the otolithic organs, specifically the utricule. Even though the response to static head tilt is also present in humans and monkeys, there is a neurophysiological difference between lateral and front-eyed animals. Indeed, in front-eyed animals, a head roll induces an ocular torsion while a head pitch induces a vertical eye movement (Bockisch and Haslwanter, 2001). However, in lateral-eyed animals, and specifically mice OCR response to a lateral head tilt will lead to a compensatory vertical eye movement (Oommen and Stahl, 2008): if the head is tilted ipsilaterally (down) the eye will go up and if the tilt is contralaterally (or up), the eye will go down.

The gain of OCR is twice more important in lateral-eyed animals (Maruta et al., 2001; Cohen et al., 2006) than it is in frontal-eyed animals for which this reflex is quite limited with a gain of approximately 10% (Collewijn et al., 1985).

Maculo-Ocular Reflex (MOR) during Off Avis Vertical Rotations (OVAR)

The MOR represents a complex reflex, as it processes otolithic inputs but also requires functional canalar activity. The maculo ocular reflex will compensate with slow and fast eye movements a constant velocity stimulation if the axis is shifted instead of being earth-based. OVAR (Off vertical axis rotations) will induce persistent unidirectional nystagmus that compensates for the stimulation in both direction and velocity (Hess and Dieringer, 1990). In the mice, OVAR induces in the first few nystagmus a canal and otolithic-dependent response, and after a few rotations at a constant velocity, an otolithic-only response, see **Figure 16** (Beraneck et al., 2012).
This reflex not only depends on otolithic and canalar signals; it also depends on a central processing involving the so-called velocity storage pathway (Angelaki et al., 1992).

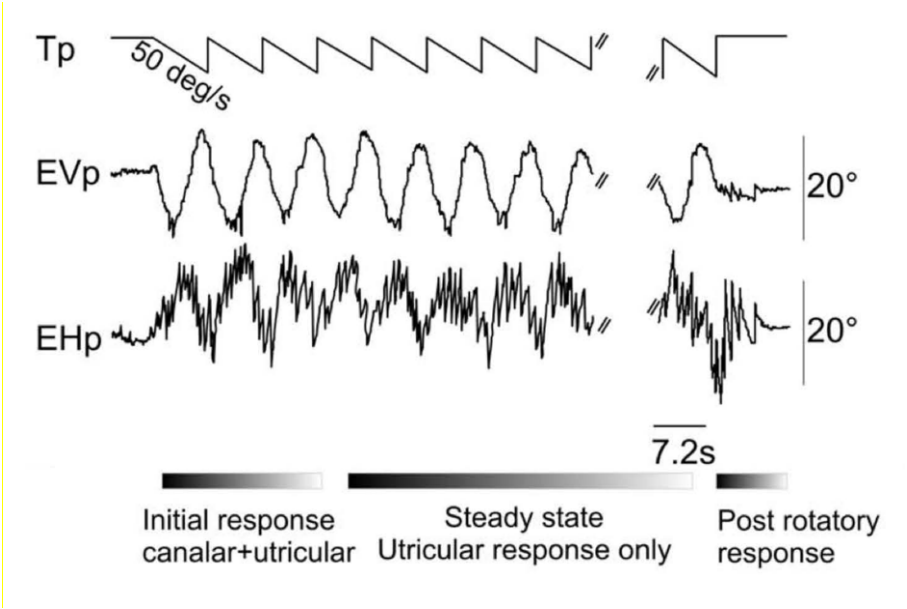

Figure 16: Maculo-ocular reflex during Off Vertical Axis Rotations (OVAR). The vestibular turntable (Tp) is rotated continuously at 50°/s in the counterclockwise direction, and the vertical (EVp) and horizontal (EHp) eye movements are recorded

during the stimulation. The horizontal component of the eye response is composed of nystagmus in both clockwise and counterclockwise directions. The initial response can be attributed to a mixed canalar and utricular stimulation, while the steady state is associated only with a utricular response. The post-rotatory response is in part the result of the velocity storage (See "velocity storage section") (Modified from Beraneck et al., 2012).

iv· VELOCITY STORAGE

The vestibular system integrates multiple sources of vestibular-related inputs (canalar and otolithic) to other sensory, e.g visual inputs. However, those inputs originating from very different systems respond to a given movement with different time constants. The velocity storage has been described as a brainstem/cerebellum mechanism that aims to properly process multisensory integration (Laurens & Angelaki, 2011). While a good deal about this mechanism remains unclear (see **Table 2)**, the role of the velocity storage system can be represented in diverse physiological conditions.

Vestibular inputs are encoded from the primary afferents to the vestibular central neurons, but both answers a continuous constant velocity stimulation with different time constants. Indeed, the constant velocity will induce a decrease in the primary afferent signals, but the reduction of the nerve signal will take longer. This delay has been attributed to the velocity retained in the velocity storage system (VSM) in the brainstem. Hence, the mechanisms of velocity storage have been described as the transformation of the short time constant of the semi-circular canals (5-7 s) into the longer time constant of the neural sense of rotations (15-20s, Waespe and Henn, 1977).
In addition, the angular vestibulo-ocular reflex responds preferentially to short and fast movements and as such presents an optimal performance for high-frequency stimulations. To counter its relatively weak performance at low frequencies, the velocity storage amplifies and prolongs this poor vestibular signal by integrating canalar and

otolithic inputs (Laurens and Angelaki, 2011). Finally, the semi-circular canals cannot encode constant velocity stimulations (Goldberg and Fernandez, 1971), while the otolithic-related activity stays present all during a constant velocity stimulation. The velocity storage retains the velocity stored during the steady response and is represented in a persistent motor response after the offset of the vestibular stimulation (Raphan et al., 1979).

Similarly, VN neurons can be activated by optokinetic stimulations (Beraneck and Cullen, 2007) and visual inputs can be used to improve the sub-optimal performances of the aVOR at low frequencies. As described in the "Optokinetic reflex characteristics" section, the OKR response can be divided into two components, one direct and the other indirect that is associated with a gradual increase of the velocity of the response slow phases during optokinetic stimulation. In absence of vestibular inputs, this velocity builds up and manifests as persistency of the response after the end of the stimulation (OKAN, after optokinetic nystagmus) (Cohen et al., 1977 p.77). However, in the presence of vestibular inputs, the velocity storage is able to use visual and vestibular information to predict future velocity even if the system is not updated with new information, in order to improve the estimation of the rotation (Karmali, 2019).

Recent studies have found the presence of the velocity storage mechanisms (VSM) neurons in the medial and superior vestibular nuclei in monkeys (Yakushin et al., 2017) and humans (Rühl et al., 2022). Though the velocity storage is present in a large number of species including monkeys and humans, as previously stated it is considered leaky and weak in mice (van Alphen et al., 2001).

Functional importance	*Paper*
Time constant matching	Waespe et al, 1977, Karmali et al, 2019
Integration of canalar and otolithic inputs during constant velocity stimulation	(Angelaki and Hess, 1996)
Predictive OKR	(Miki et al., 2020)
Motion sickness	(Cohen et al., 2003; Idoux et al., 2018; Lackner and DiZio, 2020)

Table 2: Velocity storage functional importance and bibliography.

PLASTICITY OF GAZE STABILIZATION

Vestibular inputs are crucial for normal life to maintain posture, balance, stabilize gaze and for spatial orientation and navigation. Maintaining good and sufficient responses to the vestibular inputs is thus paramount. As such, and to avoid any error making the functional vestibular pathway ineffective, the vestibular pathway is required to be able to adapt its performance and compensate for any errors. This chapter will be divided into three sections i) introduce the VOR and OKR as models of cerebellum-dependent adaptation, ii) consider the consequences of vestibular lesions and the system's mechanisms to compensate for the lesion-induced deficit, and iii) describe the functional link between OKR and VOR and its effect on adaptation and compensation.

I· GAZE STABILIZATION ADAPTATION: A MOTOR LEARNING MODEL

VOR and OKR, as other coordinated movements, can be described in two components: the amplitude and the timing of the response. The cerebellum plays a crucial role in the maintenance and adaptation of these components. To this extent, both reflexes have been used as a stand-in to study the adaptation mechanisms in the cerebellum as vestibular and visual inputs are easily modifiable and quantifiable.

i· ADAPTATION PARADIGMS

VOR and OKR motor learning paradigms are well used in the mice, the model of this thesis. Both reflexes and their adaptation mechanisms are conserved in most animals and are quite well-known in mice (review in (De Zeeuw et al., 2021). Video-oculography is a convenient and non-invasive technique to record eye movements while

modulating external inputs, by a screen and a vestibular turntable, making the mice a relevant model in this domain of research. Mice OKR and VOR are reported to be similar to humans (Stahl, 2004) and the availability of genetics tools and the use of mutants are good reasons why the mouse model is a good model for cerebellum-dependent adaptation.

Adaptation paradigms aim to create a visual-vestibular mismatch. The visual error signal that will be induced by the mismatch will drive the adaptation. VOR paradigms can adapt to a higher gain (gain-up adaptation, **Figure 17 A**) with an out-of-phase screen or to a lower gain (gain-down adaptation **Figure 17 B**) if the screen and stimulation are synchronized (Voges et al., 2017). OKR adaptation paradigm is composed of training sessions of visual stimulation rotations in both directions. The visual stimulation should be of enough high contrast and of low frequency to induce an optimized coding of the retinal slip and a bigger adaptation (Pham et al., 2022a). An example of OKR training I developed during my thesis is reported in Appendix 1.

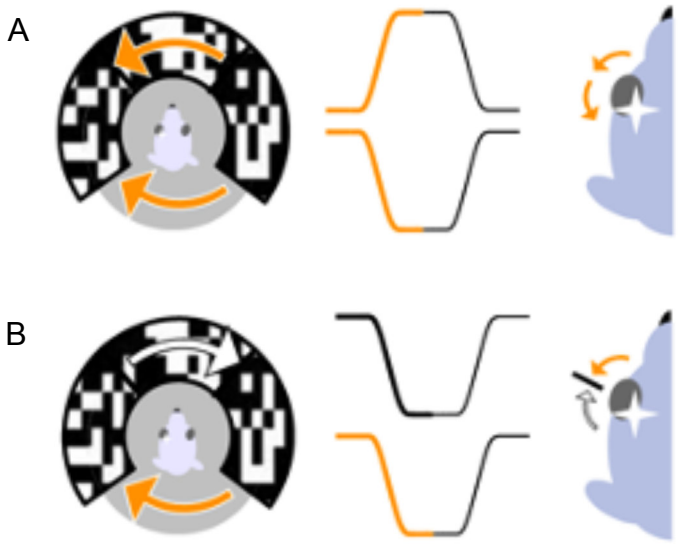

Figure 17: VOR adaptation set-up. A) VOR gain-up training: the screen and the turntable are rotated out-ot-phase leading to a bigger amplitude of eye responses. B) VOR gain-down training: the screen and the turntable are rotated in phase and reducing the amplitude of the compensatory eye response. (Voges et al, 2017).

ii· ADAPTATION MECHANISMS

As described in the previous sections, both VOR and OKR are dependent on the cerebellum for their fine-tuning and their adaptation, making them efficient models of adaptation and motor learning through the cerebellum. The cerebellum does not play a role in the direct horizontal VOR pathway but its adaptation is cerebellum-dependent and the VOR adaptation is considered a model of cerebellum-dependent motor learning.

VOR and OKR adaptation mechanisms in the cerebellum were hypothesized by Marr, 1969 and Albus, 1971 to be mainly due to the modified synapse of Purkinje cells (PC) and Parallel fibres (PF) in the cerebellum in response to an error signal. Furthermore, Ito and colleagues proposed that the adaptation of the hVOR occurred in the Horizontal-zone of the flocculus because the PC vestibular sensitivity is modified due to the climbing fibres (CF) (that conveyed vestibular information to the PC/PF synapse) plasticity (Ito, 1970). In the case of the adaptation of OKR, visual inputs are conveyed directly to the flocculus and the same mechanism of the VOR adaptation can occur; the visual-related CF modified the responsiveness of the H-zone PC (Katoh et al., 1998). In the cellular context, adaptation was thought to be the result of long-term potentiation (LTP) or long-term depression (LTD) at the PF level induced by retina slip inputs in the CF of the H-zone (Ito, 1989 p.89). Since then, several studies have shown that VOR adaptation is driven by LTD at the PC-PF synapses (Kakegawa et al., 2018).

However, the PC-PF plasticity cannot completely explain the VOR adaptation: Schonewille and colleagues used genetically-modified mice with altered LTD and observed that motor learning (gain down and gain up) was not impaired (Schonewille et al., 2011). While LTD could be considered not crucial for adaptation in the flocculus, there might be multiple types of synaptic plasticity instigating adaptation that take over when one is defective. On the other hand, in mice whose granule cells were silenced with LTD and LTP impaired, responses to the gain-down paradigm were preserved in the mutants but not responses to the gain-up paradigm (Galliano et al., 2013). The Marr-Albus-Ito hypothesis was further challenged by Miles and Lisberger: they proposed that

instead of an LTD at the PC-PF synapses in the flocculus, the adaptation was induced in the brainstem and modulated by the error signals generated by the PC in the flocculus (Miles and Lisberger, 1981).

While the initial idea of adaptation was that it was driven by the plasticity of a specific synapse, new studies have shown that adaptation is best described as the coordination of multiple types of plasticity occurring in different areas of the brain.
Indeed, Ito and Schonewille's hypotheses are not mutually exclusive and co-habit if we consider the timing component of VOR adaptation: adaptation can occur in a short period but can also be consolidated if the paradigm is imposed for a long duration (also in OKR, Shutoh and al, 2006). This change from short-term adaptation to memory consolidation is in part due to the transfer of plasticity site from the cerebellum to other areas for long-term storage (Yamazaki et al, 2015). Horizontal VOR adaptations are thought to be induced first by LTD at the PF-PC synapses in the floccular H-Zone mediated by the climbing fibres inputs to the cerebellum: this is the short-term adaptation, fast and not reliably retained. Then the adaptation memory is transferred in response to several repetitions into long-term memory in the brainstem via mossy fibre-like projections (Ito, 2013). This transfer of plasticity is also found in OKR adaptation as an optokinetic training protocol leads to higher neuronal excitability in the brainstem, at the level of the vestibular nuclei (Shutoh et al., 2006). Long-term retention of the adaptation at the level of the brainstem has been bolstered by the work of our group, as Carcaud and colleagues as they demonstrated a modulation of the MVN neurons' properties after a long-term visuo-vestibular mismatch (Carcaud et al., 2017). The plasticity of the vestibular neurons after a VOR adaptation paradigm is also delayed compared to the Purkinje cells' plasticity, reinforcing the cerebellum-to-brainstem pathway of consolidation (Jang et al., 2020). The OKR adaptation depends on similar short and long-term mechanisms: short-term memory is formed in the H-Zone between the PC and PF with LTD, and long-term is induced by the LTP in the brainstem (Yamazaki et al., 2015).

The consolidation of the memory of adaptation is related to the spacing learning effect (repetitions of trials with rest) compared to the massed learning effect (with no resting interval) leading to a more robust memory (Kornmeier and Sosic-Vasic, 2012). However, it has been recently proven that spacing learning leads to a more robust consolidation of hOKR than hVOR, which implies there are still different pathways of adaptation and consolidation between the two reflexes depending on the training parameters or the learning paradigm (Pham et al., 2022b).

To conclude, gaze stabilizing reflexes are models of cerebellum-dependent adaptation whose amplitude can be decreased or increased. The mechanisms of adaptation are numerous and involve plasticity occurring at the synaptic and cellular levels within the vestibular cerebellum and brainstem vestibular nuclei. While adaptation can occur as the result of a controlled paradigm that leads to temporary and reversible changes, comparable cellular mechanisms are also triggered during post-lesional plasticity as a response to a complete loss of vestibular inputs.

II· POST-LESIONAL VESTIBULAR PLASTICITY

i· COMPENSATION OF THE VESTIBULAR SYSTEM FOLLOWING UVL

The bilaterality of vestibular endorgans is crucial to maintaining proper gaze stabilization, posture and spatial orientation (Dieterich and Brandt, 2018) and its importance in the system has been investigated early on by lesion studies. Indeed, French physiologist Pierre-Marie Flourens reported in 1824 that a lesion done to the semi-circular canals did not induce deafness but led to an imbalance and nystagmus in lesioned animal (Wiest, 2015), and furthermore, the animal recovered after a unilateral lesion in a matter of weeks or months. This restoration is called vestibular compensation and has been further studied ever since, in most vertebrates and for both unilateral or bilateral lesions (either simultaneously or two delayed unilateral lesions in Betcherew's case). While lesion studies are good models to study compensation mechanisms in the

animal, it should be noted that they only partially reproduce many vestibular pathologies that disrupt the function in acute crisis, with fluctuating loss of vestibular inputs.

Static and dynamic components of the vestibular compensation

Unilateral vestibular lesion (UVL) first induces an acute vestibular syndrome, an ensemble of symptoms that are the immediate result of the loss of one inner ear as well as long-term consequences (**Figure 16**). The immediate or static symptoms are spontaneous nystagmus, head and body tilt, barrel rolling and circular walking. UVL also induces dynamic symptoms such as altered balance control in complex situations or vestibular-related reflex deficits such as VOR or the vestibulo-spinal reflex. The alteration in VOR gains is asymmetric with the ipsilesional VOR greatly reduced while the contralesional loss is limited, in the mice but also in other species (Beraneck et al., 2008). While static symptoms recover in a matter of days thanks to the compensation, dynamic symptoms persist for a longer time and the compensation remains often incomplete.

In mice, static symptoms are recovered in about a few days to weeks while the dynamics deficits are never completely compensated for (Lacour and Bernard-Demanze, 2015). In the very acute timeframe of the UVL (1 to 3 days after the lesion) diverse cellular mechanisms are participating in the recovery (as reviewed in Tighilet et al., 2019). The crucial step of the deficit compensation is the functional restoration, i.e rebalancing the electrophysiological signals between the two vestibular nuclei: reducing the activity of the ipsilesional VN and increasing the activity of the contralesional VN. In non-lesioned animals, the activity of the bilateral vestibular nuclei is normally regulated by the vestibular commissural pathway, to maintain a balanced firing rate between both vestibular complexes. However, after a unilateral vestibular lesion, the commissural pathway is partly responsible for the oculomotor and postural symptoms and their recovery (Ris and Godaux, 1998). Indeed, the symptoms are the result of a severe imbalance of the firing rate between the ipsilesional MVN neurons and the hyperactive

contralateral MVN neurons due to the inhibitory effect of the commissural vestibular pathway. However, during compensation, there is a re-balancing of the commissural vestibular pathway in order to re-establish a balance between the bilateral MVN neurons' resting fire rate (reviewed in (Olabi et al., 2010).

Dynamics deficits are recovered through several mechanisms. They differ in dynamics but aim to compensate for vestibular deficits in the long term. The intrinsic properties of the bilateral vestibular nuclei neurons are modulated and an asymmetry of firing pattern is created, with a dominance of tonic discharge (type A neurons) in the ipsilesional side and tonic/type B dominance in the contralateral side (Beraneck and Idoux, 2012). The plasticity-induced change of the bilateral vestibular nuclei homeostasis is reinforced by the increased inhibitory expression of GABA in the ipsilesional vestibular nucleus after UVL (Bergquist et al., 2008) and the restoration of the static deficit induced by this GABA activity (Heskin-Sweezie et al., 2010).

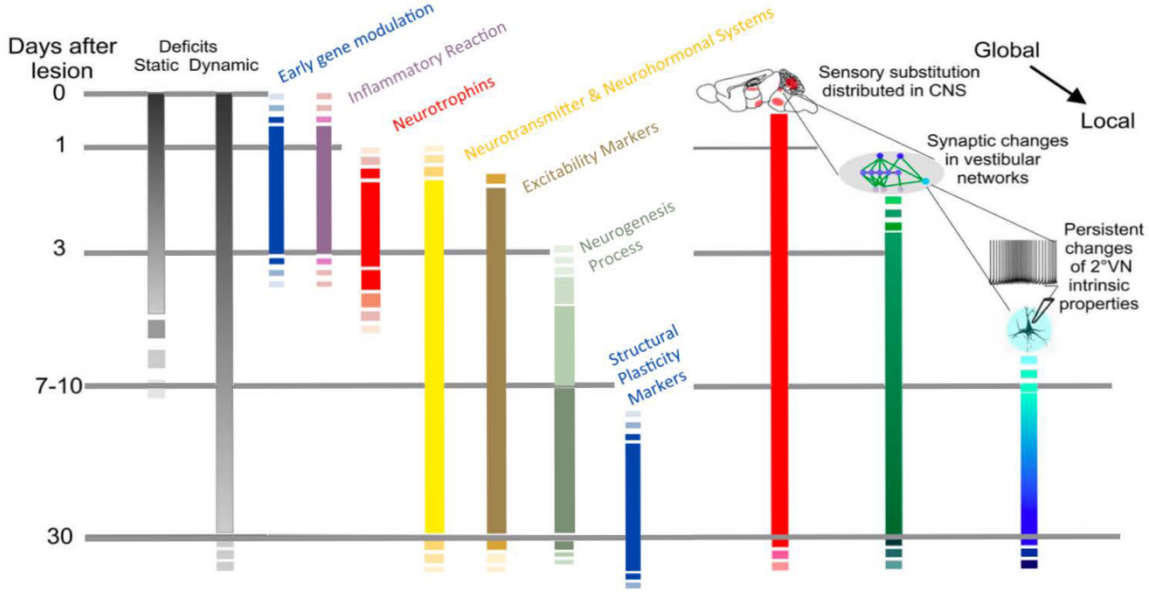

Figure 18: Timeframe of the vestibular compensation and the different mechanisms occurring during the static and dynamic deficit period. (From Beraneck & Idoux, 2012 & Tighilet et al, 2019).

Global to local compensation

Compensation can be described as two parallel channels of plasticity (static and dynamic) and this is reflected in the changes induced in the system at different levels, from global i.e whole brain to local i.e vestibular neurons (see **Figure 18**). The changes occur first in a global manner to compensate for the behavioural consequences of the unilateral lesion, such as sensory substitution involving non-vestibular areas. Along with the substitution, changes are ingrained further into the vestibular-related network and then at the cellular level. Several plasticity mechanisms elicit changes in the dynamic of the network, as previously described above. At the cellular level, plasticity is consolidated with changes at the synaptic level, followed by changes in the intrinsic properties of vestibular neurons (Beraneck and Idoux, 2012).

The cerebellum, which integrates also visual inputs coming down the OKR pathway, is also involved in the recovery, though not necessary, after a unilateral vestibular lesion. Cerebellum-deficient mice have an altered compensation of the static deficits whose recovery is delayed compared to the WT mice (Beraneck et al., 2008). Mutant mice's recovery of dynamic symptoms, with the VOR as a proxy, is also impaired as the compensation appeared to be incomplete. While the cerebellum is crucial for long-term VOR restoration, vestibular compensation required cerebellum and non-LTD-dependent pathways (Faulstich et al., 2006). Vestibular compensation could in part be induced by the creation of new neurons in the long-term maintenance of compensation behaviours. In the cat, UVL induces neurogenesis in the ipsilateral vestibular nuclei side of the lesion (Tighilet et al., 2007; El Mahmoudi et al., 2022). Neurogenesis has been proven in other species, but it might need a longer period of vestibular dysfunction to be put in place (Tighilet et al., 2019). Moreover, damages made to the peripheral vestibular system and especially the destruction of the afferent vestibular fibres can cause an acute inflammatory response (Dutheil et al., 2011) and it has been suggested that cell proliferation and survival are modulated by the inflammatory response (El Mahmoudi et al., 2022).

ii· SENSORY SUBSTITUTION

In the acute phase immediately following UVL, non-vestibular areas are functionally recruited, including the auditory, visual and somatosensory cortices and are used to compensate for the vestibular loss (Grosch et al., 2020). This mechanism is called sensory substitution, which is the process of using one functional sense to replace another impaired sense (Bach-y-Rita and W. Kercel, 2003). In the blind, one sensory substitution is tactile sensory information, used notably for reading in the written language Braille.

In the context of vestibular compensation, sensory substitution aims to put non-vestibular inputs at the same level of functional importance that vestibular signals, by reweighting the vestibular and non-vestibular inputs. Sensory substitution and reweighting studies are not common in animals, but sensory reweighting has been reported several times in human research. For example, studies on human spaceflight investigated sensory substitution. In response to severe vestibular changes (i.e the absence of gravitational inputs), adaptative plasticity would allow for visual and somatosensory substitution (Hupfeld et al., 2022).
In the animal model, the vestibulo-spinal reflex has been shown to substitute for the vestibular loss with increased sensitivity of the neck proprioceptive signals in neurons that do not normally respond to proprioceptive inputs (VO neurons) and its evolution correlates with the restoration of the acute symptoms (Sadeghi et al., 2011). While mechanisms of sensory substitution are not known, the unmasking of this proprioceptive substitution leads to the multisensory integration of new inputs that can improve balance and self-perception (Jamali et al., 2014). The substitution does not only occur in the vestibular nuclei through its one of the preferred targets. In the very first hours after a unilateral neurectomy, the receptor fields of the hindpaws in the somatosensory cortex were bilaterally expended through modulated thalamic-cortical inputs during the vestibular compensation (Facchini et al., 2021). Similarly, Kai and colleagues have shown in the mice the same substitution for the somatosensory cortex

after UVL, but no substitution by the visual cortex as is often the case in human studies (Dieterich and Brandt, 2010; Kai et al., 2022).

As seen above, sensory substitution is a mechanism that participates to vestibular compensation after a unilateral vestibular lesion. However, in the case of a bilateral vestibular lesion (BVL), the total loss of vestibular inputs cancels the possibility of vestibular compensation from the intact vestibular nuclei. Following a BVL, gaze stabilization is altered as the eye movements in response to head rotations in the dark are abolished (Baarsma and Collewijn, 1974). However, some compensation occurred as the postural ability was retained even to some limited extent (Thomson et al., 1991). Extra-vestibular inputs, such as neck signals, need to be integrated to balance the loss. Acting as a substitute in the VOR pathway, proprioceptive signals can improve gaze stabilization after a bilateral loss of vestibular inputs (Sadeghi et al., 2012). Normally the cervico-ocular reflex (COR) is not dominant in most species (mice, primates and humans for example), while very performant in others (birds), however, bilateral vestibular loss leads to an increase of neck inputs at the level of the VOR premotor and in the end, to better gaze stabilization.

To sum up, a unilateral lesion will be able to be compensated by a series of mechanisms occurring at different levels and using inputs from the intact side. In the case of a bilateral lesion, the behavourial consequences are mostly reduced by sensory substitution that will up-modulate a pre-existent input and thus compensate for the complete or partial loss of others.

III· VOR AND OKR INTERACTIONS

While vestibular lesions and their consequences in animals and humans have been well documented, neural mechanisms underlying sensory substitution and their dynamics are still poorly described. One obvious possibility to improve gaze stabilization after a complete loss of vestibular inputs would be to increase the use of

visual inputs and oculomotor signals. To further consider the optokinetic system as a valuable lever of sensory substitution, I will first describe the shared circuitry and functional interactions of the VOR and OKR pathways.

i· FUNCTIONAL VOR AND OKR INTERACTIONS

VOR is a well-preserved reflex whose circuitry and physiology are present in many different species. OKR is also conserved through evolution but visual discrepancies between species (such as the position of the eye on the head and the presence or absence of a fovea) can modify its neurophysiology. However, as both reflexes are present and functional, they both work synergistically to stabilize the gaze.

The fine-tuning of both reflexes is different across species. However, VOR is an open-loop reflex, meaning that it functions in the dark, in absence of visual feedback. However, its fine-tuning depends on the presence of visual inputs, in particular during development, but thorough lifespan. Mice are an altricial species that still need to develop after birth. Hence, the opening of the eyes occurs only at P10-12, which leads to the developmental tuning of OKR and VOR during the 2nd and 3rd postnatal week (Beraneck et al., 2014). Compared to adult mice, VOR is weaker in juvenile mice, while OKR is initially more performant (Faulstich et al, 2004). With the maturation of VOR with age, and the increase of its gain, OKR gain decreases slightly. The dynamic of OKR in the period of VOR immaturity can explain the persistent and almost perfect performance of VOR in light of both juvenile and adult mice. VOR and OKR work in a preferred range of motions to optimise gaze stabilisation, explained by their pathways' properties. As described in the "Sensory Pathways" section, vestibular afferents are more sensitive to motions with higher velocities while the DSGC encode preferably slow motions. This asymmetry of response is reproduced in the performance of each reflex across frequencies. As such, OKR is more proficient at low frequencies, whilst VOR is driving gaze stabilization at higher frequencies (Faulstich et al, 2004). The frequency selective dynamics of OKR and VOR provide for an almost perfect gaze stabilization in light while rotating in all ranges of frequencies.

Moreover, OKR and VOR share the same adaptative controller (the flocculus and the vestibular nuclei) and the mechanisms of adaptation during a visuo-vestibular mismatch are similar for both OKR and VOR (see the "Adaptation mechanisms" chapter) (Ito et al, 2006). Nonetheless, their plasticity mechanisms are diverse and the two gaze stabilizing reflexes are affected differently by a similar visuo-vestibular conflict. For instance, a VOR gain-down paradigm induces a decreased VOR gain as a result of the error signal, and an OKR gain increases while a VOR gain-up adaption leads to both VOR and OKR gain increase (Faulstich et al., 2004; Pham et al., 2022c).

Optokinetic plasticity after vestibular lesion

Few studies have researched the impact of a vestibular loss caused by a lesion on the optokinetic system but several suggested that an oculomotor substitution occurred in response to vestibular loss. In the vestibular nuclei, the neuronal response to dynamic optokinetic stimulation at high frequency increased in UVN cats compared to non-lesioned cats, leading to a visual substitution in a vestibular-specific frequency range (Zennou-Azogui et al., 1994). Nelson and colleagues found that, in mice, the much-described transient VOR gain decrease caused by a unilateral vestibular lesion is accompanied by an increase in the optokinetic gain with a similar dynamic (Nelson et al., 2017). However, a more recent study investigated the immediate consequences of a lesion of the vestibulo-cochlear nerve (VIIIth) on the VOR and OKR (Soupiadou et al., 2020). While OKR gain increased right after the lesion, it decreased with the same amplitude as that of the VOR. The ultimate alteration of the optokinetic reflex can be linked to the shared components of the VOR and OKR circuitry and the mechanisms involved in vestibular compensation in a unilateral lesion to rebalance the bilateral vestibular information. The two studies cited above differ in the model used and the timescales of the investigation, thus this could explain the differences seen in the adaptation of the VOR and OKR gain. Nonetheless, optokinetic inputs could be a good

substitution target to compensate for the failures of the vestibular inputs in the specific context of gaze stabilization.

This multiple plasticity is further discussed in Article 1 and 2 as we investigated VOR and OKR plasticity after either a long-lasting visuo-vestibular mismatch or a transient bilateral vestibular loss.

ii· VESTIBULAR PATHOLOGIES AND VISUAL SUBSITUTION

In the previous chapter, I described the plasticity of the vestibular and extra-vestibular signals in response to a man-made lesion or during a severe change in the environment (i.e absence of gravity). However, several pathologies are caused by vestibular dysfunction (with diverse levels of severity) and thus have dramatic consequences on a day-to-day basis. Balance, vestibular-related reflexes, self-perception or even spatial orientation are altered in vestibular deficit patients (Curthoys and Wade, 1995).

Bilateral Vestibular Failure (BVF) incidence in the population is not frequent, less than unilateral vestibulopathy (UV) or Menière's Disease (MD) (Strupp et al., 2020). The latter diseases consist of attacks lasting from a few hours in MD to a few days for UV, thus allowing for the system to recuperate from those acute attacks. Even if compensation in the case of complete vestibular loss is challenging, BVF patients can maintain a normal posture in the presence of visual inputs but retain balance and gaze stabilization issues (absent VOR) (Mergner et al., 2009). Strategies are then put into practice to compensate for vestibular failures, such as sensory substitution, motor substitution, and anticipatory mechanisms (Herdman et al., 2007). BVF patients' reliance on visual signals increases compared to people with intact vestibular function: their COR, normally insignificant in most species and here humans, increased (Bronstein et al., 1995). Optokinetic responses can also contribute to gaze stabilization at low frequencies in BVF patients (Leigh et al., 1992). Dieterich and Brandt have shown

in patients suffering from bilateral vestibular failure that optokinetic stimulation leads to a more important activation of visual and oculomotor areas than in control subjects even if the optokinetic performance were not different in both groups (Dieterich and Brandt, 2010). Nonetheless, that activation suggests that a visual sensory substitution occurs as the visual and oculomotor sensitivities have increased.

To conclude, sensory substitution could be proven to be an effective therapeutic tool as several sensory inputs can be used to help the system compensate for vestibular hypofunction (both complete or incomplete). It remains unclear whether visual and oculomotor information could be fortified following a vestibular failure and if it could adequately compensate for the dysfunctional activity of the vestibular system.

AIMS AND COURSE OF MY THESIS

This thesis studied the integration of visual and vestibular inputs within gaze control and its plasticity during unimodal and long-term perturbations. This work highlights the conjugated plasticity of the oculomotor reflexes but also the implementation of sensory substitution in response to vestibular loss.

In the first study of this thesis, we were interested in the adaptation of the OKR and the VOR during a **long-term visual perturbation** to understand the cross-plasticity of these reflexes. The protocol was designed to allow **studying both the adaptation and the recovery after the perturbation** was stopped. To do this, we used a new protocol previously developed by the team that allowed us to induce a visual-vestibular mismatch using a helmet that mice could wear for 2 weeks, without disturbing their usual behaviour. We then quantified the OKR and VOR responses after the helmet was removed to observe how reflexes adapted following this prolonged visual conflict. We also observed the dynamics of OKR and VOR adaptation over several days and their responses to different frequencies (Article 1). My contribution to the article concerns the entire OKR dataset that I completely generated, analyzed and processed for publication. I also participated in the implementation of a new analysis to discriminate the optokinetic responses between their fast and slow components.

In a second study, we followed the same rationale but this time wanted to induce a **reversible perturbation of the vestibular inputs**. To investigate the consequences of a bilateral vestibular lesion and the substitution mechanisms that make up for such a lesion, we used a "sub-chronic" pharmacological protocol to induce a chronic but transient bilateral vestibular lesion to observe the **plasticity occurring after the lesion and the dynamic of recovery thereafter** OKR and VOR were tested at different stages of the protocol to see their dynamics during and after treatment, and the integration of these two reflexes combined was also tested at the end of the protocol. To correlate the functional data to structural deficits, inner ear organs were collected at the end of the treatment and at the end of the recovery period to link the loss of specific VOR function

to the number of hair cells in the different vestibular endorgans. We found the treatment equally affects the otolith and canal organs, and the loss of type I hair cells induced by IDPN strongly correlates with the loss of function. We showed that the bilateral vestibular dysfunction led to an increase of the optokinetic reflex gain in a specific range of frequency in which gaze stabilization normally strongly depends on vestibular information. We also report that while the vestibular loss of function could theoretically be compensated for by the OKR increase, the integration of visual and vestibular inputs remained either sub-optimal or absent, leading to impaired gaze stabilization even after recovery.

During my thesis, I was also able to participate in several collaborative studies. In particular, I carried out vestibular phenotyping of mice whose mutation in the poc5 gene led in some human cases to idiopathic scoliosis (Appendix 1). By the means of tests specific to the two organs of the inner ear (semicircular canals (VOR) and otoliths (OCR)), **I was able to study whether this mutation led to vestibular disorders in a pathology model**. In mutant mice with a POC5 KO genotype, no alteration of the vestibular function was found, as KO and WT mice have similar responses to aVOR, OCR and even OVAR, a more sensitive but less specific vestibular test. This dataset could in the future be part of a publication reporting the effect of POC5 mutation in the mouse. I also collaborated in another study to test mutant mice that lacked the transmembrane protein SUSD4, which is present in the cerebellum and brainstem. SUSD4 is normally involved in the activity-dependent degradation of an AMPA receptor subunit. Its absence led to an alteration of LTD. LTD is necessary for plasticity and in particular, for the adaptation of oculomotor reflexes, including the optokinetic reflex. To this end, **I set up an adaptation protocol that led to an increase in OKR gain through a long training session**, as well as a new approach to analyze OKR responses that leads to a more rigorous quantification of OKR signals by obtaining the amplitude of the response (gain) and the timing (phase). I was able to test this protocol on these mutant mice (Appendix 2), and they show no difference to the WT mice in response to the OKR adaptation. The alteration in LTD in the cerebellum in those mice does not lead to an altered adaptation.

While the main focus of this thesis is on behavioural oculomotor data, I acquired, used and developed cellular techniques through 2 additional projects during my thesis.

In the first one, I also produced results of neural tracer injections in order to mark a specific population in collaboration with Louis Richevaux. I was able to use retrograde labelling to highlight neurons projecting to the presubiculum, a subcortical structure involved in spatial orientation, and more precisely the head direction circuit, by integrating visual and vestibular signals. This work led to a publication in Jove, Richevaux et al. 2019 on which I am second author. I later used this same strategy to try to label neurons projecting to an up-stream structure of this same circuit, the supragenual nucleus. However, in mice, the model used for these injections, this structure is extremely small and I did not succeed in injecting a sufficient quantity of marker precisely enough to trace the neurons of this pathway. A bigger model, such as rats, or another way of injecting neuronal tracers should be considered.

In the last project, which would be further addressed in the perspectives section, I set up a system of in vivo neuron recording with tetrodes coupled to visual and vestibular stimulations as well as to eye movement recording. I also set up the offline analysis system to link a neuron's discharge (with a spike sorting and clustering free software) to the position of the eyes or the head. However, one of the limitations of this set-up lies in the use of head-fixed animals in recording head direction cells, whose movements are therefore passive. Though it limits the recording of neurons to those whose coding is not solely dependent on the active component of the movement, the set-up is functional for further experiments involving the recording of vestibular neurons coupled with visual and vestibular stimulations (see General Discussion).

「 · CHAPITRE 2 · 」

― METHODOLOGY ―

I· VIDEO-OCULOGRAPHY AND SENSORY STIMULATIONS

i· VIDEO OCULOGRAPHY EYE TRACKING SYSTEM

Eye tracking is a technique used to record eye movements, as well as gaze direction, during a task. Charles Bell first classified the different kinds of eye movements and described them as under the control of the brain (Bell, 1823). The functional association between eye movements and brain processes was further investigated with novel methods to measure eye movements in amplitude and timing (Wade and Tatler, 2005). Nowadays there are several methods of eye tracking systems in mice such as the eye coil on head-fixed animals (Boyden and Raymond, 2003), and magnets that can be used on freely-moving mice (Payne and Raymond, 2017). However, those techniques have the disadvantage of being invasive. In our lab, we use another eye-tracking method, video oculography which was created for head-fixed animals but has been recently used on freely-moving animals as well (Meyer et al., 2018; Michaiel et al., 2020).

Video oculography is a non-invasive technique that has been developed in the mouse recently (Stahl et al 2004). It allows a precise recording of the eye movements for both the horizontal and vertical components in response to vestibular or visual stimulations without any impairment to the animal's eye (compared to eye coils or magnets). Our studies involved the use of sensory stimulations to induce eye movements and as such having head-fixed animals inherent to video oculography was not an issue.

Our set-up uses the eye-tracking system ISCAN (ETL-200, ISCAN, Burlington, MA) modified to fit mice with a macro lens that shortens the working distance at 100mm (Stahl et al., 2000). The system was calibrated to obtain the perfect angle between the eye and the camera for optimal locations of the pupil and reference CR in the centre of the camera.

The pupil movement is tracked by the use of IR LEDs that are positioned on the side of the camera. The light emitted by the IR is reflected on the cornea (corneal

reflection) creating a non-moving reference point to track the pupil's movements as the CR and pupil's linear positions, with a delay of 30ms (Stahl et al, 2000). Those linear positions, recorded with a sampling rate of 1kHz, need to be translated into angular rotations by taking into account the axis of the eyeball and the axis of the camera (Stahl et al, 2000). This is performed with the following equation, with Rp being the radius of the rotation of the pupil:

$$E = \arcsin (CR-P)/Rp.$$

ii· GAZE STABILISATION REFLEXES STIMULATION

The mouse was positioned head fixed in a restraining plexiglass tube, with the nose inclined down at 30°/s to align the horizontal canals with the yaw plane. The tube was placed in the centre of the vestibular turntable that could be covered either by a white dome for the visual stimulations or a black and opaque dome for the experiments in the dark see Figure 17). For those, a solution of pilocarpine (2%) was used to induce miosis.

Optokinetic reflex tests

Optokinetic reflexes were tested either with a constant velocity or sinusoidal visual stimulation. Either way, the image projected on the dome consisted of a black background on which white dots (25 0000) were randomly distributed. The **constant velocity stimulations** (**Figure 19B)** corresponded to the image moving in either direction (clockwise or counterclockwise) at different velocities: 2.5, 5, 7.5, and 10°/s. This stimulation was used previously by the team while the **sinusoidal stimulations** had to be implanted (**Figure 19A**). A waveform of different frequencies tested (0.1, 0.2, 0.33, 0.5 and 1 Hz) was created on Spike 2 software and digitally transferred to the PsychoToolBox Matlab Pipeline to induce a sinusoidal stimulation of those frequencies.

The amplitude of each stimulation would be modified directly in MatLab so the peak velocity for each frequency would be 10°/s.

Vestibular-related reflex tests

Horizontal angular vestibulo-ocular reflexes were induced by performing horizontal sinusoidal rotations for 0.2, 0.5, 0.8, 1 and 2 Hz at a peak velocity of 30°/s (**Figure 19C). Off Vertical Axis Rotations** test corresponded to stimulations of a constant velocity, 50°/s either clockwise or counterclockwise with the table inclined with a 17° angle, inducing a nystagmus-like response (**Figure 19D**). **Ocular Counter Roll** tests were performed on a manual turntable and the vertical component of the eye response to the tilt angle of the table was recorded. The table was inclined at different angles (0° to 40°) both clockwise and counterclockwise (**Figure 19E)**. VOR in the light tests, called here **Combined Gaze Reflex** (CGR) were performed with sinusoidal stimulation at 0.2, 0.5 and 1Hz at a peak velocity of 30°/s with a fixed image projected on the dome (**Figure 19F)**.

iii· Quantification of the VOR and OKR Gain

The two main components of the response of the majority of the reflexes (sinusoidal OKR and VOR) tested are the gain and the phase. The gain represents the amplitude of the reflex and is calculated as the ratio of the response of the eye to the stimulation (head or visual flow). Its values are quantified between 0 and 1, 1 being a perfect compensation. The phase corresponds to the timing of the reflex and its perfect value is 0. Both components are modified with frequency and velocity.

Other parameters were also analyzed, such as the velocity of the slow phases of the optokinetic or the OCR gain that can be calculated as the slope of the vertical response of the eye in response to static tilts.

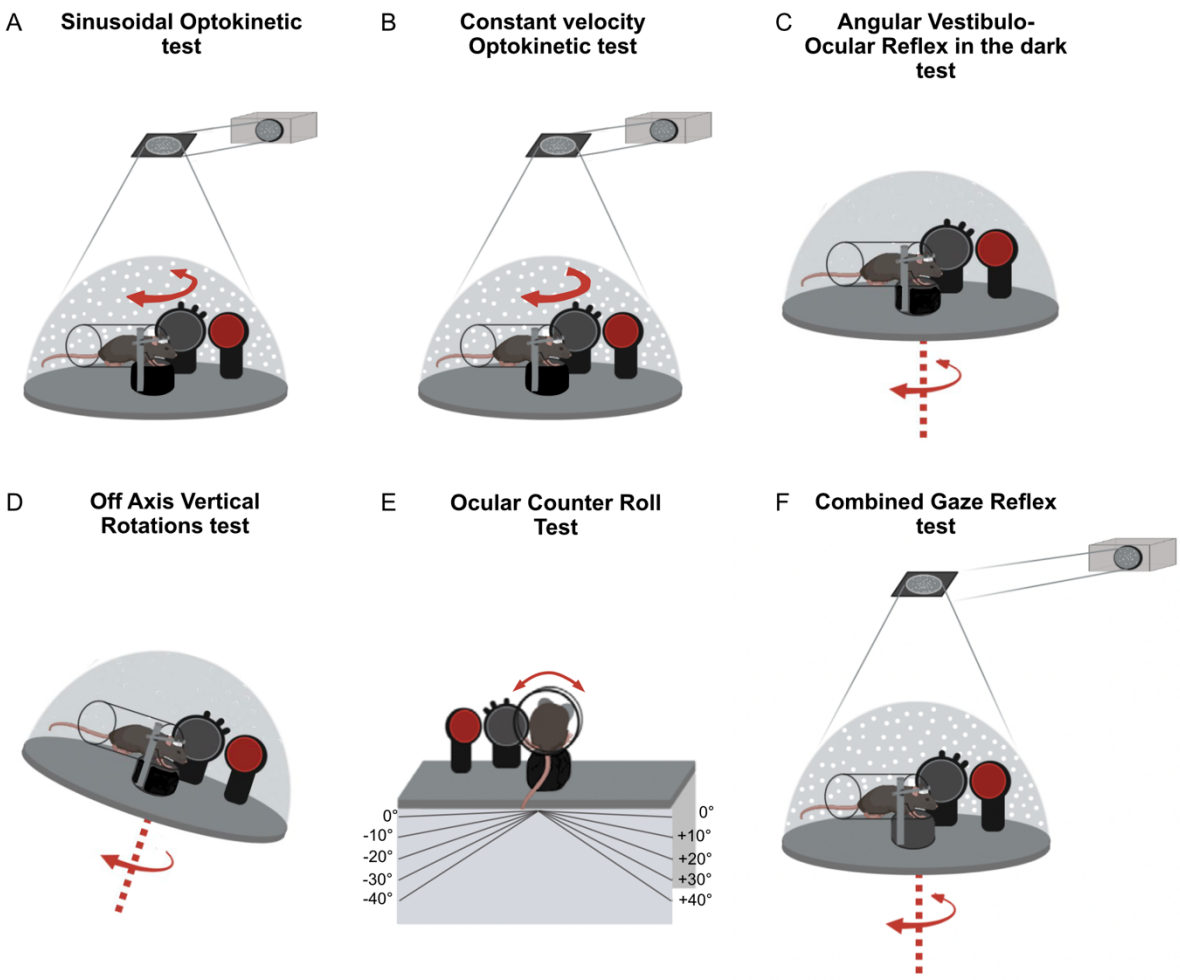

Figure 19: Gaze stabilization reflexes stimulation. The mouse is positioned head-fixed in a plexiglass tube and orientated such that its left eye movements are recorded thanks to the camera and the CR. The mouse is either covered by a white dome (A, B and F) or a black dome (C and D). A) Sinusoidal Optokinetic test B) Constant velocity Optokinetic test C) Horizontal Angular vestibulo-ocular reflex in the dark test D) Off Axis Vertical Rotations test E) Ocular Counter Roll Test F) Combined Gaze Reflex.

II· VISUO-VESTIBULAR MISMATCH PROTOCOL

The visuo-vestibular mismatch protocol used in Article 1 was developed to induce a long-term sensory conflict in mice in order to study its effect on oculomotor reflexes. This protocol was developed by the team and previously used in several papers. It

induces a visuo-vestibular mismatch occurring during their normal behaviour without any further probing from the experimenter and as such reduces bias. This protocol required a headpost implanted on the mouse skull to hold its head fixed during video-oculography tests on which the visuo-vestibular device was fixed.

i· Headpost implantation surgery

The mouse was anaesthetized with isoflurane (2%) half an hour after being injected with buprenorphine. The eyes were covered with ophthalmic gels to avoid dryness and the head was shaved. The head was cleaned with an antiseptic solution and a local anaesthesia (lidocaine hydrochloride) was injected subcutaneously. A longitudinal incision was made to expose the skull. The skull was cleaned with a saline solution and a scalpel was used to gently removed the membrane covering the skull while minimizing the bleeding. The headpost was glued to the skull between the lambda and bregma perpendicularly to the midline suture. A dental cement was further used to protect and maintain fixation of the headpost on the skull as its proper implantation was crucial and ensure the rest of the protocol. Once the cement dried around the headpost, the opened skin of the head was sutured behind the headpost. The mouse was allowed to recover under red light to avoid hypothermia following the end of the anesthesia.

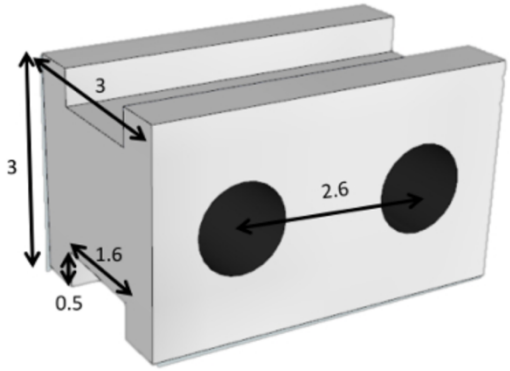

Figure 20: Headpost implanted on the skull of the mouse (From Barros et al, 2019)

ii· VVM device

The helmet-like device was made of opaque poly lactic acid (PLA) plastic created by a 3D printer (**Figure 20 Figure 21A)**. This plastic was lighter and the shape of the device made it possible for the mouse to do its normal activity in the cage. The devices were either used like it was produced, called “no-pattern”, or stripes of black nailed polish were placed on the device (**Figure 21B**). This “pattern” device would create a retinal slip; whenever the mouse is moving, the visual signal would be locked in the black stripes. On the other hand, the “no pattern” device would not lead to any retinal slip as there would not be any error signal.

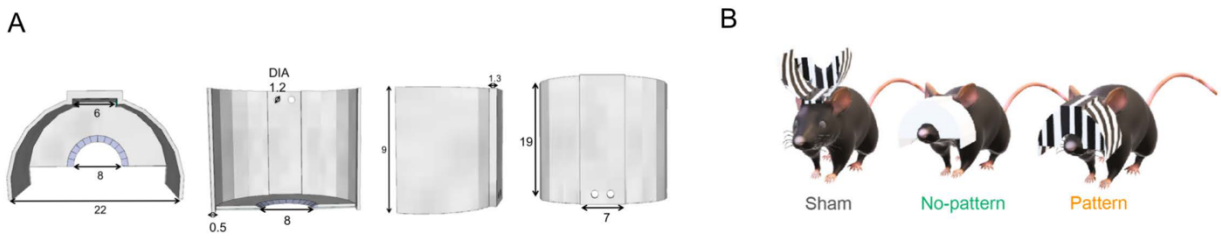

Figure 21: Adaptation device. A) Device size specifications B) VVM conditions: SHAM, No pattern, and Pattern (From Barros et al, 2019 and Barros et al, 2020)

iii· Adaptation protocol

The VVM device was attached after the first session of OKR or VOR test on the headpost by small screws. To limit experimental bias, the OKR group were measured twice before the start of the adaptation protocol. The helmet was secured tightly so it would not move and impair the mouse's ability to normally behave in its cage. After the device fixation and until the protocol was over, the well-being of the mouse and its weight were surveilled. The mouse wore the VVM device for 14 days. VOR sinusoidal

simulations, sinusoidal and constant velocity OKR stimulations (**Figure 19A, B and C**) were performed right after the helmet was removed, and on days 1, 2, and 6.

III· TRANSITORY VESTIBULAR IMPAIRMENT PROTOCOL

This protocol developed in Article 2 was used to induce a long-term but transitory sensory loss. The pharmaceutic treatment of IDPN has been previously used by Llorens and colleagues. They used acute injections that led to profound and irreversible damage to the vestibular functions (Greguske et al, 2019). More recently they proved that diluting IDPN in the drinking water, "sub-chronic treatment" allowed for a persistent and reversible vestibular impairment after the removal of IDPN from the water (Gregunske et al 2021). We used this same protocol to study the compensations occurring after a vestibular sensory loss, notably a visual compensation.
A similar headpost to the one in the previous study (see above "Headpost implantation") was used to maintain mice head-fixed during testing and with the same implantation protocol.

i· IDPN treatment

VOR and OKR (see **Figure 19 A to E**) were measured twice before the beginning of the IDPN treatment to ensure the measure would not be impacted by experimental bias. Mice were then treated with IDPN at a 30mM concentration in their drinking water for six weeks and the reflexes were tested every two weeks (3 measures for a mouse during the IDPN treatment). Bibs were changed every week and the mice's health followed regularly. After the Week 6 measure began the washout period and bibs were filled with only water. Similarly, the reflexes were tested every two weeks, thus 3 measures during the washout and a total of 7 measures for each mouse during the entire timeframe of the protocol.

ii· Histological studies

Mice were sacrificed at W6 (at the end of the IDPN treatment) or at W12 (at the end of the washout period), and their inner ears were removed in order to quantify the number of hair cells in the horizontal semi-circular canals and the utricule. Hair cells were classified as type I or type II hair cells with different markers to observe the consequences of IDPN treatment on the specific types.

IV· IN VIVO ELECTROPHYSIOLOGY

To complement the recording of the oculomotor reflexes, I implemented the vestibular turntable with an in vivo electrophysiological wireless set-up. The overall goal was to record head direction cells in the thalamus simultaneously with eye movements in order to compare the neural coding with either the head position or the eye. To do so, tetrodes had to be implanted in the subcortical regions of the mice and electrophysiological signals had to be analyzed offline. While no head direction was properly recorded, *in vivo* electrophysiology recordings will be implemented in further experiments (see “Perspectives”).

i· Tetrode fabrication

A total of 4 tetrodes were implanted chronically, and the 16 electrodes were lowered in the region of interest by a microdrive (MDR-01M1, Axona). The tetrodes were made of an insulated 17µm diameter core platinium-iridium that is cut to an appropriate length (20cm) and then folded twice to form a bundle of four wires. That bundle was placed in a motorized Tetrode Twister to insure proper torsion, with 40 clockwise

rotations. Once properly twisted, a heating gun was used at 160° on the end of the newly formed tetrode to fuse the wires together. The tetrode was removed from the Twister, and the four branches were exposed and inserted into the canula of the microdrive.

To connect the electrodes to the recording device (W16 HS, Multi-Channel System), a nano-miniature connector (A79044-001, Omnetics) was fastened on the Microdrive with dental acrylic (Dentalon Plus, Heraeus). Each electrode was connected to one wire of the omnetic connector until the 16 electrodes were connected with 16 wires, each connection covered with silver conductive paint (Electrolube, HK Wentworth Limited). Two other wires from the connector would be later used as the reference electrode and ground. After each tetrode was inserted in the canula, its impedance was calculated in a saline solution with the NanoZ device (Neuro Nexus Technologies) to verify the quality of the connection. When each electrode was properly connected, both the tetrodes and the wires from the Omnetics were covered with nail polish to secure the ensemble. Once the polish was dried, the tetrodes were cut to an appropriate length (4mm for the antero-dorsal thalamic nucleus, 6mm for the vestibular nuclei) and the impedance was further reduced with a gold plating solution until the typical final impedance values ranged from 150 to 350kOhm.

ii· Craniotomy and Microdrive implantation surgery

The mouse was anaesthetized with isoflurane (2%) after an injection of buprenorphine half an hour before the induction of the anaesthesia. The mouse was placed on a stereotaxic frame and the head was shaved. As the surgery took more than an hour, the mouse was placed on a warming pad to ensure proper body temperature during the anaesthesia. The eyes were covered with ophthalmic gel to avoid dryness. The head was sterilized with an antiseptic solution and lidocaine hydrochloride was injected under the skin of the head. The skull was then exposed from between the eye to the end of the cranial bone. The skull was cleaned with a saline solution and the

muscles on the back of the skull were slightly pushed back to make room for the headpost apparatus. Bregma and lambda were aligned and the anteroposterior and mediolateral position of the region of interest were used to proceed to a craniotomy with a 0,5mm drill above the ROI. The hole had a final diameter of 1mm to fit the canula containing the tetrodes. The dura was gently removed to allow passage for the electrodes. It was important to avoid unnecessary bleeding that could coagulate and block the electrodes. The microdrive and its attached connectors and tetrodes were lowered straight into the brain until the tetrodes were in the brain, above the region of interest. Vasoline was applied around the tetrodes to protect them and seal the craniotomy. The microdrive was glued to the skull (C&B Metabond, Sun Medical CO, LTD). Two other craniotomies of a lesser diameter were performed on the skull of the mouse: one to implant the reference electrode in the cortex, and the other to insert a small screw in the cranial bone to which the ground reference was connected with silver conductive paint. Dental acrylic was used to cover the ground and the reference electrodes, as well as the bottom part of the Microdrive and to secure the ensemble on the skull. At the back of the skull, the headpost used to maintain the mouse head-fixed was glued then secured with dental acrylic. The skin of the initial incision was glued using Vetbond (3M) around the Microdrive to ensure no loose skin will drop unto the eyes. The mouse recovered under red light to avoid hypothermia with softened food and housed one mouse in a cage.

iii· Recording sessions

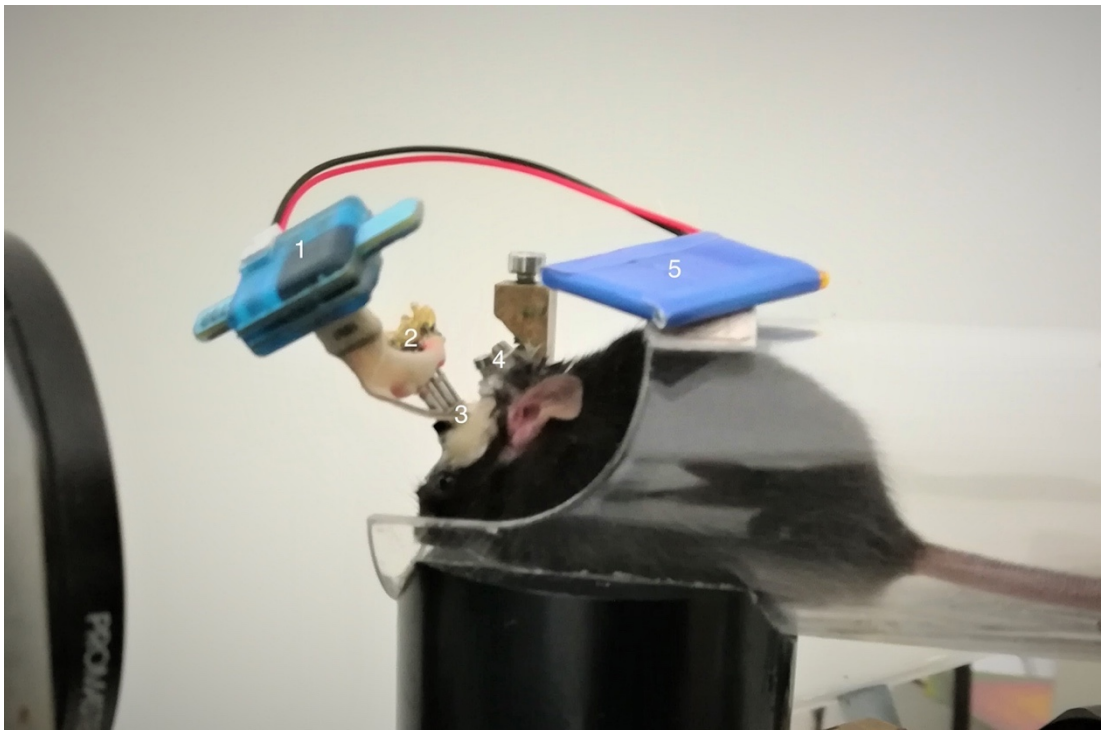

Figure 22: *In vivo* electrophysiological recording in a head-fixed and awake mouse. 1) 16 channels wireless head stage 2) the 4 tetrodes connected to the omnetics connector 3) Microdrive 4) headpost 5) battery of the head stage.

The mouse was held head-fixed in a plexiglass tube on the vestibular turntable and the left eye movements were tracked by video-oculography and transmitted to the Spike 2 software (see **Figure 22**). Electrophysiological signals were acquired continuously at 20kHz with a Multi-Channel System Wireless 16-channels headstage. Signals were online filtered with a 300Hz high pass filter, a 5kHz low pass filter and a Notch filter at 50Hz. TTL pulses were digitally sent from the Spike2 software to the electrophysiological signals recording software to synchronize the electrophysiological, eye and head signals. To record head direction cells, I used a trajectory that explored 450° (270° clockwise and 180° counterclockwise) with changing velocities up to 50°/s. This trajectory was used in two conditions: in the dark or in the light.

iv· Offline analysis

Electrophysiological signals were analyzed offline with the Tridesclous pipeline on Python. Tridesclous is a recent free Python using software that was developed to do automated spike sorting (Garcia and Pouzat, 2015). Tetrodes were analyzed together and clusters of neurons were selected based on the pruning shears method and then manually curated. Time stamps of each spike of each cluster were exported and then compared to the position of the mouse head exported by Spike 2 software. A python-based script was used to plot spike time with its corresponding angle in order to create polar-plots of the neuron's spiking activity.

「 · CHAPITRE 3 · 」

― RESULTS ―

ARTICLE 1 - Long term visuo-vestibular mismatch in freely behaving mice differentially affects gaze stabilizing reflexes.

This project is based on a VOR adaptation by using a visual-vestibular perturbation, the effectiveness of which has already been proven and published by our group.

Indeed, Carcaud and colleagues have set up this protocol to study the long-term adaptation mechanisms of the VOR (Carcaud et al, 2017). To this end, a helmet-like device with black stripes was used to reproduce conventional gain-down VOR adaptations for a long period of time by consistently inducing visuo-vestibular mismatch for 14 days. The VOR tested after the removal of the VVM device was reduced by 50% at all tested frequencies, proving the effectiveness of this new method similarly to a gain-down VOR adaptation induced during passive movements over long training periods. The cellular mechanisms in the brainstem associated with the observed decrease in VOR gain are also investigated. The VVM protocol leads to a decrease in the efficacy of the synapses between the vestibular nerve and the MVN neurons as shown by the reduction of the excitatory postsynaptic current (EPSC) in VVM mice after stimulation of the vestibular nerve. Moreover, MVN neurons can be classified following electrophysiological studies into two categories: type A and type B neurons which differ in properties and projections (Beraneck and Idoux, 2012). VVM-induced adaptation leads to altered excitability of type A specifically. To sum up this work, the VVM protocol used for the first time in mice by our group induces a VOR gain decreases as a result of a long-term adaptation that is consolidated in the brainstem.

The VVM protocol was also used in a study investigating motion sickness in mice and its consequences on the vestibular system through vestibulo-related reflexes (Idoux et al, 2018). After inducing motion sickness, the vestibular sensitivity is altered as the

VOR gain was decreased. The VVM protocol was also used for 14 days and through it decreased (as seen in Carcaud et al, 2017) the VOR gain, the induction of motion sickness did not decrease further the VOR. Indeed, the visual perturbation had a similar effect to anti-motion sickness drugs on the vestibular function, maybe by reducing the vestibular system sensitivity.

The VVM was further optimized in Barros et al, 2019 in regards to the weight of the VVM apparatus on the mouse head.

However, several questions remained quite unclear after the previous studies. Notably, the effect of the VVM protocol on the optokinetic reflex was only investigated at one constant velocity. As such, we proceed to test the VOR and OKR before and after the VVM adaptation for different frequencies to observe if the protocol had an effect on the OKR and how it would compare to the decrease observed in the VOR. We confirmed the adaptation-induced VOR decrease as well as an OKR loss that however, did not reach the same amplitude as the VOR.

We also considered the persistency of the adaptation on both reflexes by testing the gaze stabilization reflexes on the day of the removal of the device (as previously done by Carcaud et al, 2017 and Barros et al, 2019), but also on day 1, day 2 and day 6. We observed a reflex-specific persistence of the adaptation as the VOR is affected longer than the OKR, 2 days for the VOR and one day for the OKR. Furthermore, we found that the reflexes were differentially affected at lower frequencies, with larger reductions and tenacity compared to higher frequencies.

Moreover, the influence of visual inputs during the VVM that can be described mainly as a visual perturbation was further investigated by using two sets of VVM devices. One was similar to the one used previously, with high-contrast black stripes inducing retinal slip during movements, while the other was deprived of stripes and thus elicited little to no retinal slip. However, we observed similar dynamics in both VOR and OKR decrease and recovery, as the lack of visual inputs seems to mainly drive the VVM adaptation.

In conclusion, following a long-term visuo-vestibulo mismatch protocol, the VOR is more severely decreased than the OKR and recovers with a longer delay. However, both reflexes presented a frequency-specific adaptation and recovery for lower frequencies.

scientific reports

Check for updates

OPEN

Long term visuo-vestibular mismatch in freely behaving mice differentially affects gaze stabilizing reflexes

Filipa França de Barros✉, Louise Schenberg, Michele Tagliabue & Mathieu Beraneck✉

The vestibulo-ocular reflex (VOR) and the optokinetic reflex (OKR) work synergistically to stabilize gaze in response to head movements. We previously demonstrated that a 14-day visuo-vestibular mismatch (VVM) protocol applied in freely behaving mice decreased the VOR gain. Here, we show for the first time that the OKR gain is also reduced and report on the recovery dynamics of both VOR and OKR after the end of the VVM protocol. Using sinusoidally-modulated stimulations, the decreases in VOR and OKR were found to be frequency-selective with larger reductions for frequencies < 0.5 Hz. Constant-velocity OKR stimulation tests demonstrated that the persistent components of the OKR were not modified while the transient, initial responses were. To identify the signals driving VOR and OKR reductions, we compared the responses of mice exposed to a high-contrast and no-contrast VVM. Despite being more robust in the high-contrast conditions, reductions were largely comparable and recovered with a similar time course. An analysis that directly compared VOR and OKR responses revealed that, alterations in the VOR were of significantly larger amplitude with significantly slower dynamics of recovery. Our findings are evidence for a frequency-selective influence of visual signals in the tuning of gaze stabilizing reflexes in normal mice.

During everyday life, natural head movements in mammals cover a large range of frequencies and velocities[1–3]. To avoid blurry vision, image displacements on the retina are minimized by compensatory eye movements. These eye-in-space movements are referred to as gaze stabilization eye movements, which result from the transformation of sensory signals into extraocular motor commands[4]. Vertebrates possess two gaze stabilizing reflexes -the optokinetic reflex (OKR) and the vestibulo-ocular reflex (VOR)—that act synergistically to compensate for environmental and self-movements. The OKR responses rely on direction-selective retinal ganglion cells that are efficient for relatively slow motions of the visual scene (± 3°/s in mice)[5,6]. Consequently, the OKR gain is inversely proportional to the velocity of the visual stimulus[7]. On the other hand, the vestibular acceleration-sensitive neurons responsible for VOR are more sensitive to mid-to-high frequency range head motions[8]. In addition, the OKR can respond to constant-velocity visual motions while the vestibular system encodes only non-constant, transient head velocities[6]. The optokinetic and vestibulo-ocular reflexes are therefore functionally complementary, their combination enables efficient gaze stabilization and allows to discriminate self-generated from externally imposed movements in most naturally encountered situations.

The VOR works as an open-loop system[9,10]: it is completely functional in the dark, i.e., inner ear vestibular signals generate compensatory eye movements even in the absence of visual feedback. In rodents, the initial development of the VOR relies on the early maturation of the vestibular circuitry even before eye-opening (P12-14)[11–14]. Nevertheless, visual inputs are critical for the development and proper functioning of VOR: its fine-tuning depends on the visual feedback that informs on the efficacy of the compensatory eye movements. In the absence of vision, such as in congenitally or adventitiously blind people, the VOR is impaired[15]. The gain of the vestibulo-ocular reflex improves after the opening of the eyes in mice, while the phase shifts toward smaller phase leads[9]. In addition, vision critically influences the time constant of the velocity storage[16], the development of vestibular nuclei neurons[17] and the acquisition of their plastic properties[14,18,19].

We recently reported a visuo-vestibular mismatch (VVM) protocol which consists in a high-contrast patterned device wore by the animal for 14 consecutive days while freely behaving in its cage[20]. Using this VVM, we demonstrated in adult mice that the long-term visual perturbation leads to neural modifications in the direct

Integrative Neuroscience and Cognition Center, CNRS, Université de Paris, 75006 Paris, France. ✉email: filipa.barros@parisdescartes.fr; mathieu.beraneck@u-paris.fr

vestibulo-ocular pathway[21]. Specifically, VVM led to a drastic reduction of the VOR, associated with changes in the efficacy at the synapse between vestibular afferents and medial vestibular neurons as well as modifications of the intrinsic properties of a subpopulation of central vestibular neurons[21].

Nevertheless, our previous study let several questions unanswered. First, it remains unclear which neural signals (*e.g.* oculomotor error/retinal slip)[22–24] drive VVM plasticity. To answer to this question in the present study mice were tested either with a high- or no-contrast VVM device. If the retinal slip is among the signals driving plasticity, we expect different VOR gain reduction in the 2 conditions. Second, whether the changes in the VOR are paralleled with changes in the OKR remains elusive. To better understand the interplay between VOR and OKR, both reflexes were measured throughout the protocol. Lastly, few studies have explored the capacity of the VOR to recover following alteration in mice[25]. To determine how VOR and/or OKR recover after VVM, the gaze stabilizing reflexes were measured before the VVM protocol, right after its conclusion, and until recovery to pre-VVM levels.

Results

Effect of the visuo-vestibular mismatch and recovery of the vestibulo-ocular reflex. To measure the effect of each device (Fig. 1a; see "Methods") on the VOR response, video-oculography was performed in darkness using sinusoidal turntable rotations (Fig. 1b). Figure 1c shows examples of the oculomotor response of mice of each of the three groups the day the device was removed (day 0, after 14 days of visuo-vestibular mismatch), during a 0.5 Hz stimulation at a fixed peak velocity of 30°/s. A striking difference can be qualitatively observed between the amplitude of the eye movements of Sham mice (n = 8) compared to No-pattern (n = 16) and Pattern (n = 15) mice, with smaller compensatory eye oscillation for the latter. Figure 1d quantitatively illustrates the evolution over time of the mean gain of the VOR for the three groups, which results in a statistically significant interaction between the effect of the tested *Day* and of the *VVM group* (repeated measures ANOVA, *Day* × *VVM group interaction effect:* $F_{8,108} = 5.33$, $p < 10^{-4}$). As expected, before the visuo-vestibular mismatch the gain of the reflex was the same for the three groups of mice, and the Sham group did not show significant modulations over the whole duration of the protocol. On the other hand, at day 0, Pattern and No-pattern groups showed a significant decrease of the VOR gain and both had significantly lower gains than Sham (Newman–Keuls post-hoc test: at day 0 Sham vs Pattern, $p < 10^{-4}$; Sham vs No-pattern, $p < 10^{-4}$). At day 1, the gain of both Pattern and No-pattern groups had significantly recovered with respect to day 0 (Newman–Keuls post-hoc test: day 0 vs day 1, No-pattern, $p = 0.0002$; Pattern, $p = 0.0004$), but still showed significant differences compared to Sham (Newman-Keuls post-hoc test: at day 1, Sham vs Pattern, $p < 10^{-4}$; Sham vs No-pattern, $p = 0.019$). From day 2 on, there was no significant difference between the VOR gain of the three *VVM groups*.

To determine whether the effect of the Pattern and No-pattern protocols on the VOR is modulated by the frequency of the stimulation, the VOR gain (Fig. 1e) and phase (Fig. 1f) are illustrated as bode plots for each test day. Frequency specific effects were revealed by the significant statistical interactions between the effects of the *Day*, *VVM group* and *stimulation Frequency*, on both the gain and the phase of the VOR (repeated measures ANOVA, *Day x VVM group x stimulation Frequency interaction effect*, Gain: $F_{24,324} = 1.92$, $p = 0.007$; Phase: $F_{24,300} = 5.05$, $p < 10^{-5}$). More precisely, at day 0 the VOR gain of the Pattern and No-pattern groups dropped significantly compared to Sham (Fig. 1e) for all tested frequencies (Newman–Keuls post-hoc test, at day0 Sham vs Pattern at 0.2 Hz, $p = 0.0002$; at 0.5 Hz, 1 Hz and 2 Hz, all $p < 10^{-4}$; Sham vs No-Pattern at 0.2 Hz, $p = 0.0005$; 0.5 Hz and 1 Hz, $p < 10^{-4}$; at 2 Hz, $p = 0.007$). On day 1 the VOR gain of the Pattern group remained significantly reduced (Newman–Keuls post-hoc test, at day1 Sham vs Pattern at 0.2 Hz, $p = 0.0014$; 0.5 Hz, $p = 0.0003$; 1 Hz, $p = 0.002$; 2 Hz, $p = 0.0006$) whilst for the No-pattern group only the lowest frequencies (0.2 and 0.5 Hz) remained significantly reduced (Newman–Keuls post-hoc test, at day1, Sham vs No-pattern at 0.2 Hz, $p = 0.0177$; at 0.5 Hz, $p = 0.0026$).

On day 2 only the Pattern group VOR gain at 0.5 Hz is still different from the Sham (Newman–Keuls post-hoc test, at day2 Sham vs Pattern at 0.5 Hz, $p = 0.0049$). At day 6 significant differences can no longer be detected between the three VVM groups. Regarding the phase, Fig. 1f shows that the VVM had an effect only at day 0 and this effect is opposite for the low and high frequencies: greater phase lag at 0.2 Hz (Newman–Keuls post-hoc test, at day0: Sham vs No-pattern at 0.2 Hz, $p < 10^{-4}$; Sham vs Pattern at 0.2 Hz, $p < 10^{-4}$) and greater phase leads at 1 and 2 Hz (Newman–Keuls post-hoc test, at day0: Sham vs No-pattern and Sham vs Pattern at: 1 Hz and 2 Hz, all $p < 10^{-4}$).

Overall, these results suggest that the VOR responses of the Pattern and No-pattern groups recovered a regular timing (phase) faster than an adequate amplitude of response (gain). Moreover, there were only limited differences in the gain reductions and recovery dynamics of the VOR responses between the Pattern and No-pattern groups. These results suggest that the high-contrast visual input of the Pattern device did not substantially influence the processes triggered by the visuo-vestibular mismatch.

Effect of the VVM and recovery during sinusoidal optokinetic stimulation. To investigate whether the visuo-vestibular mismatch affects the optokinetic reflex in the frequency domain, animals were first tested using sinusoidal rotations of a dotted pattern (Fig. 2a) at a fixed peak speed of 10°/s and at different frequencies in range 0.2–1 Hz. In response to sinusoidal oscillations of the dotted pattern, all mice responded with slow phases that smoothly tracked the visual stimulation (Fig. 2b). On day 0, a decrease in the amplitude of the eye movements was observed for No-pattern (n = 8) and Pattern (n = 12) groups, when compared to Sham (n = 6) (compare traces on Fig. 2b). Figure 2c illustrates for all VVM groups the global tendency for OKR gain changes along the tested days (repeated measures ANOVA, *Day x VVM group,* $F_{6,69} = 2.2$, $p = 0.053$). On day 0, the Pattern and No-pattern groups had a significantly diminished OKR gain (Newman-Keuls post-hoc test, at day0 Sham vs Pattern $p = 0.0294$; Sham vs No-pattern, $p = 0.0046$). On day 1, both Pattern and No-pattern groups showed

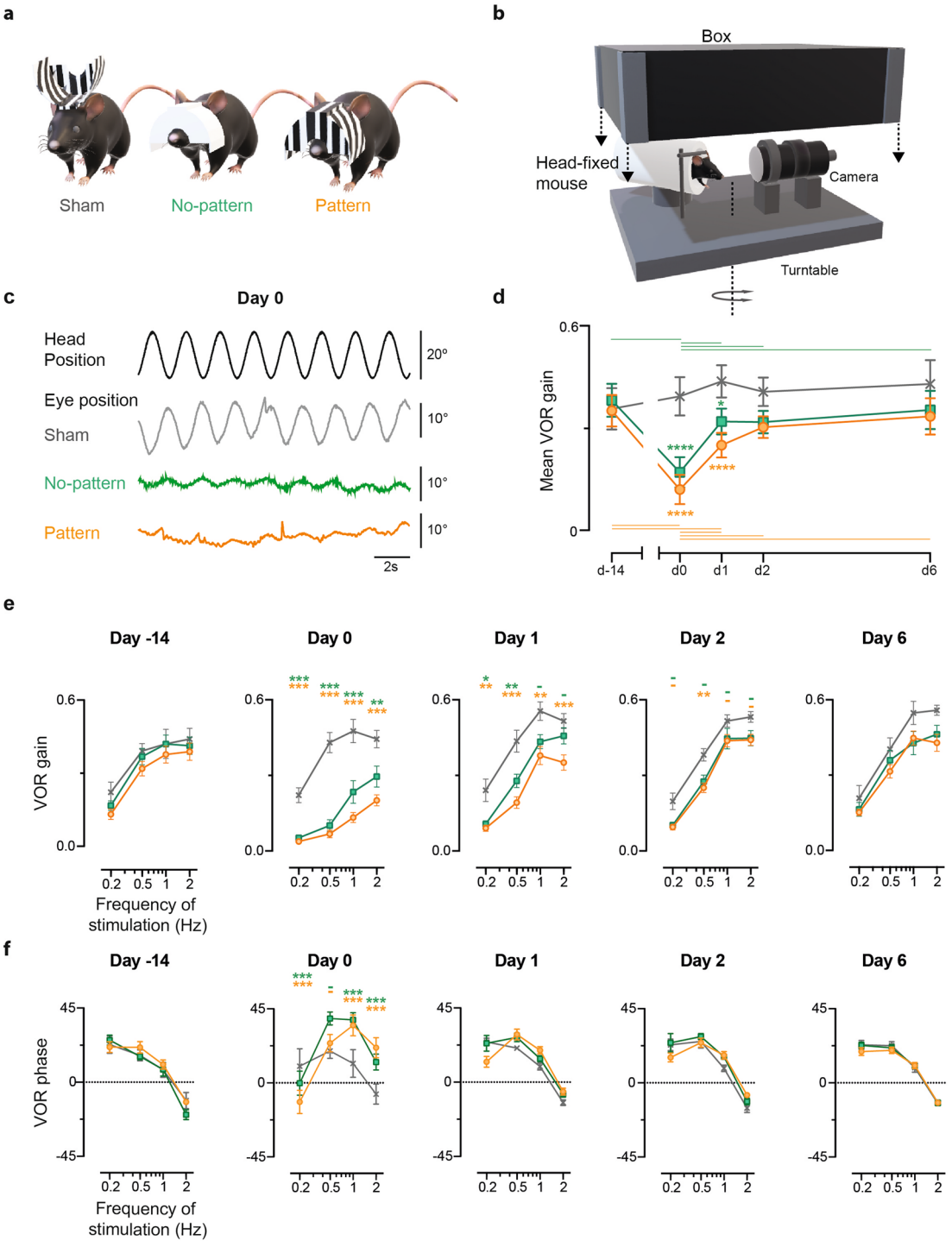

Figure 1. Effects of the VVM on the VOR. (**a**) Representation of mice wearing the three different types of devices used in the protocol; Pattern (left), No-pattern (middle) and Sham (right). (**b**) Depiction of the set-up to test VOR; the mouse is head-fixed and secured in a plexiglas tube during horizontal rotations of the turntable at a fixed peak velocity (30°/s) and variable frequencies (0.2-2 Hz). 3D renderings (a and b) were obtained using Paint 3D (Microsoft Corporation). (**c**) Example raw traces of VOR responses recorded on day 0 at 0,5 Hz for Sham (grey), No-pattern (green) and Pattern (orange). Head rotations in the dark evoked compensatory eye movements in the opposite direction. VVM-exposed mice showed altered eye movements. (**d**) Sham (n = 8), No-pattern (n = 16) and Pattern (n = 15) mean VOR gain along the entire protocol (20 days). The mean VOR (**e**) gain and (**f**) phase are at all tested days are plotted for the different frequencies of stimulation. The significance of the gain and phase changes compared to Sham are indicated next to each point in the graph. Horizontal lines represent intra-group significant differences between the tested days. Error bars represent ± SEM; Newman Keuls post-hoc test $^{*}p < 0.05$; $^{**}p < 0.01$; $^{***}p < 10^{-3}$.

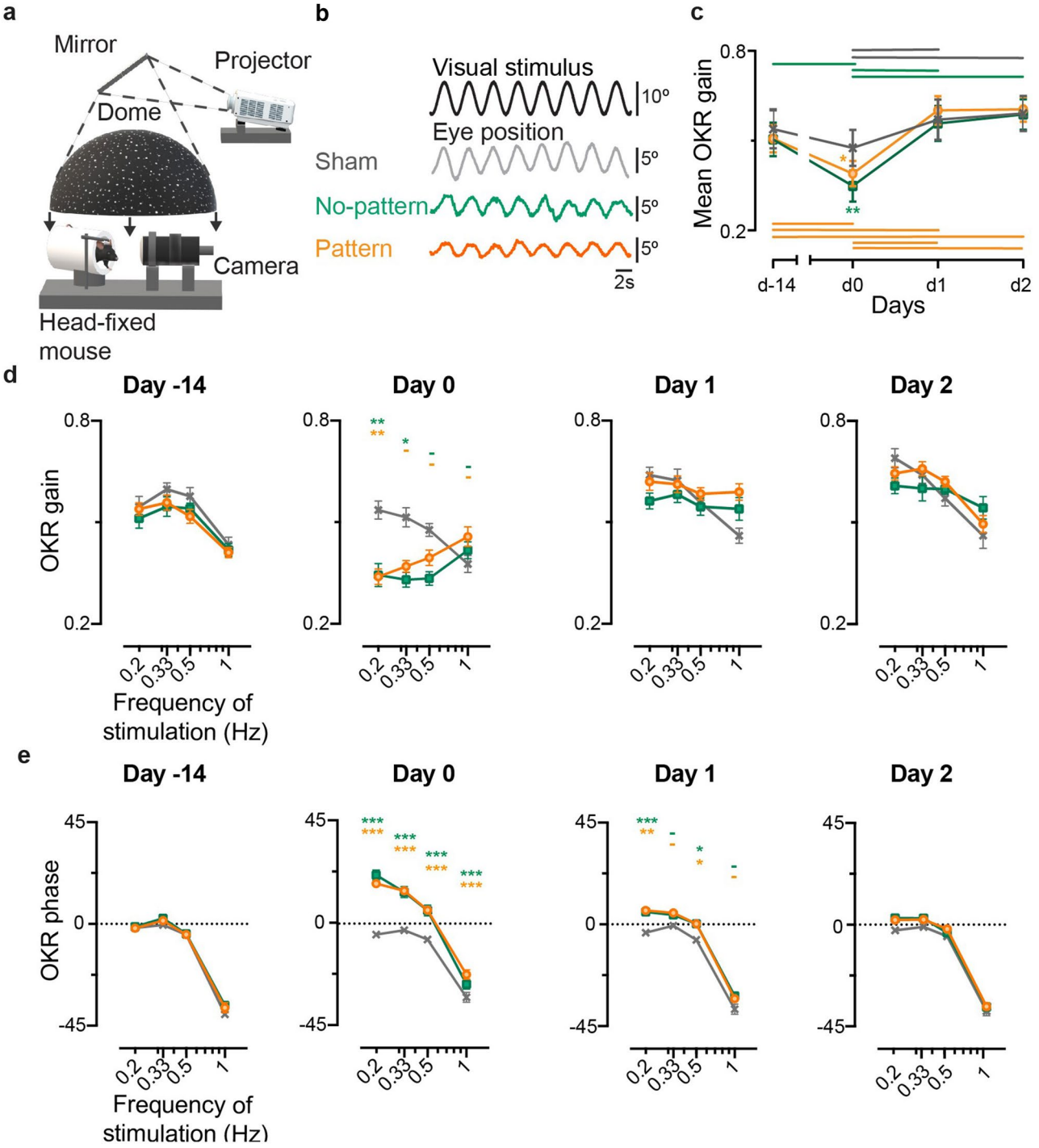

Figure 2. Effects of the VVM on OKR. (**a**) Representation of the set-up used to test OKR. A dotted background was projected into a mirror while the mouse was kept head-fixed. 3D model obtained using Paint 3D (Microsoft Corporation). (**b**) Example raw traces of the OKR response to a stimulation at 0.33 Hz at peak velocity of 10°/s for each condition; Sham (grey), No-pattern (green) and Pattern (orange). The eye position smoothly follows the optokinetic stimulus. (**c**) Kinematics of the mean OKR gain of Sham (n = 6), No-pattern (n = 8) and Pattern (n = 12) during the tested days. Horizontal lines represent intra-group significant differences between the tested days. OKR gain (**d**) and phase (**e**) at each of the different frequencies tested along each day. The significance of both gain and phase are indicated on top of each point in the graph for No-pattern (first line, green) and Pattern (second line, orange). Error bars represent ± SEM; Newman Keuls post-hoc test $^{*}p < 0.05$; $^{**}p < 0.01$; $^{***}p < 10^{-3}$.

a significant OKR gain recovery (Newman-Keuls post-hoc test, day0 vs day1: No-pattern, $p = 0.0001$; Pattern, $p = 0.0002$), resulting in no differences between the three groups from day 1 onwards.

To investigate if the alteration of the OKR response was dependent on the frequency tested, the gain (Fig. 2d) and phase (Fig. 2e) were plotted as a function of the stimulation frequency for each day. Frequency-specific effects were revealed by the significant statistical interactions between the effects of the *Day*, *VVM group* and *stimulation Frequency*, on both the gain and the phase of the OKR (repeated measures ANOVA, *Day x VVM group x stimulation Frequency interaction effect*, Gain: $F_{18,207} = 2.6288$, $p = 0.0005$; Phase: $F_{18,207} = 3.2987$, $p < 10^{-4}$). Figure 2d shows that the above-mentioned effect at day 0 is mainly due to a reduction of the OKR gain for stimulations at the lowest tested frequencies (0.2 Hz and 0.33 Hz) (Newman-Keuls post-hoc test, at day 0 Sham vs Pattern at 0.2 Hz: $p = 0.006$; Sham vs No-pattern at 0.2 Hz: $p = 0.0015$; at 0.33 Hz: $p = 0.0146$). On this day, a significant phase shift towards a greater phase lead was also observed across all stimulation *Frequencies* for both Pattern and No-pattern groups (Newman–Keuls post-hoc test, day0, Sham vs Pattern at all frequencies: $p < 10^{-4}$; Sham vs No-pattern at 0.2 Hz, 0.33 and 0.5 Hz: $p < 10^{-4}$; at 1 Hz: $p = 0.0078$). On day 1, for all frequencies the OKR gain of both Pattern and No-pattern groups was no longer different from the Sham group. However, the timing of the OKR responses was still affected on Pattern and No-pattern groups, with remaining significant differences between these groups and Sham at 0.2 and 0.5 Hz (Newman–Keuls post-hoc test, day1, Sham vs Pattern at 0.2 Hz: $p = 0.0001$; at 0.5 Hz: $p = 0.0296$; Sham vs No-pattern at 0.2 Hz: $p = 0.0004$; at 0.5 Hz: $p = 0.0282$;). At day 2, both gain and phase had completely recovered, and no further differences were found between the three *groups*.

In conclusion, sinusoidal stimulations at different frequencies showed that significant gain and phase changes occurred in the OKR pathway following the VVM protocols. However, the reduction of the OKR responses appeared to last no more than one day and to predominantly affect the responses to low stimulation frequencies.

Effect of the VVM in response to constant velocity optokinetic stimulation. To further investigate how the optokinetic response is affected by the visuo-vestibular mismatch protocol, we also tested on another group of mice the OKR using long-lasting (60 s) full-field stimulations at constant velocities of 2.5, 5, 7.5 and 10°/s. Mice responded to the OKR stimulations with nystagmus-like responses consisting in series of slow phases in the direction of the stimulus, interrupted by quick-phases that recenter the eye in its orbit. Figure 3a displays example raw traces at day 0 at a velocity of 7.5°/s and Temporo-Nasal direction for Sham (n = 8), No-pattern (n = 16) and Pattern (n = 15) groups. Throughout each 60 s-long stimulation, the slow phases evoked were characterized by their number, amplitude and duration (at day 0, see Supplementary Fig. S1). For all groups, the number of slow phases significantly increased as a function of the stimulus velocity while their duration decreased (repeated measures ANOVA, *Velocity* effect, Number: $F_{3,90} = 31.886$, $p < 10^{-4}$; Duration: $F_{3,93} = 26.846$, $p < 10^{-4}$). No significant differences were found between the number and duration of slow phases between the three groups (repeated measures ANOVA, *VVM group* effect, Number: $F_{2,30} = 1.3783$, $p = 0.27$; Duration: $F_{2,31} = 3.0007$, $p = 0.065$). The amplitude of the slow phases also significantly increased with the stimulus velocity (repeated measures ANOVA, *Velocity* effect, Amplitude: $F_{3,93} = 13.648$, $p < 10^{-4}$). However, the amplitude of the slow phases was significantly different between Sham and Pattern groups (repeated measures ANOVA, *VVM group* effect, Amplitude: $F_{2.31} = 5.4568$, $p = 0.0093$; Newman–Keuls post-hoc test, day0, Sham vs Pattern $p = 0.0096$).

The dynamics of the OKR response are illustrated on Fig. 3b; each line presents the gains of the slow phases performed, per mouse, along the stimulation at 7.5°/s at day-14, day0 and day1. As previously described in the mouse[26–28], before the VVM protocol (day-14), the intensity of the optokinetic responses decreased over time during the 60 s duration of the optokinetic stimulation. This dynamic was quantified by comparing the mean gain of the first slow phase evoked after stimulus onset and the gain of the last slow phase evoked for all the different stimulations (2.5–10°/s) tested (Fig. 3c). There was a significant interaction between the *VVM Groups*, *Day* and *Component* (repeated measures ANOVA, *Day x VVM group x Component interaction effect*, Gain: $F_{6,90} = 4.6741$, $p = 0.0035$). Before the VVM (day-14), the mean gain of the first slow phases was significantly higher than the mean gain of the last slow phases for all the tested groups (Fig. 3c, day-14, Newman–Keuls post-hoc test, Sham, $p = 0.0002$; Pattern, $p = 0.0002$; No-pattern, $p = 0.0013$). At day 0, while this dynamic was unchanged in the Sham group, the response of Pattern and No-pattern groups showed rather different profiles. Specifically, the gain of the first slow phase was significantly reduced (day 0, Newman–Keuls post-hoc test; Sham vs Pattern, $p = 0.0002$; Sham vs No-pattern, $p = 0.0008$) while the gain of the last slow phase was not. At day 1, the mean gain of the first slow phases had mostly recovered for both Pattern and No-pattern groups (Newman–Keuls post-hoc test, day1, Sham vs Pattern, $p = 0.3802$; Sham vs No-pattern, $p = 0.3399$). However, the dynamic of their response was not yet back to normal (no significant decrease between first and last slow phase; Newman–Keuls post-hoc test, day1, First slow phase vs Last slow phase: Pattern, $p = 0.0754$; No-pattern, $p = 0.0746$). All these parameters had fully recovered on day 2.

Overall, the modifications of OKR responses observed during constant-velocity stimulation suggest that it was the transient, initial component of the OKR that was mostly affected by the visuo-vestibular mismatch, while the sustained, late component was not.

Comparison between VOR and OKR gain changes as a result of the VVM protocol. Results presented so far demonstrate that 2 weeks of visuo-vestibular mismatch led to a significant alteration of the vestibulo-ocular reflex (Fig. 1) which recovered in about 2 days, while alteration of optokinetic reflex recovered in about 1 day (Fig. 2). Overall, the general effects were similar between Pattern and No-pattern mice. In order to directly compare the dynamics and magnitude of the changes in VOR and OKR while taking into account the non-specific effects, for each stimulation modality and day, we subtracted the mean responses of the Sham (VOR n = 8; OKR n = 6) group from those of the No-pattern (VOR n = 16; OKR n = 8) and Pattern (VOR n = 15; OKR

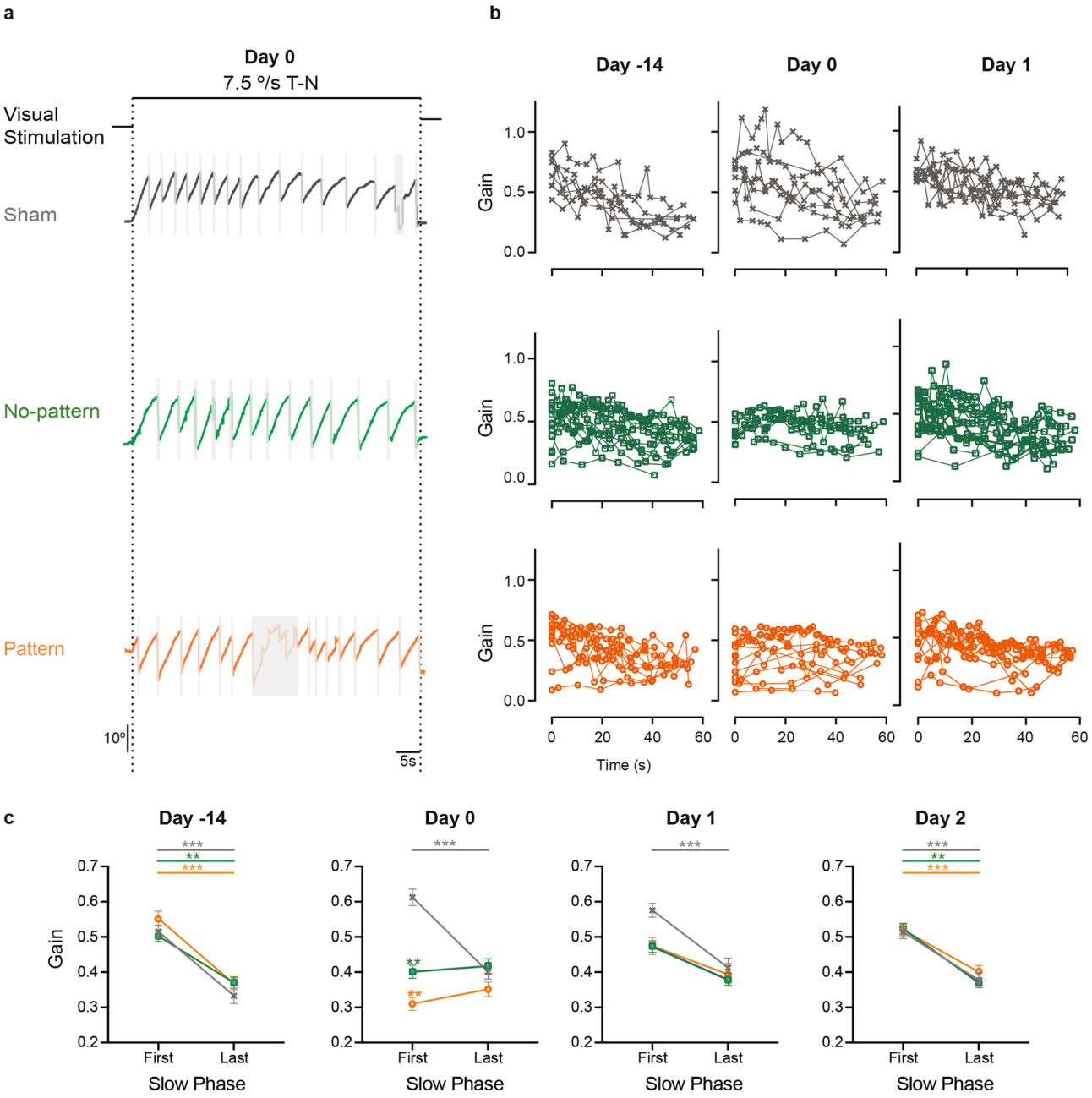

Figure 3. Effects of the VVM on OKR nystagmus. (**a**) Example raw traces for each group (Sham n = 8, grey; No-pattern n = 16, green; Pattern n = 15, orange) of the OKR response to the 60 s-long stimulation at 7.5°/s in temporo-nasal direction (black line). The grey rectangles mark the segments that were not considered in the analysis of the eye movements (quick phases or recording artefacts). Only slow phases were computed to characterize the response over the duration of the visual stimulation. (**b**) To illustrate the dynamic of responses over the stimulation period, the individual slow phases gains were plotted over time for 7.5°/s constant velocity stimulation in temporo-nasal direction. In the VVM-treated groups, the first response after stimulus onset (the first slow phase), appears lower after the VVM protocol. To quantify this difference, the gains of the first and last slow phases in response to all velocities and directions were averaged (**c**). When computed, the difference between the first and last SP gains reveals that before the VVM, the three groups had similar first and last gains while, on day 0, VVM-treated groups had lower first slow phase gains. On day 1, these gains have increased and at day 2, they are identical to Sham. The significant differences compared to Sham are indicated on top of each point in the graphs for No-pattern (green asterisks) and Pattern (orange asterisks) groups, respectively. Error bars represent ± SEM; Newman Keuls post-hoc test $^{*}p < 0.05$; $^{**}p < 0.01$; $^{***}p < 10^{-3}$.

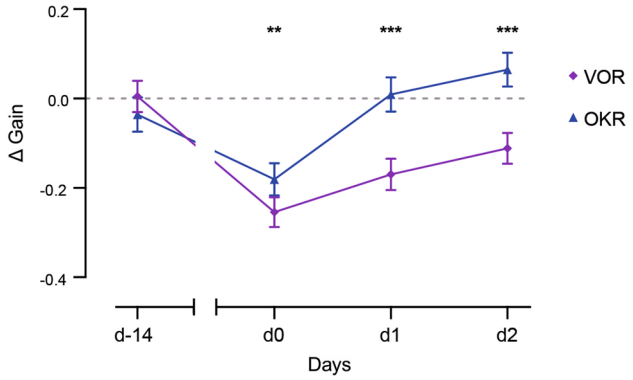

Figure 4. Comparison of the amplitude and dynamics of VOR and OKR gain changes over time. Global gain changes in VOR (purple diamonds) and OKR (blue triangles) over time were compared by subtracting the mean responses of the Sham group from those of the VVM-exposed mice (ΔGain). Differences between VOR and OKR responses of both VVM-exposed groups are represented with black asterisks. Error bars represent ± SEM; Newman Keuls post-hoc test $*p<0.05$; $**p<0.01$; $***p<10^{-3}$.

n = 12) groups for all tested frequencies (ΔGain; Fig. 4). There was a significant interaction between the *Day*, and *Stimulation modality* (repeated measures ANOVA, *Day x Stimulation modality interaction effect*, $F_{3,117}=23.579$, $p<10^{-4}$). At day-14, ΔGain for both VOR and OKR were, as expected, not different from 0, and not significantly different from each other (Newman–Keuls post-hoc test, d-14: VOR vs OKR, $p=0.1041$). On day 0, day 1 and day 2, the ΔGain magnitude of VOR was significantly larger than the ΔGain for OKR at all tested days (Newman–Keuls post-hoc test, day0: VOR vs OKR $p=0.0014$; day1 and day2: VOR vs OKR, $p<10^{-4}$). The ΔGain of OKR was only significantly smaller than the initial d-14 value at day0 (Newman–Keuls post-hoc test, day-14 vs day0 for OKR: $p=0.0001$); the optokinetic responses were therefore no longer affected after the first day of recovery. On the other hand, the ΔGain of VOR was significantly different from day-14 at day 0 (Newman–Keuls post-hoc test, day-14 vs day0 for VOR, $p=0.0001$), day 1 (day-14 vs day1 for VOR, $p=0.0001$) as well as at day 2 (day-14 vs day2, $p=0.0001$). This shows that, across the tested frequencies, VOR responses of Pattern and No-pattern mice are still abnormally reduced at day 2. Overall, this comparative analysis demonstrates that alteration in the OKR and VOR pathways differ both in terms of amplitude and dynamic of recovery.

Discussion

This study shows a concurrent decrease of VOR and OKR following 14 days of a visuo-vestibular mismatch protocol. This concomitant reduction of OKR and VOR efficacy differs from what was previously reported following short–term (< 3 days) adaptation protocols in studies that also used mice as animal models[9,29]. These short-term VOR gain-down and gain-up adaptation protocols (1/2 h learning, up to 1 h follow-up) showed a moderate but significant increase in the OKR, in line with early reports in the rabbit[30]. It was suggested that, like during optokinetic learning, retinal slip might serve as a learning signal during short-term VOR adaptation[22,31] and lead to potentiation in the optokinetic pathway[9]. Here, we used 2 different devices: one whose surface was completely blank (No-pattern), that would not generate any retinal slip when the eyes move, and another one with a high-contrast (Pattern). Our results show that both devices led to a significant reduction in both OKR and VOR, and no major alterations could be specifically ascribed to one or the other. The Pattern group showed larger VOR gain reductions as well as a slightly longer recovery time, but these differences were not compelling. From these experiments, it is therefore not possible to conclude whether the presence of the Pattern effectively led to a stronger "retinal slip", which would represent an important error-signal driving the adaptation described in short-term protocols[31]. Another possibility would be that the retinal slip generated in the pattern group, and the complete absence of visual sensory feedback in the no-pattern group, would lead to comparable changes in VOR and OKR through completely different mechanisms. Moreover, the calibration of the VOR and OKR not only depends on retinal slip per se, but on the precise matching of different neural signals (e.g., head/eye velocities; relative phase of head vs eye movement[23]), it is therefore possible that the persistent perturbation of other gaze-related signals would be the main determining factor driving the changes observed in both groups.

Since the early 80s, long-term visual impairment protocols have been used in mammals to study the interaction of the vestibular and visual systems for gaze stabilization. The species used in these experiments vary from humans[32] and non-human primates[33,34] to cats[35,36], rabbits[37,38], and more recently, mice[20,21]. The inspiration for our protocol lies in the long-term adaptation experiments conducted in primates, in which the use of telescopic spectacles changed the visuo-vestibular interactions during head-free movements[33,34]. Several features of our results resemble the ones on these preceding studies. First, following a fixed-field protocol (fixed images viewed through lenses, providing a field of view fixed with respect to the head), the VOR in dark was decreased by 60–70% in 3–4 days[33]. The amplitude of this decrease is comparable to the decrease of VOR reported here following the VVM. OKR was also found to decrease by up to 50%, depending on the OKR velocity tested[39]. Specifically, the OKR deficit was positively correlated with velocities and concerned the closed-loop, velocity storage-dependent, pathway, as well as the optokinetic after nystagmus (OKAN) (see below[39]). Notably, comparable results were obtained during experiments in which animals were dark-reared to understand the role of visual

inputs in the development of VOR and/or OKR. In rabbits that were dark-reared for 7 months[37], the gain of the VOR in dark decreased ~ 70% at low frequencies and ~ 50% at high frequencies. The OKR gain also decreased by ~ 30%. OKAN responses were not affected. After 24 h in a normal light, both VOR and OKR increased and kept on improving for the next 3 months but remained permanently suboptimal[37]. In cats dark-reared until adulthood, the VOR in the dark was also found to be decreased by ~ 70%[35]. Again, the OKR was decreased by ~ 25% at low velocities, and even worsened as the velocity of the optokinetic stimulation increased. The velocity-storage dependent responses, including OKAN, were also markedly affected. It is noteworthy that, despite obvious visual and oculomotor differences, the abovementioned animal models confronted with protocols of long-term visual impairments, showed drastic reductions in VOR paralleled by a mild reduction of OKR efficacy. This observation would suggest that the basic mechanisms/circuitries involved are likely shared among mammals. Thus, the mouse model as well as VVM protocol can serve as valuable means to understand the signal-driven calibration of gaze stabilizing pathways.

While the VOR pathway constitutes a 3-neuron direct reflex arc[21], several subcircuits contribute to different features of the optokinetic responses. Two distinct pathways related to different retinal ganglion cells appear, for instance, to manage the initial (transient) and late (sustained) phases of the OKR response[27]. In the following paragraph we discuss the results obtained using the transient sinusoidal and the constant-velocity lasting OKR tests, and their relations to VOR. In response to transient sinusoidal stimulation, we observed a frequency-selective decrease in the OKR responses. This decrease concerned the lowest frequencies tested (below 0.5 Hz). These results mirror the frequency-selective decrease observed in the VOR: at day 0, the larger gain reduction is observed for the lower frequencies tested (0.2 and 0.5 Hz). The VOR phase shift also differs between low (increased phase leads) and high (increased phase lags) frequencies. In the present freely behaving protocol, the visuo-vestibular mismatch mainly occurs in the range of natural head-movements. Previous studies have demonstrated that the mouse head movements produced during home-cage recordings or open-field active exploration are dominated by low frequencies[1,2,21]. The strongest effects observed on OKR and VOR at low frequencies could therefore relate to the statistics of the natural head-movements. Another explanation would be that the VVM mainly alters VOR/OKR in the range where visual information is the dominant sensory input signaling if eye movements are compensatory. Faulstich and colleagues[9] demonstrated that, in mice, OKR and VOR have a mutually complementary working range; the OKR accounts for most of the gaze stabilization at frequencies below 0.5 Hz, while the VOR takes over above 0.5 Hz (mouse[9], see also rabbit[30]). How the frequency-specific changes in OKR and VOR following VVM relates to the timing rules of plasticity in the flocculus[40,41] and to the inter-dependency of these 2 reflexes[42] should be the focus of future dedicated studies. Interestingly, other features of optokinetic response were revealed by the constant-velocity OKR tests. In particular, the gain of the first slow phase measured after stimulus onset was smaller in Pattern and No-Pattern mice compared to Sham (Fig. 3c). As the stimulation continued, the Sham mice OKR response decreased steadily (as previously reported[26–28]) whereas, Pattern and No-Pattern mice exhibited a consistently low response (Fig. 3b) that did not show any additional decrease. A degradation of the transient pathway could explain both the difference between the Pattern/No-Pattern and Sham mice during the sinusoidal stimulation and the loss in the initial OKR long-lasting response. In addition, a similar late OKR response for all mice groups suggests that the persistent pathway would be only marginally affected by the VVM protocol. Another mechanism involved in the response to a constant-velocity and lasting optokinetic stimulation is the velocity storage, which manifests in vertebrates as a build-up in the response during continued high velocity optokinetic stimulation and as a persistency in the response after stimulus offset[43,44]. However, in mice the velocity storage is considered "leaky"[45] and does not generate much after nystagmus response (OKAN)[28,45]. A change affecting the velocity storage could therefore participate to the difference seen in the early, but not late, response to the long-lasting OKR responses. Since the velocity storage mechanism depends on the recruitment of vestibular brainstem circuitry[46–49], whose excitability was shown to be decreased after VVM[42], one hypothesis would be that the VVM impaired the capacity to recruit the brainstem circuitry common to OKR and VOR.

A key point in understanding the dynamic of plasticity of OKR and VOR networks, is the interaction between the cellular mechanisms located in the flocculi and the long-term consolidation of the motor learning in the brainstem[21,50–52]. Jang and colleagues[53] have recently demonstrated that the brainstem consolidation following a gain-up VOR training was dependent on the synergy of synaptic and intrinsic plasticity within Purkinje cells. In the case of an iterated VOR gain-up training, plastic brainstem modifications were reported as the combination of an increase in both the vestibular afferents-central vestibular neurons synapse as well as an increase in the excitability of central vestibular neurons. Notably, this result mirrors the results obtained by Carcaud and colleagues[21] which demonstrated that a VOR gain reduction was accompanied by a decrease of the efficacy of the synapse between the vestibular afferents and the central vestibular neurons, accompanied by a decrease in the excitability of a subpopulation of central vestibular neurons. Collectively, these studies demonstrate that VOR gain modifications depend on synaptic and intrinsic plastic changes in the brainstem.

Overall, the visuo-vestibular mismatch protocol performed in freely behaving mice led to a frequency-specific reduction of the gain of both VOR and OKR. The changes observed in the OKR were of lower intensity and recovered more rapidly than the changes in the VOR. Based on the recent findings on cellular mechanisms associated with learning in gaze stabilization networks, future experiments conducted on mouse and model studies will help to better understand the cellular mechanisms associated with OKR/VOR tuning and their interactions.

Methods

Ethics. A total of 65 male C57/BL6J mice, age 6–10 weeks, was used for the described protocol. Animals were used in accordance with the European Communities Council Directive 2010/63/EU. All efforts were made to minimize suffering and reduce the number of animals included in the study. All procedures were approved by the ethical committee for animal research of the University of Paris (CEEA.34).

Headpost implantation surgery and animal care. Surgical procedures, postoperative care, device fixation and animal surveillance during the protocol were performed as described previously[20,21]. Briefly, mice anesthetized with isoflurane gas had their heads shaved with small clippers. Then, lidocaine hydrochloride (2%; 2 mg/Kg) was injected locally before a longitudinal incision of 1.5 cm was made to expose the skull. Just anterior to the lambda landmark, a small custom-built headpost (3 × 3 × 5mm; poly lactic acid) was cemented (C&B Metabond; Parkell Inc., Edgewood, NY) and laterally covered with resin (Heraeus) for protection. Animals were fully recovered 30 min after the end of the surgery, yet buprenorphine (0.05 mg/kg) was provided for postoperative analgesia and they were closely monitored for the following 48 h.

Long-term visuo-vestibular mismatch protocol. The custom-built devices were secured on top of the mouse headpost for 14 days. The device consisted of a 0.9 g helmet-like structure that completely covered the mouse's head. The front of the device was adapted to the animal's anatomy so that the nose was not covered, and its width allowed for grooming and barbering behaviors. Given its dimensions[20] and small distance to the eye (5 mm), the device completely covers the entire binocular field and monocular horizontal fields of view[54], and most (85%) of the field on the vertical axis. The lower edges of the device are in the part of the visual field that the mouse would normally cover with head movements[55,56] and which is poorly represented in retinotopic space[57]. To preserve light-dependent physiology and nychthemeral rhythm, the device was made of slightly opaque PLA so that the animal could no longer see the surrounding, but still received luminance stimulation. Design and 3D printer specifications of this device were previously detailed[20]. VOR and OKR responses were recorded before the beginning of the VVM protocol. Then, mice were designated to 1 of the 3 visuo-vestibular mismatch devices (Fig. 1a): Sham (n = 14), 'No-pattern' (n = 24) or 'Pattern' (n = 27). 'No-pattern' devices were blank (white PLA color) while 'Pattern' ones had black 3 mm stripes drawn onto their surfaces. These stripes were previously used to create a high-contrast fixed visual signal during self-generated head movements[21]. Sham mice had the device fixed upside-down so that they were exposed to the same procedure except for the visuo-vestibular mismatch[21]. After securing the device into the headpost with a pair of screws, it was ensured that the nose of the mouse was aligned with the center of the device's snout aperture and that no pressure was being directly applied to it.

Animals were housed in groups of 5 composed of at least 1 mouse of each condition. Moistened food and hydrogel were placed on the cage's floor to facilitate feeding on the first two days after the fixation of the device. Mice were left with the implanted devices for 14 days. To ensure their well-being, mice were daily weighted and surveilled. After this two-week period, the device was removed and video-oculography was performed at different timepoints.

Video-oculography recording sessions. Eye movements were recorded with a non-invasive video-oculography system (ETL-200, Iscan; acquisition rate 120 Hz) following the methodology previously described (Stahl et al. 2000). Eye and Image/head position signals were sampled at 1 kHz, digitally recorded (CED power1401 MkII) with Spike 2 software and analyzed off-line in Matlab (Matlab, The MathWorks, Natick, MA, USA; RRID: SCR:001622) programming environment. The experimental set-up (see Figs. 1b and 2a) and methods of data acquisition are akin to those described in[21,58]. In sum, mice were put in a custom-built Plexiglas tube and head-fixed at ~ 30° nose-down position to align the horizontal canals to the yaw plane[59,60]. This restraint assembly was fixed on a rotating platform on top of an extended rig with a servo-controlled motor. Recording sessions were performed in a temperature-controlled room (21 °C) and lasted up to 45 min. To study the effects of the device on the gaze stabilizing reflexes, mice underwent a recording session before (*day-14*) having the device implanted, immediately after its removal (*day0*), 1 (*day1*), 2 (*day2*) and 6 (*day6*) days afterwards. To minimize the exposure to the visual scene, the recording session on *day 0* began immediately after the device was removed in a room with low luminance. Mice were then left in standard lighting and housing conditions.

Vestibulo-ocular reflex tests and analysis. VOR tests were performed with all sources of light turned off except for computer screens. The turntable was surrounded by a black box to isolate the animal from any remaining light, creating a final luminance inside the box of < 0.02 lx (Luxmeter Lux-1337 Iso-tech). To prevent excessive pupil dilatation, pilocarpine 2% was instilled into the eye.

To evaluate the angular vestibulo-ocular reflex, different vestibular stimulations were used. Horizontal vestibulo-ocular reflex (VOR) recordings consisted of sinusoidal angular rotations around the vertical axis at 0.2, 0.5, 1 and 2 Hz at a peak velocity of 30°/s. The angular amplitude of the table movement was adjusted accordingly. At least 10 cycles were analyzed *per* frequency/velocity. The compensatory eye movements were studied by calculating their gain and phase in each condition. Briefly, the gain is the ratio between the response (eye) velocity and stimulus (head) velocity. The phase is the temporal shift between the eye and table rotations, expressed in degrees of the sinusoidal cycle. Detailed VOR gain and phase calculation are reported in[21].

Optokinetic reflex tests and analysis. To record the OKR, head-fixed mice were surrounded by a 40 cm wide dome (see Fig. 2a) and all sources of light were turned off except for the optokinetic stimulus projector.

Optokinetic stimulations consisted in 25,000 white dots (max width 0.075°) randomly distributed on a black background. The light intensity inside the dome during the test was around 185 lx.

Two types of optokinetic stimuli were tested: *sinusoidal* and *constant velocity* stimulations. The *sinusoidal* one allowed a direct comparison with the VOR responses in the frequency domain[9], whilst the classical *constant velocity* stimulation allowed better discriminating between the transient and sustained responses of the OKR[27]. To avoid cross-effects, both the two OKR tests were performed on different groups of mice.

The *optokinetic sinusoidal stimulations* were tested *at different frequencies (0.2; 0.33, 0.5; 1 Hz; peak velocity of 10°/s)* using monocular stimulation. OKR response was expressed as gain and phase determined by least-squares optimization method, similar to the VOR gain and phase[21].

Optokinetic constant velocity (2.5; 5; 7.5; 10°/s) binocular stimulations in alternated clockwise (or naso-temporal (N-T) to the recorded eye) and counterclockwise (or temporo-nasal (T-N) to the recorded eye) directions. On each day, mice were tested during a unique trial in each direction and each velocity, that is a total of 8 different trials/day. The stimulation lasted 60 s and was separated by at least 60 s of darkness. Analysis of the generated optokinetic nystagmus (alternation of slow and quick phases[61]) was performed on the slow phases after automatic removal of the quick phases using a detection threshold set at 50°/s. Slow phases shorter than 1 s were discarded. To study the individual dynamics of slow phases, each was fitted to an exponential curve in order to reduce noise in parameter estimation. The slow phase gain was computed as the ratio between the amplitude of the interpolated eye displacement and the amplitude of the stimulus displacement, on the same time window. The ocular response was analyzed for the entire duration of the stimulation and the gain of the initial and last slow phase was used to describe its transient and persistent components respectively. The mean number, amplitude and duration of the slow phases during the stimulation were also computed.

Statistical analyses. For both VOR and OKR sinusoidal stimulation experiments the effect of the protocol on the reflex gain and phase were statistically tested by performing a mixed-model ANOVA with the *VVM group* (Sham, Pattern and No-pattern) as between-individual independent factor and the Day (d-14, day0, day1, day2, and, for VOR only, day6) and the stimulation *Frequency* (for VOR: 0.2, 0.5, 1, 2 Hz; for OKR 0.2, 0.33, 0.5, 1 Hz) as within-individual independent factors. The main effects of these factors, as well as their interactions, were tested.

For the continuous OKR stimulation a mixed-model ANOVA was used to test the effect and the interaction between the following independent variables: *VVM group* (Sham, Pattern and No-pattern), as between-individual factor, and the *Day* (d-14, day0, day1, day2), stimulation *Velocity* (2.5, 5, 7.5, 10°/s), *Direction* (T-N, N-T) and *Component* [transient (first slow phase) and sustained (last slow phase)] as within-individual independent factors. A mixed-model ANOVA was also used for evaluating the effects of the *VVM group, Velocity* and *Direction* on the number, amplitude and duration of the OKR slow phases at day0.

For the comparison between the OKR and VOR sinusoidal stimulation experiments, for each stimulation modality and for each day, we first subtracted the average gain of the Sham group to those of the Pattern and No-pattern group. Then, we applied a mixed-model ANOVA with the *stimulation modality* (OKR and VOR) as between-individual independent factors and the *Day* (d-14, day0, day1, day2) as within-individual independent factors. For this analysis the mice of Pattern and No-pattern groups were pooled together.

For all analyses the significance threshold was set at $p < 0.05$ and Newman–Keuls post-hoc test was performed whenever a significant main effect or interaction was detected. Data were analyzed using Statistica (StatSoft Inc.) software.

Data availability

The VVM protocol used in this study is explained in detail in the published article[20]. The datasets generated during the current study are available in the Mendeley Data repository, https://dx.doi.org/10.17632/r56jxvyycv.1.

Received: 17 July 2020; Accepted: 26 October 2020
Published online: 18 November 2020

References

1. Beraneck, M., McKee, J. L., Aleisa, M. & Cullen, K. E. Asymmetric recovery in cerebellar-deficient mice following unilateral labyrinthectomy. *J. Neurophysiol.* **100**, 945–958 (2008).
2. Carriot, J., Jamali, M., Chacron, M. J. & Cullen, K. E. The statistics of the vestibular input experienced during natural self-motion differ between rodents and primates. *J. Physiol.* **595**, 2751–2766 (2017).
3. Carriot, J., Jamali, M., Chacron, M. J. & Cullen, K. E. Statistics of the vestibular input experienced during natural self-motion: Implications for neural processing. *J. Neurosci.* **34**, 8347–8357 (2014).
4. Straka, H., Simmers, J. & Chagnaud, B. P. A new perspective on predictive motor signaling. *Curr. Biol.* **28**, R232–R243 (2018).
5. Dhande, O. S. *et al.* Genetic dissection of retinal inputs to brainstem nuclei controlling image stabilization. *J. Neurosci.* **33**, 17797–17813 (2013).
6. Masseck, O. A. & Hoffmann, K.-P. Comparative neurobiology of the optokinetic reflex. *Ann. N. Y. Acad. Sci.* **1164**, 430–439 (2009).
7. Stahl, J. S. Using eye movements to assess brain function in mice. *Vis. Res.* **44**, 3401–3410 (2004).
8. Cullen, K. E. Vestibular processing during natural self-motion: Implications for perception and action. *Nat. Rev. Neurosci.* **20**, 346–363 (2019).
9. Faulstich, B. M., Onori, K. A. & du Lac, S. Comparison of plasticity and development of mouse optokinetic and vestibulo-ocular reflexes suggests differential gain control mechanisms. *Vis. Res.* **44**, 3419–3427 (2004).
10. Robinson, D. A. Control of eye movements. In *Handbook of Physiology Section II : The Nervous System,* 1275–1320 (The William and Wilkins Co, Philadelphia, 1981).
11. Lannou, J., Cazin, L., Precht, W. & Toupet, M. Optokinetic, vestibular, and optokinetic-vestibular responses in albino and pigmented rats. *Pflugers Arch.* **393**, 42–44 (1982).

12. Curthoys, I. S. The development of function of horizontal semicircular canal primary neurons in the rat. *Brain Res.* **167**, 41–52 (1979).
13. Curthoys, I. S. The vestibulo-ocular reflex in newborn rats. *Acta Otolaryngol.* **87**, 484–489 (1979).
14. Beraneck, M., Lambert, F. M. & Sadeghi, S. G. Functional Development of the Vestibular System: Sensorimotor Pathways for Stabilization of Gaze and Posture. in (eds Romand, R. & Varela-Nieto, I.) *Development of Auditory and Vestibular Systems* 449–488 (Academic Press, 2014).
15. Sherman, K. R. & Keller, E. L. Vestibulo-ocular reflexes of adventitiously and congenitally blind adults. *Invest. Ophthalmol. Vis. Sci.* **27**, 1154–1159 (1986).
16. Seemungal, B. M., Glasauer, S., Gresty, M. A. & Bronstein, A. M. Vestibular perception and navigation in the congenitally blind. *J. Neurophysiol.* **97**, 4341–4356 (2007).
17. Puyal, J. *et al.* Developmental shift from long-term depression to long-term potentiation in the rat medial vestibular nuclei: Role of group. I. Metabotropic glutamate receptors. *J. Physiol. (Lond.)* **553**, 427–443 (2003).
18. Beraneck M. & Lambert F.M. Differential organization of intrinsic membrane properties of central vestibular neurons and interaction with network properties. in *The Senses: A Comprehensive Reference*, Vol. 6 (eds Fritzsch, B. & Straka, H.) 273–289 (Elsevier, Academic Press, 2020).
19. Grassi, S., Dieni, C., Frondaroli, A. & Pettorossi, V. E. Influence of visual experience on developmental shift from long-term depression to long-term potentiation in the rat medial vestibular nuclei. *J. Physiol. (Lond.)* **560**, 767–777 (2004).
20. França de Barros, F., Carcaud, J. & Beraneck, M. Long-term sensory conflict in freely behaving mice. *J. Vis. Exp.* https://doi.org/10.3791/59135 (2019).
21. Carcaud, J. *et al.* Long-lasting visuo-vestibular mismatch in freely-behaving mice reduces the vestibulo-ocular reflex and leads to neural changes in the direct vestibular pathway. *eNeuro* **4**(1), ENEURO.0290-16.201. https://doi.org/10.1523/ENEURO.0290-16.2017 (2017).
22. Boyden, E. S., Katoh, A. & Raymond, J. L. Cerebellum-dependent learning: The role of multiple plasticity mechanisms. *Annu. Rev. Neurosci.* **27**, 581–609 (2004).
23. Shin, S.-L., Zhao, G. Q. & Raymond, J. L. Signals and learning rules guiding oculomotor plasticity. *J. Neurosci.* **34**, 10635–10644 (2014).
24. Lac, S., Raymond, J. L., Sejnowski, T. J. & Lisberger, S. G. Learning and memory in the vestibulo-ocular reflex. *Annu. Rev. Neurosci.* **18**, 409–441 (1995).
25. Boyden, E. S. & Raymond, J. L. Active reversal of motor memories reveals rules governing memory encoding. *Neuron* **39**, 1031–1042 (2003).
26. Beraneck, M. & Cullen, K. E. Activity of vestibular nuclei neurons during vestibular and optokinetic stimulation in the alert mouse. *J. Neurophysiol.* **98**, 1549–1565 (2007).
27. Sugita, Y., Miura, K., Araki, F., Furukawa, T. & Kawano, K. Contributions of retinal direction-selective ganglion cells to optokinetic responses in mice. *Eur. J. Neurosci.* **38**, 2823–2831 (2013).
28. Kodama, T. & du Lac, S. Adaptive acceleration of visually evoked smooth eye movements in mice. *J. Neurosci.* **36**, 6836–6849 (2016).
29. Wakita, R. *et al.* Differential regulations of vestibulo-ocular reflex and optokinetic response by β- and α2-adrenergic receptors in the cerebellar flocculus. *Sci. Rep.* **7**, 3944 (2017).
30. Collewijn, H. & Grootendorst, A. F. Adaptation of optokinetic and vestibulo-ocular reflexes to modified visual input in the rabbit. In *Progress in Brain Research, vol. 50* (eds Granit, R. & Pompeiano, O.) 771–781 (Elsevier, Amsterdam, 1979).
31. Dean, P. & Porrill, J. Decorrelation learning in the cerebellum: Computational analysis and experimental questions. *Prog. Brain Res.* **210**, 157–192 (2014).
32. Gonshor, A. & Jones, G. M. Extreme vestibulo-ocular adaptation induced by prolonged optical reversal of vision. *J. Physiol.* **256**, 381–414 (1976).
33. Miles, F. A. & Eighmy, B. B. Long-term adaptive changes in primate vestibuloocular reflex. I. Behavioral observations. *J. Neurophysiol.* **43**, 1406–1425 (1980).
34. Miles, F. A. & Lisberger, S. G. Plasticity in the vestibulo-ocular reflex: A new hypothesis. *Annu. Rev. Neurosci.* **4**, 273–299 (1981).
35. Harris, L. R. & Cynader, M. The eye movements of the dark-reared cat. *Exp. Brain Res.* **44**, 41–56 (1981).
36. Jones, G. M. & Davies, P. Adaptation of cat vestibulo-ocular reflex to 200 days of optically reversed vision. *Brain Res.* **103**, 551–554 (1976).
37. Collewijn, H. Optokinetic and vestibulo-ocular reflexes in dark-reared rabbits. *Exp. Brain. Res.* **27**, 287–300 (1977).
38. Ito, M., Jastreboff, P. J. & Miyashita, Y. Adaptive modification of the rabbit's horizontal vestibulo-ocular reflex during sustained vestibular and optokinetic stimulation. *Exp. Brain Res.* **37**, 17–30 (1979).
39. Lisberger, S. G., Miles, F. A., Optican, L. M. & Eighmy, B. B. Optokinetic response in monkey: underlying mechanisms and their sensitivity to long-term adaptive changes in vestibuloocular reflex. *J. Neurophysiol.* **45**, 869–890 (1981).
40. Suvrathan, A. & Raymond, J. L. Depressed by learning—heterogeneity of the plasticity rules at parallel fiber synapses onto purkinje cells. *Cerebellum* **17**, 747–755 (2018).
41. Suvrathan, A., Payne, H. L. & Raymond, J. L. Timing rules for synaptic plasticity matched to behavioral function. *Neuron* **92**, 959–967 (2016).
42. Holland, P. J. *et al.* A neuroanatomically grounded optimal control model of the compensatory eye movement system in mice. *Front. Syst. Neurosci.* **14**, 13 (2020).
43. Laurens, J. & Angelaki, D. E. The functional significance of velocity storage and its dependence on gravity. *Exp. Brain Res.* **210**, 407–422 (2011).
44. Cohen, B., Matsuo, V. & Raphan, T. Quantitative analysis of the velocity characteristics of optokinetic nystagmus and optokinetic after-nystagmus. *J. Physiol. (Lond.)* **270**, 321–344 (1977).
45. van Alphen, A. M., Stahl, J. S. & De Zeeuw, C. I. The dynamic characteristics of the mouse horizontal vestibulo-ocular and optokinetic response. *Brain Res.* **890**, 296–305 (2001).
46. Blazquez, P. M., de Carrizosa, M.A.D.-L., Heiney, S. A. & Highstein, S. M. Neuronal substrates of motor learning in the velocity storage generated during optokinetic stimulation in the Squirrel Monkey. *J. Neurophysiol.* **97**, 1114–1126 (2007).
47. Miki, S., Urase, K., Baker, R. & Hirata, Y. Velocity storage mechanism drives a cerebellar clock for predictive eye velocity control. *Sci. Rep.* **10**, 6944 (2020).
48. Cohen, B., Dai, M., Yakushin, S. B. & Raphan, T. Baclofen, motion sickness susceptibility and the neural basis for velocity storage. *Prog. Brain Res.* **171**, 543–553 (2008).
49. Yakushin, S. B., Raphan, T. & Cohen, B. Coding of Velocity Storage in the Vestibular Nuclei. *Front. Neurol.* https://doi.org/10.3389/fneur.2017.00386 (2017).
50. Kassardjian, C. D. The site of a motor memory shifts with consolidation. *J. Neurosci.* **25**, 7979–7985 (2005).
51. Shutoh, F., Ohki, M., Kitazawa, H., Itohara, S. & Nagao, S. Memory trace of motor learning shifts transsynaptically from cerebellar cortex to nuclei for consolidation. *Neuroscience* **139**, 767–777 (2006).
52. Raymond, J. L. & Medina, J. F. Computational principles of supervised learning in the cerebellum. *Annu. Rev. Neurosci.* **41**, 233–253 (2018).

53. Jang, D. C., Shim, H. G. & Kim, S. J. Intrinsic plasticity of cerebellar purkinje cells contributes to motor memory consolidation. *J. Neurosci.* **40**, 4145–4157 (2020).
54. Samonds, J. M., Choi, V. & Priebe, N. J. Mice discriminate stereoscopic surfaces without fixating in depth. *J. Neurosci.* **39**, 8024–8037 (2019).
55. Wallace, D. J. *et al.* Rats maintain an overhead binocular field at the expense of constant fusion. *Nature* **498**, 65–69 (2013).
56. Kretschmer, F., Tariq, M., Chatila, W., Wu, B. & Badea, T. C. Comparison of optomotor and optokinetic reflexes in mice. *J. Neurophysiol.* **118**, 300–316 (2017).
57. Sterratt, D. C., Lyngholm, D., Willshaw, D. J. & Thompson, I. D. Standard Anatomical and visual space for the mouse retina: Computational reconstruction and transformation of flattened retinae with the retistruct package. *PLoS Comput. Biol.* **9**, e1002921 (2013).
58. Beraneck, M. & Idoux, E. Reconsidering the role of neuronal intrinsic properties and neuromodulation in vestibular homeostasis. *Front Neurol.* **3**, 25 (2012).
59. Calabrese, D. R. & Hullar, T. E. Planar Relationships of the Semicircular Canals in Two Strains of Mice. *JARO* **7**, 151–159 (2006).
60. Oommen, B. S. & Stahl, J. S. Eye orientation during static tilts and its relationship to spontaneous head pitch in the laboratory mouse. *Brain Res.* **1193**, 57–66 (2008).
61. Cahill, H. & Nathans, J. The optokinetic reflex as a tool for quantitative analyses of nervous system function in mice: application to genetic and drug-induced variation. *PLoS ONE* **3**, e2055 (2008).

Acknowledgements

The authors thank M. Patrice Jegouzo and Laure-Hélène Bernard, Olivia Cattaneo and Thibault Patti for their technical help during the experiments. This work was supported by the *Centre National d'Etudes Spatiales*, the *Centre National de la Recherche Scientifique* and the *Université de Paris*. F.B. & M.B. received support from the *Agence Nationale de la Recherche* (ANR-15-CE32-0007-02). This study contributes to the IdEx Université de Paris ANR-18-IDEX-0001.

Author contributions

F.F.B., M.T., M.B.: Conceptualization. F.F.B., L.S., M.T., M.B.: Methodology. L.S., M.T., M.B.: Software. F.F.B., L.S., M.T., M.B.: Formal analysis. F.F.B., L.S., M.B.: Investigation. F.F.B., M.B.: Writing original manuscript. F.F.B., L.S., M.T., M.B.: Writing—review and editing. F.F.B., L.S., M.T., M.B.: Visualization. F.F.B., M.T., M.B.: Supervision. M.B.: Project administration. M.T., M.B.: Funding acquisition.

Competing interests

The authors declare no competing interests.

Additional information

Supplementary information is available for this paper at https://doi.org/10.1038/s41598-020-77026-w.

Correspondence and requests for materials should be addressed to F.F.d. or M.B.

Reprints and permissions information is available at www.nature.com/reprints.

Publisher's note Springer Nature remains neutral with regard to jurisdictional claims in published maps and institutional affiliations.

ARTICLE 2 – Suboptimal visuo-vestibular integration following transient vestibular loss.

Vestibular diseases have a fairly high incidence in the population and are characterized by attacks during which vestibular functions are impaired. These attacks are followed by periods of recovery. Currently, animal models of unilateral or bilateral vestibular lesions do not allow the mechanisms of such pathologies to be completely reproduced because the lesions induced are permanent. However, they have made it possible to highlight the multiple mechanisms that are put in place to induce vestibular compensation. Sensory substitution, in particular, processes to increase the efficiency and sensitivity of non-vestibular sensory information so that it can contribute in place of the damaged sensory inputs (Sadeghi et al, 2012).

In this project, we use 3,3′-iminodiproprionitrile (IDPN) that is able to induce a bilateral functional vestibular loss quantified by VOR when injected acutely, i.e. permanently. However, it has recently been shown that it is possible to produce a so-called "sub-chronic" protocol by diluting IDPN in the drinking water of mice (Gregunske et al, 2021). Sub-chronic IDPN causes transient vestibular dysfunction associated with hair cell loss, as vestibular function and hair cells are recovered when IDPN is removed from the water.

Thus, we associated the use of a sub-chronic IDPN protocol with vestibular-related reflexes test to quantify the function of specific vestibular endorgans during transient loss. We also performed histological staining after treatment and after recovery to observe the effect of the protocol on hair cell numbers. Thus, we report that subchronic IDPN induces a transient canalar and otolithic lesion whose amplitude correlates with the number of hair cells in each organ.

We were also interested in the mechanisms of substitution following a bilateral lesion, in particular a visual substitution. For this purpose, we also performed

optokinetic stimulations in order to quantify the effect of the lesion on the OKR gain. The loss of vestibular function is indeed accompanied by an increase in OKR performance in a frequency-specific manner and presents slightly shifted dynamics compared to the VOR.

Finally, we investigated the functional visuo-vestibular integration after a transient lesion protocol. We observed a suboptimal integration in treated mice despite a partial recovery of their vestibular function and an increase in their OKR capacity. Moreover, we show here that visual-vestibular integration is clearly dependent on vestibular information.

Overall, this project demonstrates the use of the IDPN subchronic protocol to induce transient vestibular loss as well as the correlation between the function of specific vestibular organs and their respective number of hair cells. Furthermore, we show that the visual substitution that occurs to compensate for vestibular loss is specific to frequencies for which vestibular function is normally dominant. Finally, the integration of visual and vestibular inputs in gaze stabilization is sub-optimal after vestibular recovery and as such is mostly dependent on vestibular inputs.

This article is in its pre-print version.

Visuo-vestibular sensory substitution following ototoxic alteration of type I hair cells

or

Suboptimal visuo-vestibular integration following ototoxic alteration of type I hair cells

Louise Schenberg[1], Aïda Palou Miranda[2]*, François Simon[1], *Tess Bonnard[1], Charles-Elliot Barton[1], Desdemona Fricker[1], Michele Tagliabue[1], Jordi Llorens[2,3], Mathieu Beraneck[1,*]*

1-Université Paris Cité, CNRS UMR 8002, INCC - Integrative Neuroscience and Cognition Center, F-75006, Paris, France.

2- Departament de Ciències Fisiològiques, Institut de Neurociènces, Universitat de Barcelona, Barcelona, Catalunya, Spain

3-Institut d'Investigació Biomèdica de Bellvitge, Barcelona, Catalunya, Spain.

*** Corresponding authors:**

Louise Schenberg, CNRS UMR 8002, Université Paris Cité, 45 rue des St-Pères, Paris 75270, France. Email: louise.schenberg@u-paris.fr

Dr. M. Beraneck. CNRS UMR 8002, Université Paris Cité, 45 rue des St-Pères, Paris 75270, France. Email: mathieu.beraneck@cnrs.fr

Funding: This work is supported by the Centre National d'Etudes Spatiales, the Centre National de la Recherche Scientifique, and the Université Paris Cité. MB and LS received funding from the Agence Nationale de la Recherche (ANR-20-CE37-0016 INVEST). MB, FS & DF received funding from the ERANET NEURON Program VELOSO. APM & JL received funding from the ERANET NEURON Program VELOSO.

Acknowledgment: this study contributes to the IdEx Université de Paris ANR-18-IDEX-0001. This work has benefited from the support and expertise of the animal facility of BioMedTech Facilities at Université Paris Cité (Institut National de la Santé et de la Recherche Médicale Unité S36/Unité Mixte de Service 2009).

Author contribution: Conceptualization: JL ; MB. Methodology: LS ; APM ; FS ; MT ; JL ; MB. Formal analysis: LS ; APM ; MT ; JL ; MB. Investigation: LS ; APM ; TB ; CEB . Writing original manuscript: LS ; MT ; MB. Writing review and editing: LS ; APM ; FS ; TB ; CEB ; DF ; MT ; JL ; MB. Visualization: LS ; APM ; MT ; JL ; MB. Supervision: LS ; DF ; MT ; JL ; MB. Project administration: JL; MB. .Funding acquisition: DF, JL; MB.

Declaration of interests: The authors declare no competing interests.

Abstract (200mots)

The functional complementarity of the vestibulo-ocular reflex and optokinetic reflex allows for optimal gaze stabilization in light. While sensory substitution has been reported following a complete vestibular loss, the capacity of the visual system to compensate for partial vestibular loss remains to be determined. Here, we first demonstrate the efficacy of a “sub-chronic” IDPN ototoxic protocol in inducing transient and partial vestibular loss by quantifying the organ-specific vestibulo-ocular function. Immunostaining directed against hair-cell and synapse-related proteins revealed that the 6 weeks of IDPN subchronic treatment equally affects the canal- and otolith-dependent VORs and that organ-specific loss of type I hair cells correlates with individual mice impairments. The decrease in VOR performance is paralleled with an increase in the gain of the OKR occurring in a specific range of frequencies where VOR normally dominates gaze stabilization, compatible with a sensory substitution process. However, the combined visuo-vestibular responses remain suboptimal in the long term, despite significant recovery in the VOR individually correlated with recovery in type I HC. The integrity in the vestibular pathway therefore appears necessary to insure optimal integration of visual inputs for gaze stabilization. Overall, these results shed light on the dynamic of multisensory reweighting in patients suffering from fluctuating peripheral vestibular malfunction.

Introduction

The vestibular system is well-conserved among vertebrates, in which it serves essential functions such as balance, postural control and gaze stabilization (Straka et al., 2016). Beyond these well-recognized roles, vestibular signals also contribute to cognitive processes e.g spatial orientation and navigation (Cullen, 2019), or body representation (Lopez et al., 2012; Facchini et al., 2021). Because of its involvement in many basic functions important in our daily life, vestibular pathologies affecting the inner ear are associated with a significant deterioration of the well-being of patients (Möhwald et al., 2020) and represent an important public health concern (Agrawal et al., 2009, 2013).

Research on post-lesion plasticity following permanent vestibular loss has shed light on the neural plastic mechanisms that follow a chronic unilateral or bilateral vestibular lesion, a process termed “vestibular compensation” (Brandt et al., 1997; Cullen et al., 2010; Beraneck and Idoux, 2012). The adaptive plasticity taking place after the lesion is known to involve dynamical multisensory reweighting of e.g proprioceptive and visual inputs and of internal efferent copies (Cullen et al., 2010; Sadeghi et al., 2012). While permanent lesions offer the experimental opportunity to characterize drastic cellular and molecular changes triggered by the total silencing of the vestibular endorgans, those imperfectly mimic clinical situations where degradation of peripheral vestibular function is only partial and/or transient.

To better model fluctuating inner ear function, protocols based on weeks-long exposure to an ototoxic substance, 3,3’-iminodiproprionitrile (IDPN) were first introduced in the rat (Seoane et al., 2001; Sedó-Cabezón et al., 2014, 2015; Martins-Lopes et al., 2019a) and more recently in the mouse (Greguske et al., 2019). Exposure to IDPN in drinking water at low doses allowed for a so-called “subchronic” ototoxicity, leading to a partial and reversible extrusion of sensory inner ear hair cells. Using behavioural assays, the subchronic IDNP protocol was shown to cause postural and locomotor deficits (Martins-Lopes et al., 2019a). However, its effects on the gaze stabilizing reflexes, namely the vestibulo-ocular and optokinetic reflexes, have not yet been described.

The primary objective of the present study was first to assess how subchronic exposure to IDPN is affecting the different vestibular endorgans. To that end, we took advantage of our recently described methodology (Simon et al., 2020, 2021) using canal-specific and otolith-specific tests. Quantification of the vestibulo-ocular reflexes is a sensitive and specific method

to assess the functionality of the sensory-motor vestibular pathway, it is the most used test in clinics, and highly correlates to quality-of-life reports in patients suffering from acute peripheral pathologies (Möhwald et al., 2020).

The secondary objective is to determine whether visual substitution occurs following a transient vestibular loss. Optogenetic stimulation of the vestibular pathway demonstrated the recruitment of circuits involved in visual processing at the midbrain, thalamic and cortical regions (Leong et al., 2019). Recent imaging studies in rodents have shown that acute vestibular loss triggers brain-wide adaptive plasticity (Zwergal et al., 2016; Grosch et al., 2021), involving circuits known to be involved in visual processing. In addition, it was previously shown that OKR plasticity is triggered during vestibular compensation following a permanent vestibular lesion (Faulstich et al., 2006; Nelson et al., 2017). Another objective of this study is therefore to quantify optokinetic plasticity and its dynamic in a pathological situation where the inner ear deficit is only partial and transient.

We report that 6 weeks of IDPN subchronic treatment equally affects the canal- and otolith-dependent vestibulo-ocular reflexes and that organ-specific loss of type I hair cells correlates with individual mice impairments. We show that optokinetic adaptive plasticity is frequency-specific and dynamically lags VOR changes. OKR changes occur in the frequency range where the vestibular inputs are physiologically dominating compensatory gaze-stabilizing reflexes. Finally, the integration of vestibular and visual inputs remains impaired in IDPN-treated mice despite the functional improvement of their vestibulo-ocular reflexes, leading to suboptimal gaze stabilization. These results shed light on the dynamic of multisensory reweighting in patients suffering from fluctuating peripheral vestibular malfunction.

Results

Effects of the subchronic treatment of IDPN on the canal- and otolith-dependent VOR.

To investigate the effects of the IDPN on vestibulo-ocular reflexes (VOR), animals were exposed "subchronically" to the ototoxic compound in the drinking water for six weeks (Treatment period), followed by 6 weeks of standard drinking water without IDPN (Washout period). The vestibulo-ocular reflexes were quantified every two weeks using canal-specific and otolith-specific tests. Horizontal sinusoidal rotations in the dark were performed and oculomotor responses were obtained using video-oculography (Figure 1A) to study the impact of the IDPN on the canal-dependent angular VOR (aVOR). Raw aVOR traces obtained before treatment (W0), after 6 weeks of treatment (W6) and after 6 additional weeks of washout (W12) for a sinusoidal stimulation of 1Hz at 30°/s velocity are shown in Figure 1B. At W6 the amplitude of the eye movements is distinctly reduced compared to W0, while at W12 the amplitude of the response appears only partially restored. The dynamic of decrease and recovery of the mean aVOR gain over the course of the protocol is reported in Figure 1C for both IDPN (n=21) and SHAM (n=22) groups. There is a significant interaction between the effect of the tested week and group (Weeks x Group interaction, $F(6,246)=29.232$, $p<10^{-4}$). Before treatment, both groups respond similarly to the sinusoidal stimulations and their aVOR gain remains unchanged until 2 weeks of treatment (W2). However, starting W4 the aVOR gain of IDPN group significantly decreases in respect to W0 (Newman-Keuls post hoc test: IDPN W0 vs W4 $p<10^{-4}$) and is significantly lower compared with the SHAM group (W4, IDPN vs SHAM $p<10^{-4}$). The aVOR gain of the IDPN group remains lower compared to SHAM through the rest of the protocol with a minimum value at W6 corresponding to ~2/3 of aVOR loss (IDPN W4 vs W6 $p<10^{-4}$, IDPN W6 vs W8 $p=0.0411$). During the washout period, IDPN mean aVOR gain remains significantly lower compared to SHAM (W8 IDPN vs SHAM $p<10^{-4}$, W10 IDPN vs SHAM $p<10^{-4}$, W12 IDPN vs SHAM $p<10^{-4}$). At the end of the six weeks of washout, the mean aVOR significantly improved (IDPN W6 vs W12 $p<10^{-4}$) to levels observed at W4 (IDPN W4 vs W12 $p=0.5621$).

Similar trends were observed for all tested frequencies in the range 0.5-2Hz (supplementary Figure 1A, top panels; Weeks x Group x Frequencies interaction $F(24,984)=3.6092$, $p<10^{-4}$). VOR gain decrease was paralleled with significant phase leads that affected all tested frequencies at week 6 (Supplementary Figure 1B, ANOVA repeated measures Weeks x Group

Interactions F(6, 144)=5.5490, $p<10^{-4}$). Overall, canalar responses remained unaffected until week 2, but the amplitude and/or timing of the aVOR is abnormal from week 4 until the end of the protocol, despite a significant recovery of angular VOR responses observed during the washout period.

To determine whether otolith-dependent VOR is also affected by the IDPN, ocular-counter roll responses were tested during static lateral inclination in the range ±40° (OCR; Figure 1D). Examples of raw traces and quantification of the response are shown in Figure 1E, while the gain of the OCR of each group is plotted in Figure 1F (n=13 IDPN, n=14 SHAM). The amplitude of the responses of the IDPN group was significantly different from that of the SHAM (ANOVA repeated measures Weeks x Group Interaction F(6, 150)= 7.7411 $p<10^{-4}$). We note that there was a significant difference between SHAM and IDPN during the initial measurements at W0. However, at this timepoint mice were not yet separated into different groups. This incidental difference completely disappeared on the measurement performed at W2 (W2 IDPN vs SHAM p=0.8135). While the gain of the SHAM group stays in a 0.5-0.6 range over the protocol's duration, the responses of the IDPN group significantly decrease at W4 compared to the SHAM group (W4 IDPN vs SHAM $p<10^{-4}$). This decrease is larger at W6 weeks (IDPN W4 vs W6 p=0.023) and stays significantly different from the SHAM group until W8. At W10 and W12, the OCR of IDPN group recovers to a level comparable to the SHAM group (W10 IDPN vs SHAM p=0.1262, W12 IPDN vs SHAM p=0.3385).

Sub-chronic treatment of IDPN was also investigated through the dynamic OVAR test (Supplementary Figure 1C), which primarily reflects maculo-ocular (dominantly otolithic) responses integrated by central vestibular pathways. The bias of the MOR decreased significantly compared to the SHAM group (ANOVA Weeks x Group, F(6, 132)= 10,076, $p<10^{-4}$) starting W2 of treatment (W2 IDPN vs SHAM p=0,0018), demonstrating that ototoxicity already affects the inner ear at this early time point. The maximal decrease is reached at W6 (W6 IDPN vs SHAM p=0.00012) and recovery leads to normal responses at W12 (W12 IDPN vs SHAM p=0.4709).

Comparison of otolith- and canal-dependent plasticity in individuals.

To compare the dynamic of canal- and otolith-dependent VOR alterations, the 1Hz VOR and OCR gain measured in the same individuals from the IDPN groups (n=13) are plotted together (Figure 2A). Alteration in canal- and otolith-dependent responses follow a very similar time

course with a decrease 2 weeks after the beginning of IDPN exposure, a trough reached at week 6, and a progressive recovery during the following washout period. Comparisons between OCR gain and VOR gain at the other tested frequencies are shown in Supplementary Figure 2. Despite minor variations in the modulation of the responses, the dynamic of aVOR and OCR alterations were rather comparable in all tested frequencies.

To investigate further the organ-specific responses, the individual values of VOR gain at 1Hz (left panel) and OCR slope (right panel) are plotted in Figure 2B. These plots show the variability of the responses observed in different individuals. 2/3 of the mice had aVOR responses lowered by >50%, while 1/3 had milder aVOR impairments. For the large majority, however, the aVOR gain is markedly decreasing between week 4 and week 6 and starts to recover on week 8 (compare individual slopes on Figure 2B). Similarly, OCR gains were variable between individuals, however, the dynamic of the variations in otolith-dependent responses follows a pattern comparable to that of the canal-dependent changes.

To determine whether the changes in canal- and otolith-dependent responses are proportional, individual variations in gain since pre-treatment of the aVOR (1Hz) and OCR are compared at W6 (Figure 2C) and W12 (Figure 2D). At week 6, there is a significant correlation between the amplitude of the changes observed in aVOR and OCR, such that canalar and otolithic loss of function is proportional (slope of regression line:0.5586, r^2=0.5243, p=0.0051). Despite the general recovery, this significant correlation is preserved at week 12: the recovery in canal-dependant responses is proportional to the recovery in otolith-dependent responses (slope of regression line:0.5566, r^2=0.5581, p=0.0033). Overall, these results suggest that the subchronic IDPN treatment similarly affects the vestibulo-ocular reflexes that depend on semi-circular canals and on the otolithic organs, respectively.

Effects of the IDPN exposure on the number of hair cells in the vestibular epithelia.

To correlate the vestibular loss of function to the structural changes induced by the ototoxic compound, the vestibular epithelia were dissected and labelled to assess the number of hair cells in the organs. One horizontal semi-circular and one utricule were harvested at Week 6 for n=7 IDPN and n=4 SHAM, and at Week 12 for n=8 IDPN and n=4 SHAM, and each organ epithelium was divided into the central and peripheral region to differentiate the possible participation of zone- and organ-specific hair cells (HC) to the vestibular function. Vestibular hair cells are labelled with type-specific immunomarkers in both endorgans. 6-week long

treatment of IDPN exposure leads to a reduced number of type I hair cells labelled with Spp1 and Caspr1 in the canal crista (Figure 3A1) and in the otolith macula (Figure 3B1). Indeed, the number of Spp1+ and Caspr1+ cells is significantly reduced in all regions at Week 6 compared to the SHAM (Spp1+ p=0.0322, Caspr1 p=0.0268; Supplementary Figure 3A1 and B1 for the peripheral zones). However, the treatment does not induce a loss of type II hair cells as the number of Calre+ cells in the IDPN group is similar to the SHAM in all regions of either vestibular endorgans (Figure 3A1, B1). At Week 12 the number of type I hair cells labelled in the IDPN-treated mice are no longer significantly different from the SHAM group in either endorgans (Figure 3A2 for crista; Figure 3B2 for macula). Immunostaining data obtained by a confocal microscope are pictured in Figure 3A3 for the horizontal semi-circular canals and Figure 3B3 for the utricule. While the labelling of the calretinin remains constant, the labelling of Spp1 and Caspr1 decreases at Week 6.

The numbers of type I and II HC in the central region of the horizontal semi-circular canals are plotted as a function of the mean aVOR gain for mice at Week 6 and Week 12, IDPN and SHAM (Figure 3C1 and C2 for type I and C3 for type II). Both markers of type I HC (Caspr1 and Spp1) are significantly correlated with the aVOR gain (Spp1 r^2=0.5128 p=0.0001, Caspr1 r^2=0.4948 p=0.0002, Figure 3C1 and C2) whereas the number of type II HC in the vestibular organ does not correlate with the loss of function. The numbers of hair cells of type I and II are similarly plotted in relation to the OCR gain (Spp1 r^2=0.6011 p<0.0001, Caspr1 r^2=0.6342 p<0.0001, Figure3 D1 and D2 for type I and D3 for type II). Again, the otolithic function is correlated with the number of type I, and not type II in the central region. The correlation between organ-specific function and the number of type I HC is also found in the peripheral regions of these organs (See Supplementary Figure 3C1, C2 for the horizontal semi-circular canals, and Figure3 D1, D2 for the utricule).

Finally, to see if the correlation is due to the recovery occurring between Week 6 and Week 12, the number of CASPR+ cells of IDPN Week 12 mice are plotted as a function either of their aVOR gain at W12 (pink squares) or their aVOR gain at W6 (black circles), with the respective gain linked by an arrow (Figure3 E). The linear regression at W12 is also represented. The recovery of the vestibular function induces a shift toward the correlation line, reinforcing the notion that the recovery of function is a consequence of the increase in the number of hair cells that occurs during the recovery period.

Globally IDPN induces a loss of canalar and otolithic functions, both strongly correlated with the ototoxic effect of the treatment on type I, and not type II, hair cells in the central and peripheral zones of vestibular endorgans.

Effects of the subchronic treatment of IDPN on the optokinetic reflex.

To determine the effects of the subchronic treatment of IDPN on the optokinetic reflex, mice were tested with sinusoidal rotations of a virtual drum (Figure 4A). An example of raw traces of the evoked horizontal eye movements is shown in Figure4B before treatment and every 4 weeks for a 0.5Hz and 10deg.s^{-1} visual stimulation. The mean OKR gain for all tested frequencies is plotted in Figure 4C (n=12 SHAM, n=12 IDPN). There is a significant interaction between Weeks and Group ($F(6,132)=2.9845$, $p=0.0091$). The mean IDPN OKR gain reaches a peak value at W8 (IDPN W0 vs W8 $p=0.00037$) where it is significantly larger than the gain of SHAM (W8 IDPN vs SHAM $p=0.0216$). After W8, the gain slightly decreases but its value stays larger than the SHAM group even at W12 (W12 IDPN vs SHAM $p=0.046$).

To determine whether this OKR plasticity is frequency-specific, the gain is plotted for every frequency tested for W0, W4, W8, and W12 (Figure 4D). Response at the lowest tested frequencies (0.1 and 0.2 Hz) are not significantly affected (W8 IDPN vs SHAM for 0.1Hz $p=0.7439$, for 0.2Hz $p=0.9999$); on the other hand, the response to higher frequencies (0.33, 0.5 and 1 Hz) are significantly increased (ANOVA Weeks x Group x Frequencies interaction $F(24, 528)=6.5870$ $p<10^{-4}$). At Week4, there is a significant difference between the IDPN and SHAM group at 1Hz (W4 IDPN vs SHAM 1Hz $p=0.0248$). At W8, all frequencies >0.33Hz are significantly increased compared to the SHAM group (W8 IDPN vs SHAM 0.33Hz $p=0.027687$; 0.5Hz $p=0.0025$, 1Hz $p=0.00015$). At W12, the gain remains high for both 0.5 and 1Hz whereas the gain at 0.33Hz is no longer significantly larger than the SHAM group (W12 IDPN vs SHAM 0.33Hz ns; 0,5Hz $p=0.0069$, 1Hz $p=0.00078$). Notably, these changes in gain for frequencies >0.33Hz were not accompanied by changes in the timing (phase) of the OKR (Figure 4E) (ANOVA, Weeks x Group x Frequencies interaction $p=0.3802$).

Relations between VOR decrease and optokinetic increase

To correlate the changes in vestibular pathway with the frequency-specific changes observed in the optokinetic pathway, we compared the responses in aVOR and OKR obtained at the frequencies that were common between the 2 tests (i.e 0.2 Hz, 0.5 HZ and 1Hz) for n=12 IDPN

and n=12 SHAM. Figure 5A shows their mean aVOR and OKR gains during the 12 weeks of the protocol. The changes in the OKR pathway are delayed compared to the changes in the VOR pathway as the peak in OKR at week 8 occurs after the trough observed at week6 for the VOR. To determine whether the changes in VOR and OKR are proportional, we compared the decrease and increase in the mean ΔaVOR and ΔOKR gain of the common frequencies after 8 weeks of treatment, the condition in which the changes in OKR are maximal. The vast majority (n=11) of IDPN-exposed mice showed a decrease in aVOR and an increase in OKR (top left quadrant corner; mean±50% confidence interval is shown as a shaded area). However, there was no correlation between the amplitude of the VOR decrease and the amplitude of the OKR increase, i.e mice that had the greatest VOR loss did not show the largest OKR increase (slope in the regression line: 0.1107). Comparing the IDPN and SHAM individuals however suggests that the OKR increase is related to the treatment, as this same coupling between VOR/OKR variations was never observed for SHAM mice.

To further explore the relation between vestibular and optokinetic modifications, we then compared the changes at the frequencies that were common between both VOR and OKR tests (0.2, 0.5, and 1HZ; figure 5C). At 0.2Hz, there is a significant decrease in aVOR (IDPN W0 vs W8 0.2Hz $p<10^{-4}$), however, the OKR is not modified. On the other hand, significant VOR decrease at 0.5 and 1Hz (IDPN W0 vs W8 0.5Hz $p<10^{-4}$, 1Hz $p<10^{-4}$) is accompanied by significant OKR increase at 0.5 and 1HZ (IDPN W0 vs W8 0.5Hz $p<10^{-4}$, 1Hz $p<10^{-4}$). To examine this frequency-selective increase of the OKR gain, the percentage of change in the OKR gain is plotted as a function of the vestibular weight, determined as the ratio between aVOR value divided by the aVOR+OKR value measured at week 0. The *vestibular weight*, therefore, represents the frequency-dependent relative influence of the vestibular signal on gaze stabilization. Figure 5D shows that at week 8, the change in the OKR occurred at the frequencies for which the vestibular weight was dominant (>50%), and that the increase in OKR is positively correlated with the vestibular weight at a given frequency (slope of the regression line: 1.235; $r^2=0.6299$; $p<0.0001$). Overall, these results suggest that the increase in OKR gain observed at high frequencies could correspond to a “visual substitution” occurring preferentially in the range in which the vestibular inputs are normally dominating gaze stabilization.

Vestibular impairment leads to suboptimal visuo-vestibular integration

To investigate whether OKR increase constitutes a "visual substitution" that maintains an optimal gaze stabilization at light despite vestibular loss, we investigated how IDPN mice integrate vestibular and visual inputs. To this end, a session of combined visual and vestibular stimulation (VOR in light, here referred as *Combined Gaze Response* or CGR condition) was performed at week 12. The predicted CGR was calculated as the sum of aVORd (VOR in dark) and OKR responses tested individually and compared with measured performance during combined visuo-vestibular stimulation. As expected, in SHAM animals (figure 6A), the CGR gain measured corresponds well with a simple summation of the VORd and OKR gain (compare blue line and blue shaded area in Figure 6A) and is high (>0.7) in all conditions. The right panel in figure A shows the individual values obtained for SHAM (n=8) individuals for the vestibular-only (aVORd), visual-only (OKR), and visuo-vestibular (CGR) conditions, respectively. At 1Hz, the combined response is normally dominated by vestibular inputs as shown in the left panel. In the IDPN group (n=12), predicted CGR gain is slightly lowered compared to SHAM group by ~0.1 in the 3 tested conditions. However, the measured CGR of IDPN mice does not match their predicted CGR, such that the combined visuo-vestibular response is low (~0.5) at all frequencies. This would suggest that at W12, IDPN mouse cannot optimally integrate visual and vestibular inputs to stabilize gaze. Figure 5C illustrates the relationship between the predicted and measured CGR gain for all tested frequencies and animals. For Sham animals, CGR gain values are next to the unity dotted line that represents a perfect match between predicted and tested CGR. For IDPN mice, the responses form 2 clusters that do not correspond to different frequencies (all frequencies are present in either subgroup). The first cluster is intermingled with the SHAM responses, with measured values slightly lower than predicted values. The second cluster represents measured CGR gain <0.4. We noted that 12/13 of these measures belong to 4 particular IDPN mice with a CGR<0.4 and detail of their responses is shown on Figure 6D. This plot (Figure 4D) illustrates that for these individuals (n=4), the low predicted CGR is a consequence of their collapsed VORd responses, as their OKR responses are high at 0.5 and 1Hz, as previously described. Surprisingly, this subset of IDPN presents measured CGR that are below predicted CGR (as expected from plot 6C), but that is also below the responses in the visual-only condition. For these individuals, the response in the visuo-vestibular condition is actually worsened compared to the visual-only condition. This effect is further illustrated in the subplot of figure 6D showing that at 1HZ, individual OKR

values are higher than CGR values (two-tailed non-parametric t-test, p=0.0286). Figure 6E illustrates the responses of the IDPN mice (n=8) with CGS>0.4. As expected, their OKR and VOR responses are globally respectively higher and lower compared to SHAM (ANOVA repeated measures, VOR Group effect p=0.0234, OKR Group effect p=0.00126). As a sum of these 2 variations, their predicted CGR remains in the range of the SHAM group, such that the increased OKR could theoretically substitute for the decrease in VORd (ANOVA repeated measures, predicted CGR Group effect p=0.6934). However, this is not the case as their measured visuo-vestibular responses remain significantly lower than the predicted CGR (Group effect CGR p=0.001178). Thus, even in IDPN mice that show a significant recovery of vestibular responses and a potentiated OKR, the integration of visual and vestibular inputs remains suboptimal.

Discussion

IDPN as a model of partial and transitory loss of vestibular function

IDPN was long established as an ototoxic compound targeting vestibular hair cells in the different vestibular endorgans of rats (Llorens et al., 1993, 1994; Llorens and Demêmes, 1994) and later in guinea-pig, frogs and mice (Soler-Martin et al., 2006; Greguske et al., 2019). Its ototoxic vestibular effects have previously been used as a tool to study extraocular muscle development (Brueckner et al., 1999) or more recently to induce permanent vestibular loss in mice (Yang et al., 2019; Zeng et al., 2020) and study cell regeneration (Sayyid et al., 2019). The sub-chronic, reversible, protocol used in our study was validated in rats (Sedó-Cabezón et al., 2015; Martins-Lopes et al., 2019b; Maroto et al., 2021) and mice (Boadas-Vaello et al., 2017; Greguske et al., 2019) with postural / locomotor quantification of vestibular loss. We for the first time demonstrate that the subchronic protocol leads to a progressive and reversible loss of vestibulo-ocular reflexes. These previous studies further demonstrated some of the cellular mechanisms that lead to the progressive loss of vestibular functions: ototoxic effects lead to the early dismantlement of calyx junction, followed by synaptic uncoupling, both of which were shown to be reversible, while continuation of the IDPN treatment would lead to hair cell extrusion and long-term lesion. Hair cell loss was also demonstrated to occur in a central to peripheral order within vestibular epithelia, and in crista to utricule to saccule order (see Sedó-Cabezon et al. 2015). Greguske et al. (2019) convincingly demonstrated that type I hair cells show greater sensitivity than type II hair cells to IDPN subchronic exposure (Maroto et al.

2021). Given these data, a primary goal of the present study was to try to correlate the loss of VOR functions to organ-specific, zone-specific, and cell-type-specific effects.

Loss and substantial recovery of the vestibular function quantified by VOR measures were found to be correlated with the number of type I hair cells in both canals and otoliths. A parallel was previously established between hair cell integrity and VOR following ototoxic protocols in mice (Cassel et al., 2019; Yang et al., 2019; Zeng et al., 2020), but these were established at the population level. Here, we for the first time specifically correlated the loss of hair cells and loss of VOR function both at the individual level and in an organ-specific way. aVOR and OCR tests demonstrated a parallel decrease in canal- and otolith-dependent functions, respectively. The 6 weeks-long treatment was followed by a 6 weeks-washout period, allowing a significant but partial recovery of the aVOR, and complete recovery of the OCR. The individual correlations between these functional tests and the number of hair cells counted in the ampullae and maculae of the mice were found to be particularly significant, both during the trough (week 6) of VOR function and after the recovery period (week 12) (see Figure 3, C, D, E). We, however, did not find any difference between the hair cell loss in the central vs peripheral zones of the organs, and can therefore not conclude on any putatively differential implication in the VORs. Overall, these organ-specific structure-function correlations confirm that the vestibulo-ocular reflex can serve as a proxy indicating the status of the vestibular endorgans. It further validates the use of the aVOR and OCR as relevant tests reflecting hair cell integrity at the level of the ampullae and maculae, respectively.

A differential loss of type I versus type II hair cells

The subchronic treatment affected type I HC more than type II HC, in accordance with previous reports (Llorens et al. 1993; Maroto et al. 2021). Susceptibility to IDPN was also reported to variate between different mouse strains (Boadas-Vaello et al., 2017; Wilkerson et al., 2018). Interestingly, we used a different strain of mice than the one used in a previous subchronic experiment (Greguske et al. 2019) and have neither observed a loss of type II HC, nor differences between males and females.

Hence, IDPN treatment induces a loss of cell markers specific to type I hair cells, with no effects on type II markers. Two types of markers were used to identify type I HC. Spp1 targeted a protein located on the neck of the hair cell (McInturff et al., 2018), while Caspr1 is located at the calyceal junction of the afferent terminal, and has been proven to be necessary for the

functionality of the synapse between the hair cell and its connected afferent (Sousa et al., 2009). Though it is not possible to compare for one individual the number of cells before and after treatment, the number of cells labelled for either of these proteins decreased significantly compared to SHAM group, whose numbers are consistent between W6 and W12. The loss of Caspr1 marker induced by IDPN acute or sub-chronic treatment has been linked to hair cell extrusion from the calyx terminal (Greguske et al., 2019; Maroto et al., 2021). In theory, the loss of vestibular function observed in both canal- and otolith-dependent VOR at W6 could be linked to the extrusion of type I hair cells. In adult rodents, however, the regeneration of hair cells leads to the formation of cells with type II HC features (González-Calvo et al., 2021), so the recovery of type I cellular markers at W12 is likely not a result of cell regeneration. The recovery in the number of type I HC therefore suggest that most were not extruded. In addition, we observed a similar loss of Spp1 marker at W6, normally located in the neck of the hair cell. As such the loss of vestibular function could rather be attributed to a global disorganization of the synapse, leading to a transitory decrease of e.g the Spp1 and CAPR1 protein. In accordance with this hypothesis, the number of Spp1 and Caspr1 positive cells after the washout period at W12 was not significantly different from the SHAM group and correlated to the recovery of the vestibular function observed at W12 for the IDPN mice. The altered expression of proteins in type I HC induced by the sub-chronic treatment of IDPN seems to be reversible in most individuals. One possibility is that definitive extrusion of type I HC occurred in the most susceptible individuals that did not show a recovery after the end of treatment. It was previously reported in the pigeon that type I HC and calyx afferents take longer (12 weeks) to regenerate following aminoglycosyde toxicity, while type II and boutons endings regenerated in a week (Zakir and Dickman, 2006). Similarly, recovered innervation for type I HC was delayed compared to type II HC in mice (Kim et al., 2022). A longer recovery period could be investigated in the case of the severely-affected mice to confirm the absence of recovery on the long term.

Evidence for the role of type I HC in the vestibulo-ocular pathways

To our knowledge, the direct implication of type I and type II hair cells in the VOR was never directly tested. Type I and type II HC differ by many features, including their anatomical location within the epithelium, electrophysiological properties, morphology and innervation by afferents (Eatock and Songer, 2011). Seemingly, irregular afferents have been described as

predominantly innervating the central area and striolar zones of the ampullae and maculae with calyx and dimorphic synaptic contacts, while regular afferents make dimorphic and buttons contacts predominantly within the peripheral zones of cristae and extrastriolar zones of maculae (Goldberg, 2000; Eatock and Songer, 2011; Contini et al., 2022).

Functionally, regular afferents recorded in the monkey show lower detection threshold than irregular afferents (Sadeghi et al., 2007), while irregular show higher gains and phase leads (mouse: Lasker et al., 2008; Cullen, 2019), and would be better optimized for encoding high dynamic stimuli (Cullen, 2019). Seminal studies have suggested that irregular afferents would constitute ~1/3 of the excitatory drive received by central neurons responsible for the VOR (Highstein et al., 1987; Boyle et al., 1991), and functional ablation targeting irregular afferents that VOR might function normally with only regular afferent inputs(Minor and Goldberg, 1991).

Based on these data, it would be tempting to infer that the most regular and tonic elements of the vestibular periphery are the only ones responsible for the VOR. However, the correspondence between hair cells properties and afferents properties is only partial, such that the two phasic/irregular and tonic/regular channels for head motion signals are constituted of both types of HC and afferents (Eatock and Songer 2011; Beraneck and Straka, 2011). It has also been recently shown that both types of hair cells contribute to VeSP responses, previously described as mostly type I-specific (Sayyid et al, 2019). Our data further contradict such a simplified scheme as the vestibulo-ocular reflex is severely affected by the specific loss of type I HC in both central and peripheral parts of the vestibular endorgans. Carey and colleagues (1996) previously reported a better correlation of VOR recovery with type I than with type II HC following ototoxic lesions in the chick. Overall, the result of ototoxic studies, including this one, demonstrate a fundamental role of type I HC in the encoding of vestibular signals that drive the vestibulo-ocular reflexes, even in the relatively low range of head movements tested in this study (Carriot et al., 2017). Our results are compatible with the hypothesis of a convergence of heterogeneous peripheral neural elements at the level of central vestibular nuclei, where intrinsic properties of central vestibular neurons (Straka et al., 2005; Beraneck and Idoux, 2012) supplemented by network properties (Beraneck et al., 2007; Pfanzelt et al., 2008; Beraneck and Straka, 2011) would differentially integrate vestibular signals further processed in the different vestibular pathways (Sadeghi and Beraneck, 2020).

Visuo-vestibular integration after IDPN treatment

OKR plasticity following vestibular loss concerned gain, and not phase, modifications for frequencies >0.33Hz. Previous studies have reported an increase in OKR gain following a permanent vestibular lesion for a non-specific range of frequencies (Shinder et al., 2005; Faulstich et al., 2006; Nelson et al., 2017). One key to understanding the frequency-specific OKR plasticity could be the physiological dominance of vestibular inputs in the gaze stabilisation process at high frequencies (Faulstich et al., 2004). The visual inputs could be reweighted and potentiated specifically in the range where the vestibular loss has the most impact on gaze stabilization (Fig. 5).

The VOR and OKR work synergistically to stabilize gaze by compensating for head and visual surround movements, respectively (França de Barros et al., 2020). If the reflexive eye movements are not perfectly compensatory, an error signal (retinal slip) is produced that drive adaptation of the VOR (Boyden et al., 2004; Dean and Porrill, 2014; Shin et al., 2014) and OKR (Glasauer, 2007; Kodama and du Lac, 2016). In an effort to understand the integration of VOR and OKR, Holland and colleagues (2020) recently proposed that OKR would predict the retinal slip not compensated by VOR. Within that framework, the changes in the OKR could happen preferentially as a function of the vestibular weight, i.e in the range of movements where the loss of vestibular inputs generates the largest retinal slip. The increase in OKR gain is in theory substituting for the decrease in the VOR, such that the predicted CGR of IDPN mice compares to that of SHAM. However, even after VOR recovery, the integration remained sub-optimal in the mice with a high CGR. In mice with a low CGR, the combination of VOR and OKR is not only sub-optimal but also less performant than the unimodal (OKR) reflex. The integration of visual and vestibular inputs is occurring in several structures, including in the cerebellar flocculi (Jang et al., 2020) and brainstem (Carcaud et al., 2017) (see review De Zeeuw et al., 2021). In the case of vestibular loss, most of the defects are expected to concern the central vestibular neurons involved in the VOR, which also integrate visual inputs (ES, or eye-sensitive neurons; Beraneck and Cullen, 2007). After a unilateral neurectomy performed in the cat, vestibular neurons in the Deiters nuclei responded to higher frequencies during visual stimulation (Zennou-Azogui et al., 1994), a change compatible with the hypothesis that OKR gain increase partly takes place in the vestibular nuclei. It was shown that inhibitory floccular inputs (including OKR) and excitatory vestibular inputs often colocalized on the dendrites of central vestibular neurons. One possibility is therefore that the massive disorganization of vestibular

inputs led in the long term to synaptic and intrinsic changes at the level of central vestibular neurons (Beraneck and Idoux 2012; Carcaud et al. 2017), thus impairing their capacity to integrate both signals.

Material & Methods

Ethics

A total of 56 C57/BL6J mice in an equal partition of males and females were used for the protocol. Animals were used in accordance with the European Communities Council Directive 2010/63/EU. All efforts were made to minimize suffering and reduce the number of animals included in this study. All procedures were approved by the ethical committee for animal research of the Université Paris Cité.

Headpost implantation surgery and animal care

Surgical procedures, postoperative care, device fixation and animal surveillance during the protocol were performed as described previously in França de Barros et al., 2019, 2020. Briefly, mice anaesthetized with isoflurane gas had their heads shaved with small clippers. Then, lidocaine hydrochloride (2%; 2mg/Kg) was injected locally before a longitudinal incision of 1.5 cm was made to expose the skull. Just anterior to the lambda landmark, a small custom-built headpost (3x3x5mm; poly lactic acid) was cemented (C&B Metabond; Parkell Inc., Edgewood, NY) and laterally covered with resin (Heraeus) for protection. Animals were fully recovered 30 min after the end of the surgery, yet buprenorphine (0.05mg/kg) was provided for postoperative analgesia and they were closely monitored for the following 48 hours.

Sub chronic ototoxic exposure

28 mice were treated with 3,3'-iminodiproprionitrile (IDPN, Sigma Aldrich, 317306, 90%) for 6 weeks (IDPN group) at 30mM concentration of IDPN in their drinking water. After 6 weeks of treatment, a washout period of 6 weeks followed. Previous experiments (Greguske et al., 2021) had demonstrated that at these concentrations, ototoxic lesions produced by IDPN are reversible; we, therefore, refer to this transitory alteration as a *subchronic* protocol. The SHAM group was tested the exact same way but was not exposed to IDPN in their drinking water. Video-oculography tests were performed before the beginning of the treatment and once every two weeks until week 12 (W12), for a total of 7 sessions of tests for each mouse.

Experimental groups

3 different batches of mice were used, each composed of both IDPN-treated mice and SHAM. The mice of the first one (n=19) were subjected only to vestibular stimulations, to test the effect of IDPN on the canal-related or otolith-related VOR responses during the 12 weeks of protocol. The second group (n=24), designed to compare the dynamic of VOR and OKR changes was tested with angular VOR stimulations, otolithic test, optokinetic (visual) stimulations, and combined vestibular and visual stimulation (VOR in light; referred to as Combined Gaze Response or CGR). The third group (n=11) designed to correlate ototoxic effects of IDPN on vestibular hair cells (HC) and VOR function was tested for canal-related or otolith-related VOR responses, before treatment and after 6 weeks of treatment and immediately used for immunochemistry experiments (see below). A subset of the second group (n=12 out of 24) was also used for immunochemistry experiments at the end of the 12 weeks of protocol.

Video oculography recordings sessions

The recording procedure is similar to the one presented in Carcaud et al. 2017 & França de Barros et al. 2020. The animals were head-fixed in a custom build Plexiglas tube, and their head was oriented in a 30° nose down position to align the horizontal canals to the yaw plane. Their left eye movements were recorded using a non-invasive video oculography system (ETL -200 Iscan, acquisition rate 120Hz, Stahl et al 2000). Eye, head, and virtual drum (OKR stimulation) position signals were digitally recorded (CED mk3 power 1401, acquisition rate 1kHz) with Spike 2 software. Signals were analysed offline in Matlab (Matlab, the MathWorks, Natick, MA, USA; RRID, SCR:001622) programming environment. The restraining apparatus was fixed on a rotation platform on top of an extended rig with a servo-controlled motor. Single VOR or OKR recording sessions lasted no longer than 45 minutes in total.

Vestibular stimulations and analysis

All vestibular-specific tests were performed in a temperature-controlled room with all sources of light turned off except for computer screens. The turntable was further surrounded with a closed box to isolate the animal from remaining light, with a final luminance inside the box <0.02 lux. Myosis was induced with topical 2% pilocarpine applied 10 minutes before experimentation.

Vestibulo ocular reflex in dark (VORd) tests were performed in the dark with the mouse surrounded by an opaque black dome (Fig1.A). Sinusoidal angular rotations around the vertical axis were used to record the horizontal angular vestibulo-ocular reflex (aVOR), at different frequencies: 0.2, 0.5, 0.8; 1 and 2Hz at a peak velocity of 30°/s.

Angular vestibulo-ocular reflex analysis is similar to the one described in Carcaud et al. 2017. Segments of data with saccades were excluded from VOR slow-phase analysis. For horizontal sinusoidal rotations, at least 20 cycles were analyzed for each frequency. VOR gain and phase were determined by the least-squares optimization of the equation:

$$EH_v(t) = g \cdot \{[HH_v \cdot (t - t_d)] + \mathrm{C^{te}}\}$$

where EHv(t) is eye horizontal velocity, g (gain) is a constant value, HHv (t) is head horizontal velocity, td is the dynamic lag time (in msec) of the eye movement with respect to the head movement, and C^{te} is an offset. The td was used to calculate the corresponding phase (ϕ°) of eye velocity relative to head velocity. The Variance-Accounted-For (VAF) of each fit was computed as

$$1 - \left[\frac{var(est - EHv)}{var(EHv)}\right]$$

where *var* represents variance, *est* represents the modeled eye velocity, and *EHv* represents the actual eye horizontal velocity. VAF values for VOR measures were typically between 0.70 – 1 (>95% of recordings), where a VAF of 1 indicates a perfect fit to the data. Trials for which the VAF was less than 0.5 were excluded from the analysis.

Static Ocular Counter-roll reflex were performed as described in Simon et al. 2021 by measuring the vertical eye movement generated in response to different roll angles. The table was moved from left to right in incremental steps of 10° (from 0 to 40deg), with static periods of at least 10s between oscillations (Fig1.D) to record the stabilized eye elevation and declination. The OCR gain corresponds to the slope of the linear regression of the vertical eye angle *vs* the head tilt angles (Oomen and Stahl, 2008).

Off vertical axis rotation (OVAR) tests were performed with the vestibular turntable tilted with a 17° off-axis angle following the methodology described in Beraneck et al. 2012 & Idoux et al., 2018. 50°/s continuous stimulations were performed in a counter-clockwise and then clockwise direction. OVAR generates a continuous change in the head tilt angle, compensated through a maculo-ocular reflex (MOR) by the generation of a horizontal nystagmus compensating for the table constant rotation. This oculomotor response was quantified following the methodology described in Idoux et al 2018. First, quick-phases were identified and removed. During rotations, the velocity of horizontal slow phases is modulated (modulation, μ) around a constant bias (β). Both parameters (μ and β) were calculated from the sinusoidal fit of eye horizontal slow-phase velocity using the least-squares optimization of the equation:

$$SP(t) = \beta + \mu \cdot sin[2\pi \cdot f_0 \cdot (t + t_d)]$$

where SP(t) is slow-phase velocity, β is the steady-state bias slow phase velocity, μ is the modulation of eye velocity, f_0 is the frequency of table rotation, t_d is the dynamic lag time (in msec) of the eye movement with respect to the head movement. The bias (Maculo-ocular reflex Bias) is reported here as the main index of the MOR response (Hess and Dieringer, 1990; Beraneck et al., 2012).

Optokinetic reflexes tests and analysis

Horizontal optokinetic stimulations were performed as previously described in França de Barros et al. 2020. The mice were placed under a semi-opaque plastic dome and all sources of light were turned off. The projected stimulation consisted of a randomly distributed white dots pattern on a black background image (250000 white dots, max width 0.075°). The optokinetic sinusoidal stimulations were tested at 0.1, 0.2, 0.33, 0.5 and 1Hz at a peak velocity of 10°/s. The gain and phase were obtained by the same least-squares optimization method described above for the aVOR. To prevent putative cross effects between visual and vestibular stimulations, VOR and OKR test sessions order were performed on separate days.

Combined visual and vestibular stimulations

Combined visual and vestibular stimulations measuring the combined gaze reflex (CGR) consisted of horizontal vestibular stimulations while projecting the fixed dotted pattern used

for OKR on the surrounding dome. Horizontal angular sinusoidal rotations were performed at frequencies of 0.2, 0.5 and 1Hz with a peak velocity of 30°/s. The CGR gain and phase quantification were performed following the same methodology as for aVOR. To avoid interference, these were performed on n=8 SHAM and n=12 IDPN after the end of the VOR and OKR test sessions on week 12. To test the effects at week 6, a specific group of mice (n= 4 SHAM and n=8 IDPN) was tested at week 0 and week 6.

Immunolabelling of the hair cells

Two groups of mice (n=11 at W6 and n=12 at W12) were used to perform immunofluorescence analysis on hair cells in the vestibular endorgans. Mice were anaesthetized with an overdose of intraperitoneal injection of ketamine hydrochloride (10%)/xylazine (5%) and decapitated. The histology was done following the protocol of Maroto et al., 2021. The vestibular epithelia (one horizontal canal and one utricule) were dissected and fixed for 1h in a 4% solution of paraformaldehyde (PFA). PFA was washed twice with phosphate-buffered saline (PBS) and the samples were placed at 2° for effective embedding and then stored at -20°. Before the immunochemistry, samples were put at room temperature and rinsed twice in PBS. While under slow agitation, the samples were incubated twice, first for 1h with a 4% Triton X-100 (Sigma Aldrich) in PBS to permeabilise and a second time for 1h in 0,5% Triton X-100 1% fish gelatin (CAS #9000-70-8, Sigma-Aldrich) in PBS to block. The incubation with the primary antibodies was then performed in 0,1M Triton X-100, 1% fish gelatin in PBS at 4° for 24h. After rinsing, the second antibodies were incubated in the same conditions. The 2nd antibodies were rinsed and the vestibular epithelia were mounted on slides with fluoromount (F4680, Sigma-Aldrich) and were visualised with a confocal microscope Zeiss LSM880 (with an objective of 63x NA:1;4). To properly analyse the whole vestibular epithelium, Z-stacks of 0,5 µm were performed and observed with ImageJ (National Institute of Mental Health, Bethesda, Malyland, USA). The primary antibodies used were rabbit anti-Myosin VIIa (Myo7a) (Proteus Biosciences, #25-6790), mouse anti-contactin-associated protein (Caspr1) (Neuromab #75-001), guinea pig anti calretinin (Synaptic Systems #214-104) and goat anti-osteopontin (Spp1) (R&D Systems #AF08). Their respective secondary antibodies were Dylight 405 donkey anti-rabbit ifG H+L (Jackson Immuno Research #711-475-152, Alexa Fluor 488 donkey anti-mouse IgG H+L (Life Technologies #A21202), Alexa Fluor donkey anti-guinea-pig IgG H+L (Jackson

ImmunoResearch #706-605-148) and Alexa Fluor 555 donkey anti-goat IgG H+L (Invitrogen #A21432).

The hair cells in two vestibular organs (horizontal semi-circular canals and utricule) were counted in the W6 group and the W12 group. The global number of hair cells was assessed with the cytoplasmic labelling of the anti-Myo7a antibody (Hasson et al., 1997). Type I hair cells were labelled using two different antibodies: anti-Spp1 in the neck of the type I HC (McInturff et al., 2018) and the presence of anti-Caspr1 in the calyceal junctions of the calyx (Sousa et al., 2009 p.20). Type II hair cells were distinguished by the colocalization of Myo7a and calretinin (Maroto et al, 2021).

Statistical analysis

For both OKR and VOR stimulations, the effect of the protocol on the gain and phase were statistically tested by performing a mix-model ANOVA. The *treatment* (SHAM or IDPN) was considered as between individual independent factor with the *Weeks* (W0, W2, W4, W6, W8, W10, W12) and the *Frequencies* (0.1, 0.2, 0.33, 0.5 and 1Hz for the OKR; 0.2, 0.5, 0.8, 1 and 2Hz for the VOR) were considered as within individual independent factors. The main effects of those factors and their interactions were tested and reported. In the case of the OCR and OVAR, mix-model ANOVA was used with only *Weeks* considered as within factors. For the CGR, measured at W6 and W12, mix-model ANOVA was used with only the *Frequencies* used as within factors. For the comparison between the OKR and VOR Δ gain, a repeated measures ANOVA was applied on the Δ gain (Wx-W0) with the *stimulation modality* (OKR or VOR) as between individual independent factor and the *Weeks* as within individual independent factor. For the correlation between TILT and VOR, as well as the measured and theoretical CGR gain a linear regression model was fitted.

The effect of IDPN exposure on the hair cell count was reported with a Kruskal Wallis test.

For all analyses the significance threshold was set at $p<0.05$ and Newman Keuls post hoc test was performed if the main effect or an interaction was found significant.

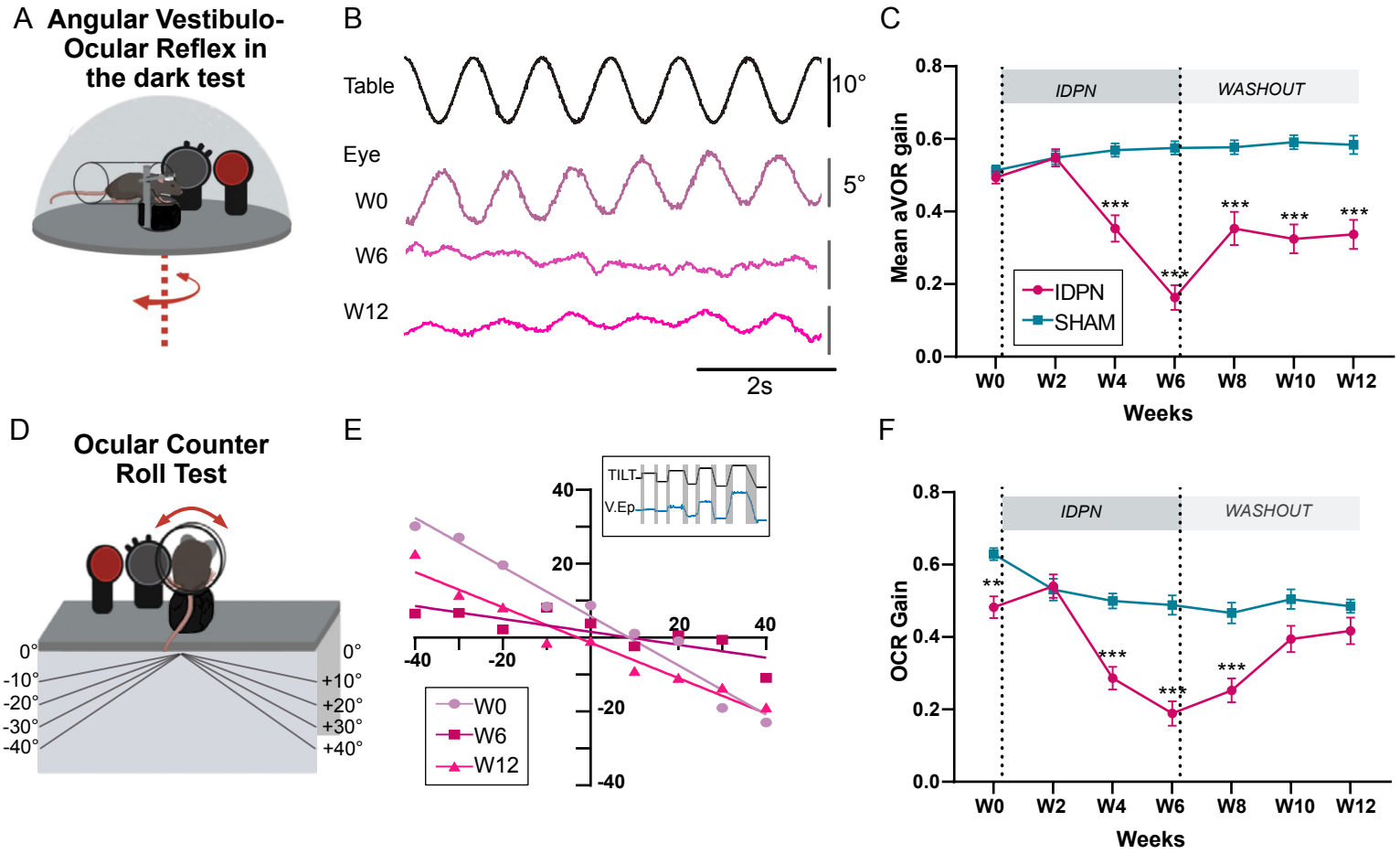

Figure 1: Effects of subchronic IDPN on canal- and otolithic- dependent VOR.

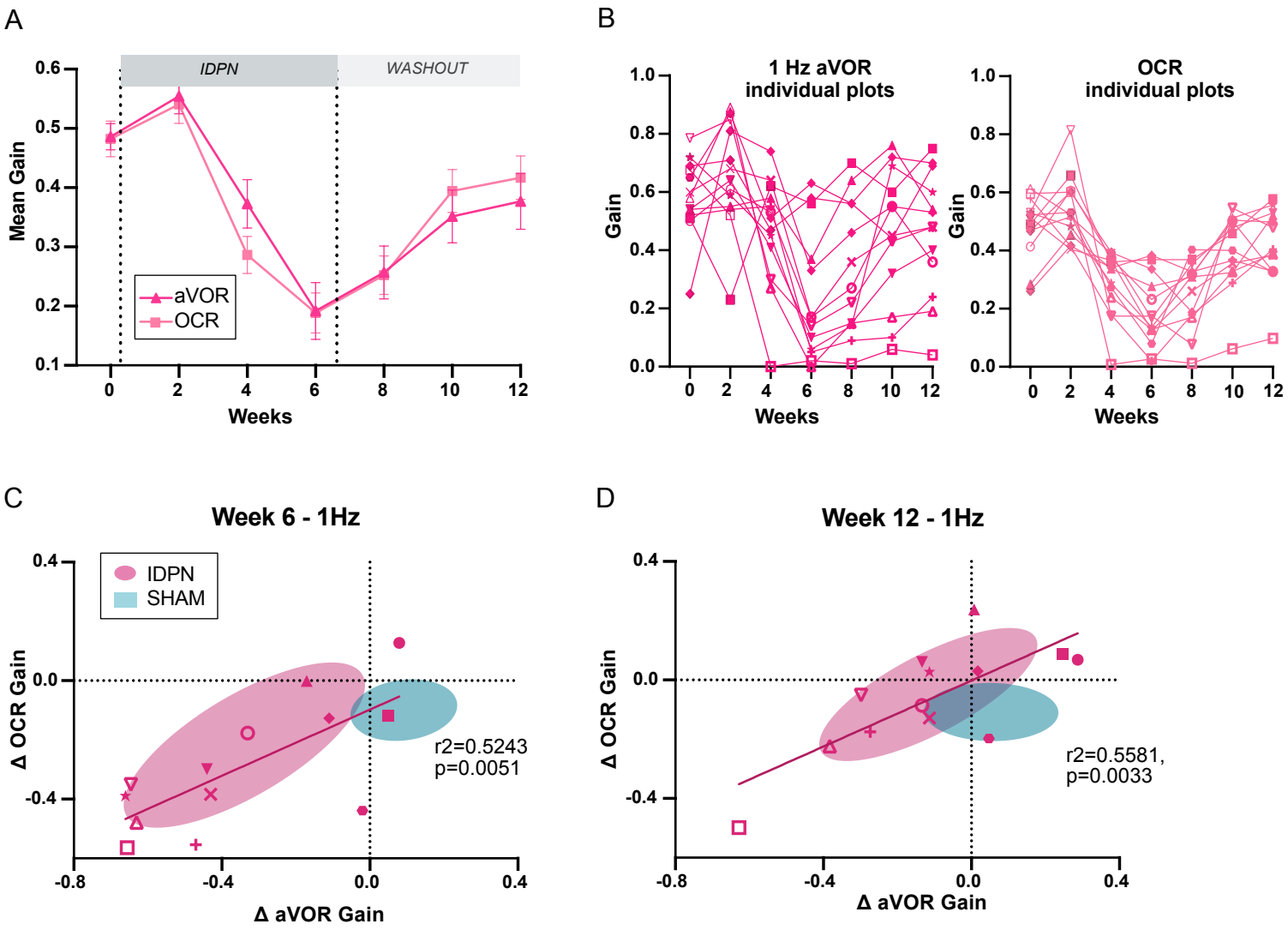

Figure 2: Comparison of the dynamics of canalar and otolithic loss of function.

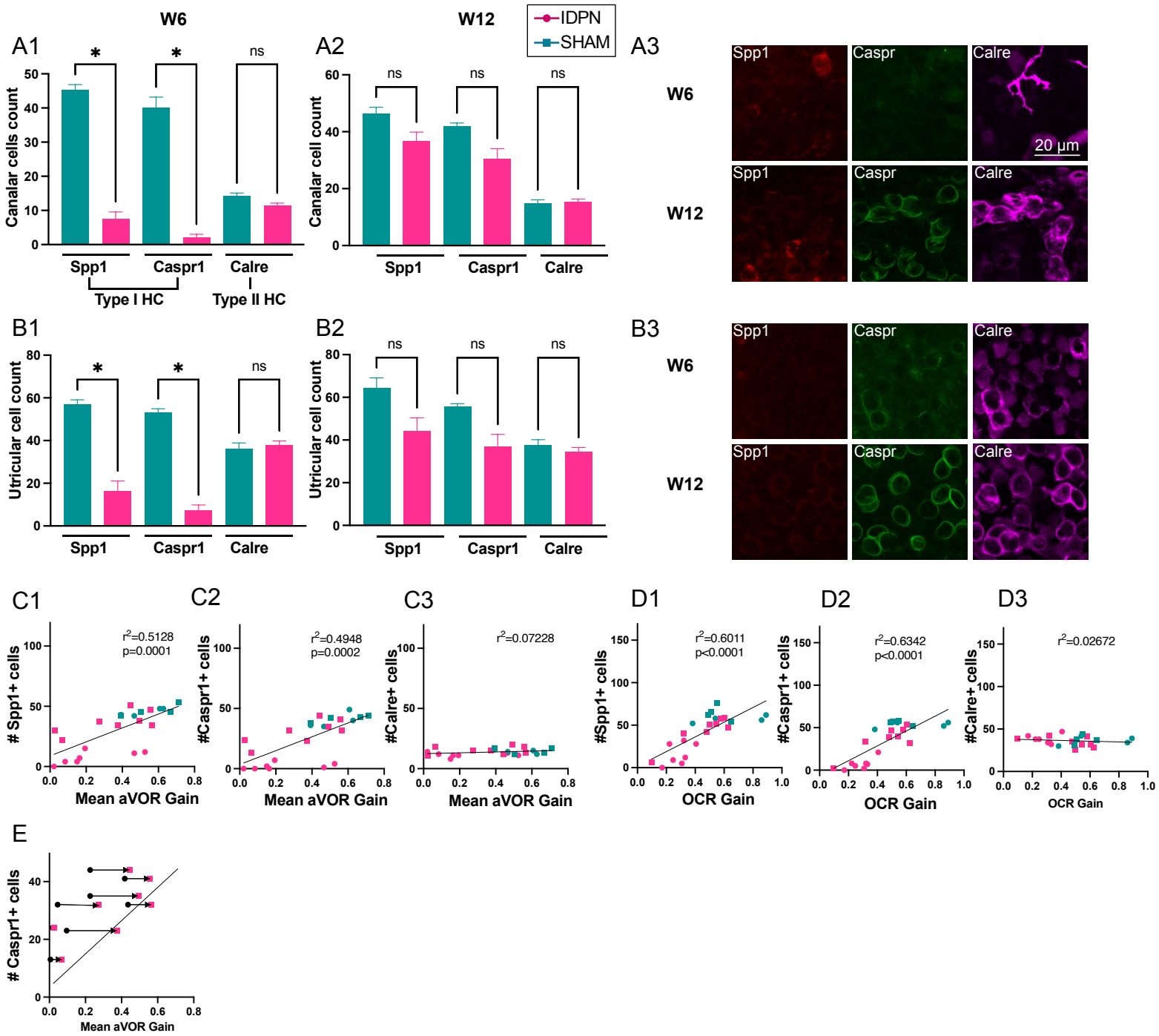

Figure 3: Effects of the IDPN on the number of hair cells in the central regions of the horizontal SCC ampulla and striolar region of the utricule Macula.

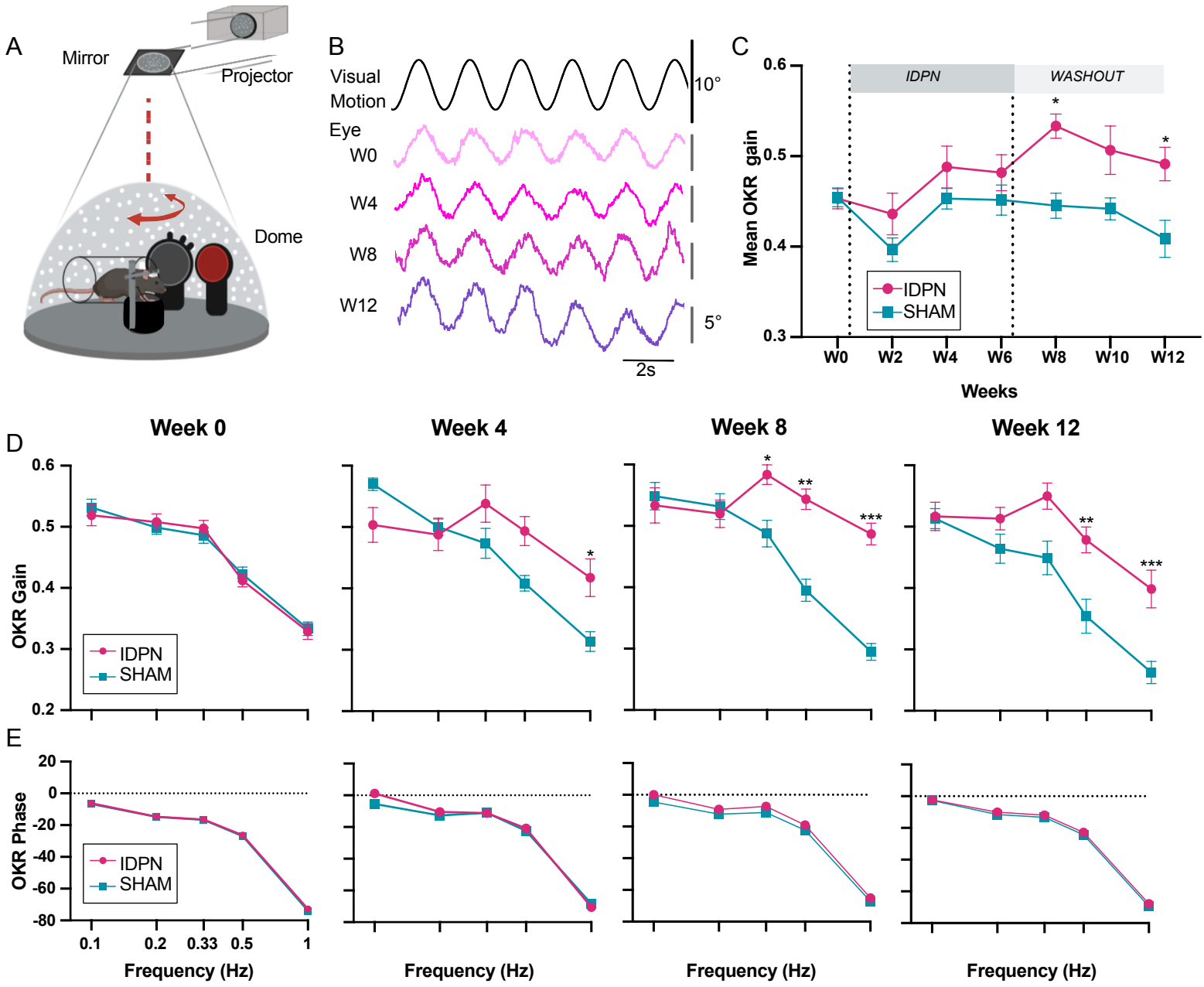

Figure 4: Effects of subchronic IDPN treatment on the OKR.

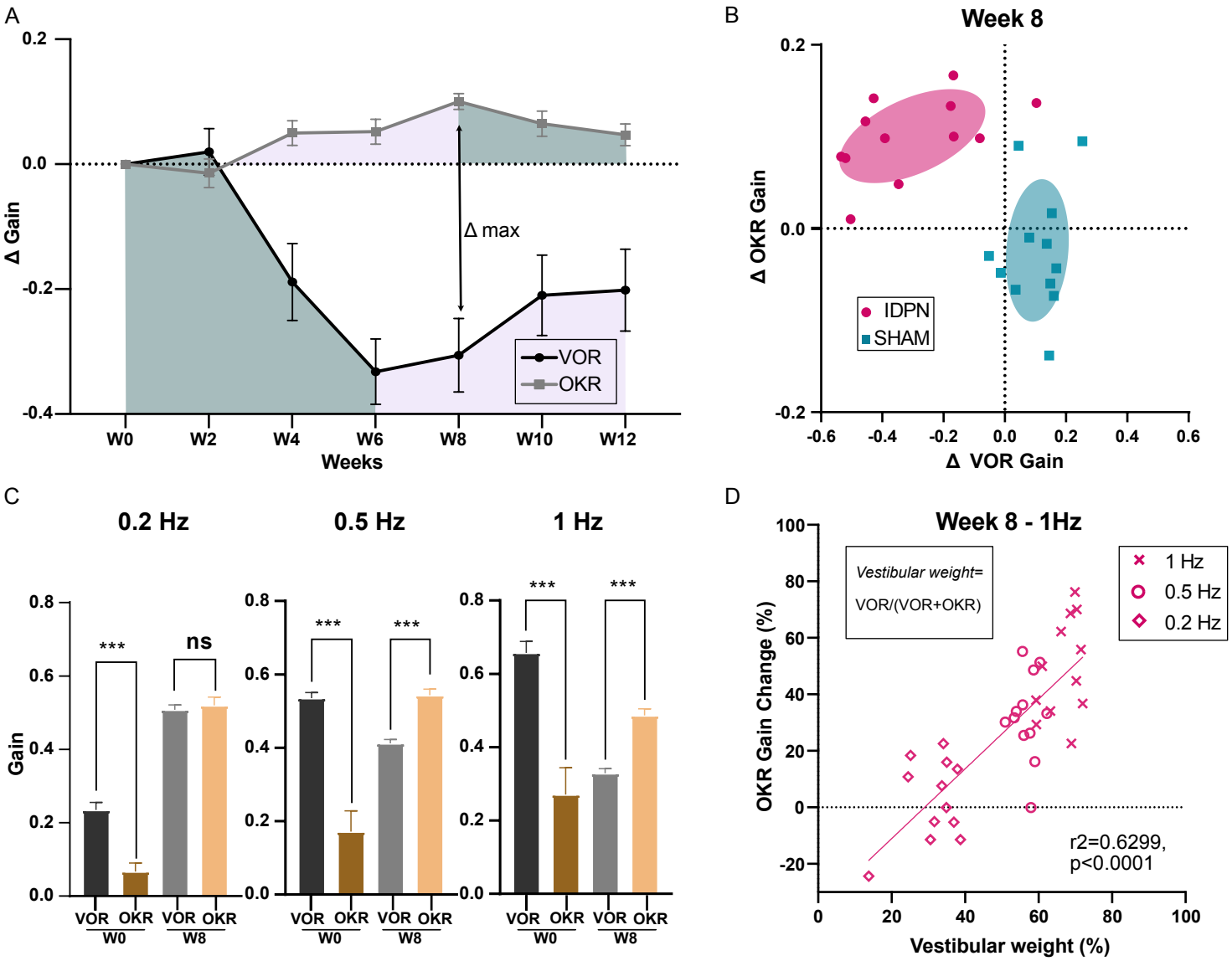

Figure 5: Dynamics of the IDPN treatment on OKR and aVOR.

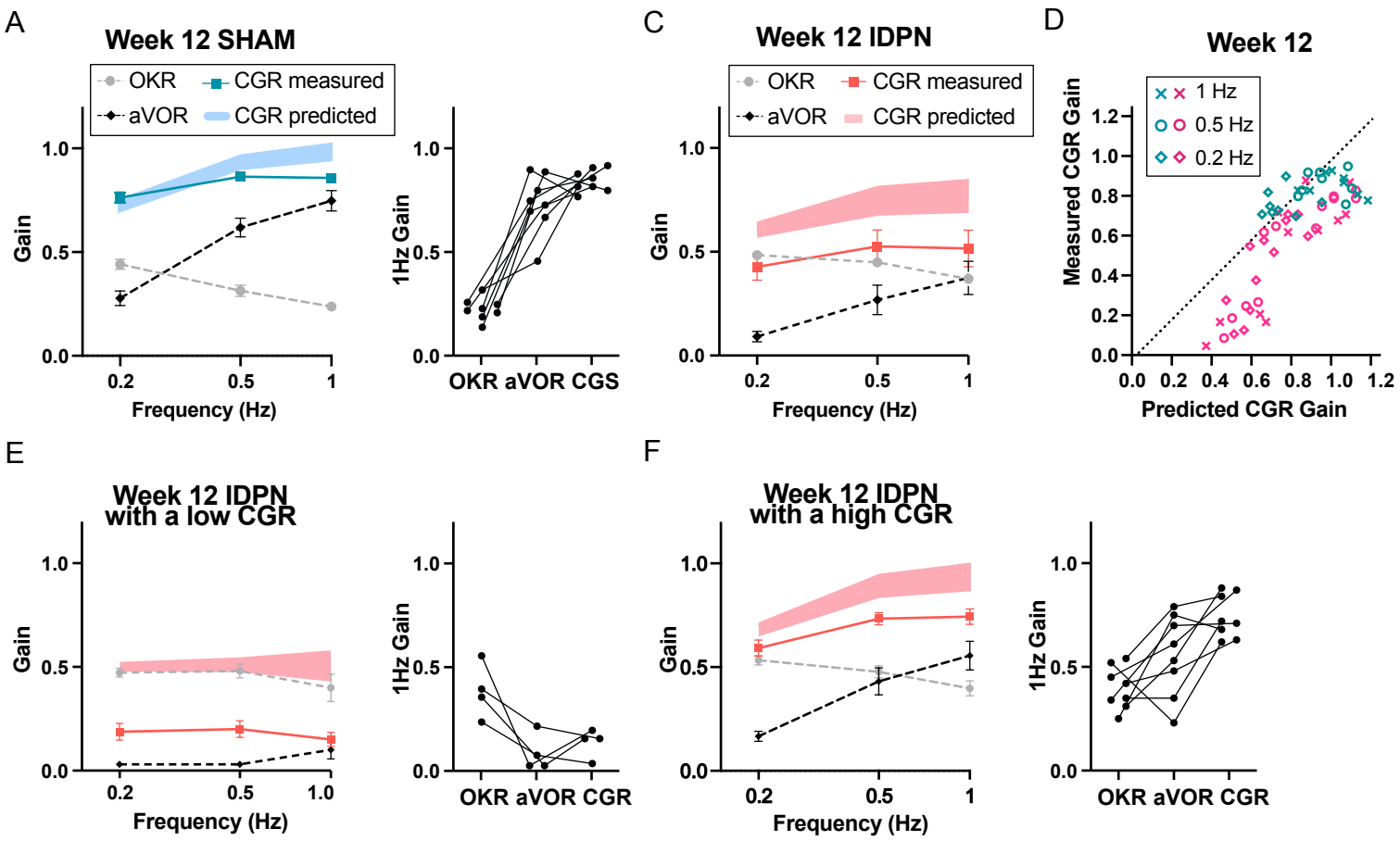

Figure 6: Suboptimal integration of visual and vestibular inputs.

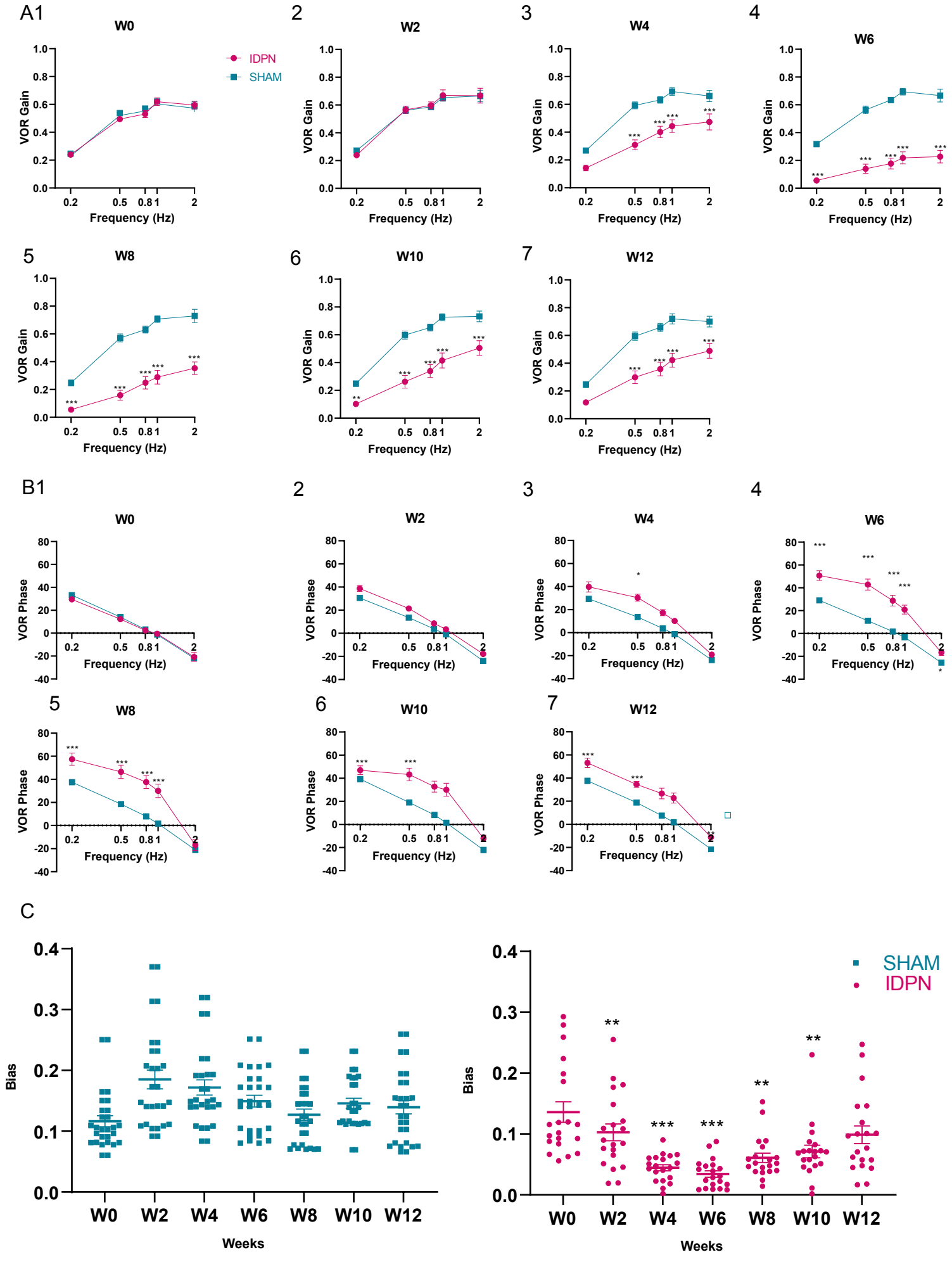

Supplementary Figure 1: Effects of subchronic IDPN on canalar- and otolith-dependent VOR.

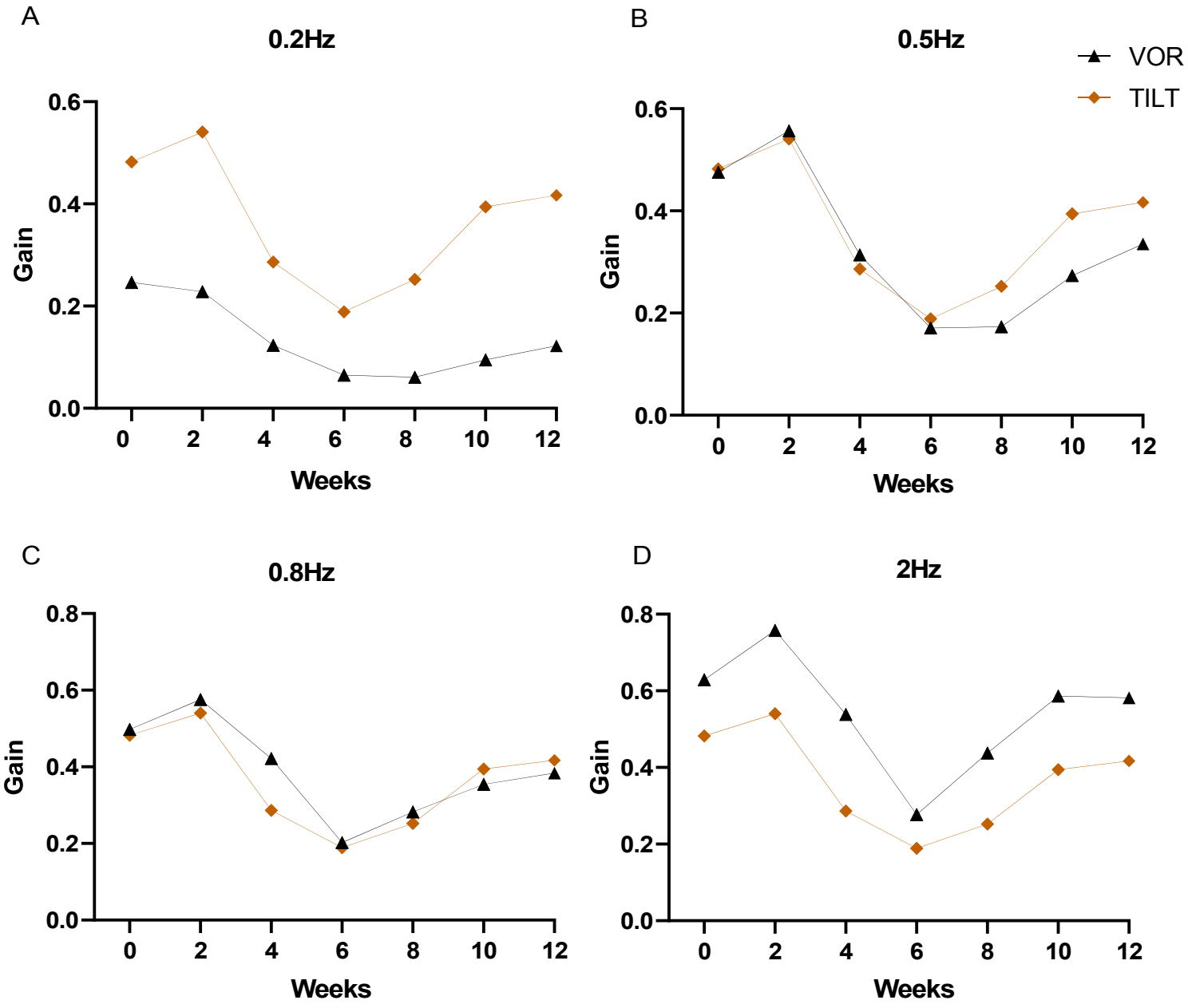

Supplementary Figure 2: dynamics of canalar and otolithic loss of function for all frequencies.

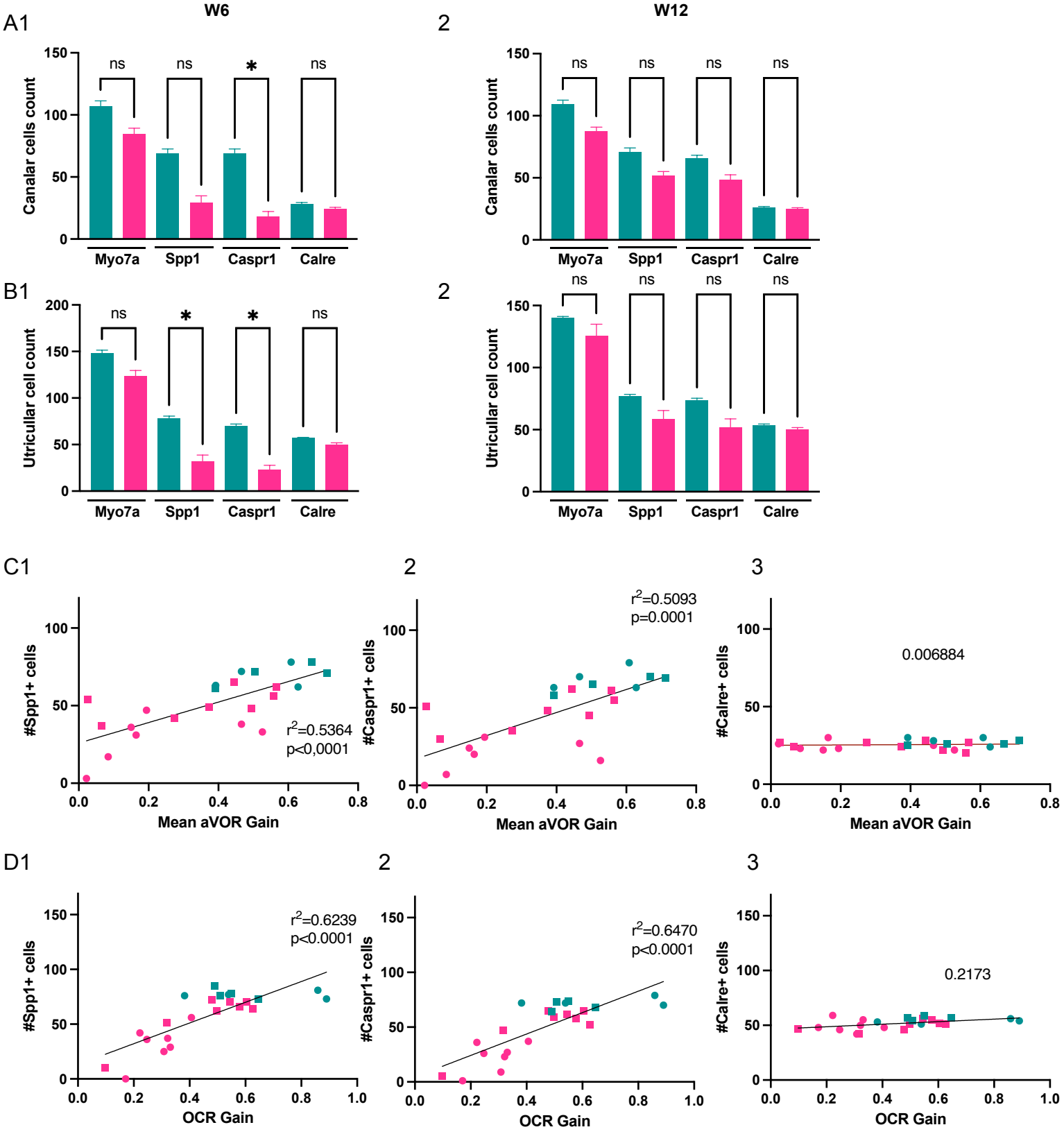

Supplementary Figure 3: Effects of the IDPN on the number of hair cells in the peripheral regions of the horizontal SCC ampulla and extrastriolar utricule Macula.

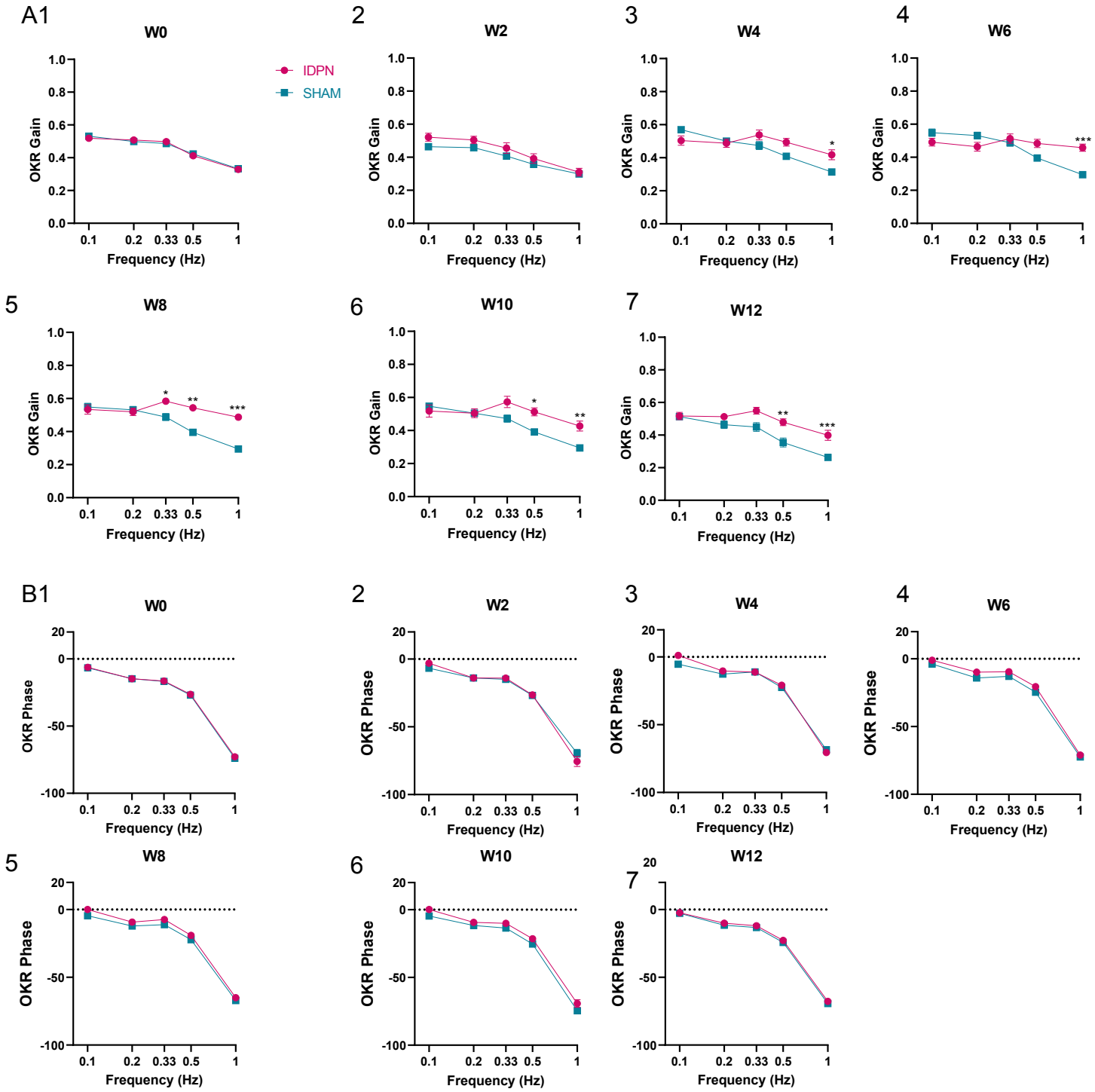

Supplementary Figure 4: Effect of the IDPN on optokinetic reflex amplitude and timing.

FIGURE LEGENDS

Figure 1: Effects of subchronic IDPN on canal- and otolithic- dependent VOR.

A) aVOR set-up.

B) Examples of raw traces of a 1Hz at 30°/s aVOR in the dark (table) recorded before (WO), and after 6 weeks of IDPN (W6) and 6 weeks of washout (W12) of the same animal.

C) Mean aVOR gain of IDPN (n=21) and SHAM (n=22) mice during the protocol.

D) OCR test set-up.

E) Angles of eye elevation in response to Roll static angles, before (W0) and after 6 weeks of IDPN (W6) and 6 weeks of washout (W12) of the same animal. Gain of the OCR is the slope of linear regression lines (W0 r^2=0,9614, W6 r^2=0,6670, W12 r^2=0,9549). Inset: example of a raw trace of OCR at W0.

F) Mean OCR gain of IDPN (n=13) and SHAM (n=14) mice during the protocol. We note that there was a significant difference between SHAM and IDPN during the initial measurements at W0. However, at this time point mice were not yet separated into different groups. This incidental difference however completely disappeared on the measurement performed at W2. (** p<0.001, ***p<0.0001). Errors bar represents ±SEM.

Figure 2: Comparison of the dynamics of canalar and otolithic loss of function.

A) Gain of the 1 Hz aVOR and OCR during the protocol of IDPN mice.

B) Individual traces of IDPN mice (n=13) for 1Hz aVOR (left)and OCR (right).

C, D) Individual ΔaVOR gains as a function of individual ΔOCR gains at W6 (C) and W12 (D) compared to W0, for IDPN and SHAM (n=14). The linear regression of IDPN mice is represented as well as the 50% confidence interval of each group (shaded areas).
The symbols for each animal are the same in panels B, C and D.

Figure 3: Effects of the IDPN on the number of hair cells in the central regions of the horizontal SCC ampulla and striolar region of the utricule Macula.

A) Cell count of type I and type II HC for W6 mice (1) and W12 mice (2) in the central horizontal ampulla. Blue is SHAM; Pink is IDPN. A3) Immunolabelling of type I HC (Spp1+ and Caspr1+) and type 2 HC (Calre +) for the SHAM, IDPN W6 and IDPN W12 groups.

B) Cell count of type I and type II HC for Week 6 mice (1) and Week 12 mice (2) in central utricular maculae. B3) Immunolabelling of type I HC (Spp1+ and Caspr1+) and type 2 HC (Calre +) for the SHAM, IDPN W6 and IDPN W12 groups in the central utricular maculae.

C) Individual number of central Spp1+ type I HC (1), Caspr1 + type I HC (2) and Calre+ type II HC (3) as a function of the aVOR gain for the W6 (circle) and W12 (squares) groups. The linear regression of both groups (n=23 mice) and the goodness of their fit is represented.

D) Individual number of central Spp1+ type I HC (1), Caspr1 + type I HC (2) and Calre+ type II HC (3) as a function of the OCR gain for the W6 (circle) and W12 (squares) groups. The linear regression and the goodness of fit are calculated on points (n=23 mice).

E) Comparison of the number of Caspr1 type I HC as a function of the aVOR gain at W6 (black and circle) and at W12 (pink and square) for each IDPN mice of the W12 group (n=8). Note that all points are shifted toward the regression line (redrawn from C2), indicating that the number of cells at W12 better correlates with the recovered aVOR.

Figure 4: Effects of subchronic IDPN treatment on the OKR.

A) OKR set-up.

B) Example of raw traces of the same animal of a 0,5Hz at 10°/s OKR recorded before (W0), after 4 weeks of IDPN treatment (W4), 2 weeks (W8) and 6 weeks of washout (W12).

C) Mean OKR gain of IDPN (n=12) and SHAM (n=12) mice during the protocol.

D) OKR gain and (E) phase for IDPN (n=12) and SHAM (=12) for each frequency at W0, W4, W8 and W12.

(* $p<0.05$ ** ; $p<0.001$***; $p<0.0001$). Errors bar represents ±SEM.

Figure 5: Dynamics of the IDPN treatment on OKR and aVOR.

A) Mean Δ aVOR and Δ Gain for 0.2, 0.5 and 1Hz for IDPN (n=12) and SHAM (n=12) mice.

B) Individual ΔaVOR gains as a function of individual ΔOKR gains. The 50% confidence interval of each group is represented in the shaded areas.

C) aVOR and OKR gains of IDPN mice (n=12) at W0 and W8 for all common frequencies: 0.2, 0.5 and 1Hz.
D) Percentage of the individual vestibular weight (inset), as a function of the percentage of the individual OKR gains change for IDPN (n=12) for 0.2, 0.5 and 1 Hz. The linear regression is represented.
(* p<0.05 ** ; p<0.001***; p<0,0001). Errors bar represents ±SEM.

Figure 6: Suboptimal integration of visual and vestibular inputs.

A, B, D, E) Left panels: OKR, aVOR, CGR predicted and measured gains for all frequencies. Right panels: individual OKR, aVOR and CGR for 1 Hz at Week 12. A, SHAM mice (n=8); B, IDPN mice(n=12); D, IDPN mice with a low value of measured CGR (n=4); E, IDPN mice with a high value of measured CGR (n=8)

Table 1 Statistics table of the aVOR gain for the IDPN treated group.

W0	W2	W4	W6	W8	W10	W12	
	ns	***	***	***	***	***	W0
ns		***	***	***	***	***	W2
***	***		***	***	ns	ns	W4
***	***	***		*	***	***	W6
***	***	***	*		***	***	W8
***	***	ns	***	***		ns	W10
***	***	ns	***	***	ns		W12

Table 2: Statistics table of the OKR gain for the IDPN treated group.

W0	W2	W4	W6	W8	W10	W12	
	ns	ns	ns	***	ns	ns	W0
ns		ns	ns	***	**	ns	W2
ns	ns		ns	ns	ns	ns	W4
ns	ns	ns		*	ns	ns	W6
***	***	ns	*		ns	ns	W8
ns	**	ns	ns	ns		ns	W10

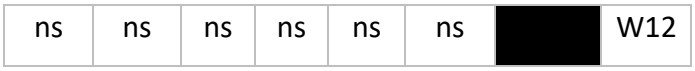

Supplementary Figure 1: Effects of subchronic IDPN on canalar- and otolith-dependent VOR.

A, B) aVOR (A) Gain and (B) Phase across all frequencies and weeks tested for IDPN (n=21) and SHAM (n=22) mice.
C) OVAR MOR bias for IDPN (n=13) and SHAM (n=14) mice during the protocol.
(*p<0.05, ** p<0.001, ***p<0.0001). Errors bar represents ±SEM.

Supplementary Figure 2: dynamics of canalar and otolithic loss of function for all frequencies. Gain of the A)0.2Hz, B) 0.5Hz C) 0.8Hz and D) 2Hz aVOR and OCR during the protocol for IDPN mice(n=13).

Supplementary Figure 3: Effects of the IDPN on the number of hair cells in the peripheral regions of the horizontal SCC ampulla and extrastriolar utricule Macula.
A) Cell count of peripheral horizontal semi-circular canal type I and type II HC for Week 6 mice (1) and Week 12 mice (2). B) Cell count of peripheral utricular type I and type II HC for Week 6 mice (1) and Week 12 mice (2). C) Individual number of peripheral Spp1+ type I HC (1), Caspr1 + type I HC (2) and Calre+ type II HC (3) as a function of the aVOR gain for the W6 group (circle) and W12 (squares). The linear regression of both groups (n=23 mice) and the goodness of their fit is represented. D) Individual number of peripheral Spp1+ type I HC (1), Caspr1 + type I HC (2) and Calre+ type II HC (3) as a function of the OCR gain for the W6 group (circle) and W12 (squares). The linear regression of both groups (n=23 mice) and the goodness of their fit is represented.

Supplementary Figure 4: Effect of the IDPN on optokinetic reflex amplitude and timing.
A) OKR Gain across all frequencies and weeks tested B) OKR Phase across all frequencies and weeks tested. (*p<0.05, ** p<0.001, ***p<0.0001). Errors bar represents ±SEM.

References

Agrawal Y, Carey JP, Della Santina CC, Schubert MC, Minor LB (2009) Disorders of Balance and Vestibular Function in US Adults: Data From the National Health and Nutrition Examination Survey, 2001-2004. Arch Intern Med 169:938.

Agrawal Y, Ward BK, Minor LB (2013) Vestibular dysfunction: Prevalence, impact and need for targeted treatment Chabbert C, ed. J Vestib Res 23:113–117.

Beraneck M, Bojados M, Le Séac'h A, Jamon M, Vidal P-P (2012) Ontogeny of Mouse Vestibulo-Ocular Reflex Following Genetic or Environmental Alteration of Gravity Sensing Gilestro GF, ed. PLoS ONE 7:e40414.

Beraneck M, Cullen KE (2007) Activity of Vestibular Nuclei Neurons During Vestibular and Optokinetic Stimulation in the Alert Mouse. J Neurophysiol 98:1549–1565.

Beraneck M, Idoux E (2012) Reconsidering the Role of Neuronal Intrinsic Properties and Neuromodulation in Vestibular Homeostasis. Front Neurol 3 Available at: http://journal.frontiersin.org/article/10.3389/fneur.2012.00025/abstract

Beraneck M, Pfanzelt S, Vassias I, Rohregger M, Vibert N, Vidal P-P, Moore LE, Straka H (2007) Differential Intrinsic Response Dynamics Determine Synaptic Signal Processing in Frog Vestibular Neurons. J Neurosci 27:4283–4296.

Beraneck M, Straka H (2011) Vestibular signal processing by separate sets of neuronal filters Peusner KD, ed. J Vestib Res 21:5–19.

Boadas-Vaello P, Sedó-Cabezón L, Verdú E, Llorens J (2017) Strain and Sex Differences in the Vestibular and Systemic Toxicity of 3,3'-Iminodipropionitrile in Mice. Toxicol Sci:kfw238.

Boyden ES, Katoh A, Raymond JL (2004) CEREBELLUM-DEPENDENT LEARNING: The Role of Multiple Plasticity Mechanisms. Annu Rev Neurosci 27:581–609.

Boyle R, Carey JP, Highstein SM (1991) Morphological correlates of response dynamics and efferent stimulation in horizontal semicircular canal afferents of the toadfish, Opsanus tau. J Neurophysiol 66:1504–1521.

Brandt T, Strupp M, Arbusow V, Dieringer N (1997) Plasticity of the vestibular system: central compensation and sensory substitution for vestibular deficits. Adv Neurol:297–309.

Brueckner JK, Ashby LP, Prichard JR, Porter JD (1999) Vestibulo-ocular pathways modulate extraocular muscle myosin expression patterns. Cell Tissue Res 295:477–484.

Carcaud J, França de Barros F, Idoux E, Eugène D, Reveret L, Moore LE, Vidal P-P, Beraneck M (2017) Long-Lasting Visuo-Vestibular Mismatch in Freely-Behaving Mice Reduces the Vestibulo-Ocular Reflex and Leads to Neural Changes in the Direct Vestibular Pathway. eneuro 4:ENEURO.0290-16.2017.

Carey JP, Fuchs AF, Rubel EW (1996) Hair cell regeneration and recovery of the vestibuloocular reflex in the avian vestibular system. J Neurophysiol 76:3301–3312.

Carriot J, Jamali M, Chacron MJ, Cullen KE (2017) The statistics of the vestibular input experienced during natural self-motion differ between rodents and primates: Natural vestibular input in rodents and monkeys. J Physiol 595:2751–2766.

Cassel R, Bordiga P, Carcaud J, Simon F, Beraneck M, Le Gall A, Benoit A, Bouet V, Philoxene B, Besnard S, Watabe I, Pericat D, Hautefort C, Assie A, Tonetto A, Dyhrfjeld-Johnsen J, Llorens J, Tighilet B, Chabbert C (2019) Morphological and functional correlates of vestibular synaptic deafferentation and repair in a mouse model of acute onset vertigo. Dis Model Mech:dmm.039115.

Contini D, Holstein GR, Art JJ (2022) Simultaneous Dual Recordings From Vestibular Hair Cells and Their Calyx Afferents Demonstrate Multiple Modes of Transmission at These Specialized Endings. Front Neurol 13:891536.

Cullen K (2019) Vestibular processing during natural self-motion: implications for perception and action. :41.

Cullen KE, Minor LB, Beraneck M, Sadeghi SG (2010) Neural substrates underlying vestibular compensation: Contribution of peripheral versus central processing. J Vestib Res 19:171–182.

De Zeeuw CI, Lisberger SG, Raymond JL (2021) Diversity and dynamism in the cerebellum. Nat Neurosci 24:160–167.

Dean P, Porrill J (2014) Decorrelation Learning in the Cerebellum. In: Progress in Brain Research, pp 157–192. Elsevier. Available at: https://linkinghub.elsevier.com/retrieve/pii/B9780444633569000078.

Eatock RA, Songer JE (2011) Vestibular Hair Cells and Afferents: Two Channels for Head Motion Signals. Annu Rev Neurosci 34:501–534.

Facchini J, Rastoldo G, Xerri C, Péricat D, El Ahmadi A, Tighilet B, Zennou-Azogui Y (2021) Unilateral vestibular neurectomy induces a remodeling of somatosensory cortical maps. Prog Neurobiol 205:102119.

Faulstich BM, Onori KA, du Lac S (2004) Comparison of plasticity and development of mouse optokinetic and vestibulo-ocular reflexes suggests differential gain control mechanisms. Vision Res 44:3419–3427.

Faulstich M, van Alphen AM, Luo C, du Lac S, De Zeeuw CI (2006) Oculomotor Plasticity During Vestibular Compensation Does Not Depend on Cerebellar LTD. J Neurophysiol 96:1187–1195.

França de Barros F, Carcaud J, Beraneck M (2019) Long-term Sensory Conflict in Freely Behaving Mice. J Vis Exp:59135.

França de Barros F, Schenberg L, Tagliabue M, Beraneck M (2020) Long term visuo-vestibular mismatch in freely behaving mice differentially affects gaze stabilizing reflexes. Sci Rep 10:20018.

Glasauer S (2007) Current Models of the Ocular Motor System. In: Developments in Ophthalmology, 2007 (Straube A, Büttner U, eds), pp 158–174. Basel: KARGER. Available at: https://www.karger.com/Article/FullText/100485.

Goldberg JM (2000) Afferent diversity and the organization of central vestibular pathways. Exp Brain Res 130:277–297.

González-Calvo I et al. (2021) Sushi domain-containing protein 4 controls synaptic plasticity and motor learning. eLife 10:e65712.

Greguske EA, Carreres-Pons M, Cutillas B, Boadas-Vaello P, Llorens J (2019) Calyx junction dismantlement and synaptic uncoupling precede hair cell extrusion in the vestibular sensory epithelium during sub-chronic 3,3'-iminodipropionitrile ototoxicity in the mouse. Arch Toxicol 93:417–434.

Greguske EA, Llorens J, Pyott SJ (2021) Assessment of cochlear toxicity in response to chronic 3,3'-iminodipropionitrile in mice reveals early and reversible functional loss that precedes overt histopathology. Arch Toxicol 95:1003–1021.

Grosch M, Lindner M, Bartenstein P, Brandt T, Dieterich M, Ziegler S, Zwergal A (2021) Dynamic whole-brain metabolic connectivity during vestibular compensation in the rat. NeuroImage 226:117588.

Hasson T, Gillespie PG, Garcia JA, MacDonald RB, Zhao Y, Yee AG, Mooseker MS, Corey DP (1997) Unconventional Myosins in Inner-Ear Sensory Epithelia. J Cell Biol 137:1287–1307.

Hess BJM, Dieringer N (1990) Spatial Organization of the Maculo-Ocular Reflex of the Rat: Responses During Off-Vertical Axis Rotation. Eur J Neurosci 2:909–919.

Highstein SM, Goldberg JM, Moschovakis AK, Fernandez C (1987) Inputs from regularly and irregularly discharging vestibular nerve afferents to secondary neurons in the vestibular nuclei of the squirrel monkey. II. Correlation with output pathways of secondary neurons. J Neurophysiol 58:719–738.

Holland PJ, Sibindi TM, Ginzburg M, Das S, Arkesteijn K, Frens MA, Donchin O (2020) A Neuroanatomically Grounded Optimal Control Model of the Compensatory Eye Movement System in Mice. Front Syst Neurosci 14:13.

Idoux E, Tagliabue M, Beraneck M (2018) No Gain No Pain: Relations Between Vestibulo-Ocular Reflexes and Motion Sickness in Mice. Front Neurol 9:918.

Jang DC, Shim HG, Kim SJ (2020) Intrinsic Plasticity of Cerebellar Purkinje Cells Contributes to Motor Memory Consolidation. J Neurosci 40:4145–4157.

Kim GS, Wang T, Sayyid ZN, Fuhriman J, Jones SM, Cheng AG (2022) Repair of surviving hair cells in the damaged mouse utricle. Proc Natl Acad Sci 119:e2116973119.

Kodama T, du Lac S (2016) Adaptive Acceleration of Visually Evoked Smooth Eye Movements in Mice. J Neurosci 36:6836–6849.

Lasker DM, Han GC, Park HJ, Minor LB (2008) Rotational Responses of Vestibular–Nerve Afferents Innervating the Semicircular Canals in the C57BL/6 Mouse. J Assoc Res Otolaryngol 9:334–348.

Leong ATL, Gu Y, Chan Y-S, Zheng H, Dong CM, Chan RW, Wang X, Liu Y, Tan LH, Wu EX (2019) Optogenetic fMRI interrogation of brain-wide central vestibular pathways. Proc Natl Acad Sci 116:10122–10129.

Llorens J, Demêmes D (1994) Hair cell degeneration resenting from 3,3'-imiodiprpiunitril toxicity in the rat vestibular epithelia. Hear Res:78–86.

Llorens J, Demêmes D, Sans A (1993) The behavioural syndrome caused by 3'3-Iminodipropionitrile and related nitriles in the rat is associated with degeneration of the vestibular sensory hair cells. Toxicol Appl Pharmacol:199–210.

Llorens J, Demêmes D, Sans A (1994) The toxicity of IDPN on the vestibular system of the rat: new insights on its effects on behavior and neurofilament transport. NeuroToxicology:199–210.

Lopez C, Schreyer H-M, Preuss N, Mast FW (2012) Vestibular stimulation modifies the body schema. Neuropsychologia 50:1830–1837.

Maroto AF, Barrallo-Gimeno A, Llorens J (2021) Relationship between vestibular hair cell loss and deficits in two anti-gravity reflexes in the rat. Hear Res 410:108336.

Martins-Lopes V, Bellmunt A, Greguske EA, Maroto AF, Boadas-Vaello P, Llorens J (2019a) Quantitative Assessment of Anti-Gravity Reflexes to EvaluateVestibular Dysfunction in Rats. J Assoc Res Otolaryngol 20:553–563.

Martins-Lopes V, Bellmunt A, Greguske EA, Maroto AF, Boadas-Vaello P, Llorens J (2019b) Quantitative Assessment of Anti-Gravity Reflexes to EvaluateVestibular Dysfunction in Rats. J Assoc Res Otolaryngol 20:553–563.

McInturff S, Burns JC, Kelley MW (2018) Characterization of spatial and temporal development of Type I and Type II hair cells in the mouse utricle using new cell-type-specific markers. Biol Open 7:bio038083.

Minor L, Goldberg J (1991) Vestibular-nerve inputs to the vestibulo-ocular reflex: a functional-ablation study in the squirrel monkey. J Neurosci 11:1636–1648.

Möhwald K, Hadzhikolev H, Bardins S, Becker-Bense S, Brandt T, Grill E, Jahn K, Dieterich M, Zwergal A (2020) Health-related quality of life and functional impairment in acute vestibular disorders. Eur J Neurol 27:2089–2098.

Nelson AB, Faulstich M, Moghadam S, Onori K, Meredith A, du Lac S (2017) BK Channels Are Required for Multisensory Plasticity in the Oculomotor System. Neuron 93:211–220.

Pfanzelt S, Rossert C, Rohregger M, Glasauer S, Moore LE, Straka H (2008) Differential Dynamic Processing of Afferent Signals in Frog Tonic and Phasic Second-Order Vestibular Neurons. J Neurosci 28:10349–10362.

Sadeghi SG, Beraneck M (2020) Task-Specific Differentiation of Central Vestibular Neurons and Plasticity During Vestibular Compensation. In: The Senses: A Comprehensive Reference, pp 290–308. Elsevier. Available at: https://linkinghub.elsevier.com/retrieve/pii/B978012809324524145X.

Sadeghi SG, Minor LB, Cullen KE (2007) Response of Vestibular-Nerve Afferents to Active and Passive Rotations Under Normal Conditions and After Unilateral Labyrinthectomy. J Neurophysiol 97:1503–1514.

Sadeghi SG, Minor LB, Cullen KE (2012) Neural Correlates of Sensory Substitution in Vestibular Pathways following Complete Vestibular Loss. J Neurosci 32:14685–14695.

Sayyid ZN, Wang T, Chen L, Jones SM, Cheng AG (2019) Atoh1 Directs Regeneration and Functional Recovery of the Mature Mouse Vestibular System. Cell Rep 28:312-324.e4.

Sedó-Cabezón L, Boadas-Vaello P, Soler-Martín C, Llorens J (2014) Vestibular damage in chronic ototoxicity: A mini-review. NeuroToxicology 67.

Sedó-Cabezón L, Jedynak P, Boadas-Vaello P, Llorens J (2015) Transient alteration of the vestibular calyceal junction and synapse in response to chronic ototoxic insult in rats. Dis Model Mech:dmm.021436.

Seoane A, Demêmes D, Llorens J (2001) Pathology of the rat vestibular sensory epithelia during subchronic 3,3′-iminodipropionitrile exposure: hair cells may not be the primary target of toxicity. Acta Neuropathol (Berl) 102:339–348.

Shin S-L, Zhao GQ, Raymond JL (2014) Signals and Learning Rules Guiding Oculomotor Plasticity. J Neurosci 34:10635–10644.

Shinder ME, Perachio AA, Kaufman GD (2005) VOR and Fos response during acute vestibular compensation in the Mongolian gerbil in darkness and in light. Brain Res 1038:183–197.

Simon F, Pericat D, Djian C, Fricker D, Denoyelle F, Beraneck M (2020) Surgical techniques and functional evaluation for vestibular lesions in the mouse: unilateral labyrinthectomy (UL) and unilateral vestibular neurectomy (UVN). J Neurol 267:51–61.

Simon F, Tissir F, Michel V, Lahlou G, Deans M, Beraneck M (2021) Implication of Vestibular Hair Cell Loss of Planar Polarity for the Canal and Otolith-Dependent Vestibulo-Ocular Reflexes in Celsr1–/– Mice. Front Neurosci 15:750596.

Soler-Martin C, Diez-Padrisa N, Boadas-Vaello P, Llorens J (2006) Behavioral Disturbances and Hair Cell Loss in the Inner Ear Following Nitrile Exposure in Mice, Guinea Pigs, and Frogs. Toxicol Sci 96:123–132.

Sousa AD, Andrade LR, Salles FT, Pillai AM, Buttermore ED, Bhat MA, Kachar B (2009) The Septate Junction Protein Caspr Is Required for Structural Support and Retention of KCNQ4 at Calyceal Synapses of Vestibular Hair Cells. J Neurosci 29:3103–3108.

Straka H, Vibert N, Vidal PP, Moore LE, Dutia MB (2005) Intrinsic membrane properties of vertebrate vestibular neurons: Function, development and plasticity. Prog Neurobiol 76:349–392.

Straka H, Zwergal A, Cullen KE (2016) Vestibular animal models: contributions to understanding physiology and disease. J Neurol 263:10–23.

Wilkerson BA, Artoni F, Lea C, Ritchie K, Ray CA, Bermingham-McDonogh O (2018) Effects of 3,3′-Iminodipropionitrile on Hair Cell Numbers in Cristae of CBA/CaJ and C57BL/6J Mice. J Assoc Res Otolaryngol 19:483–491.

Yang X, Zhou S, Wu J, Liao Q, Wang C, Liu M, Qu L, Zhang Y, Cheng C, Chai R, Zhang K, Yu X, Huang P, Liu L, Xiong W, Chen S, Chen F (2019) Surgery-free video-oculography in mouse models: enabling quantitative and short-interval longitudinal assessment of vestibular function. Neurosci Lett 696:212–218.

Zakir M (2006) Regeneration of Vestibular Otolith Afferents after Ototoxic Damage. J Neurosci 26:2881–2893.

Zeng S, Ni W, Jiang H, You D, Wang J, Lu X, Liu L, Yu H, Wu J, Chen F, Li H, Wang Y, Chen Y, Li W (2020) Toxic Effects of 3,3 ' -Iminodipropionitrile on Vestibular System in Adult C57BL/6J Mice *In Vivo*. Neural Plast 2020:1–11.

Zennou-Azogui Y, Xerri C, Harlay F (1994) Visual sensory substitution in vestibular compensation: neuronal substrates in the alert cat. Exp Brain Res 98 Available at: http://link.springer.com/10.1007/BF00233983.

Zwergal A, Schlichtiger J, Xiong G, Beck R, Günther L, Schniepp R, Schöberl F, Jahn K, Brandt T, Strupp M, Bartenstein P, Dieterich M, Dutia MB, la Fougère C (2016) Sequential [18F]FDG µPET whole-brain imaging of central vestibular compensation: a model of deafferentation-induced brain plasticity. Brain Struct Funct 221:159–170.

「 · CHAPITRE 4 · 」

— GENERAL DISCUSSION —

My thesis focused on the study of visuo-vestibular integration through the plasticity mechanisms of the vestibulo-ocular or optokinetic reflexes in the mouse model. To do this, I used tools that allowed me to modulate one of the main inputs of this system to study the consequences on the two reflexes. In the first part of this discussion, I will first address some methodological considerations surrounding the methods used in this thesis. I will then address the conceptual points arising from my works concerning the direct VOR pathway and the visual and vestibular integration in gaze stabilizing reflexes. This discussion will also feature final perspectives.

i· Methodological considerations

The use of video-oculography in head-fixed mice allows accurate measurements to be obtained non-invasively (Stahl et al, 2004). It requires only minor surgery with rapid recovery. As demonstrated in article 2, the implantation of a headpost is robust and allows recordings to be obtained for a mouse over a long period of time. The headpost does not cause discomfort to the mouse, nor does it interfere with its natural lifestyle.

Importance of visual perturbation in a long-term motor learning protocol

The headset used in the protocol of Article 1 has the advantage of requiring only the headpost to be put on and allows for a purely visual disturbance to be generated during active mouse movements. This methodology differs from traditional VOR/OKR adaptation protocols which consist of head-fixed mouse training iterated many times at specific frequencies (Voges et al, 2017). The implementation of this protocol is not only simple but also allows the adaptation to occur liberated from the passive components (or unnatural frequencies compared to the active movements of the mouse in its environment) of standard adaptation protocols. The quantified results clearly prove that

this technique is a relevant model to study long-term visuo-vestibular adaptation (Article 1).

We used two different helmets to see the influence of visual contrast on the adaptation of gaze stabilization reflexes. In theory, the white helmet induced little visual error, while the helmet with black lines induced retinal blur and thus a larger error message. However, we obtained similar changes for both groups, for both the vestibular and visual reflexes. These results indicate that the nature of the visual alteration is not essential to this adaptation process; and that it is the perturbation of visual feedback itself and not the magnitude of the possible error message (retinal slip) that drove the adaptation. We, therefore, refer to this adaptation as a "decalibration". Although we have no differences in the amplitude of decalibration after the removal of the two helmets, we do observe a difference in recovery. It has been shown in humans that visual contrast modulates the extent of VOR adaptation over a short training period (Mahfuz et al., 2018). It would be interesting to see if we could observe a difference in the dynamics of the calibration process between these two different helmet conditions by testing the gaze stabilization reflexes at intermediate during the 14 days of adaptation. The high contrast on the pattern helmet might help induce a decrease in the VOR and OKR gain earlier than the no-pattern device.

Sub chronic IDPN treatment as a relevant model of vestibulopathy

As mentioned above, we were also able to follow the dynamics of vestibulo-ocular and optokinetic reflexes during a pharmacologically induced lesion. IDPN can be injected acutely and thus cause bilateral damage to the vestibular organs without the possibility of recovery (Zeng et al., 2020 ; Simon et al, in prep.). However, this model does not reproduce the pathological reality of many vestibular diseases. Indeed, most of these diseases cause alterations in the form of acute attacks that can last up to several hours in the case of for instance Menière's disease (Gürkov et al., 2016). The use of IDPN sub-chronically could be argued to be more relevant since it induces severe vestibular alterations but also as there is recovery when the treatment is interrupted. Thus, it is possible to model a fluctuant pathology and observe the different substitution

mechanisms that take place during and after treatment. We observed a significant vestibular alteration at six weeks but this varied between individuals. Indeed, not all mice are similarly affected by the same concentration of IDPN, although this is not related to the sex of the animals, and they also do not recover in a similar way. The correlation between vestibular function and hair cell numbers observed indicates that the variability in response is indeed due to the ototoxicity of IDPN. The variability observed could be related to an inter-individual resistance to the drug or to the consumption of the IDPN-water mix by the mice.

Another consideration regarding the IDPN protocol is that it induces a simultaneous bilateral lesion. There is a so-called Betcherew effect observed when the lesions are not simultaneous but one after the other with a delay between the two, which can happen in vestibular pathologies (for example neuritis)(Kim et al., 2022). The compensation following the first lesion is therefore again unbalanced by the second lesion. After a unilateral vestibular lesion, it has been shown that an increase in OKR gain is obtained (Nelson et al., 2017), the dynamics of which follow the recovery of vestibular function that is compensated by multiple mechanisms. IDPN thus stands as a good model to study plastic mechanisms in the context of a transient, partial, and bilateral loss of vestibular function.

ii· A clear role of type I hair cells in the VOR circuitry

The data obtained in article 2 also allow us to distance ourselves from the hypothesis that information from type II hair cells and regular afferents represents the majority of information within the VOR pathway (Cullen et al, 2019). In the inner ear, type I cells are predominantly innervated by irregular afferents that have been described as carrying vestibular information dependent on high stimulation frequencies and therefore were thought less likely to participate in VOR generation. Here, only type I cells are affected by the ototoxicity of IDPN, yet the VOR is severely impaired. Additionally, we do not observe any modulation related to a specific frequency range, in either the initial decrease of VOR or in the partial recovery of vestibular

function. It seems clear that the stimuli received by the mechanoreceptors of type I hair cells are involved in the elaboration of the signal used in the VOR pathway. However, it has been described that the primary afferents found in the periphery of the vestibular sensory organs are predominantly regular and may also connect to type I cells (Eactock & Songer, 2011); furthermore, we find a histology/function correlation in the central as well as in the peripheral regions of the utricle and semicircular canals. Thus, although it is impossible in this IDPN protocol to separate the contribution of regular and irregular afferents in the VOR circuit, it is clear that type I cells are involved. While type II HC are specifically not altered by IDPN exposition, recent studies have shown that it is possible to induce a specific loss of type II HC in the vestibular apparatus using a genetically modified mice line (Stone et al., 2021). The contribution of type II hair cells in the VOR pathway could be inferred from performing gaze stabilization reflexes tests on type II HC-deficit mice.

iii· OKR and VOR during adaptation and plasticity

Shared adaptation of the VOR and OKR after a VVM protocol

We used a helmet previously tested by our team to induce long motor learning driven by the visuo-vestibular mismatch. The VVM protocol induces an alteration of the VOR but also to a lesser extent in OKR responses. Indeed, the VOR gain is decreased by about 60% while the OKR gain is decreased by 30%. If we compare this protocol to the more conventional adaptation protocols, we can consider that it compares with a gain-down VOR protocol, due in particular to the visual disturbance. It has been shown that the VOR shift induced by wearing the helmet is associated with a modulation of the MVN neurons (Carcaud et al, 2017). The flocculus is the site of a rapid initial adaptation of the OKR (Shutoh et al, 2006) before being transmitted to the brainstem, and here, a flocculus lesion induces suppression of the optokinetic reflex after the VVM protocol (Carcaud et al, 2017). The difference in the magnitude of functional loss of the two reflexes after the VVM protocol could be due to a difference in the location of the adaptive process (reviewed in De Zeeuw et al, 2021), but also to a

different sensitivity of MVN neurons to visual and vestibular inputs (i.e different sensory weight).

Visual substitution following a bilateral vestibular lesion

There are multiple compensatory mechanisms set in place following a vestibular injury. If the lesion is unilateral, the postural symptoms that accompany the acute phase following the lesion are compensated for by various processes using the remaining intact vestibular information to rebalance the system (Beraneck and Idoux, 2012). Substitution mechanisms with non-vestibular sensory information are also used but are less privileged as vestibular information is still available, also to a lesser extent (Sadeghi et al, 2012). In the case of bilateral lesions, sensory substitutions by non-vestibular signals remain the only possible mechanisms to induce functional recovery. Here we observe a visual substitution that takes place with a delay compared to the vestibular dysfunction. The magnitude of the OKR gain increase is less than the vestibular loss. However, it is robust enough that it theoretically compensates for the vestibular loss.

It would be interesting to investigate the properties of central vestibular neurons after bilateral injury in the presence of visual substitution. Within the MVN, the neurons encoding head and eye movements and participating in the VOR pathway are the PVPs, or ES in the mouse. Substitution mechanisms may involve rebalancing by PVP or FTN neurons that also encode eye position. To test this hypothesis, the MVN neurons could be recorded in vivo during the treatment of IDPN to test the possible modulations during the different stimulations and if there is a modulation of the excitability or sensitivity of these neurons also coding the eye component. The delay observed between the severe vestibular loss and the increase in optokinetic gain may be due in particular to an adaptation mechanism occurring first in the flocculus and with a delay transferred into a change in the activity of the MVN.

In addition, the information transmitted to the central vestibular nuclei is also modulated by the presence of efferent fibres within the peripheral vestibular system (Raghu et al, 2019). These efferent fibres innervate type I and type II cells in an excitatory manner in mammals (Sadeghi et al., 2009) and participate in the compensation that follows vestibular injury (Hübner et al., 2017). They may be involved in the substitution mechanisms induced by a bilateral lesion of the vestibular system. Moreover, efferent fibres allow the decrease in sensitivity of peripheral vestibular organs (Chagnaud et al., 2015) during active locomotion. Yet, active locomotion is part of the rehabilitation therapy protocol for vestibular pathologies (Lacour and Bernard-Demanze, 2015). We have not tested the IDPN mice with tests other than the VOR and postural tests, and it would be intriguing to see if there is an effect of locomotion, if it could induce a positive effect on recovery or if vestibular disruption induces a modulation in the activity of those efferent fibres.

Frequency-specific adaptation of gaze stabilization reflexes

The cross-range performance of the VOR and OKR has been known for a long time (Faultisch et al, 2004). The VOR performs particularly well at high frequencies, while the OKR leads gaze stabilization at low frequencies. This complementarity makes it possible to obtain the optimal compensatory eye movements possible for all frequencies. This notion of a specific range for each reflex is found in the two studies presented in this thesis.

Indeed, the VVM protocol (Article 1), through its visual perturbation, induces a decrease in OKR gain specific to low frequencies. The decrease of the VOR is found at all frequencies, but the low and intermediate frequencies were the most marked. Moreover, during recovery, the decalibration was more robust at low frequencies. Here, the alterations are mainly found at frequencies where visual inputs are dominant.

In the case of the IDPN protocol (Article 2) although we have a decrease in VOR gain at all tested frequencies, the increase in OKR gain occurs only for frequencies that

are normally associated with a better performing VOR than OKR. To show the importance of this cross-frequency range, I introduced the concept of vestibular weight. The vestibular weight allows us to highlight the dominance of vestibular information on gaze stabilization, and in particular its weight at high frequencies. This visual substitution concentrated on high frequencies must necessarily pass through a reweighting of visual inputs that is specific to this range, similar to that observed in humans after unilateral vestibular lesions (Lubetzky et al., 2019). As visual substitution is still present during the recovery of vestibular functions, it might be possible to potentiate this reweighting to obtain a greater vestibular recovery or a better visuo-vestibular integration, by conducting optokinetic learning during the recovery period. And indeed, optokinetic stimulations have been a pertinent part of vestibular therapy reeducation to improve gaze stabilization that is altered during vestibular hypofunction (Whitney et al., 2016).

Visuo-vestibular integration in gaze stabilization is dominated by vestibular inputs

Following the profound but transient impairment of vestibular function caused by the IDPN protocol, I was able to quantify the integration of visual and vestibular inputs through VOR in the light, referred to as Combined Gaze Reflex, CGR. The results obtained in control mice showed that the visual-vestibular integration within the vestibular system quantified by CGR was a near-perfect summation of unimodal reflexes. This allowed me to compare the gains obtained following CGR to a predicted value in animals with disrupted vestibular function. I was able to demonstrate suboptimal integration in affected mice, which differs depending on the remaining vestibular function. Thus, although visual substitution is sufficient for some mice to perfectly compensate for vestibular loss, integration remains functionally reduced. Moreover, when the vestibular loss is too great, integration is quantitatively inferior to the optokinetic reflex. This sub-optimal function involves the structures responsible for visuo-vestibular integration, the vestibular nuclei, but also the cerebellum which is necessary for the adaptation of both reflexes. As the cerebellum is able to generate an

internal model to compare the self-made movement with the sensory-feedback movement and then send it to the central vestibular system (Brooks and Cullen, 2009), it is possible that long-term vestibular dysfunction leads to the alteration of this internal model which then induces a poor integration of vestibular and visual signals within the central nuclei.

Overall, those results have contributed to understanding gaze stabilizing reflexes integration and adaptation. However, the specific mechanisms of plasticity and sensory substitution occurring in the central vestibular nuclei remain unclear and would necessitate electrophysiological recordings.

iv· Perspectives

The integration of visual and vestibular information is not only essential for the production of gaze stabilization reflexes during passive movement but also during locomotion. However, while passive stimulation results in a steady VOR, active locomotion is associated with an extinct VOR (also in humans, Dietrich and Wuehr, 2019), which was demonstrated to depend in the xenopus tadpole on an efferent spinal locomotor copy participating to compensatory eye movements (Lambert et al., 2012). It was very recently confirmed in mice that this motor efferent copy comes from spinal cervical CPGs (Barros et al., 2022). In addition, a signal from the vestibular efferent system updates the hair cells and their afferents to locomotion dynamics (Straka and Chagnaud, 2017).

I have been involved in the development of preliminary results on VOR extinction during locomotion. We subjected a mouse running on a wheel to horizontal sinusoidal vestibular stimulations and observed compensatory eye movements on the same plane. These data allowed us to obtain an ANR grant to study the coupling between locomotion and gaze stabilization. We are currently developing a system in order to

couple the visuo-vestibular stimulation to locomotion and electrophysiology in the alert mouse.

During my thesis, I indeed set up a wireless *in vivo* recording system in the awake, head-fixed mouse. The recording of vestibular neurons by tetrodes can be coupled with visual, vestibular or combined stimulations, to distinguish and separate neurons according to their responses to stimuli. It will, then, be possible to study the mechanisms underlying the sensory substitution observed in article 2, as well as the modulation of vestibular neurons during locomotion. I hope to develop this line of research in the coming months.

「 · CHAPITRE 5 · 」

— APPENDIX —

APPENDIX I: VESTIBULAR PHENOTYPING

This project aimed to test the vestibular phenotype of mutant mice, KO for the POC5 gene. POC5 protein is located in the centrioles where it is required for the elongation of the primary cilium of cells by encoding a protein that is present in the distal part of the centrioles (Hassan et al, 2019). POC5 is necessary for the normal cell cycle progression. POC5 could be involved in scoliosis, a lateral deformity of the spine whose origins are still not well known (neurologic, musculoskeletal or connective tissue disorders); when its origins are not explained by the presence of another disease, scoliosis is called idiopathic and those account for 60% of scoliosis, and affects 3% of the population (Rosenberg 2011). A mutation in the poc5 gene is associated with 10% of idiopathic scoliosis in some French-Canadian families and could be a therapeutic target (Patten et al, 2015). Guillaume Dugué and his team used a mutant mouse model carrying the same mutation as in humans (single nucleotide polymorphism in the POC5 gene). Some idiopathic scoliosis are also accompanied by vestibular functional alterations and it is with the aim of observing whether the same vestibular disorder exists in the mutant mouse model that I carried out vestibular phenotyping tests. In order to be as precise as possible in the absence or existence of a vestibular disorder, specific tests of the vestibular organs were performed. Thus, the operationality of the semicircular canals is demonstrated by the angular vestibulo-ocular reflex (here with sinusoidal vestibular stimulations), at different frequencies (0.2, 0.5, 0.8, 1 and 1.5Hz at a spike speed of 30°/s) and that of the otoliths by the ocular counter roll, in which the mouse is tilted statically at several angles. Another test, the OVAR (at 50°/s, constant speed, clockwise and counterclockwise) was carried out in order to have an overall view of the vestibular system, being non-specific but more sensitive. The measurements were performed on 6 mutant mice and 7 WT mice. The overall results indicate an absence of an altered vestibular phenotype in these POC5 mutant mice, which respond to the three tests in a similar manner to the WTs. The POC5 mutation is not associated with every case of scoliosis and this mutation might not be enough to induce scoliosis in humans and in mice.

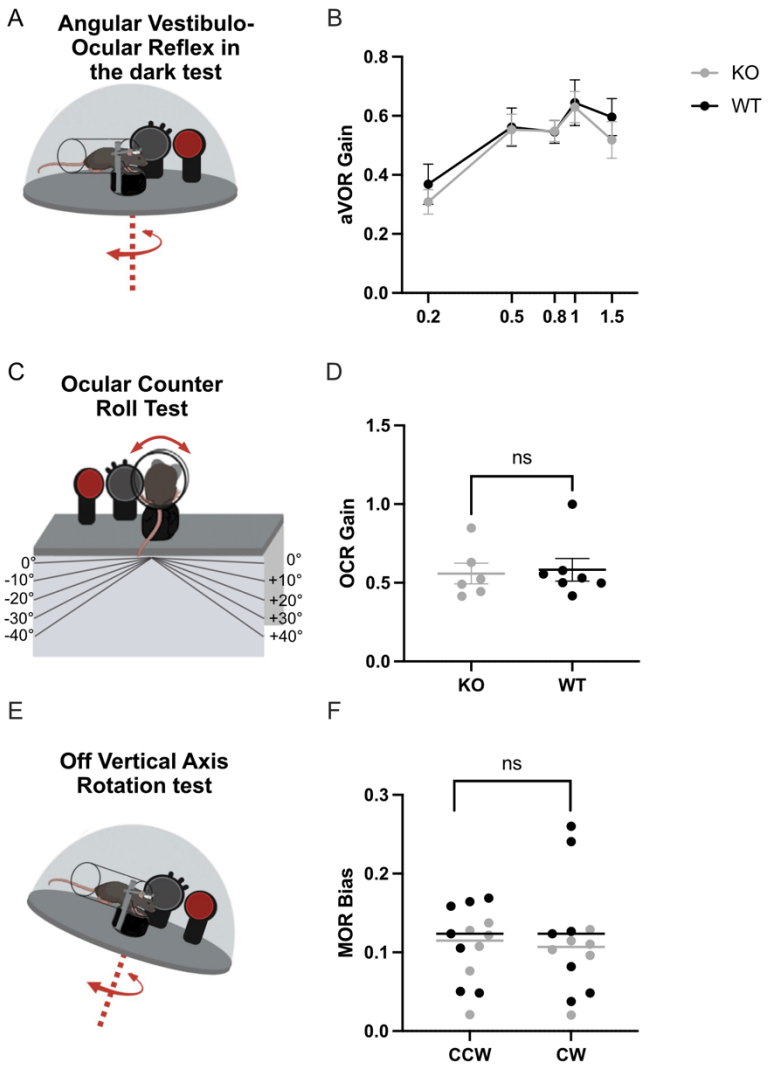

Figure 23: Appendix I A) Horizontal aVOR set-up B) aVOR responses of WT (black) and POC5 mutants (grey) at different frequencies ((0.2, 0.5, 0.8, 1 et 1.5Hz at a 30°/s velocity peak.) C) Ocular Counter Roll set-up D) OCR gain of WT (black) and POC5 KO (grey). E) OVAR setp-up F) Responses of WT (black) and POC5 KO (grey) to OVAR test (50°/s clockwise and counterclockwise stimulations)

APPENDIX II : OKR ADAPTATION

This project, in collaboration with Dr. Inés Gonzáles Calvo and Dr. Fekrije Selimi, aimed to test the adaptation of the optokinetic reflex following a long learning session in mutant mice. These mice lacked the transmembrane protein with a SUSHI domain, SUSD4 that is located in the cerebellum and brainstem. SUSD4 is normally involved in the activity-dependent degradation of an AMPA receptor subunit. Its absence leads to LTD deficiency and facilitation of LTP at the synapse between Purkinje cells and parallel fibres, as well as a phenotype affected by motor and coordination problems (Gonzáles-Calvo et al, 2021). As plasticity in the cerebellum is controlled in part by LTD/LTP, we used an OKR adaptation protocol to test the modulation of learning in these mutant mice. OKR adaptation is a pertinent model of cerebellum-dependent plasticity. To set-up the adaptation protocol I tested several paradigms in order to select a proper one. We realized that using an image that covered fully the dome did not lead to an increase in the OKR gain; it is possible that the reflection of the dots on the camera lenses creata conflict with the training protocol. To remove this perturbation, we used during the training session an image that covered half of the dome. However, during the OKR test, we used a full-dome image.

This protocol consists of sinusoidal visual stimulation at a certain frequency (0.33Hz with a maximum speed of 10°/s) for one hour. The OKR is measured by video-oculography before the beginning of the training session, and then at regular intervals of 15 minutes (a total of 5 measurements per mouse). The tests were performed on n=18 KOs and n=18 WTs, but the analysis focused on the mice whose increase in gain after one hour-long adaptation reflected an increase of at least 20% over the pre-training value (n=12 WTs and n=12 KOs). The data showed that the absence of SUSD4 did not result in a difference in OKR adaptation.

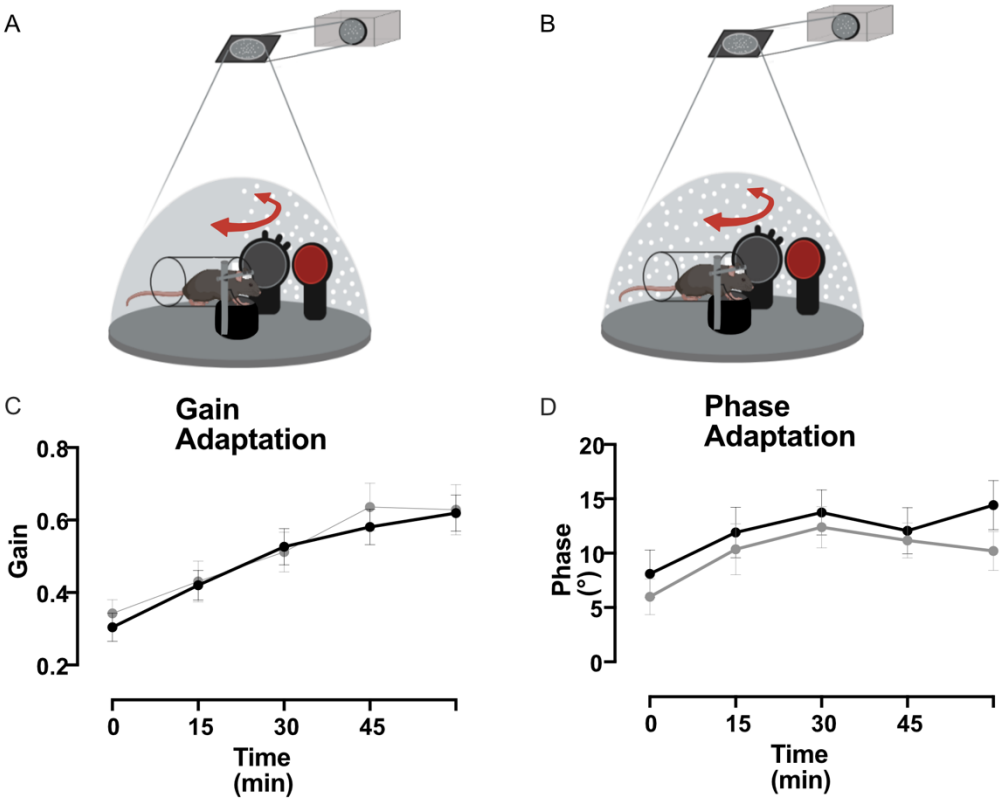

Figure 24: Appendix II. A) OKR adaptation set-up. B) OKR test set-up. C) OKR gain over an hour-long training session for WT mice (black) and SUSD4 KO mice (grey). B) OKR phase increase over the OKR adaptation training session for WT mice (black) and SUSD4 KO (grey).

APPENDIX III : NEURONAL TRACING

Neuronal tracing is an effective technique in order to study populations of neurons. Multiple tools exist, such as anterograde and retrograde tracers that respectively mark either the region the target areas project into or the areas where the projections to the targeted regions emerge from. In the study of the vestibular system, and further downstream the head direction (HD) circuit, neuronal tracing allows us to follow the integration of different inputs in an anatomical way, that can be completed by *in vivo* electrophysiology. It can also be used in order to stimulate a specific afferent for *in vitro* experiments, as is the main goal behind the paper presented in Appendix 3.

In the HD circuit, vestibular inputs are forwarded to the antero-dorsal thalamus nucleus (ADN) which then projects into the presubiculum, and HD cells are found in both of those structures (Yoder et al, 2014). To study the specific connectivity between the AND and the presubiculum, it is possible to mark ADN afferents that can be optogenetically stimulated and recorded. *In vivo* stereotaxic injections of anterograde virus-mediated channelrhodopsin are used to target the ADN neurons that project to the presubiculum. Properties of presubiculum neurons in brain slices can then be recorded while transfected neurons (ADN-projecting) can be stimulated by light. This approach allows for targeting neurons receiving specific inputs.

Video Article

In Vivo Intracerebral Stereotaxic Injections for Optogenetic Stimulation of Long-Range Inputs in Mouse Brain Slices

Louis Richevaux[1,2], Louise Schenberg[1,2], Mathieu Beraneck[1,2], Desdemona Fricker[1,2]

[1]CNRS (Integrative Neuroscience and Cognition Center, UMR 8002)

[2]Université Paris Descartes, Sorbonne Paris Cité

Correspondence to: Louis Richevaux at louis.richevaux@parisdescartes.fr, Desdemona Fricker at desdemona.fricker@parisdescartes.fr

URL: https://www.jove.com/video/59534
DOI: doi:10.3791/59534

Keywords: Neuroscience, Issue 151, stereotaxic injection, channelrhodopsin, optogenetics, electrophysiology, acute brain slice, whole-cell patch-clamp recording, neuronal morphology, hippocampus, synaptic transmission

Date Published: 9/20/2019

Citation: Richevaux, L., Schenberg, L., Beraneck, M., Fricker, D. In Vivo Intracerebral Stereotaxic Injections for Optogenetic Stimulation of Long-Range Inputs in Mouse Brain Slices. *J. Vis. Exp.* (151), e59534, doi:10.3791/59534 (2019).

Abstract

Knowledge of cell-type specific synaptic connectivity is a crucial prerequisite for understanding brain-wide neuronal circuits. The functional investigation of long-range connections requires targeted recordings of single neurons combined with the specific stimulation of identified distant inputs. This is often difficult to achieve with conventional and electrical stimulation techniques, because axons from converging upstream brain areas may intermingle in the target region. The stereotaxic targeting of a specific brain region for virus-mediated expression of light-sensitive ion channels allows selective stimulation of axons originating from that region with light. Intracerebral stereotaxic injections can be used in well-delimited structures, such as the anterior thalamic nuclei, in addition to other subcortical or cortical areas throughout the brain.

Described here is a set of techniques for precise stereotaxic injection of viral vectors expressing channelrhodopsin in the mouse brain, followed by photostimulation of axon terminals in the brain slice preparation. These protocols are simple and widely applicable. In combination with whole-cell patch clamp recording from a postsynaptically connected neuron, photostimulation of axons allows the detection of functional synaptic connections, pharmacological characterization, and evaluation of their strength. In addition, biocytin filling of the recorded neuron can be used for post-hoc morphological identification of the postsynaptic neuron.

Video Link

The video component of this article can be found at https://www.jove.com/video/59534/

Introduction

Defining connectivity between brain regions is necessary to understand neural circuits. Classical anatomical tracing methods allow establishing interregional connectivity, and lesion studies help to understand the hierarchical organization of information flow. For example, brain circuits for spatial orientation and head direction signaling involve the directional flow of information from the thalamus to the presubiculum. This has been demonstrated by lesion studies of antero-dorsal thalamic nuclei (ADN) that degrade the head direction signal in the downstream dorsal presubiculum, as well as the parahippocampal grid cell signal[1,2].

The functional connectivity between brain areas is more difficult to establish at a cellular and subcellular level. In the hippocampus, a highly organized anatomy allows to investigate pathway-specific synaptic connections using electrical simulation in the slice preparation. Stimulation electrodes placed in stratum radiatum of CA1 can be used to specifically stimulate Schaffer collateral input from CA3[3]. Stimulating electrodes placed in stratum lacunosum moleculare of CA1 will activate the perforant path input to CA1[4,5]. Electrical stimulation activates neurotransmitter release from axon terminals; however, it activates neurons with somata near the stimulation site as well as axons of passage. It is therefore of limited use for studying afferents from defined brain regions when fibers of different regions of origin intermingle in the target structure, as is typically the case in the neocortex.

Neurons may also be stimulated with light. Optical methods include the photoactivation of caged glutamate, which can be combined with one- or two-photon laser scanning. Multiple closely spaced sites may be stimulated sequentially, with no mechanical damage to the tissue[6]. This has been successfully used to map synaptic receptors as well as activate individual neurons[7]. While glutamate uncaging can be used for local circuit analysis, it does not allow for specific activation of long-range inputs.

A method of choice for the investigation of long-range connectivity in neuronal circuits is the use of virus-mediated channelrhodopsin expression. Using in vivo stereotaxic injections as described here, the expression of light-gated ion channels can be targeted and spatially restricted to a desired brain region. In this way, channelrhodopsins are effective for mapping excitatory or inhibitory connectivity from one region to its target. Transfected axons terminals may be stimulated with light in a brain slice preparation, and patch-clamp recordings as a read-out allow examination of the functions and strengths of specific circuit components in the brain[8]. The optogenetic approach combined with stereotaxic

injection of a virus offers unprecedented specificity and genetic control[9]. Stimulating with light additionally allows for both high temporal and spatial precision[10,11].

The presubiculum is a six-layered cortical structure at the transition of the hippocampus and the para-hippocampal formation[12,13]. It receives important synaptic input from the ADN[11] but also from several other cortical and subcortical regions[14]. Thus, the selective stimulation of thalamic axons terminals within a presubicular slice is not possible with electrical stimulation nor glutamate uncaging. Described in this protocol are methods to determine functional connectivity between brain regions (ADN and presubiculum) using precise stereotaxic injections of viral vectors expressing light-gated channels. Also described is the photostimulation of axons terminals of projecting neurons in their target region, coupled with whole-cell patch-clamp recordings of post-synaptic neurons in the brain slice preparation.

Protocol

All procedures were performed in accordance with the European Community Council Directive (2010/63/EU) and approved by the ethics committee of Paris Descartes University. The experimenter must obtain authorization for the procedure to comply with local regulations.

1. Planning of the experiment

1. Define the brain area to be targeted. Determine the stereotaxic coordinates of the injection site with the help of a mouse brain atlas[15]. For the right antero-dorsal thalamic nucleus (ADN), the coordinates are: -0.82 posterior, 0.75 lateral, -3.2 depth (mm) relative to bregma. Coordinates may need to be adjusted for animals of different age, sex, or strain.
2. Confirm and document the exactitude of the coordinates by injecting a fluorescent tracer (150 to 300 nL) observable with an epifluorescence microscope in a pilot experiment (**Figure 1A,B).**
3. Define the type of virus to be injected. Store the virus in 6 µL aliquots at -80 °C as recommended by the producer. Bring 1 aliquot placed on ice to the surgery room, for injection of one to six animals on a given day. Biosafety regulations for the use of AAV may depend on the country or institution, and the use of a PSM 2 hood may be required.
   NOTE: Here, we use a AAV2/5 serotype expressing Chronos, a fast channelrhodospin-2 variant, fused to green fluorescent protein under the control of the Synapsin promoter: AAV5.Syn.Chronos-GFP.WPRE.bGH.

2. Stereotaxic surgery

1. Install a stereotaxic frame equipped with a pump holder on a stable standard laboratory bench. Adjust stereoscope so as to clearly see the zone where the animal's head will be placed. Use a LED light source for illumination. Rotate the stereoscope away to access the pump holder, which is not needed for the first steps of the surgery.
2. Install a 10 µL Hamilton syringe equipped with a 33 G beveled metal needle in the pump holder. Test the ejection system with water.
3. Anesthetize a 4- to 5-week old C57BL6 mouse with an intraperitoneal injection of a mix of ketamine hydrochloride and xylazine (100 mg/kg and 10 mg/kg, respectively). Prepare a mix of 1 mL of ketamine and 0.5 mL of xylazine in 8.5 mL of 0.9% NaCl. This will result in 10 mg/mL ketamine and 1 mg/mL xylazine in the mix. Of this mix, inject intraperitoneally 10 µL per gram of the animal's body weight. Duration of anesthesia is about 1 h.
4. Verify that the animal is well-anesthetized with a toe pinch. Then, pull out the tongue to facilitate breathing. Shave the cranial hair.
5. Inject 20 µL of lidocaine hydrochloride (4 mg/mL; 2 mg/kg) under the skin of the head for local anesthesia and wait 5 min for the effect to begin. To avoid eye damage due to dryness, cover the eyes with topical ophthalmic ointment.
6. To expose the skull, create a straight cut in the scalp with small surgery scissors. Place the animal in a stereotaxic frame, inserting the ear bars slightly rostral to the actual ear to rest on the bone and pull down the skin, which should create good access to the skull. Tighten into place. Install the nose piece.
7. Maintain the body of the animal horizontally at the level of the head using a height-adjusted support. Place a heating pad under the mouse to keep it at physiological temperature.
8. Clean the skull by applying 0.9% NaCl with a cotton swab to remove soft tissue from the bone. Use the stereoscope for the rest of the surgery.
9. Adjust the skull so that the bregma-lambda axis is level, moving up or down the nose and teeth piece. This necessitates iterative measures of bregma and lamba, as both will change following adjustment of the nose level.
10. Find the location of the injection site on the skull. Adjust the injection needle above the injection site according to posterior and medial coordinates and mark the skull with a disposable needle. Move the injection needle upward by 4 cm.
11. Use a 0.5 mm burr with a drill to realize a 1 mm diameter craniotomy on the mark, at one-half of maximum speed. Swab eventual bleeding with a paper tissue.
12. Empty the water contained in the Hamilton syringe for storage by completely ejecting it with the pump. Only the needle will still be filled with water. The needle is washed between each use with pure deionized water. Sterilization is not required.
13. Take the aliquot of virus that is to be used for this day. Make sure that the viral solution is not frozen anymore but has remained cooled (close to 0 °C, on ice). Only briefly remove from the ice to obtain 700 nL with a micropipette for small volumes. Deposit the drop on a 5 cm x 5 cm piece of paraffin film. Avoid creating bubbles. Put the remaining viral solution back on ice.
    NOTE: The drop volume should be greater than the desired injection volume (700 nL for 200 nL injected). This will give a safety margin in case some of the liquid is lost during the transfer and allows performing a small test ejection (step 2.16) before proceeding.
14. Place the paraffin film on top of the craniotomy. Plunge the needle in the drop of viral solution without changing the antero-posterior and lateral position.
15. Use the "withdraw" function of the pump to fill the syringe with about 500 nL of viral solution disposed on the paraffin film. Do this under visual control (stereoscope), watch the drop disappear, and make sure not to aspirate air.
16. Make sure the syringe has been filled correctly. Verify the functioning of the ejection system by driving down the plunger to test eject a small drop of liquid of 50 nL under visual control. Wipe the drop.

17. Insert the needle into the brain to the chosen depth, by turning the knob controlling the dorso-ventral axis of the stereotaxic apparatus clockwise. Push the "run" button (speed 15 nL/min per volume of 150 nL injected). A small volume (50-300 nL, depending on the virus used) is slowly ejected over 10 min with an automatic pump.
18. Wait 10 min after the injection to avoid leaking from the injection site. Then, slowly remove the needle over 3-5 min by turning the knob controlling the dorso-ventral axis counterclockwise.
19. Rotate the vertical part of the stereotaxic frame with the syringe away from the animal. Immediately wash the needle in clean distilled water by filling-emptying it several times, in order to avoid clogging. Store the syringe filled with water.
20. Remove the mouse from the stereotaxic frame. Suture the skin with 4-0 polyamide suture filament. Make three or four stiches, tied with 2-1-1 standard surgical knots.
21. Place the mouse in a heated cage until it completely wakes up from anesthesia, and provide water and soaked food in a Petri dish placed on the ground. If the heat source is below the cage, use a spacer grid to avoid overheating.
    NOTE: According to local guidelines, a single dose of ketoprofen (2-5 mg/kg, subcutaneously) or buprenorphine (0.05-0.1 mg/kg, subcutaneously) may be applied to prevent pain.
22. When the animal is fully awake, return it to its home cage and monitor its well-being, particularly on the day following injection. Check for signs of pain. If any behavioral modification is observed, the animal is weighed to monitor its body weight.
23. Depending on the virus used, the time for full expression may vary. Here, we allow 3 weeks for expression of AAV5.Syn.Chronos-GFP.

3. Solutions for acute slice recordings and fixation

1. Prepare stock solutions of 10x concentrated cutting solution (125 mM NaCl, 25 mM sucrose, 2.5 mM KCl, 25 mM $NaHCO_3$, 1.25 mM NaH_2PO_4, and 2.5 mM D-glucose) and artificial cerebrospinal fluid (ACSF) solution (124 mM NaCl, 2.5 mM KCl, 26 mM $NaHCO_3$, 1 mM NaH_2PO_4, and 11 mM D-glucose) in pure deionized water prior to electrophysiology experiments. Store these solutions at 4 °C in 1 L bottles without $CaCl_2$ and $MgCl_2$.
2. On the day of the experiment, dilute the stock solutions of cutting solution and ACSF 10x to a final volume of 0.5 L each. Agitate with a magnetic stirrer and oxygenize by bubbling with 95%/5% O_2/CO_2. Add divalent ions to obtain final concentrations of 0.1 mM $CaCl_2$ and 7 mM $MgCl_2$ for the cutting solution, and 2 mM $CaCl_2$ and 2 mM $MgCl_2$ for ACSF.
3. Prepare the potassium-gluconate based pipette solution to contain: 135 mM K-gluconate, 1.2 mM KCl, 10 mM HEPES, 0.2 mM EGTA, 2 mM $MgCl_2$, 4 mM MgATP, 0.4 mM Tris-GTP, 10 mM Na_2-phosphocreatine, and 2.7–7.1 mM biocytin for post-hoc cell morphology revelation. Adjust the solution's pH to 7.3 and osmolarity to 290 mOsm. Store 1 mL aliquots at -20 °C.
4. Prepare 0.1 M PBS by diluting BupH PBS dry-blend powder pouches in 500 mL of distilled water, resulting in 0.1 M sodium phosphate, 0.15 M NaCl, pH 7.2.
5. To prepare 1 L of 4% PFA solution, dilute 111 mL of 36% liquid PFA and 90 mL of 10x PBS solution in distilled water.
6. Prepare 30% sucrose solution containing 150 g of sucrose in 500 mL of 0.1 M PBS.

4. Preparation of brain slices

1. Prepare the bench space with absorbent bench paper before perfusion.
2. Install a drip about 1 m above the bench for gravity-fed perfusion. Attach a 24 G butterfly needle.
3. Surround the cutting chamber of the vibratome with ice and store it in a freezer.
4. Anesthetize the mouse with intraperitoneal injection of the same ketamine-xylazine mixture used for surgery. Assess the stage of the anesthesia by pinching the toe with forceps. When fully asleep, inject 100 µL of heparin (5000 U.I./mL) intraperitoneally.
5. Fix the animal with adhesive tape on the absorbent paper, lying on its back. Open the thoracic cage by cutting the ribs on the left and right sides with small scissors, from the diaphragm upwards. Maintain the thoracic cage open with the help of adhesive tape.
6. Clamp the descending aorta with a hemostat and perfuse via the left ventricle of the heart with 4 °C cooled and oxygenated (95%/5% O_2/CO_2), cutting the solution through the 24 G butterfly needle. After 5 s, open the right atrium with small scissors.
7. After 5 min of perfusion, when the organs are bloodless, stop the perfusion. Decapitate the animal with big scissors and immerge the head into 4 °C cooled and oxygenated cutting solution in a Petri dish.
8. To extract the brain, cut the skin from neck to nose, then section the last vertebrae from the skull with scissors. Manually retract the skin and use small scissors to open the skull, cutting it along the midline, from caudal to rostral, upward to between the eyes.
9. Carefully remove the parietal bone and caudal part of frontal bone with curved or bone forceps. Extract the brain with a small rounded spatula by inserting the instrument between the brain and the cranial floor, sectioning the olfactory bulb, optic nerve and other cranial nerves, and cerebellum.
10. Gently submerge the brain in ice-cold cutting solution (4 °C) in a beaker. Position the brain on filter paper to gently dry the cortical surface. Glue the brain cortex-down to the specimen holder of a vibratome, with the caudal side facing the blade, in order to cut horizontal brain slices.
11. Fill the cutting chamber with ice-cold oxygenated cutting solution so the brain is fully immerged. Make a cut on the left hemisphere (contralateral to the injected side) to avoid potential left-right ambiguity on slices.
    CAUTION: Always oxygenate the solution and protect slices from light exposure.
12. Cut 300 µm thick slices with the vibratome, at a speed of 0.07 mm/s at 1 mm amplitude. At this stage, it is recommended to briefly check the Chronos-GFP expression in the thalamus using a fluorescent flashlight (440-460 nm) and corresponding filter glasses (500 nm long pass).
13. Isolate the hippocampal region with a scalpel and transfer it to a chamber positioned in a beaker filled with bath-warmed (34 °C), oxygenated (95%/5% O_2/CO_2) ACSF.
14. After 15 min, take the chamber out of the heated water bath and let the slices rest at room temperature, still oxygenated for at least 45 min until use.

5. Whole-cell patch-clamp recording

1. Gently transfer a brain slice containing the hippocampal complex with a custom-made glass transfer pipette to the recording chamber mounted on an upright microscope. A transfer pipette is made of a shortened Pasteur pipette (inner diameter 6.5 mm) attached to a rubber

pipette bulb. Continuously perfuse the recording chamber (3 mL) with 34 °C (warmed) ACSF bubbled with 95%/5% O_2/CO_2. Set the speed of the peristaltic pump to 2-3 mL/min.
2. Briefly examine Chronos-GFP expression in axon terminals in the region of interest with blue LED illumination (470 nm) and observe with a 4x objective. GFP fluorescence is visualized through an appropriate emission filter, with a CCD camera image displayed on a computer screen.
3. Place a slice anchor made from a U-shaped platinum wire with tightly spaced nylon strings ("harp") on the slice to maintain it.
4. Change to a 63x immersion objective and adjust the focus. Check for axons expressing Chronos-GFP and choose a pyramidal neuron for patch recording.
5. Move the objective upward.
6. Pull pipettes using a Brown-Flaming electrode puller from borosilicate glass. The puller is set to produce pipettes with approximately 1 µm in tip diameter. Fill the pipettes with K-gluconate-based internal solution.
7. Mount the pipette in the pipette holder on the head-stage. Lower the pipette in the chamber and find the tip under the objective. Pipette resistance should be between 3–8 MΩ. Apply a light positive pressure with a syringe so as to see a cone of solution outflow out of the pipette and progressively lower the pipette and objective to the surface of the slice.
8. Patch the cell in voltage-clamp configuration: approach the identified neuron and delicately press the pipette tip onto the soma. The positive pressure should produce a dimple on the membrane surface. Release the pressure to create a giga-ohm seal (>1 GΩ resistance). Once sealed, set the holding voltage to -65 mV. Break the membrane with a sharp pulse of negative pressure: this is achieved by applying strong suction to a tube connected to the pipette holder.
9. Record in whole-cell current clamp mode the responses of the neuron to hyperpolarizing and depolarizing current steps (**Figure 2A**).
NOTE: This protocol will be used to determine active and passive intrinsic properties of the cell. Custom-written MATLAB routines are used for off-line analysis[10,16].
10. Record in current- or voltage-clamp postsynaptic responses to whole-field 475 nm LED stimulation of afferent fibers expressing Chronos. Stimulate with trains of 10 stimulations of 2 ms durations at 20 Hz (**Figure 2B,C**). Light intensity may vary from 0.1–2 mW.
NOTE: Light intensity was measured with a digital handheld optical power console equipped with a photodiode sensor, positioned under the objective. Response latencies of 2–4 ms are characteristic for a monosynaptic connection.
11. To investigate the nature of the synaptic transmission between the long-range afferents and the recorded neuron, different pharmacological agents may be used. To pharmacologically distinguish direct, monosynaptic responses from indirect responses via network activation, add 1 µM TTX and 100 µM 4-AP to the ACSF.
NOTE: Bath application of glutamate receptor blockers allows to determine the nature of the neurotransmitter that is released and the identity of postsynaptic receptors. For example, AMPA type glutamate receptors will be blocked by NBQX (10 µM) and NMDA receptors by APV (100 µM). Depending on the aim of the study, protocols may be conceived to investigate voltage dependence of synaptic responses or response dynamics over time.
12. Wash with original ACSF solution to patch another cell, or transfer the slice containing a biocytin-filled neuron in a small vial filled with 4% PFA.
13. After overnight fixation in 4% PFA, wash the slice in 0.1 M PBS (2x for 5 min, 1x for 20 min).
14. Store in 30% sucrose at 4 °C.

6. Biocytin revelation

1. Transfer the fixed slices containing biocytin-filled neurons onto a glass blade in a drop of 30% sucrose and perform three cycles of freezing-thawing: place the blade onto dry ice disposed in a styrofoam box for 1 min until drops of sucrose are completely frozen, then press the blade against the hand palm to thaw.
2. Wash the slice 3x in 0.1 M PBS (2x for 5 min, 1x for 1 h and 50 min), gently agitated. Do not exceed 2 h for the last washing.
3. Pre-incubate the slice at RT for 2 h in agitated buffer solution containing 2% milk powder (0.4 g in 20 mL) to saturate non-specific sites and 0.5% Triton X100 (0.1 mL in 20 mL) to permeabilize the membranes in 0.1 M PBS.
4. Incubate overnight at 4 °C in a solution containing 2% milk powder, 1% Triton X100, streptavidin-Cy5 conjugate (1/500), and DAPI (1/1000) in 0.1 M PBS, gently agitated.
5. Wash the slice three times in 0.1 M PBS (2x for 5 min, 1x for 2 h). The last wash can last longer, up to 4 h, to reduce background staining.
6. Before mounting the slice, use an epifluorescence microscope at 10x magnification configured to observe Cy5 fluorescent markers in order to identify the side of the slice containing the marked cell in a chamber filled with PBS.
7. Transfer the slice onto a blade, cell-side up, dry it with a paper tissue, and mount it using high-resistance mounting medium.
8. Use an epifluorescence microscope at 10x magnification in Cy5 and DAPI configuration to examine the cell body location, and in GFP configuration to observe the marked afferents, or a high-resolution confocal microscope at 20x for detailed somatic, axonal, and dendritic morphology (**Figure 2D,E**). Filter settings are detailed in the **Table of Materials**.

Representative Results

The procedure presented here was used to express a blue light-sensitive channelrhodopsin (Chronos) fused to GFP in the antero-dorsal nucleus of the thalamus (ADN), by stereotaxic injection of anterograde adeno-associated virus. The stereotaxic coordinates were determined according to a mouse brain atlas and tested by injecting 200 nL of fluorescent tracer fluoro-ruby. The animal was sacrificed 10 min after the injection, and the brain was extracted and fixated overnight. Coronal brain sections were prepared to examine the injection site, which was correctly placed in and limited to ADN (**Figure 1A,B**).

In order to express Chronos-GFP in neurons of ADN, we injected 300 nL of AAV5.Syn.Chronos-GFP.WPRE.bGH. Three weeks after the injection, acute horizontal brain slices were prepared. **Figure 1C** shows a brain slice containing the thalamic injection site in the right hemisphere, with GFP expression in green. Upon inspection with an epi-fluorescence microscope equipped with a 4x objective, GFP labeled thalamic axons were observed in the presubiculum (**Figure 1C,D**). It was noted that thalamic axons densely innervated the superficial layers I and III of the presubiculum (**Figure 1D**).

The activity of presubicular neurons in layer III was recorded in the whole-cell patch-clamp configuration. Hyperpolarizing and depolarizing current steps were applied while recording the membrane potential variations (**Figure 2A**). Data was stored on a computer for later offline analysis of active and passive membrane properties. Presubicular layer III principal cells typically possessed a negative resting potential close to -63 mV and required depolarizing current injections to drive the membrane potential to firing threshold. A full description of their intrinsic properties has been published[11].

Stimulating ADN axon terminals expressing Chronos-GFP elicited excitatory post-synaptic potentials (EPSPs) in presubicular layer III principal cells in current clamp mode (**Figure 2B**). Depending on light intensity, the EPSPs could reach action potential threshold. Postsynaptic responses were also observed in voltage-clamp mode as excitatory post-synaptic currents (EPSCs) were elicited (**Figure 2C**). Onset latencies of EPSCs evoked by light stimulations were short (median, 1.4 ms[10]), indicating a direct synaptic contact between thalamic axons and layer III presubicular neurons. Persisting EPSCs in TTX-4AP condition confirmed this monosynaptic activation. It is noteworthy that these cells responded reliably to the light stimulations of afferent axons with a regular firing pattern.

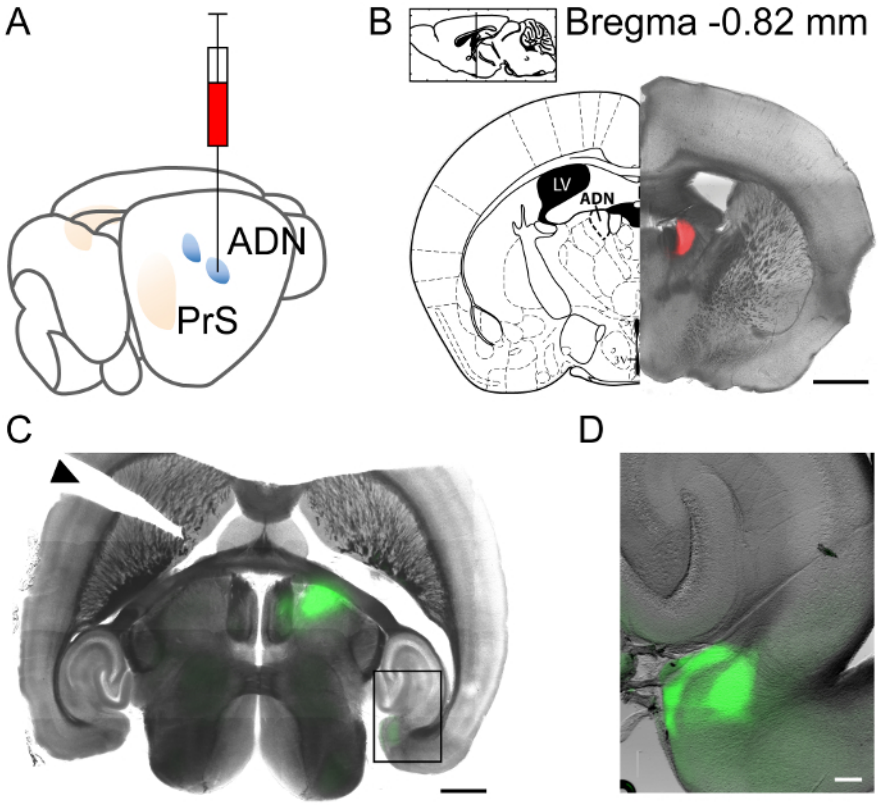

Figure 1: Stereotaxic injection in the anterodorsal thalamic nucleus (ADN). (**A)** Schematic representation of the injection. (**B)** Injection site confirmation with fluoro-ruby in a coronal section. Inset indicates antero-dorsal level and distance from bregma. (**C**) Horizontal slice following AAV-Chronos-GFP injection in the thalamus. The axonal projections to the ipsilateral presubiculum should be noted. An incision on the left side of the slice (indicated by a black triangle) marks the contralateral hemisphere. (**B, C**) Scale bar 1 mm. (**D)** Magnified view of inset in (**C)** with ADN projections to the presubicular superficial layers. Scale bar = 100 µm. Please click here to view a larger version of this figure.

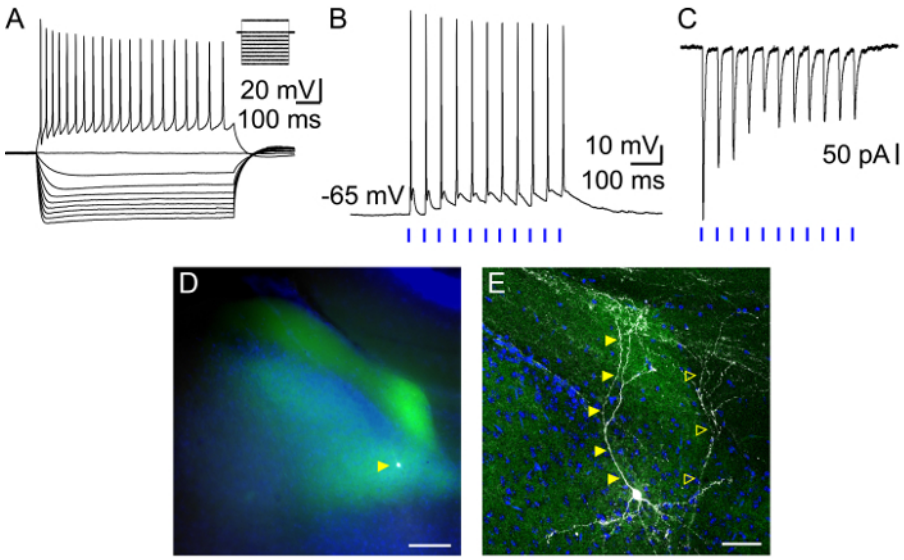

Figure 2: Presubicular layer III neuron: intrinsic properties, response to light stimulation of thalamic afferents, and post-hoc revelation of cell morphology. (**A)** Firing pattern and membrane potential variations of layer III neuron for hyperpolarizing and depolarizing current steps. (**B, C)** Responses of layer III neuron to 2 ms light stimulations (blue bars) of thalamic axons recorded in (**B**) current-clamp and (**C**) voltage-clamp modes. (**D, E)** Layer III pyramidal neuron (white, indicated by filled yellow triangle) surrounded by thalamic axons expressing Chronos-GFP (green) in presubicular superficial layers with DAPI staining (blue) in horizontal slice imaged with an epifluorescence microscope (**D,** scale bar = 100 µm) and confocal microscope at a high magnification (**E**, scale bar = 50 µm). The cell in (**A)** is indicated with filled yellow triangles. A second, partially filled neuron is present in this slice indicated with empty yellow triangles. Please click here to view a larger version of this figure.

Discussion

In vivo viral injection to express light-sensitive opsins in a defined brain area is a choice method for the optogenetic analysis of long-range functional connectivity[10,11,17,18]. Stereotaxic injections offer the possibility to precisely target a specific area of the brain. The coexpression of an opsin with a fluorescent reporter conveniently allows evaluation of the successful expression and confirmation of the precise injection site. The use of AAV serotype 2/5 typically restricts expression to the targeted brain region. In this way, a restricted population of neurons is transfected, expressing light-sensitive ion channels in their cell bodies and axon terminals. In subsequent ex vivo slice experiments, it is possible to stimulate these axon terminals with light pulses directly in their target area, while reading out successful synaptic transmission via patch-clamp recording of a post-synaptically connected neuron. The above protocol is robust and convenient, and some additional notes may help performance of successful experiments.

Different types of anesthesia may be used. Described here is the intraperitoneal injection of a ketamine-xylazine combination as an easy-to-use, short-term anesthesia with convenient analgesia[19]. The depth and duration of anesthesia may vary to some extent. In some cases, it may be necessary to inject another half-dose of ketamine-xylazine during the protocol. Isoflurane anesthesia can be a good alternative to induce more quickly and better control the depth of anesthesia. Coordinates of injection sites may be determined with the help of a mouse brain atlas. In practice, coordinates need to be tested and adjusted, if necessary.

Clean working conditions are also key. It is recommended to use disposable protective gear, including gloves, a mob cap, and a lab coat. When positioning the animal in the stereotaxic frame, special attention should be paid to the comfort of the animal, which will greatly improve efficiency of the anesthesia. The body of the animal should be aligned with the head and neck. The most critical step in positioning the animal and before craniotomy is adjustment of the bregma-lambda axis. Especially when targeting deep brain structures, even a small deviation will generate errors when lowering the injection needle into the brain. In some cases, one may deliberately choose and calculate an oblique needle trajectory.

The injection volume is a determinant factor for obtaining precisely localized opsin expression. A small volume is ideal to privilege a tightly restricted transfection zone. Higher volumes may be useful to cover the full extent of a large target area. If a large area needs to be covered, such as the septum[18], it may be helpful to place several small injections with a range of neighboring coordinates. The interval until the ex vivo electrophysiological recording is also critical. A minimum time for full expression is necessary. While 3 weeks seem to be an optimal delay for these experiments[11], the necessary delay may vary depending on the virus, its serotype, and the distance to the postsynaptic brain region.

The approach described here is even more powerful when combined with injections in transgenic animals. Previous work has exploited different mouse lines for subtypes of GABAergic neurons, in order to specifically target either PV- or SST-expressing interneurons for patch-clamp recordings[20]. Simultaneous double recording of neighboring PV and pyramidal neurons or SST and pyramidal neurons then allows comparison of strengths of long-range inputs between two neuron types[11]. This yields results that are standardized with respect to one neuron type. This standardization is particularly important in cases where the expression levels of opsins vary between different animals or different slices.

Slice health is essential for high-quality patch-clamp recordings. Constant oxygenation of the slices is crucial, and a slow cutting speed significantly improves slice surface quality. A slice thickness of 300 µm preserves, to some extent, the microcircuit integrity in horizontal presubicular sections, including pyramidal neurons with their cell bodies, dendritic and local axonal ramifications, and local synaptic connections. The type of light-gated channels chosen to induce activation of afferent fibers will greatly influence the stimulation parameters (duration, light

intensity). Chronos is a blue light-sensitive channelrhodopsin, and a broad range of illumination wavelengths can be used for activation (peak sensitivity around 500 nm, even with minimal light intensity of 0.05 mW/mm^2, also activated at 405 nm, and up to 530 nm[21]). Furthermore, Chronos has fast kinetics properties in comparison to classical ChR2, which enables high frequency stimulations and reliable activation of long-range projections[22]. In combination with the expression of Chrimson, a red-shifted opsin variant, the independent optical excitation of distinct neural populations becomes feasible.

Disclosures

The authors declare no competing financial interests.

Acknowledgments

We thank Bertrand Mathon, Mérie Nassar, Li-Wen Huang, and Jean Simonnet for their help in the development of previous versions of the stereotaxic injection protocol and Marin Manuel and Patrice Jegouzo for technical help. This work was supported by the French Ministry for Education and Research (L. R., L. S.), Centre National des Etudes Spatiales (M. B.), and Agence Nationale de la Recherche Grant ANR-18-CE92-0051-01 (D. F.).

References

1. Goodridge, J. P., Taube, J. S. Interaction between the postsubiculum and anterior thalamus in the generation of head direction cell activity. *The Journal of Neuroscience: The Official Journal of the Society for Neuroscience.* **17** (23), 9315–9330 (1997).
2. Winter, S. S., Clark, B. J., Taube, J. S. Spatial navigation. Disruption of the head direction cell network impairs the parahippocampal grid cell signal. *Science (New York, N.Y.).* **347** (6224), 870–874 (2015).
3. Fan, Y. *et al.* Activity-dependent decrease of excitability in rat hippocampal neurons through increases in I(h). *Nature Neuroscience.* **8** (11), 1542–1551 (2005).
4. Takahashi, H., Magee, J. C. Pathway Interactions and Synaptic Plasticity in the Dendritic Tuft Regions of CA1 Pyramidal Neurons. *Neuron.* **62** (1), 102–111 (2009).
5. Dolleman-van der Weel, M. J., Lopes da Silva, F. H., Witter, M. P. Interaction of nucleus reuniens and entorhinal cortex projections in hippocampal field CA1 of the rat. *Brain Structure & Function.* **222** (5), 2421–2438 (2017).
6. Callaway, E. M., Yuste, R. Stimulating neurons with light. *Current Opinion in Neurobiology.* **12** (5), 587–592 (2002).
7. Fino, E. et al. RuBi-Glutamate: Two-Photon and Visible-Light Photoactivation of Neurons and Dendritic spines. *Frontiers in Neural Circuits.* **3**, 2 (2009).
8. Mao, T. et al. Long-range neuronal circuits underlying the interaction between sensory and motor cortex. *Neuron.* **72** (1), 111–123 (2011).
9. Zhang, F. *et al.* Optogenetic interrogation of neural circuits: technology for probing mammalian brain structures. *Nature Protocols.* **5** (3), 439–456 (2010).
10. Simonnet, J. *et al.* Activity dependent feedback inhibition may maintain head direction signals in mouse presubiculum. *Nature Communications.* **8**, 16032 (2017).
11. Nassar, M. *et al.* Anterior Thalamic Excitation and Feedforward Inhibition of Presubicular Neurons Projecting to Medial Entorhinal Cortex. *Journal of Neuroscience.* **38** (28), 6411–6425 (2018).
12. Fricker, D. et al. Pyramidal cells of rodent presubiculum express a tetrodotoxin-insensitive Na+ current. *The Journal of Physiology.* **587** (Pt 17), 4249–4264 (2009).
13. Simonnet, J., Eugène, E., Cohen, I., Miles, R., Fricker, D. Cellular neuroanatomy of rat presubiculum. *The European Journal of Neuroscience.* **37** (4), 583–597, (2013).
14. Simonnet, J., Fricker, D. Cellular components and circuitry of the presubiculum and its functional role in the head direction system. *Cell and Tissue Research.* **373** (3), 541–556 (2018).
15. Paxinos, G., Franklin, K. B. J. *The Mouse Brain in Stereotaxic Coordinates.* Academic: New York. (2013).
16. Huang, L.-W. et al. Laminar Localization and Projection-Specific Properties of Presubicular Neurons Targeting the Lateral Mammillary Nucleus, Thalamus, or Medial Entorhinal Cortex. *eNeuro.* **4** (2), (2017).
17. Cruikshank, S. J., Urabe, H., Nurmikko, A. V., Connors, B. W. Pathway-specific feedforward circuits between thalamus and neocortex revealed by selective optical stimulation of axons. *Neuron.* **65** (2), 230–245 (2010).
18. Gonzalez-Sulser, A. *et al.* GABAergic Projections from the Medial Septum Selectively Inhibit Interneurons in the Medial Entorhinal Cortex. *Journal of Neuroscience.* **34** (50), 16739–16743 (2014).
19. Mathon, B. *et al.* Increasing the effectiveness of intracerebral injections in adult and neonatal mice: a neurosurgical point of view. *Neuroscience Bulletin.* **31** (6), 685–696, (2015).
20. Nassar, M. *et al.* Diversity and overlap of parvalbumin and somatostatin expressing interneurons in mouse presubiculum. *Frontiers in Neural Circuits.* **9**, 20, (2015).
21. Klapoetke, N. C. *et al.* Independent optical excitation of distinct neural populations. *Nature Methods.* **11** (3), 338–346, (2014).
22. Hass, C. A., Glickfeld, L. L. High-fidelity optical excitation of cortico-cortical projections at physiological frequencies. *Journal of Neurophysiology.* **116** (5), 2056–2066, (2016).

LIST OF ABBREVIATIONS

a/hVOR: angular/ horizontal Vestibulo-Ocular Reflex

ADN: Antero-Dorsal Thalamic Nucleus

AHP: After Hypopolarization

ANOVA: Analysis of Variance

AOS: Accessory Optic System

BFV : Bilateral Vestibular Failure

CF : Climbing Fibres

COR: Cervico-Ocular Reflex

CPG: Central Pattern Generator

CR: Corneal Reflection

DC: Dorsal cap of Kooy

DSGC: Direction-selective Ganglion Sells

DTN: Dorsal Terminal Nuclei

DVN: Descending Vestibular Nucleus

EH: Eye-Head neurons

EOMs: Extra-Ocular Muscles

EPSC: Excitatory Post-Synaptic Current

FTN: Floccular-target Neurons

GABA : γ-Aminobutyric acid

HC: Hair Cells

HD: Head-Direction

IDPN: 3,3′-Iminodipropionitrile

IP: Intraperitoneal

IR: Infrared

KO: Gene Knock-Out

LTD : Long-Term Depression

LTN: Lateral Terminal Nuclei

LTP : Long-Term Potentiation

LVN: Lateral Vestibular Nucleus

MIFs: Multiply Innervated Fibres

MLF: Medial Longitudinal Fasciculus

MN: Motoneuron

MOR: Maculo-Ocular Reflex

MR: Medial Recti

MTN: Medial Terminal Nuclei

MVN: Medial Vestibular Nucleus

N-T: Naso-Temporal

NOT: Nucleus of the Optic Tract

NPH: Nucleus Prepositus Hypoglossi

NRTP: Nucleus reticularis Tegmenti Pontis

OKAN: Optokinetic After Nystagmus

OKN : Optokinetic Nystagmus

OKR: Optokinetic Reflex

OVAR : Off Vertical Axis Rotation

PBS: Phosphate Buffer Solution

PC: Purkinje Cells

PF: Parallel Fibres

PVP : Position-Vestibular-Pause neurons

SEM: Standart Error of the Mean

SIFs: Single Innervated Fibres

SVN: Superior Vestibular Nucleus

T-N: Temporo-Nasal

UVL : Unilateral Vestibular Lesion

VN: Vestibular Nuclei

VO : Vestibular-Only neurons

VSP: Velocity Storage Mechanisms

VSP: Vestibulo-Spinal Reflex

VVM: Visuo-Vestibular mismatch

WT: Wild Type

LIST OF FIGURES AND TABLES

THE FOLLOWING FIGURES ARE REPRODUCED IN THIS MANUSCRIPT WITH THE AUTHORS/EDITORS PERMISSION.

BIBLIOGRAPHY

Agrawal Y, Carey JP, Della Santina CC, Schubert MC, Minor LB (2009) Disorders of balance and vestibular function in US adults: data from the National Health and Nutrition Examination Survey, 2001-2004. Arch Intern Med 169:938–944.

Agrawal Y, Ward BK, Minor LB (2013) Vestibular dysfunction: Prevalence, impact and need for targeted treatment. J Vestib Res Equilib Orientat 23:113–117.

Angelaki DE (2004) Eyes on Target: What Neurons Must do for the Vestibuloocular Reflex During Linear Motion. J Neurophysiol 92:20–35.

Angelaki DE, Cullen KE (2008) Vestibular System: The Many Facets of a Multimodal Sense. Annu Rev Neurosci 31:125–150.

Angelaki DE, Hess BJ (1996) Three-dimensional organization of otolith-ocular reflexes in rhesus monkeys. I. Linear acceleration responses during off-vertical axis rotation. J Neurophysiol 75:2405–2424.

Angelaki DE, Perachio AA, Mustari MJ, Strunk CL (1992) Role of irregular otolith afferents in the steady-state nystagmus during off-vertical axis rotation. J Neurophysiol 68:1895–1900.

Anon (n.d.) Optogenetic fMRI interrogation of brain-wide central vestibular pathways | PNAS. Available at: https://www.pnas.org/doi/10.1073/pnas.1812453116 [Accessed August 31, 2022].

Arnold DB, Robinson DA, Leigh RJ (1999) Nystagmus induced by pharmacological inactivation of the brainstem ocular motor integrator in monkey. Vision Res 39:4286–4295.

Baarsma EA, Collewijn H (1974) Vestibulo-ocular and optokinetic reactions to rotation and their interaction in the rabbit. J Physiol 238:603–625.

Bach-y-Rita P, W. Kercel S (2003) Sensory substitution and the human–machine interface. Trends Cogn Sci 7:541–546.

Baird RA, Desmadryl G, Fernandez C, Goldberg JM (1988) The vestibular nerve of the chinchilla. II. Relation between afferent response properties and peripheral innervation patterns in the semicircular canals. J Neurophysiol 60:182–203.

Barlow HB, Hill RM, Levick WR (1964) Retinal ganglion cells responding selectively to direction and speed of image motion in the rabbit. J Physiol 173:377–407.

Barmack NH (2003) Central vestibular system: vestibular nuclei and posterior cerebellum. Brain Res Bull 60:511–541.

Beraneck M, Bojados M, Le Séac'h A, Jamon M, Vidal P-P (2012) Ontogeny of Mouse Vestibulo-Ocular Reflex Following Genetic or Environmental Alteration of Gravity Sensing Gilestro GF, ed. PLoS ONE 7:e40414.

Beraneck M, Cullen KE (2007) Activity of Vestibular Nuclei Neurons During Vestibular and Optokinetic Stimulation in the Alert Mouse. J Neurophysiol 98:1549–1565.

Beraneck M, Idoux E (2012) Reconsidering the Role of Neuronal Intrinsic Properties and Neuromodulation in Vestibular Homeostasis. Front Neurol 3 Available at: http://journal.frontiersin.org/article/10.3389/fneur.2012.00025/abstract

Beraneck M, Idoux E, Uno A, Vidal P-P, Moore LE, Vibert N (2004) Unilateral Labyrinthectomy Modifies the Membrane Properties of Contralesional Vestibular Neurons. J Neurophysiol 92:1668–1684.

Beraneck M, Lambert FM (2020) Differential Organization of Intrinsic Membrane Properties of Central Vestibular Neurons and Interaction With Network Properties. In: The Senses: A Comprehensive Reference, pp 273–289. Elsevier. Available at: https://linkinghub.elsevier.com/retrieve/pii/B9780128093245241424

Beraneck M, Lambert FM, Sadeghi SG (2014) Functional Development of the Vestibular System. In: Development of Auditory and Vestibular Systems, pp 449–487. Elsevier. Available at: https://linkinghub.elsevier.com/retrieve/pii/B9780124080881000154

Beraneck M, McKee JL, Aleisa M, Cullen KE (2008) Asymmetric Recovery in Cerebellar-Deficient Mice Following Unilateral Labyrinthectomy. J Neurophysiol 100:945–958.

Beraneck M, Straka H (2011) Vestibular signal processing by separate sets of neuronal filters Peusner KD, ed. J Vestib Res 21:5–19.

Bergquist F, Ludwig M, Dutia MB (2008) Role of the commissural inhibitory system in vestibular compensation in the rat: GABAergic commissural inhibition in vestibular system plasticity. J Physiol 586:4441–4452.

Boadas-Vaello P, Sedó-Cabezón L, Verdú E, Llorens J (2016) Strain and Sex Differences in the Vestibular and Systemic Toxicity of 3,3′-Iminodipropionitrile in Mice. Toxicol Sci:kfw238.

Bockisch CJ, Haslwanter T (2001) Three-dimensional eye position during static roll and pitch in humans. Vision Res 41:2127–2137.

Bohlen MO, Bui K, Stahl JS, May PJ, Warren S (2019) Mouse Extraocular Muscles and the Musculotopic Organization of Their Innervation. Anat Rec 302:1865–1885.

Bos R, Gainer C, Feller MB (2016) Role for Visual Experience in the Development of Direction-Selective Circuits. Curr Biol 26:1367–1375.

Boyden ES, Raymond JL (2003) Active Reversal of Motor Memories Reveals Rules Governing Memory Encoding. Neuron 39:1031–1042.

Brandt T, Strupp M, Arbusow V, Dieringer N (1997) Plasticity of the vestibular system: central compensation and sensory substitution for vestibular deficits. Adv Neurol 73:297–309.

Branoner F, Chagnaud BP, Straka H (2016) Ontogenetic Development of Vestibulo-Ocular Reflexes in Amphibians. Front Neural Circuits 10 Available at: http://journal.frontiersin.org/article/10.3389/fncir.2016.00091/full

Bronstein AM, Morland AB, Ruddock KH, Gresty MA (1995) Recovery from Bilateral Vestibular Failure: Implications for Visual and Cervico-ocular Function. Acta Otolaryngol (Stockh) 115:405–407.

Brooks JX, Cullen KE (2009) Multimodal Integration in Rostral Fastigial Nucleus Provides an Estimate of Body Movement. J Neurosci 29:10499–10511.

Büttner U, Büttner-Ennever JA (2006) Present concepts of oculomotor organization. In: Progress in Brain Research, pp 1–42. Elsevier. Available at: https://linkinghub.elsevier.com/retrieve/pii/S007961230551001X [Accessed October 17, 2022].

Carcaud J, França de Barros F, Idoux E, Eugène D, Reveret L, Moore LE, Vidal P-P, Beraneck M (2017) Long-Lasting Visuo-Vestibular Mismatch in Freely-Behaving Mice Reduces the Vestibulo-Ocular Reflex and Leads to Neural Changes in the Direct Vestibular Pathway. eneuro 4:ENEURO.0290-16.2017.

Carriot J, Jamali M, Cullen KE (2015) Rapid adaptation of multisensory integration in vestibular pathways. Front Syst Neurosci 9 Available at: http://journal.frontiersin.org/article/10.3389/fnsys.2015.00059/abstract

Cassel R, Bordiga P, Carcaud J, Simon F, Beraneck M, Le Gall A, Benoit A, Bouet V, Philoxene B, Besnard S, Watabe I, Pericat D, Hautefort C, Assie A, Tonetto A, Dyhrfjeld-Johnsen J, Llorens J, Tighilet B, Chabbert C (2019) Morphological and functional correlates of vestibular synaptic deafferentation and repair in a mouse model of acute-onset vertigo. Dis Model Mech 12.

Chagnaud BP, Banchi R, Simmers J, Straka H (2015) Spinal corollary discharge modulates motion sensing during vertebrate locomotion. Nat Commun 6:7982.

Cohen B, Dai M, Raphan T (2003) The Critical Role of Velocity Storage in Production of Motion Sickness. Ann N Y Acad Sci 1004:359–376.

Cohen B, Maruta J, Raphan T (2006) Plenary Lecture: Orientation of the Eyes to Gravitoinertial Acceleration. Ann N Y Acad Sci 942:241–258.

Cohen B, Matsuo V, Raphan T (1977) Quantitative analysis of the velocity characteristics of optokinetic nystagmus and optokinetic after-nystagmus. J Physiol 270:321–344.

Collewijn H, Van der Steen J, Ferman L, Jansen TC (1985) Human ocular counterroll: assessment of static and dynamic properties from electromagnetic scleral coil recordings. Exp Brain Res 59:185–196.

Contini D, Holstein GR, Art JJ (2022) Simultaneous Dual Recordings From Vestibular Hair Cells and Their Calyx Afferents Demonstrate Multiple Modes of Transmission at These Specialized Endings. Front Neurol 13:891536.

Cousins S, Cutfield NJ, Kaski D, Palla A, Seemungal BM, Golding JF, Staab JP, Bronstein AM (2014) Visual Dependency and Dizziness after Vestibular Neuritis Barton JS, ed. PLoS ONE 9:e105426.

Cullen KE, Minor LB, Beraneck M, Sadeghi SG (2009) Neural substrates underlying vestibular compensation: Contribution of peripheral versus central processing. J Vestib Res 19:171–182.

Cullen K (2019) Vestibular processing during natural self-motion: implications for perception and action. :41.

Cullen KE (2012) The vestibular system: multimodal integration and encoding of self-motion for motor control. Trends Neurosci 35:185–196.

Cullen KE, Roy JE (2004) Signal Processing in the Vestibular System During Active Versus Passive Head Movements. J Neurophysiol 91:1919–1933.

Curthoys IS, Wade SW (1995) Ocular Torsion Position and the Perception of Visual Orientation. Acta Otolaryngol (Stockh) 115:298–300.

De Zeeuw CI, Lisberger SG, Raymond JL (2021) Diversity and dynamism in the cerebellum. Nat Neurosci 24:160–167.

Desai SS, Ali H, Lysakowski A (2005a) Comparative Morphology of Rodent Vestibular Periphery. II. Cristae Ampullares. J Neurophysiol 93:267–280.

Desai SS, Zeh C, Lysakowski A (2005b) Comparative Morphology of Rodent Vestibular Periphery. I. Saccular and Utricular Maculae. J Neurophysiol 93:251–266.

Dhande OS, Estevez ME, Quattrochi LE, El-Danaf RN, Nguyen PL, Berson DM, Huberman AD (2013) Genetic Dissection of Retinal Inputs to Brainstem Nuclei Controlling Image Stabilization. J Neurosci 33:17797–17813.

Dickman JD, Angelaki DE (2002) Vestibular Convergence Patterns in Vestibular Nuclei Neurons of Alert Primates. J Neurophysiol 88:3518–3533.

Diego Manzoni (2009) Vestibulospinal Reflexes. In: Encyclopedia of Neuroscience. Windhorst Eds.

Dieterich M, Brandt T (2010) Imaging cortical activity after vestibular lesions. Restor Neurol Neurosci 28:47–56.

Dieterich M, Brandt T (2018) Global orientation in space and the lateralization of brain functions. Curr Opin Neurol 31:96–104.

Dietrich H, Wuehr M (2019) Selective suppression of the vestibulo-ocular reflex during human locomotion. J Neurol 266:101–107.

Dutheil S, Lacour M, Tighilet B (2011) Neurogenic Potential of the Vestibular Nuclei and Behavioural Recovery Time Course in the Adult Cat Are Governed by the Nature of the Vestibular Damage Gasset M, ed. PLoS ONE 6:e22262.

Dutia MB, Johnston AR (1998) Development of action potentials and apamin-sensitive after-potentials in mouse vestibular nucleus neurones. Exp Brain Res 118:148–154.

Eatock RA (2000) Adaptation in Hair Cells. Annu Rev Neurosci 23:285–314.

Eatock RA (2018) Specializations for Fast Signaling in the Amniote Vestibular Inner Ear. Integr Comp Biol 58:341–350.

Eatock RA, Songer JE (2011) Vestibular Hair Cells and Afferents: Two Channels for Head Motion Signals. Annu Rev Neurosci 34:501–534.

Eberhorn AC, Büttner-Ennever JA, Horn AKE (2006) Identification of motoneurons supplying multiply- or singly-innervated extraocular muscle fibers in the rat. Neuroscience 137:891–903.

El Mahmoudi N, Marouane E, Rastoldo G, Pericat D, Watabe I, Lapotre A, Tonetto A, Chabbert C, Tighilet B (2022) Microglial Dynamics Modulate Vestibular Compensation in a Rodent Model of Vestibulopathy and Condition the Expression of Plasticity Mechanisms in the Deafferented Vestibular Nuclei. Cells 11:2693.

Eugène D, Deforges S, Guimont F, Idoux E, Vidal P-P, Moore LE, Vibert N (2007) Developmental regulation of the membrane properties of central vestibular neurons by sensory vestibular information in the mouse: Developmental regulation of vestibular neurons membrane properties. J Physiol 583:923–943.

Eugène D, Idoux E, Beraneck M, Moore LE, Vidal P-P (2011) Intrinsic membrane properties of central vestibular neurons in rodents. Exp Brain Res 210:423–436.

Facchini J, Rastoldo G, Xerri C, Péricat D, El Ahmadi A, Tighilet B, Zennou-Azogui Y (2021) Unilateral vestibular neurectomy induces a remodeling of somatosensory cortical maps. Prog Neurobiol 205:102119.

Faulstich BM, Onori KA, du Lac S (2004) Comparison of plasticity and development of mouse optokinetic and vestibulo-ocular reflexes suggests differential gain control mechanisms. Vision Res 44:3419–3427.

Faulstich M, van Alphen AM, Luo C, du Lac S, De Zeeuw CI (2006) Oculomotor Plasticity During Vestibular Compensation Does Not Depend on Cerebellar LTD. J Neurophysiol 96:1187–1195.

França de Barros F, Bacqué-Cazenave J, Taillebuis C, Courtand G, Manuel M, Bras H, Tagliabue M, Combes D, Lambert FM, Beraneck M (2022) Conservation of locomotion-induced oculomotor activity through evolution in mammals. Curr Biol 32:453-461.e4.

Fritsches KA, Marshall NJ (2002) Independent and conjugate optokinesis in fish. J Exp Biol:12.

G. Hernández R, Calvo PM, Blumer R, de la Cruz RR, Pastor AM (2019) Functional diversity of motoneurons in the oculomotor system. Proc Natl Acad Sci 116:3837–3846.

Galliano E, Gao Z, Schonewille M, Todorov B, Simons E, Pop AS, D'Angelo E, van den Maagdenberg AMJM, Hoebeek FE, De Zeeuw CI (2013) Silencing the Majority of Cerebellar Granule Cells Uncovers Their Essential Role in Motor Learning and Consolidation. Cell Rep 3:1239–1251.

Gdowski G, Belton T, McCrea R (2001) The neurophysiological substrate for the cervico-ocular reflex in the squirrel monkey. Exp Brain Res 140:253–264.

Gdowski GT, McCrea RA (1999) Integration of Vestibular and Head Movement Signals in the Vestibular Nuclei During Whole-Body Rotation. J Neurophysiol 82:436–449.

Glasauer S, Straka H (2022) Low Gain Values of the Vestibulo-Ocular Reflex Can Optimize Retinal Image Slip. Front Neurol 13:897293.

Goldberg JM (2000) Afferent diversity and the organization of central vestibular pathways. Exp Brain Res 130:277–297.

Goldberg JM, Fernandez C (1971) Physiology of peripheral neurons innervating semicircular canals of the squirrel monkey. I. Resting discharge and response to constant angular accelerations. J Neurophysiol 34:635–660.

Goldberg JM, Fernandez C (1975) Responses Of Peripheral Vestibular Neurons To Angular And Linear Accelerations In The Squirrel Monkey. Acta Otolaryngol (Stockh) 80:101–110.

González-Garrido A, Pujol R, López-Ramírez O, Finkbeiner C, Eatock RA, Stone JS (2021) The Differentiation Status of Hair Cells That Regenerate Naturally in the Vestibular Inner Ear of the Adult Mouse. J Neurosci 41:7779–7796.

Gordon Lynn Walls (1942) The vertebrate eye and its adaptive radiation. Hafner Publishing Co.

Graf W, Gerrits N, Yatim-Dhiba N, Ugolini G (2002) Mapping the oculomotor system: the power of transneuronal labelling with rabies virus: Transneuronal labelling of eye movements networks. Eur J Neurosci 15:1557–1562.

Greguske EA, Carreres-Pons M, Cutillas B, Boadas-Vaello P, Llorens J (2019) Calyx junction dismantlement and synaptic uncoupling precede hair cell extrusion in the vestibular sensory epithelium during sub-chronic 3,3'-iminodipropionitrile ototoxicity in the mouse. Arch Toxicol 93:417–434.

Grosch M, Lindner M, Bartenstein P, Brandt T, Dieterich M, Ziegler S, Zwergal A (2021) Dynamic whole-brain metabolic connectivity during vestibular compensation in the rat. NeuroImage 226:117588.

Groves AK, Fekete DM (2012) Shaping sound in space: the regulation of inner ear patterning. Development:1.

Gürkov R, Pyykö I, Zou J, Kentala E (2016) What is Menière's disease? A contemporary re-evaluation of endolymphatic hydrops. J Neurol 263:71–81.

Hain TC, Helminski JO (2007) Anatomy and Physiology of the Normal Vestibular System.

Herdman SJ, Hall CD, Schubert MC, Das VE, Tusa RJ (2007) Recovery of Dynamic Visual Acuity in Bilateral Vestibular Hypofunction. Arch Otolaryngol Neck Surg 133:383.

Heskin-Sweezie R, Titley HK, Baizer JS, Broussard DM (2010) Type B GABA receptors contribute to the restoration of balance during vestibular compensation in mice. Neuroscience 169:302–314.

Hess BJM, Dieringer N (1990) Spatial Organization of the Maculo-Ocular Reflex of the Rat: Responses During Off-Vertical Axis Rotation. Eur J Neurosci 2:909–919.

Highstein SM, Holstein GR (2006) The Anatomy of the vestibular nuclei. In: Progress in Brain Research, pp 157–203. Elsevier. Available at: https://linkinghub.elsevier.com/retrieve/pii/S0079612305510069

Holland PJ, Sibindi TM, Ginzburg M, Das S, Arkesteijn K, Frens MA, Donchin O (2020) A Neuroanatomically Grounded Optimal Control Model of the Compensatory Eye Movement System in Mice. Front Syst Neurosci 14:13.

Horn AKE, Straka H (2021) Functional Organization of Extraocular Motoneurons and Eye Muscles. Annu Rev Vis Sci 7:793–825.

Hoy JL, Yavorska I, Wehr M, Niell CM (2016a) Vision Drives Accurate Approach Behavior during Prey Capture in Laboratory Mice. Curr Biol 26:3046–3052.

Hoy JL, Yavorska I, Wehr M, Niell CM (2016b) Vision Drives Accurate Approach Behavior during Prey Capture in Laboratory Mice. Curr Biol 26:3046–3052.

Hübner PP, Khan SI, Migliaccio AA (2017) The mammalian efferent vestibular system plays a crucial role in vestibulo-ocular reflex compensation after unilateral labyrinthectomy. J Neurophysiol 117:1553–1568.

Hupfeld KE, McGregor HR, Koppelmans V, Beltran NE, Kofman IS, De Dios YE, Riascos RF, Reuter-Lorenz PA, Wood SJ, Bloomberg JJ, Mulavara AP, Seidler RD (2022) Brain and Behavioral Evidence for Reweighting of Vestibular Inputs with Long-Duration Spaceflight. Cereb Cortex 32:755–769.

Huterer M, Cullen KE (2002) Vestibuloocular Reflex Dynamics During High-Frequency and High-Acceleration Rotations of the Head on Body in Rhesus Monkey. J Neurophysiol 88:13–28.

Idoux E, Tagliabue M, Beraneck M (2018) No Gain No Pain: Relations Between Vestibulo-Ocular Reflexes and Motion Sickness in Mice. Front Neurol 9:918.

Ito M (1970) Neurophysiological aspects of the cerebellar motor control system. Intern J Neurol Proc. Fulton Society Symposium:126–176.

Ito M (1989) Long-Term Depression. Ann Rev Neurosci:18.

Ito M (2013) Error detection and representation in the olivo-cerebellar system. Front Neural Circuits 7 Available at: http://journal.frontiersin.org/article/10.3389/fncir.2013.00001/abstract

Jamali M, Chacron MJ, Cullen KE (2016) Self-motion evokes precise spike timing in the primate vestibular system. Nat Commun 7:13229.

Jamali M, Mitchell DE, Dale A, Carriot J, Sadeghi SG, Cullen KE (2014) Neuronal detection thresholds during vestibular compensation: contributions of response variability and sensory substitution: Neuronal detection thresholds during vestibular compensation. J Physiol 592:1565–1580.

Jang DC, Shim HG, Kim SJ (2020) Intrinsic Plasticity of Cerebellar Purkinje Cells Contributes to Motor Memory Consolidation. J Neurosci 40:4145–4157.

Johnson KP, Fitzpatrick MJ, Zhao L, Wang B, McCracken S, Williams PR, Kerschensteiner D (2021) Cell-type-specific binocular vision guides predation in mice. Neuron 109:1527-1539.e4.

Kai R, Takahashi K, Tainaka K, Iwakura Y, Namba H, Saito N, Sasaoka T, Yamaguchi S, Nawa H, Horii A (2022) OPEN Cerebrocortical activation following unilateral labyrinthectomy in mice. Sci Rep:15.

Kakegawa W, Katoh A, Narumi S, Miura E, Motohashi J, Takahashi A, Kohda K, Fukazawa Y, Yuzaki M, Matsuda S (2018) Optogenetic Control of Synaptic AMPA Receptor Endocytosis Reveals Roles of LTD in Motor Learning. Neuron 99:985-998.e6.

Karmali F (2019) The velocity storage time constant: Balancing between accuracy and precision. In: Progress in Brain Research, pp 269–276. Elsevier. Available at: https://linkinghub.elsevier.com/retrieve/pii/S0079612319301141

Katoh A, Kitazawa H, Itohara S, Nagao S (1998) Dynamic characteristics and adaptability of mouse vestibulo-ocular and optokinetic response eye movements and the role of the flocculo-olivary system revealed by chemical lesions. Proc Natl Acad Sci 95:7705–7710.

Khan S, Chang R (2013) Anatomy of the vestibular system: A review Greenwald BD, Gurley JM, eds. NeuroRehabilitation 32:437–443.

Kim Y, Jin S, Kim J-S, Koo J-W (2022) Bechterew's Phenomenon in Bilateral Sequential Vestibular Neuritis: A Report of Two Cases. Front Neurol 13:844676.

Kodama T, du Lac S (2016) Adaptive Acceleration of Visually Evoked Smooth Eye Movements in Mice. J Neurosci 36:6836–6849.

Kornmeier J, Sosic-Vasic Z (2012) Parallels between spacing effects during behavioral and cellular learning. Front Hum Neurosci 6 Available at: http://journal.frontiersin.org/article/10.3389/fnhum.2012.00203/abstract

Lackner JR, DiZio P (2020) Velocity storage: its multiple roles. J Neurophysiol 123:1206–1215.

Lasker DM, Han GC, Park HJ, Minor LB (2008) Rotational Responses of Vestibular–Nerve Afferents Innervating the Semicircular Canals in the C57BL/6 Mouse. J Assoc Res Otolaryngol 9:334–348.

Lacour M, Bernard-Demanze L (2015) Interaction between Vestibular Compensation Mechanisms and Vestibular Rehabilitation Therapy: 10 Recommendations for Optimal Functional Recovery. Front Neurol 5 Available at: http://journal.frontiersin.org/article/10.3389/fneur.2014.00285/abstract

Lambert FM, Combes D, Simmers J, Straka H (2012) Gaze Stabilization by Efference Copy Signaling without Sensory Feedback during Vertebrate Locomotion. Curr Biol 22:1649–1658.

Lasker DM, Han GC, Park HJ, Minor LB (2008) Rotational Responses of Vestibular–Nerve Afferents Innervating the Semicircular Canals in the C57BL/6 Mouse. J Assoc Res Otolaryngol 9:334–348.

Laurens J, Angelaki DE (2011) The functional significance of velocity storage and its dependence on gravity. Exp Brain Res 210:407–422.

Leigh RJ, Sawyer RN, Grant MP, Seidman SH (1992) High-Frequency Vestibuloocular Reflex as a Diagnostic Tool. Ann N Y Acad Sci 656:305–314.

Leong ATL, Gu Y, Chan Y-S, Zheng H, Dong CM, Chan RW, Wang X, Liu Y, Tan LH, Wu EX (2019) Optogenetic fMRI interrogation of brain-wide central vestibular pathways. Proc Natl Acad Sci 116:10122–10129.

Lim R, Kindig AE, Donne SW, Callister RJ, Brichta AM (2011) Potassium accumulation between type I hair cells and calyx terminals in mouse crista. Exp Brain Res 210:607–621.

Lopez C, Blanke O (2011) The thalamocortical vestibular system in animals and humans. Brain Res Rev 67:119–146.

Lopez C, Schreyer H-M, Preuss N, Mast FW (2012) Vestibular stimulation modifies the body schema. Neuropsychologia 50:1830–1837.

Lorincz D, Poppi LA, Holt JC, Drury HR, Lim R, Brichta AM (2022) The Long and Winding Road—Vestibular Efferent Anatomy in Mice. Front Neural Circuits 15:751850.

Lubetzky AV, Harel D, Kelly J, Hujsak BD, Perlin K (2019) Weighting and reweighting of visual input via head mounted display given unilateral peripheral vestibular dysfunction. Hum Mov Sci 68:102526.

Mackowetzky K, Yoon KH, Mackowetzky EJ, Waskiewicz AJ (2021) Development and evolution of the vestibular apparatuses of the inner ear. J Anat 239:801–828.

Mackrous I, Carriot J, Cullen KE (2022) Context-independent encoding of passive and active self-motion in vestibular afferent fibers during locomotion in primates. Nat Commun 13:120.

Mahfuz M, Schubert MC, Todd CJ, Figtree WVC, Khan SI, Migliaccio AA (2018) The Effect of Visual Contrast on Human Vestibulo-Ocular Reflex Adaptation. J Assoc Res Otolaryngol 19:113–122.

Malinvaud D, Vassias I, Reichenberger I, Rossert C, Straka H (2010) Functional Organization of Vestibular Commissural Connections in Frog. J Neurosci 30:3310–3325.

Maruta J, Simpson JI, Raphan T, Cohen B (2001) Orienting otolith-ocular reflexes in the rabbit during static and dynamic tilts and off-vertical axis rotation. Vision Res 41:3255–3270.

Maroto AF, Barrallo-Gimeno A, Llorens J (2021) Relationship between vestibular hair cell loss and deficits in two anti-gravity reflexes in the rat. Hear Res 410:108336.

McInturff S, Burns JC, Kelley MW (2018) Characterization of spatial and temporal development of Type I and Type II hair cells in the mouse utricle using new cell-type-specific markers. Biol Open 7:bio038083.

Mehlman ML, Marcroft JL, Taube JS (2021) Anatomical projections to the dorsal tegmental nucleus and abducens nucleus arise from separate cell populations in

the nucleus prepositus hypoglossi, but overlapping cell populations in the medial vestibular nucleus. J Comp Neurol:cne.25119.

Mergner T, Schweigart G, Fennell L, Maurer C (2009) Posture Control in Vestibular-Loss Patients. Ann N Y Acad Sci 1164:206–215.

Meyer AF, Poort J, O'Keefe J, Sahani M, Linden JF (2018) A Head-Mounted Camera System Integrates Detailed Behavioral Monitoring with Multichannel Electrophysiology in Freely Moving Mice. Neuron 100:46-60.e7.

Michaiel AM, Abe ET, Niell CM (2020) Dynamics of gaze control during prey capture in freely moving mice. eLife 9:e57458.

Miki S, Urase K, Baker R, Hirata Y (2020) Velocity storage mechanism drives a cerebellar clock for predictive eye velocity control. Sci Rep 10:6944.

Miles FA, Lisberger SG (1981) Plasticity in the Vestibulo-Ocular Reflex: A New Hypothesis. Annu Rev Neurosci 4:273–299.

Möhwald K, Hadzhikolev H, Bardins S, Becker-Bense S, Brandt T, Grill E, Jahn K, Dieterich M, Zwergal A (2020) Health-related quality of life and functional impairment in acute vestibular disorders. Eur J Neurol 27:2089–2098.

Nagao S (1983) Effects of vestibulocerebellar lesions upon dynamic characteristics and adaptation of vestibulo-ocular and optokinetic responses in pigmented rabbits. Exp Brain Res 53 Available at: http://link.springer.com/10.1007/BF00239396

Nelson AB, Faulstich M, Moghadam S, Onori K, Meredith A, du Lac S (2017) BK Channels Are Required for Multisensory Plasticity in the Oculomotor System. Neuron 93:211–220.

Olabi B, Bergquist F, Dutia MB (2010) Rebalancing the commissural system: Mechanisms of vestibular compensation. J Vestib Res 19:201–207.

Oommen BS, Stahl JS (2008) Eye orientation during static tilts and its relationship to spontaneous head pitch in the laboratory mouse. Brain Res 1193:57–66.

Oyster CW, Barlow HB (1967) Direction-Selective Units in Rabbit Retina: Distribution of Preferred Directions. Sci New Ser 155:841–842.

Oyster CW, Takahashi E, Collewijn H (1972) Direction-selective retinal ganglion cells and control of optokinetic nystagmus in the rabbit. Vision Res 12:183–193.

Parnes LS, Agrawal SK, Atlas J (2003) Diagnosis and management of benign paroxysmal positional vertigo (BPPV). :13.

Payne HL, Raymond JL (2017) Magnetic eye tracking in mice. eLife 6:e29222.

Pham NC, Kim YG, Kim SJ, Kim C-H (2022a) Adaptation of Optokinetic Reflex by Training with Different Frequency and Amplitude. J Integr Neurosci 21:131.

Pham NC, Kim YG, Kim SJ, Kim C-H (2022b) Adaptation of vestibulo-ocular and optokinetic reflexes after massed and spaced vestibulo-ocular motor learning. Behav Brain Res 426:113837.

Pham NC, Kim YG, Kim SJ, Kim C-H (2022c) Adaptation of vestibulo-ocular and optokinetic reflexes after massed and spaced vestibulo-ocular motor learning. Behav Brain Res 426:113837.

Rabbitt RD (2019) Semicircular canal biomechanics in health and disease. J Neurophysiol 121:732–755.

Raghu V, Salvi R, Sadeghi SG (2019) Efferent Inputs Are Required for Normal Function of Vestibular Nerve Afferents. J Neurosci 39:6922–6935.

Raiser TM, Flanagin VL, Duering M, van Ombergen A, Ruehl RM, zu Eulenburg P (2020) The human corticocortical vestibular network. NeuroImage 223:117362.

Rancz EA, Moya J, Drawitsch F, Brichta AM, Canals S, Margrie TW (2015) Widespread Vestibular Activation of the Rodent Cortex. J Neurosci 35:5926–5934.

Raphan Th, Matsuo V, Cohen B (1979) Velocity storage in the vestibulo-ocular reflex arc (VOR). Exp Brain Res 35 Available at: http://link.springer.com/10.1007/BF00236613

Ris L, Godaux E (1998) Neuronal Activity in the Vestibular Nuclei After Contralateral or Bilateral Labyrinthectomy in the Alert Guinea Pig. J Neurophysiol 80:2352–2367.

RR Gacek (1969) The course and central termination of first order neurons supplying vestibular endorgans in the cat. Acta Otolaryngol Suppl.

Rühl M, Kimmel R, Ertl M, Conrad J, zu Eulenburg P (2022) In Vivo Localization of the Human Velocity Storage Mechanism and Its Core Cerebellar Networks by Means of Galvanic-Vestibular Afternystagmus and fMRI. The Cerebellum Available at: https://link.springer.com/10.1007/s12311-022-01374-8

Sadeghi SG, Beraneck M (2020) Task-Specific Differentiation of Central Vestibular Neurons and Plasticity During Vestibular Compensation. In: The Senses: A Comprehensive Reference, pp 290–308. Elsevier. Available at: https://linkinghub.elsevier.com/retrieve/pii/B978012809324524145X

Sadeghi SG, Goldberg JM, Minor LB, Cullen KE (2009) Efferent-Mediated Responses in Vestibular Nerve Afferents of the Alert Macaque. J Neurophysiol 101:988–1001.

Sadeghi SG, Minor LB, Cullen KE (2011) Multimodal Integration After Unilateral Labyrinthine Lesion: Single Vestibular Nuclei Neuron Responses and Implications for Postural Compensation. J Neurophysiol 105:661–673.

Sadeghi SG, Minor LB, Cullen KE (2012) Neural Correlates of Sensory Substitution in Vestibular Pathways following Complete Vestibular Loss. J Neurosci 32:14685–14695.

Sato H, Isamu Sando, Haruo Takahashi (1992) Three-Dimensional anatomy of human scarpa s ganglion.pdf. Laryngoscope.

Schonewille M, Gao Z, Boele H-J, Vinueza Veloz MF, Amerika WE, Šimek AAM, De Jeu MT, Steinberg JP, Takamiya K, Hoebeek FE, Linden DJ, Huganir RL, De Zeeuw CI (2011) Reevaluating the Role of LTD in Cerebellar Motor Learning. Neuron 70:43–50.

Sedó-Cabezón L, Boadas-Vaello P, Soler-Martín C, Llorens J (2014) Vestibular damage in chronic ototoxicity: a mini-review. Neurotoxicology 43:21–27.

Sedó-Cabezón L, Jedynak P, Boadas-Vaello P, Llorens J (2015) Transient alteration of the vestibular calyceal junction and synapse in response to chronic ototoxic insult in rats. Dis Model Mech 8:1323–1337.

Seoane A, Demêmes D, Llorens J (2001) Pathology of the rat vestibular sensory epithelia during subchronic 3,3'-iminodipropionitrile exposure: hair cells may not be the primary target of toxicity. Acta Neuropathol (Berl) 102:339–348.

Shinder ME, Perachio AA, Kaufman GD (2005) VOR and Fos response during acute vestibular compensation in the Mongolian gerbil in darkness and in light. Brain Res 1038:183–197.

Shutoh F, Ohki M, Kitazawa H, Itohara S, Nagao S (2006) Memory trace of motor learning shifts transsynaptically from cerebellar cortex to nuclei for consolidation. Neuroscience 139:767–777.

Simon F, Tissir F, Michel V, Lahlou G, Deans M, Beraneck M (2021) Implication of Vestibular Hair Cell Loss of Planar Polarity for the Canal and Otolith-Dependent Vestibulo-Ocular Reflexes in Celsr1–/– Mice. Front Neurosci 15:750596.

Simpson JI (1984) The Accessory Optic System. Annu Rev Neurosci:29.

Soupiadou P, Gordy C, Forsthofer M, Sanchez-Gonzalez R, Straka H (2020) Acute consequences of a unilateral VIIIth nerve transection on vestibulo-ocular and optokinetic reflexes in Xenopus laevis tadpoles. J Neurol 267:62–75.

Sousa AD, Andrade LR, Salles FT, Pillai AM, Buttermore ED, Bhat MA, Kachar B (2009) The Septate Junction Protein Caspr Is Required for Structural Support and Retention of KCNQ4 at Calyceal Synapses of Vestibular Hair Cells. J Neurosci 29:3103–3108.

Spaiardi P, Marcotti W, Masetto S, Johnson SL (2022) Signal transmission in mature mammalian vestibular hair cells. Front Cell Neurosci 16:806913.

Spencer RF, Porter JD (2006) Biological organization of the extraocular muscles. In: Progress in Brain Research, pp 43–80. Elsevier. Available at: https://linkinghub.elsevier.com/retrieve/pii/S0079612305510021 [Accessed September 28, 2022].

Stackman RW, Clark AS, Taube JS (2002) Hippocampal spatial representations require vestibular input. Hippocampus 12:291–303.

Stahl JS (2004) Using eye movements to assess brain function in mice. Vision Res 44:3401–3410.

Stahl JS, van Alphen AM, De Zeeuw CI (2000) A comparison of video and magnetic search coil recordings of mouse eye movements. J Neurosci Methods 99:101–110.

Stone JS, Pujol R, Nguyen TB, Cox BC (2021) The Transcription Factor Sox2 Is Required to Maintain the Cell Type-Specific Properties and Innervation of Type II Vestibular Hair Cells in Adult Mice. J Neurosci 41:6217–6233.

Straka H, Chagnaud BP (2017) Moving or being moved: that makes a difference. J Neurol 264:28–33.

Straka H, Holler S, Goto F (2002) Patterns of Canal and Otolith Afferent Input Convergence in Frog Second-Order Vestibular Neurons. J Neurophysiol 88:2287–2301.

Straka H, Vibert N, Vidal PP, Moore LE, Dutia MB (2005) Intrinsic membrane properties of vertebrate vestibular neurons: Function, development and plasticity. Prog Neurobiol 76:349–392.

Strupp M, Dlugaiczyk J, Ertl-Wagner BB, Rujescu D, Westhofen M, Dieterich M (2020) Vestibular Disorders. Dtsch Ärztebl Int Available at: https://www.aerzteblatt.de/10.3238/arztebl.2020.0300

Sugihara I (2004) Molecular, Topographic, and Functional Organization of the Cerebellar Cortex: A Study with Combined Aldolase C and Olivocerebellar Labeling. J Neurosci 24:8771–8785.

Summers MT, Feller MB (2022) Distinct inhibitory pathways control velocity and directional tuning in the mouse retina. Curr Biol 32:2130-2143.e3.

Taube JS (2007) The Head Direction Signal: Origins and Sensory-Motor Integration. :29.

Thomson DB, Inglis JT, Schor RH, Macpherson JM (1991) Bilateral labyrinthectomy in the cat: motor behaviour and quiet stance parameters. Exp Brain Res 85 Available at: http://link.springer.com/10.1007/BF00229414.

Tighilet B, Bordiga P, Cassel R, Chabbert C (2019) Peripheral vestibular plasticity vs central compensation: evidence and questions. J Neurol 266:27–32.

Tighilet B, Brezun JM, Dit Duflo Sylvie G, Gaubert C, Lacour M (2007) New neurons in the vestibular nuclei complex after unilateral vestibular neurectomy in the adult cat: Reactive neurogenesis in adult vestibular lesioned cats. Eur J Neurosci 25:47–58.

Tighilet B, Chabbert C (2019) Adult neurogenesis promotes balance recovery after vestibular loss. Prog Neurobiol 174:28–35.

van Alphen AM, Stahl JS, De Zeeuw CI (2001) The dynamic characteristics of the mouse horizontal vestibulo-ocular and optokinetic response. Brain Res 890:296–305.

Vignaux G, Chabbert C, Gaboyard-Niay S, Travo C, Machado ML, Denise P, Comoz F, Hitier M, Landemore G, Philoxène B, Besnard S (2012) Evaluation of the chemical model of vestibular lesions induced by arsanilate in rats. Toxicol Appl Pharmacol 258:61–71.

Voges K, Wu B, Post L, Schonewille M, De Zeeuw CI (2017) Mechanisms underlying vestibulo-cerebellar motor learning in mice depend on movement direction: Adaptation of compensatory eye movements in directional learning. J Physiol 595:5301–5326.

Wade N, Tatler B (2005) The Moving Tablet of the Eye: The Origins of Modern Eye Movement Research. Oxford University Press.

Waespe W, Henn V (1977) Neuronal activity in the vestibular nuclei of the alert monkey during vestibular and optokinetic stimulation. Exp Brain Res 27 Available at: http://link.springer.com/10.1007/BF00239041 [Accessed October 28, 2022].

Weng S, Sun W, He S (2005) Identification of ON-OFF direction-selective ganglion cells in the mouse retina: ON-OFF DSGCs in the mouse retina. J Physiol 562:915–923.

Whitney SL, Alghwiri AA, Alghadir A (2016) An overview of vestibular rehabilitation. In: Handbook of Clinical Neurology, pp 187–205. Elsevier. Available at: https://linkinghub.elsevier.com/retrieve/pii/B9780444634375000133

Wiest G (2015) The origins of vestibular science: The origins of vestibular science. Ann N Y Acad Sci 1343:1–9.

Wilkerson BA, Artoni F, Lea C, Ritchie K, Ray CA, Bermingham-McDonogh O (2018) Effects of 3,3′-Iminodipropionitrile on Hair Cell Numbers in Cristae of CBA/CaJ and C57BL/6J Mice. J Assoc Res Otolaryngol 19:483–491.

Wijesinghe R, Protti DA, Camp AJ (2015) Vestibular Interactions in the Thalamus. Front Neural Circuits 9 Available at: http://journal.frontiersin.org/Article/10.3389/fncir.2015.00079/abstract

Y Inoue, A Takemura, K Kawano, K Kitama, FA Miles (1998) Dependence of short-latency ocular following and associated activity in the medial superior temporal area (MST) on ocular vergence. Exp Brain Res.

Yakushin SB, Raphan T, Cohen B (2017) Coding of Velocity Storage in the Vestibular Nuclei. Front Neurol 8:386.

Yamazaki T, Nagao S, Lennon W, Tanaka S (2015) Modeling memory consolidation during posttraining periods in cerebellovestibular learning. Proc Natl Acad Sci 112:3541–3546.

Yoder RM, Taube JS (2014) The vestibular contribution to the head direction signal and navigation. Front Integr Neurosci 8 Available at: http://journal.frontiersin.org/article/10.3389/fnint.2014.00032/abstract

Yokota J-I, Reisine H, Cohen B (1992) Stimulation and Single-Unit Studies of Velocity Storage in the Vestibular and Prepositus Hypoglossi Nuclei of the Monkey. Ann N Y Acad Sci 656:966–968.

Zeng S, Ni W, Jiang H, You D, Wang J, Lu X, Liu L, Yu H, Wu J, Chen F, Li H, Wang Y, Chen Y, Li W (2020) Toxic Effects of 3,3 ′ -Iminodipropionitrile on Vestibular System in Adult C57BL/6J Mice *In Vivo*. Neural Plast 2020:1–11.

Zennou-Azogui Y, Xerri C, Harlay F (1994) Visual sensory substitution in vestibular compensation: neuronal substrates in the alert cat. Exp Brain Res 98 Available at: http://link.springer.com/10.1007/BF00233983

Zwergal A, Schlichtiger J, Xiong G, Beck R, Günther L, Schniepp R, Schöberl F, Jahn K, Brandt T, Strupp M, Bartenstein P, Dieterich M, Dutia MB, la Fougère C (2016) Sequential [18F]FDG µPET whole-brain imaging of central vestibular compensation: a model of deafferentation-induced brain plasticity. Brain Struct Funct 221:159–170.

RÉSUMÉ

Une image stable de l'environnement est cruciale pour l'équilibre, l'orientation et la navigation. La stabilisation du regard est assurée chez tous les vertébrés par les réflexes vestibulaires (VORd) et visuels (OKR) qui compensent respectivement les mouvements internes ou externes. Physiologiquement, ces deux réflexes fonctionnent en synergie pour assurer une stabilisation combinée optimale du regard. Pour comprendre l'intégration visuo-vestibulaire et sa plasticité suite à une perte sensorielle, nous avons réalisé chez la souris des perturbations visuelles ou vestibulaires. Les altérations de long-terme du VOR et de l'OKR ont d'abord été étudiées à l'aide d'un protocole de perturbations visuo-vestibulaire qui induit une réduction du gain des deux réflexes, spécifiquement pour les basses fréquences. Puis, nous avons utilisé un protocole IDPN subchronique induisant une altération transitoire des entrées vestibulaires. Nous rapportons que 6 semaines de ce traitement affectent autant le VOR canalaire et otolithique et que la perte de cellules ciliées est en corrélation avec les déficiences individuelles des souris. L'adaptation de l'OKR est en retard par rapport au VOR et se produit uniquement dans la gamme de fréquences où les entrées vestibulaires dominent physiologiquement les réflexes compensatoires de stabilisation du regard. Enfin, l'intégration des entrées vestibulaires et visuelles reste altérée après la récupération, conduisant à une stabilisation suboptimale du regard. Globalement, les résultats produits ici éclairent l'intégration des entrées visuelles et vestibulaires et fournissent de nouvelles données sur la dynamique d'adaptation qui suivent une perte sensorielle transitoire. Ces résultats sont importants pour mieux comprendre les mécanismes physiologiques qui soutiennent la repondération multisensorielle chez les patients souffrant d'une hypofonction vestibulaire fluctuante.

Mots clés : ⌜ système vestibulaire, stabilisation du regard, VOR, OKR, intégration multisensorielle ⌟

ABSTRACT

A stable image of the environment is crucial to balance, orientation and navigation. Gaze stabilization is achieved in all vertebrates by the vestibular (VORd) and visual (OKR) reflexes that compensate respectively for internal or external movements. Physiologically, both reflexes work synergistically to perform optimal combined gaze stabilization. To understand visuo-vestibular integration and its plasticity following sensory loss, we performed in the mouse visual or vestibular perturbations. VOR and OKR week-long alterations were first studied using a visuo-vestibular mismatch protocol that induced a reduction of the gain of both reflexes, specifically for the lower frequencies. Then we used a subchronic IDPN protocol inducing a transitory alteration of vestibular inputs using an IDPN subchronic ototoxic protocol. We report that 6 weeks of IDPN subchronic treatment equally affects the canal- and otolith-dependent VOR and that organ-specific loss of hair cells correlates with individual mice impairments. The OKR adaptive plasticity dynamically lags VOR changes and occurs in only in the frequency range where the vestibular inputs are physiologically dominating compensatory gaze-stabilizing reflexes. Finally, the integration of vestibular and visual inputs remains impaired after 6 weeks of washout, leading to suboptimal gaze stabilization. Globally, the results produced during my PhD shed light on the integration of visual and vestibular inputs in the mouse model and provide new data about the dynamics of adaptation that develop when a transitory sensory loss occurs. These results are of importance to better understand the physiological mechanisms that sustain the multisensory reweighting in patients suffering from fluctuating vestibular hypofunction.

Keywords :⌜ vestibular system, gaze stabilisation, VOR, OKR, multisensory integration ⌟